Synthesis and optoelectronic properties of new Fluorene-2,5-Diaryl-1,3,4-Oxadiazole hybrid materials

Oyston, Stephen

SYNTHESIS AND OPTOELECTRONIC PROPERTIES OF NEW FLUORENE-2,5-DIARYL-1,3,4-OXADIAZOLE HYBRID MATERIALS

STEPHEN OYSTON, B.SC. (HONS)

USTINOV COLLEGE

DEPARTMENT OF CHEMISTRY

UNIVERSITY OF DURHAM

A Thesis submitted for the degree of Doctor of Philosophy at the University of Durham

August 2005

STATEMENT OF COPYRIGHT

DECLARATION

The work described in this thesis was carried out in the Department of Chemistry at the University of Durham, between October 2001 and September 2004. All the work was carried out by the author unless otherwise stated, and has not previously been submitted for a degree at this or any other university.

TABLE OF CONTENTS

ABSTRACT

Synthesis And Optoelectronic Properties Of New Fluorene-2,5-Diaryl-1,3,4-Oxadiazole Hybrid Materials

Stephen Oyston, University of Durham, 2005

Novel fluorene and spirobifluorene-2,5-diaryl-1,3,4-oxadiazole hybrids **165** and **171**, respectively, have been synthesised by Suzuki cross-coupling methodology. Pyridine analogues of **165** and **171**, **184** and **185**, respectively, were also synthesised. Further extension of the π-electron framework was achieved via Wittig reaction to afford compound **177**. Single layer organic light emitting devices (OLED)s using blends of MEH-PPV as the emissive material with electron transport (ET) materials **165**, **171**, **177**, **184** and **185** have been fabricated. For all the devices studied electroluminescence (EL) originated exclusively from the MEH-PPV with external quantum efficiencies (EQE)s greatly enhanced (>two orders of magnitude) compared to pure MEH-PPV devices. The incorporation of pyridine in compounds **184** and **185** considerably enhanced the electron affinity of the systems compared to compounds **165** and **171**. For a device incorporating PEDOT:PSS in the configuration ITO/PEDOT:PSS/MEH-PPV-**185** (30 : 70% by weight)/Ca/Al an EQE of *ca.* 0.6% and a luminance efficiency of 1.2 cd A^{-1} at 10.5 V was achieved.

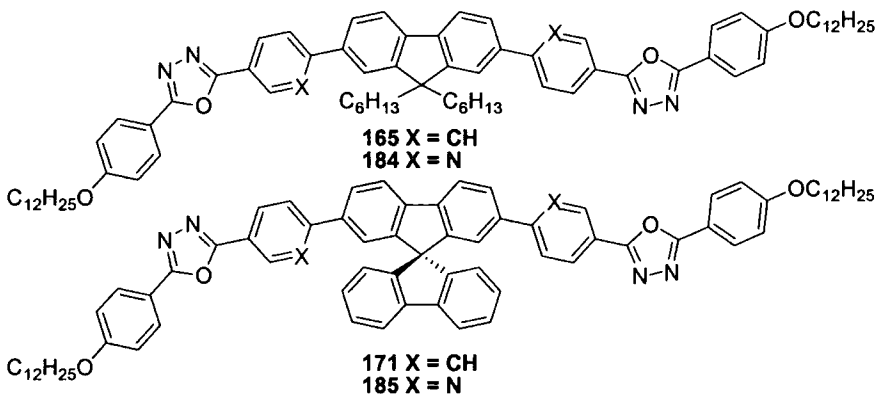

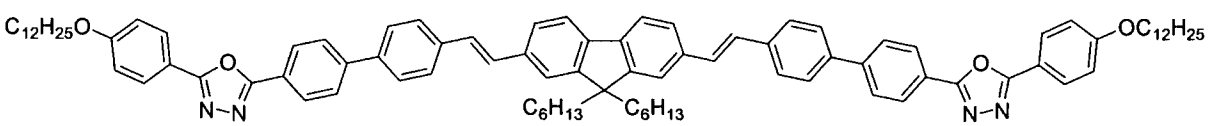

177

ACKNOWLEDGEMENTS

I would like to express my gratitude to the following people who have been involved, offering technical support, friendship and support, in the creation of this thesis.

Firstly I would like to thank my supervisor Prof. Martin R. Bryce for offering me a Ph.D. within such an interesting research field and for all his patience, support and motivating optimism.

Tremendous thanks to the past and present members of the Bryce group who made me feel at home on entering the group and have been a pleasure to work alongside over the years. Especially Changsheng for all of his excellent advice, practical assistance and constant good humour, and Igor for the many calculations and unfaltering assistance. Big thanks to the lads; Greg for the Friday night poisonings at the S.U., Paul (noodle shoes) for the burnt breakfasts and the GSAFC tour of Germany, also Ian for all the quality nights out and Steve for his David Dickinson impressions. These lads have been top housemates and drinking buddies and I thank them for their friendship throughout my time in Durham.

The academic and technical staff at the Chemistry Department for all their work in obtaining various spectra and analyses. Especially Dr. A. Kenwright for useful NMR discussions and Dr. A. Batsanov for solving crystal structures. I would also like to thank Dr. J. Ahn and Prof. M. C. Petty from the School of Engineering, University of Durham, for the OLED studies and discussions.

I would like to thank my mam and dad for all their support, financial and emotional, throughout my years at university. Without them I could not have got this far. Also my brother Paul and finally Shelly my girlfriend for her endless patience, support and encouragement whilst writing this thesis, thank you.

"Man is unique not because he does science, and he is unique not because he does art, but because science and art equally are expressions of his marvellous plasticity of mind"

- J. Bronowski, *The Ascent of Man*

ABBREVIATIONS

Alq_3	Tris-(8-hydroxyquinoline)aluminium
CuPc	Copper phthalocyanine
DCM	Dichloromethane
DSC	Differential scanning calorimetry
EI	Electron impact
EL	Electroluminescence
EML	Emitting layer
ETHB	Electron transporting hole blocking
ETL	Electron transport layer
EQE	External quantum efficiency
HOMO	Highest occupied molecular orbital
HTL	Hole transport layer
ITO	Indium tin oxide
LUMO	Lowest unoccupied molecular orbital
MEH-PPV	Poly[2-(2-ethylhexyloxy)-5-methoxy-1,4-phenylenevinylene] **15**
Mp	Melting point
NPB	[N,N'-Di(naphthalenyl)-N,N'-diphenyl](1,1'-biphenyl)-4,4'-diamine **33**
NMR	Nuclear magnetic resonance
OLED	Organic light emitting diodes
OXD	2,5-Diaryl-1,3,4-oxadiazole
PBD	5-(4-Biphenyl)-2-(4-*tert*-butylphenyl)-1,3,4-oxadiazole **5**
PEDOT	Poly(3,4-ethylenedioxythiophene)
PET	Poly(ethyleneterephthalate)
PL	Photoluminescence
PPV	Poly(*p*-phenylene vinylene) **12**
PVK	Poly(vinylcarbazole)
T_g	Glass transition temperature
THF	Tetrahydrofuran
TPD	N,N'-Diphenyl-N,N'-bis(3-methylphenyl)(1,1'-biphenyl)-4,4'-diamine **6**
UV	Ultraviolet
Vis	Visible

1 ELECTRON TRANSPORT MATERIALS FOR ORGANIC LIGHT EMITTING DIODES

There has been intense research interest recently in the use of organic materials for light emitting diodes (LEDs) since original reports of the electroluminescence (EL) properties of conjugated polymers.[1] This reinforced the immense interest in electronic and optoelectronic devices made entirely from organic materials born from the discovery in the late seventies that certain polymeric organic materials can conduct electricity almost as efficiently as copper.[2] Heeger *et al.* found that oxidation of polyacetylene with halogens (p-doping) significantly increased conductivity; this can be considered the birth of the field of conducting polymers.[3]

Organic light emitting diodes (OLEDs) offer many advantages over bulky inefficient cathode ray tubes such as low power consumption, low weight and compact flat screen technology. Also the possibility of producing inexpensive large area flat panel displays via vapour deposition, first realised by Tang and VanSlyke,[4] could provide an alternative to liquid crystal display (LCD) technology, as LCDs larger than 12 inches have proven very costly and difficult to produce.[5] Inorganic LEDs may also be challenged due to the versatility of conjugated polymers in that their physical properties (colour, emission efficiency and operating lifetimes) can be fine-tuned by manipulation of their chemical structure.[6]

Initial commercial applications of organic materials in display technologies have resulted in Pioneer Electronics introducing an organic EL monochrome display for automobiles. Multicolor OLEDs have recently seen significant incorporation in other small-format consumer electronic products such as mobile phones and portable audio players. Eastman Kodak/Sanyo launched the first full colour, active matrix OLED screen digital camera in 2003.[7] According to display industry analysis firm isuppli/Stanford Resources the global market for OLEDs will increase from $112 million in 2003 to $2.3 billion in 2008.[8] There are still many difficulties to overcome including colour emission over the full visible spectrum, higher quantum efficiencies, lower operating voltages and longer device lifetimes before OLEDs can become genuinely commercially viable.

1.1 ELECTROLUMINESCENCE OF ORGANIC MATERIALS

EL (Appendix 1) is the non-thermal conversion of electrical energy into light in a substrate whereby photon emission results from the recombination of holes and electrons within the substrate. Pope *et al.*[9] first observed EL from organic materials in 1963 by passing an electric current through a single anthracene **1** crystal. Later, Helfrich reported fluorescence in anthracene crystals using charge-injecting electrodes and attributed this to the recombination of electrons and holes within the anthracene crystal.[10] Two electrolytic solutions (positively and negatively-charged anthracene) housed in glass tubes and cemented to the surface of the crystal were responsible for charge transport of electrons and holes injected from the cathode and anode, respectively, into the anthracene crystal. EL was witnessed in the section of the anthracene crystal next to the hole-injecting anode, which suggests an imbalance of charge-carrier injection and transport. High voltages (*ca.* 400 V) were required partly due to the thickness of the crystals in both instances. This limited further breakthroughs until the 1980's when Vincett *et al.* reported EL from thin films of anthracene sublimed onto oxidised aluminium electrodes. Operating voltages were brought down to *ca.* 30 V, although low efficiencies were reported due to inefficient electron injection and poor quality anthracene films.[11]

In 1987 it became apparent that organic materials were viable for optoelectronic devices. In contrast to earlier organic EL devices, Tang and VanSlyke[4] developed an EL diode comprising a double layer of thin organic films. The first layer, an aromatic diamine **2** responsible only for hole transport, was deposited onto an indium tin oxide (ITO) substrate (*ca.* 750 Å thick). A layer of the EL material tris-(8-hydroxyquinoline)aluminium (Alq_3) **3** (*ca.* 600 Å thick) followed this. Finally a low work function alloy of magnesium and silver (10:1) was deposited as the cathode for more effective electron injection. All three layers were deposited by vacuum deposition. The simply fabricated device displayed high photon / electron quantum efficiencies of 1% with high luminous efficiencies and brightness at driving voltages below 10 V. The emission peak intensity at λ_{max} 550 nm indicated that the radiative recombination of injected electrons and holes occurs in the Alq_3 layer, as the EL emission spectrum was identical to the photoluminescence (PL) spectrum of Alq_3 thin films.

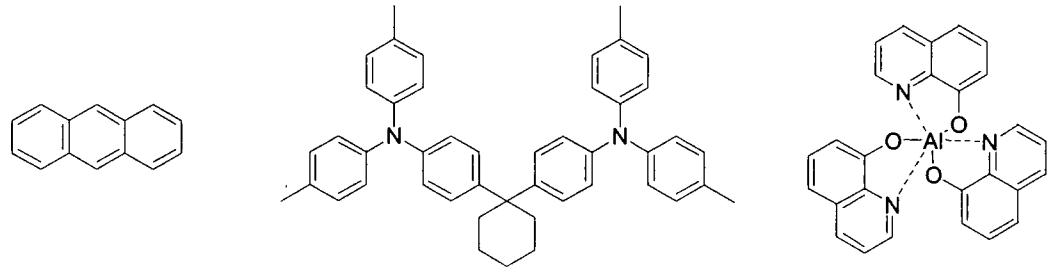

Scheme 1: Molecular structures of anthracene 1, diamine 2 and Alq_3 3 as used by Tang and VanSlyke in their double layer EL diode.[4]

Further work on multilayer thin organic film devices by Adachi *et al.*[12] using the luminescent hole transport material NSD **4** as the emitter and incorporating an electron transporting hole blocking (ETHB) material PBD **5** in the device configuration (ITO/NSD/PBD/MgAg) gave an emission intensity of ~ 1000 cd m^{-2} at a current of 100 mA cm^{-2} and a voltage of 16 V, relating to a luminous efficiency of 0.2 lm W^{-1}. Emission efficiencies of this device were 10^4 times larger than that of a single layer device (ITO/NSD/MgAg) without PBD. Also efficiencies of a bilayer device (ITO/TPD/NSD/MgAg), where TPD **6** is the hole transporting diamine derivative, were only 10^2 times larger than the single layer device. The emission spectra of the EL devices (λ_{max} 520 nm) correspond to the PL spectra of NSD thin films. No emission was evident from the PBD layer. These results established that recombination occurred in the emitter layer, with the PBD layer blocking the transport of holes whilst injecting electrons into the emitting layer.

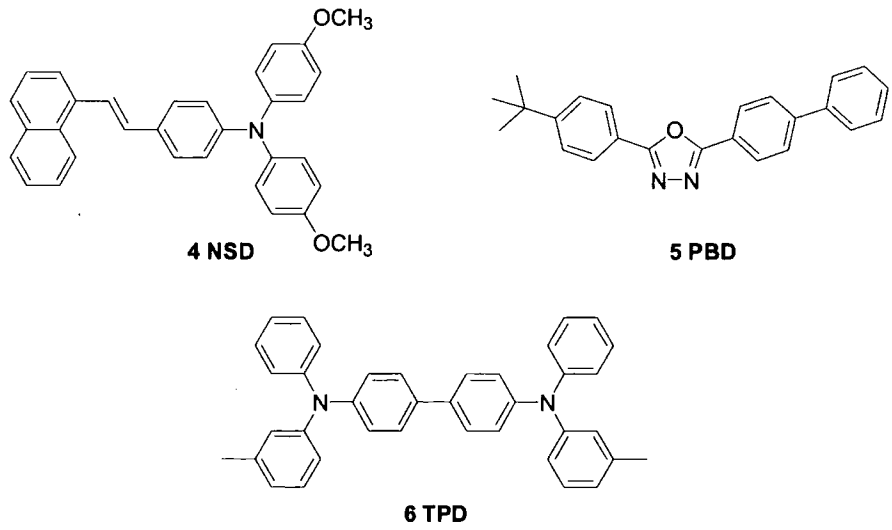

Scheme 2: Molecular structures of the hole transport materials NSD 4 and TPD 6 and the ETHB material PBD 5.

1.2 ELECTROLUMINESCENT CONJUGATED POLYMERS

Conjugated polymers are semiconductors due to π molecular orbitals being delocalised along the polymer chain. Their advantage over non-polymeric organic semiconductors is their attractive physical /mechanical properties and the possibility of solution processing to form flexible and robust structures tailored for a wide range of applications. Conjugated polymers which have large semiconductor gaps and can be prepared sufficiently pure can show high quantum yields for photoluminescence. The first example of EL from an organic polymeric semiconductor was a serendipitous discovery by the Cambridge group of Friend *et al.*, reported in 1990. Whilst studying the electrical properties of poly(*p*-phenylene vinylene) (PPV) **12** it was found that a strip of PPV sandwiched between two electrical contacts glowed green in the dark when a current was applied.[1]

1.2.1 PPV & MEH-PPV

PPV and poly[2-(2-ethylhexyloxy)-5-methoxy-1,4-phenylenevinylene] (MEH-PPV) proved pivotal materials in the development of OLEDs throughout the 1990's. PPV is a bright yellow fluorescent polymer with EL maxima at λ 551 nm (2.5 eV) and 520 nm (2.4 eV) in the yellow-green region of the visible spectrum. The polymer is insoluble and intractable. The direct synthesis of PPV has been carried out utilising some well-known coupling reactions, i.e. Wittig[13] and Heck[14] reactions. The problem with these direct syntheses from monomers is that the material produced cannot be easily processed. These physical and processing problems were overcome by the introduction of a solution-processable, sulphonium-precursor route to PPV by Wessling and Zimmerman,[15,16] which meant that solution processing by spin coating could be used to manufacture good quality thin PPV films for use in EL devices.

Scheme 3 shows the reaction of 1,4-bis(dichloromethyl)benzene **7** with tetrahydrothiophene **8** yielding the bis sulphonium salt **9**. Polymerisation of a methanolic solution of the monomer gave the colourless water-soluble viscous polyelectrolyte solution; this was then dialysed against distilled water to remove low molecular weight impurities. The molar mass of the precursor polymer **10** could not be determined. The reaction of the polyelectrolyte **10** with refluxing methanol yielded the neutral polymer **11**, which on gel permeation chromatography (GPC) gave a number average molar mass M_n of $\geq$100,000 g mol^{-1}.[17] Spin coated thin films of the precursor polymer **10** were converted to PPV by thermal

elimination of tetrahydrothiophene and HCl to form the alkene bonds. The resultant thin films of PPV **12** were homogenous, dense and uniform.

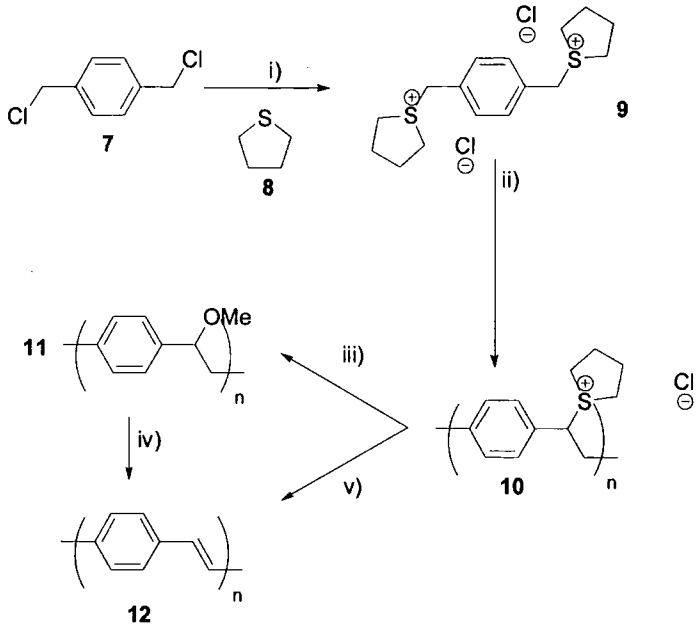

Scheme 3: Wessling and Zimmerman precursor route to PPV 12: i) 8, MeOH, 65 °C; ii) NaOH, MeOH/H_2O or Bu_4NOH, MeOH, 0 °C, neutralisation (HCl), dialysis (water); iii) MeOH, 50 °C; iv) 220 °C, HCl(g)/Ar, 22 h; v) 180-300 °C, vacuum, 12 h[6]

Ohnishi *et al.* [18] and also Braun and Heeger[19,20] have independently reported PPV derivatives that are soluble in the conjugated form. These PPV derivatives such as MEH-PPV **15**, which is the most widely studied PPV derivative (Scheme 4) and other dialkoxy-substituted derivatives of PPV owe their increased solubility and air stability to the long alkoxy side chains.

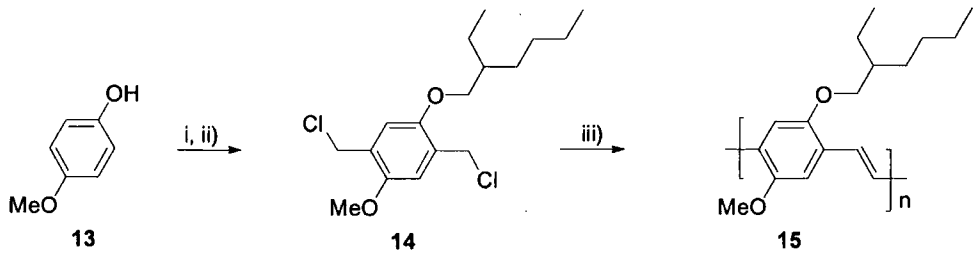

Scheme 4: Preparation of MEH-PPV 15: i) 3-(bromomethyl)heptane, KOH, EtOH, reflux, 16 h; ii) HCHO, conc. HCl, dioxane, 20°C, 18 h, reflux, 4 h; iii) KO^{t}Bu, THF, 20 °C, 24 h.[21,22]

MEH-PPV dissolves readily in solvents such as THF and $CHCl_3$, which enables direct deposition onto substrates without the need for thermal treatment during device fabrication, which was one of the major drawbacks of the Wessling precursor route. Also the EL maximum of MEH-PPV is red-shifted to λ_{max} 626 nm compared to that of PPV (λ_{max} 551 nm).

The synthesis of MEH-PPV can be achieved, as before for PPV, or by a dehydrohalogenation condensation polymerisation as developed by Gilch *et al.*[23] The Gilch route shortens the preparation by two steps and also increases yields significantly with molar masses comparable with that of the sulphonium precursor route.

Simple OLEDs employing MEH-PPV in the single layer (ITO/MEH-PPV/Ca) device structure have achieved a respectable external quantum efficiency (EQE) of 1.0%.[19] Calcium used here has a lower work function than the previously used aluminium, matching the LUMO of the MEH-PPV more effectively. However, aluminium is less reactive in the presence of moisture and air, aiding device stability.

1.3 Single Layer OLED Structures

The basic structure of OLEDs consists of a thin film of the EL material sandwiched between two electrodes, one of which must be transparent. The light emitting material can be an organic polymer, or a small non-polymeric molecule. Under an applied voltage electrons are injected from the cathode (low work function electrode) and holes are injected from the anode (high work function electrode) into the organic material where they migrate under the effect of the external electric field.[6]

Light emission is the consequence of the radiative decay of excitons in the emissive material produced by the combination of electrons and holes injected from the oppositely charged electrodes.[24] The photons of light generated escape through the transparent electrode. Figure 1 shows a representation of a simple EL device. The device is fabricated by spin coating the EL material, e.g. MEH-PPV, onto a transparent indium-tin oxide (ITO), glass or polymer substrate such as commercially available poly(ethyleneterephthalate) (PET) coated with a layer of ITO. The vacuum evaporation of a low work function metal cathode such as Al or Ca completes the EL device structure.

In such a device electrons are injected into the LUMO (forming radical anions) and the holes injected into the HOMO (forming radical cations) of the EL material. Under the external field the charges migrate along the polymer chains and combination of the radical anions and radical cations within a single conjugated segment forms singlet and triplet excited states. Spin allowed radiative emission (fluorescence) of the singlet state occurs upon relaxation to the ground state (see Appendix 1). Triplets usually relax to the ground state via a non-radiative pathway. Therefore, efficiency of these devices is limited as the probability of

triplet to singlet exciton formation from the recombination of electrons and holes is 3:1 giving a maximum efficiency of EL from the excited states of organic materials of 25%.[25] The EQE, η_{ext}, of monolayer OLEDs, *i.e.* the number of photons actually seen by the observer, is related to the number of photons emitted per electrons injected. In the case of PPV this value is low (0.05%).[1] The observed EQE, η_{ext}, is much lower than the internal efficiency, η_{int}, as given by the following relationship.[25]

$$\eta_{ext} = \eta_{int} / 2n^2$$

Equation 1: External quantum efficiency (EQE), η_{ext}, where n is the refractive index of the organic material.

The luminous efficiency, η_L, in candelas per amp (cd A^{-1}) is convenient for quantifying the properties of an OLED for display applications and is defined below.

$$\eta_L = AL / I_{OLED}$$

Equation 2: Luminous efficiency η_L, where L is the luminance of the OLED (cd m^{-2}), A is the device active area and I_{OLED} is the OLED current.

A frequently used efficiency unit is the luminous power efficiency η_P (lm W^{-1}), where η_P is the ratio of luminous power emitted in the forward direction, L_p (lm), to the total electrical power required to drive the OLED at a particular voltage (V). Luminous power efficiency is useful in interpreting the power dissipated by a device when used in a display.

$$\eta_P = L_P / I_{OLED}V$$

Equation 3: Luminous power efficiency η_p.

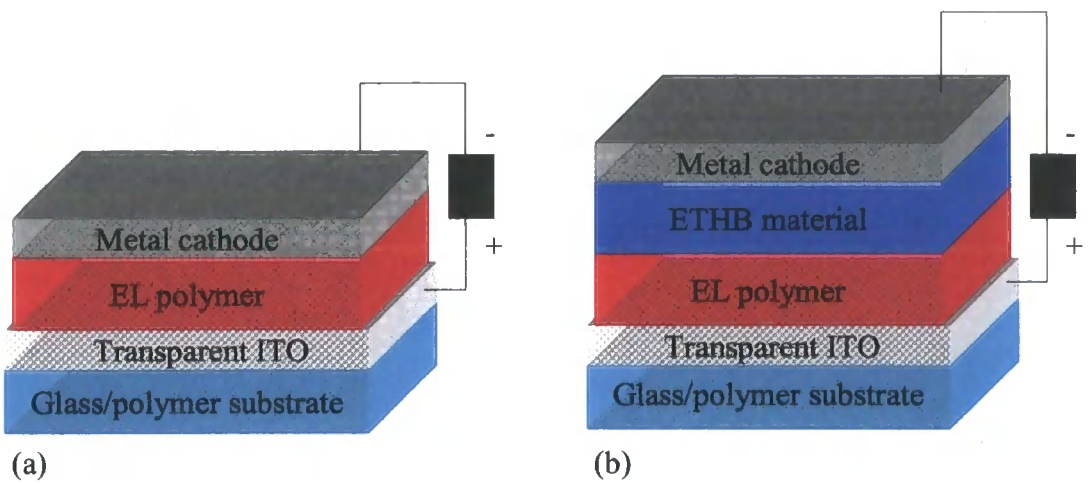

Figure 1: Schematic representation of (a) a single-layer and (b) a bilayer OLED.

A feature of the development of OLED technology is a lack of consistency between different laboratories in terms of techniques and parameters to assess device performances, with contradictory methods used for measuring quantum efficiency and device reliability. This means it is often not possible to arrive at a meaningful comparison of data on materials and fabricated devices from different publications. Forrest and co-workers have published an authorative discussion on these aspects and formal definitions of the various terms used to measure OLED efficiencies.[26]

1.3.1 Bilayer Devices Incorporating ETHB Materials

The most widely studied emissive polymers such as PPV, poly(fluorene) and their derivatives are predominantly hole transporting materials, therefore hole injection and transport predominates. Additionally, charge recombination may occur too close to the polymer/cathode interface, hence, the device efficiency is lowered due to the quenching of excitons by the metal electrode. To achieve efficient EL charge injection needs to be balanced.[27] One way to overcome these problems is the fabrication of bilayer OLEDs incorporating ETHB materials, first pioneered by Tang and VanSlyke.[4] This approach has retained the focus of international research. The ETHB material is deposited onto the emissive polymer film by spin coating or thermal evaporation before deposition of the cathode, which has a low work function matched as closely as possible to that of the LUMO of the ETHB material, to facilitate electron injection (Figure 2). The barrier to electron injection is reduced using ETHB materials; also the passage of holes is inhibited through the ETHB layer. Electrons and holes accumulate near the EL polymer/ETHB layer where recombination is confined in the EL polymer away from the cathode interface.[6] Applications of such layers in OLEDs reduce the threshold voltage whilst increasing quantum efficiency and device stability with respect to the analogous monolayer devices.

ETHB materials need to have a high electron affinity. The most widely applied ETHB materials are π-electron deficient heterocycles carrying imine nitrogen's in the aromatic ring. The polarisation of the $C^{\delta+}$-$N^{\delta-}$ bond due to the electron-withdrawing nitrogen atom lowers the energy of the HOMO and LUMO levels. This increases the electron affinity and promotes electron injection from the cathode.[25] Various π-electron deficient heterocyclic moieties have been incorporated into low molecular weight compounds and polymers for use as ETHB materials. These include 1,2,4-triazoles, 1,3,5-triazines, pyridines, pyrimidines, quinolines, quinoxalines, 1,3-oxazoles and 1,3,4-oxadiazoles.[28]

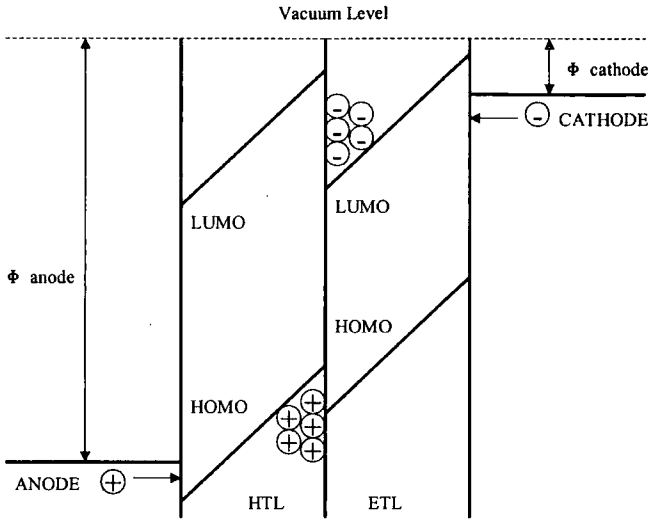

Figure 2a: Schematic energy level diagram of a generalised bilayer OLED, illustrating the accumulation of charge carriers at the interface of the hole-transporting and electron-transporting layers, HTL and ETL, respectively. (Redrawn from reference 25).

1.4 2,5-DIARYL-1,3,4-OXADIAZOLES

Most of the practical work described in this thesis concerns new 2,5-diaryl-1,3,4-oxadiazole (OXD) derivatives for OLED applications. It is appropriate, therefore, to review the important features of oxadiazoles which have paved the way for the present study. Molecular and polymeric OXDs have been widely studied due to their high thermal and chemical stability, high photoluminescent quantum yields and the electron deficient nature of the 1,3,4-oxadiazole heterocycle.[29] This class of compounds can be synthesised efficiently by a variety of methods using readily available and cheap precursors. A wide range of functionality can also be attached at the peripheral aryl groups prior to, or after, the synthesis of the ring system to give novel small molecules or polymeric compounds.

Prompted by the discovery that 2-phenyl-5-(4-biphenyl)-oxazole functioned as an efficient scintillation solute, Hayes *et al.*[30] synthesised a series of related OXDs in the 1950s. A selection of relevant derivatives is shown in Scheme 5, including PBD analogue **18**. Since then low molecular weight aromatic OXDs have been used as scintillators and laser dyes with high photoluminescent efficiencies.[31] The key breakthrough relevant to contemporary

applications of OXDs in material science came in 1989 when Adachi *et al.*[12] incorporated the OXD derivative PBD **5** as an electron transport material into a thin film bilayer EL device. This work re-ignited interest in OXD derivatives and has been pivotal to the growing field of OLED research throughout the 1990s, especially as electron transport materials for evaporated bilayer devices.

Polymers incorporating 1,3,4 oxadiazole moieties were first reported in 1961,[32] and since then a wide variety of poly(1,3,4-oxadiazole)s have been prepared: their use as advanced materials has been reviewed.[29a] Poly(1,3,4-oxadiazole)s exhibit excellent fibre and film forming capabilities, high thermal stabilities and tough mechanical properties. Consequently they have been used as heat resistant reinforcing fibers for advanced composite materials and high resistant fibers for the filtration of hot gases among other applications.[29a] Cyclic voltammetry (CV) studies of poly(arylene-1,3,4-oxadiazole)s with various arylene groups such as naphthalene, biphenyl and thienylene present in the main chain, show reversible n-doping characteristics. The mesomeric effects of the aromatic unit in the polymer backbone influence the electrochemical behaviour of these polymers.[33,34] Polymers with electron transport properties (n-type) had rarely been investigated, therefore, this property of poly(arylene-1,3,4-oxadiazole)s due to the electron affinity of the 1,3,4-oxadiazole heterocycle is of great importance.

The attractive combination of excellent thermal, mechanical and optoelectronic properties has lead to the use of poly(arylene-1,3,4-oxadiazole)s in OLEDs, with the oxadiazole group in the main chain or as a pendant substituent. They serve as electron transport layers in monolayer and bilayer OLEDs with PPV as the emissive material, or as the emitting layer themselves. Polymeric derivatives have been developed alongside new low molecular weight OXD derivatives. Both families are components in many of the latest EL devices. Previous reviews[29a,b,35] have covered developments up to 1998; the present review will focus on advances in new materials and their applications since then.

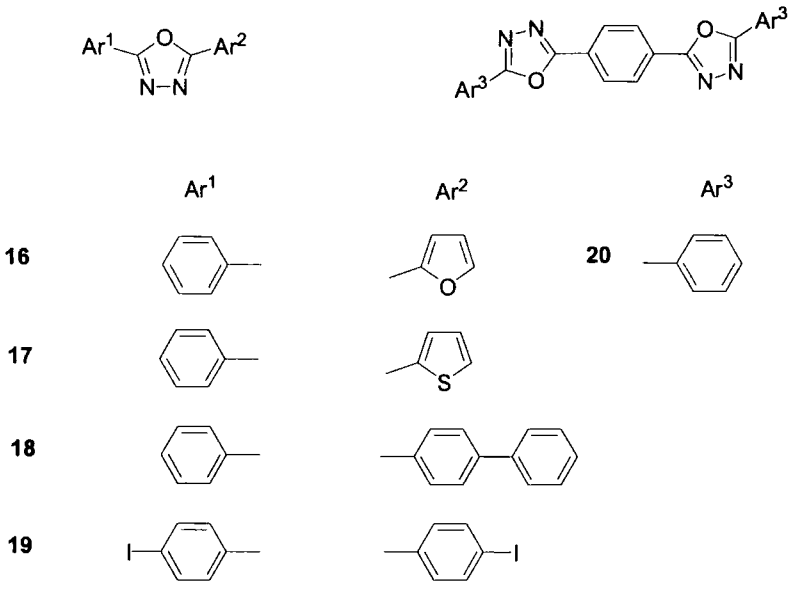

Scheme 5: Molecular structures of selected 2,5-diaryl-1,3,4-oxadiazole derivatives 16-20 synthesised by Hayes *et al.*[30]

1.4.1 Synthesis of 2,5-Diaryl-1,3,4-Oxadiazoles.

There are two main routes for the formation of OXDs each with specific advantages (Scheme 6). The first route involves nucleophilic reaction of aroyl hydrazide **21** with an acid chloride **22** to give the diaroyl hydrazine **23**. Dehydrative cyclisation using either $SOCl_2$ or $POCl_3$ yields the 2,5-diaryl-1,3,4-oxadiazole **25.**[30] The alternative route (the Huisgen route)[36] involves the preparation of an aromatic tetrazole[37] **24** via the reaction of sodium azide with the corresponding arylnitrile. The tetrazole is then reacted with the corresponding acid chloride **22** leading directly to system **25** via intramolecular ring transformation.

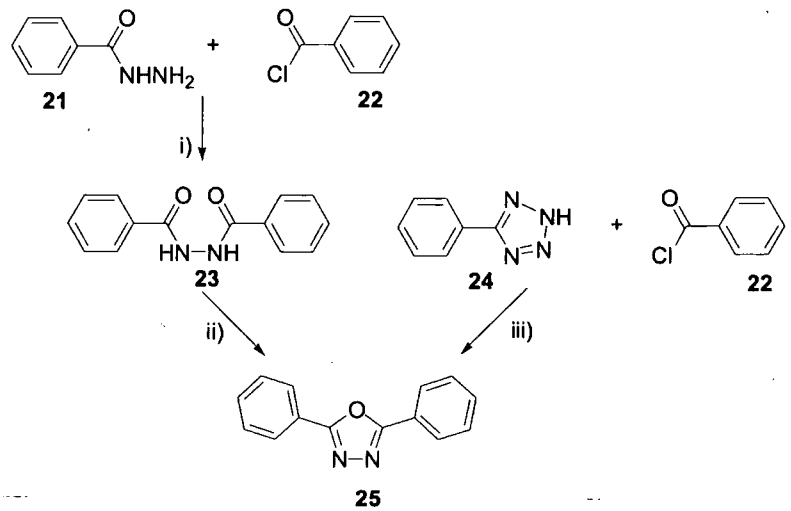

Scheme 6: Synthesis of OXD: i) Pyridine, 20 °C 0.5 h, Δ 0.5 h ; ii) $POCl_3$; iii) Pyridine Δ.

1.4.2 Low Molecular Weight Oxadiazoles as ETHB Materials

Increasing recent interest in electron transport molecular glasses has arisen from their application in OLEDs. The major prerequisites for electron transport molecular glasses are summarised in the following three points.[38]

1. Materials must give stable and uniform films. (Vacuum deposited or spin coated).
2. Materials must have large electron affinity and high electron mobility for efficient injection and transport of electrons.
3. Materials must possess large exciton energy for preventing the energy transfer of excitons produced in the emissive layer, to the electron transport layer in a bilayer device.

PBD **5** initially employed by Adachi and co-workers has been extensively studied as an ETHB material for evaporated bilayer devices.[39,12] It still plays a pivotal role in OLED research as it is available in high purity, sublimes and can be spin coated as a dispersion in a range of standard polymers. At higher temperatures crystallisation of PBD may occur and some incompatibilities with polymers exist that may lead to phase separation or crystallisation. This crystallisation can be retarded by suspending PBD in an insulating polymer such as poly(methyl methacrylate) (PMMA) as demonstrated by Brown *et al.* A mixture of PBD and PMMA was dissolved in $CHCl_3$ and spin coated onto a PPV layer in the fabrication of the bilayer OLED. Although the device thickness increased leading to an increase in voltage needed to drive the device, the internal EL efficiency increased from 0.1% (for an ITO/PPV/Ca device) to 0.8% for (ITO/PPV/PBD-PMMA/Ca).[40] Gong and co-workers[41] used poly(vinylcarbazole) (PVK) **27** with PBD as the host and tris[9,9-dihexyl-2-(phenyl-4'-(pyridin-2''-yl))fluorene]iridium(III) [$Ir(DPPF)_3$] **26** (Scheme 7) as the guest in an electrophosphorescent LED. As stated previously a maximum efficiency of EL from the excited states of organic materials will be limited to 25%, however there is evidence that for some polymers this ratio can be nearer 1 : 1.The energy of the non-emissive triplets can be harvested by energy-transfer to a phosphorescent dopant, *e.g.* transition metal complexes. The commonly used concept is to blend a low molecular weight phosphorescent dye into a polymer matrix into which holes and electrons are injected. It is important that triplet excitons should not be transferred from the triplet emitter to the host, which means that the triplet energy of the host should be higher than that of the emitter. The use of PPV **12** or poly(fluorene) derivatives (which have low triplet energies) is, therefore, limited to red or yellow triplet emitters. For higher energy triplet emitters (*i.e.*, blue or green emitters) PVK **27**

is often used. However, PVK transports holes only, so an ET material needs to be added to get balanced electron and hole currents and thereby to enhance device performance. Therefore, PBD was mixed with PVK to enable the host blend to transport both holes and electrons.[42] Electrophosphorescent emission was evident at λ_{max} 550 nm which is characteristic of $Ir(DPPF)_3$, with no emission observed from either PVK or PBD, and an EQE of 8% photons per electrons.

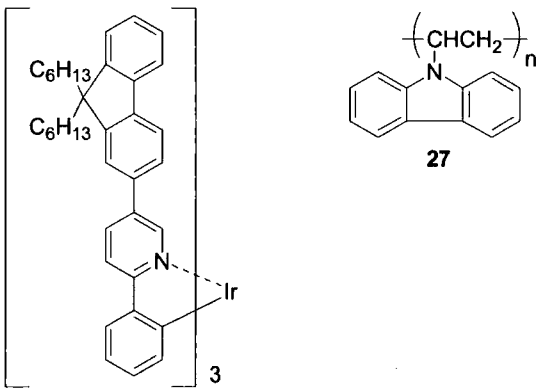

26 **27**

Scheme 7: Molecular structures of $Ir(DPPF)_3$ 26 and PVK 27.[41]

The oxadiazole dimer dye 1,3-bis(2-(4-*tert*-butylphenyl)-1,3,4-oxadiazol-5-yl)benzene (OXD-7) **28c** was synthesised based on PBD **5** along with other dimer analogs by Tsutsui and co-workers[38] in an effort to improve stability of vacuum deposited thin films without adversely affecting the electronic and optical properties. OXD-7 **28c** displayed electronic properties very similar to that of PBD, whilst vacuum deposited films of **28c** gave homogeneous glassy films with higher glass transition temperatures than PBD. Also, no degradation due to spontaneous crystallisation of the films was observed after 30 days storage.

Further work established that employing **28c** as an ETHB material in OLEDs with several different emissive layers gave significant improvements in performance over devices without the additional OXD-7 layer.[43]

Wang, working within our group, synthesised and studied ETHB properties of novel bis-1,3,4-oxadiazole-pyridine hybrids and the vinylene and phenylene analogues, including OXD-7 **28c** (Scheme 8).[44]

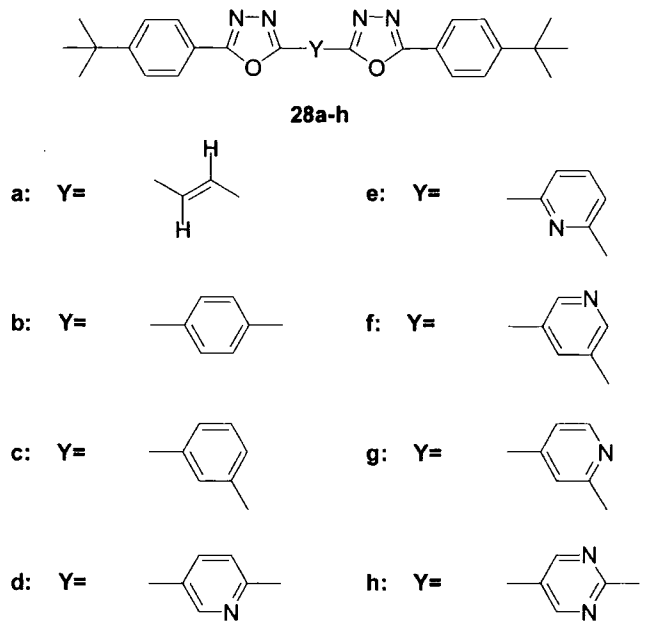

Scheme 8: Series of bis(1,3,4-oxadiazole) hybrids 28a-h studied by Wang[29d,44]

Previous studies[24,45] have shown that the introduction of a pyridine unit into the main chain of conjugated *p*-phenylene and 9,9-dialkylfluorene type polymers improves the electron transport properties of these materials which are predominantly known as hole transporting materials. As a consequence of this, pyridine and 1,3,4-oxadiazole moieties were covalently linked to explore the effect of combining two electron deficient heterocycles. Initial studies of the ETHB properties of the pyridine-1,3,4-oxadiazole hybrid PDPyDP **28d** involved a comparison of bilayer devices, based on MEH-PPV as the emitter, incorporating **28d** with the *p*-phenylene and *trans*-vinylene analogues PDPDP **28b** and PDVDP **28a**, respectively, with a device configuration of ITO/MEH-PPV/Al for the single layer and ITO/MEH-PPV/**28a,b or d**/Al for the bilayer devices. The ETHB materials were thermally evaporated on top of the MEH-PPV layer.

For the three bilayer devices incorporating ETHB materials the current versus electric field data (Figure 3a) are almost identical (suggesting similar electron transport properties). Figure 3b shows light output versus electric field curves for the four OLEDs. The turn on voltage for EL is lowered compared to that of the single layer device, the lowest being observed for the device incorporating **28d**.

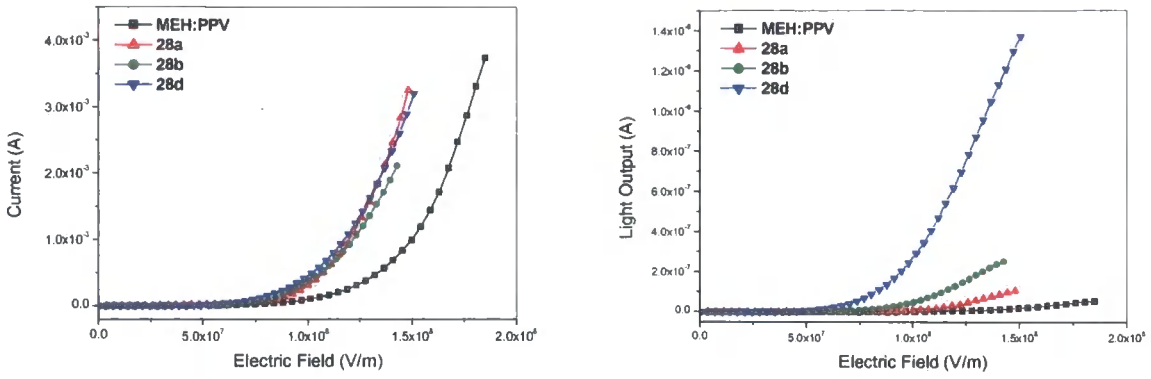

(a) (b)

Figure 3: Current versus electric field (a) and light output versus electric field (b) for both single and bilayer devices incorporating 1,3,4-oxadiazole hybrids 28a,b and d.[44]

Figure 4 shows light output versus current density curves for the four OLEDs, with approximate linear behaviour for all the devices being observed. EQEs at a current density of 50 mA cm^{-2} were recorded as 5.9 x 10^{-3}% for the single layer device. For the bilayer devices incorporating **28a**, **28b** and **28d** EQE's of 1.1 x 10^{-2}%, 4.2 x 10^{-2}% and 0.24%, respectively, were recorded. The EQE of the single layer device was, therefore, increased by a factor of 30 by incorporating an additional layer of **28d**.

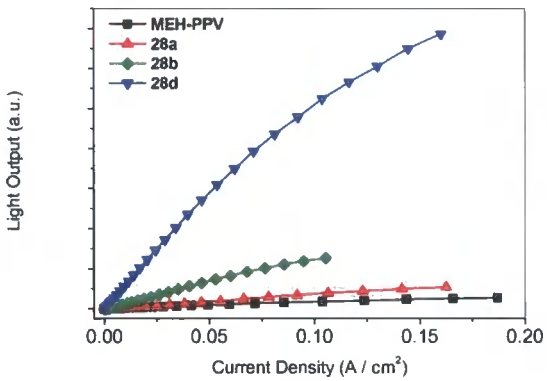

Figure 4: Light output versus current density for the single layer and bilayer devices incorporating 1,3,4-oxadiazole hybrids 28a,b and d.[44]

The EL emission from the three bilayer devices was characteristic of MEH-PPV and independent of the structure of the ETL indicating that the EL originated exclusively from the MEH-PPV material. The increased electron transport ability of PDPyDP **28d** over the two analogues **28a** and **28b** was attributed to two possible effects; the introduction of the electronegative pyridine moiety and the molecular crystal packing in the solid state. Firstly

the electron deficient pyridine ring decreases the LUMO level of the PDPyDP molecule more than that of a C=C or a benzene ring, therefore the energy barrier to electron injection into the MEH-PPV layer is reduced. The other possibility is that the electron mobility is higher in crystalline PDPyDP than in the other two materials due to molecular packing favouring the overlap of molecular orbitals in the solid state compared to that of **28a.**

Further studies[46] compared compounds **28e-g** *i.e.* the novel angular 2,6-, 3,5- and 2,4-isomers, respectively, of **28d** alongside the pyrimidine compound **28h**, which would be expected to increase electronegativity. Bilayer devices were fabricated using ITO as the anode, rubrene doped (20% by weight) MEH-PPV as the emissive material, electron transport material **28b-h**, and Al as the cathode in the configuration ITO/[MEH(Rubrene)] /**28b-h** /Al and compared with the reference single layer LED configuration of ITO/[MEH(Rubrene)]/Al. Increased EQEs were observed for all bilayer devices with respect to the reference LED which had an EQE of 0.007%, due to the ETHB material increasing electron transport. For the devices incorporating compounds **28d** and the angular isomer **28e**, the highest EQEs of 0.14% were achieved for both devices. The device incorporating the pyrimidine analogue **28h** had an EQE of 0.12% comparable to that using the linear phenylene system **28b,** with an EQE of 0.11%. It was concluded that the compounds **28e** and **28h** have comparable EQEs to the efficient material PDPyDP **28d**, which is more efficient than the widely studied OXD-7 **28c**, for which an EQE of 0.06% was recorded.

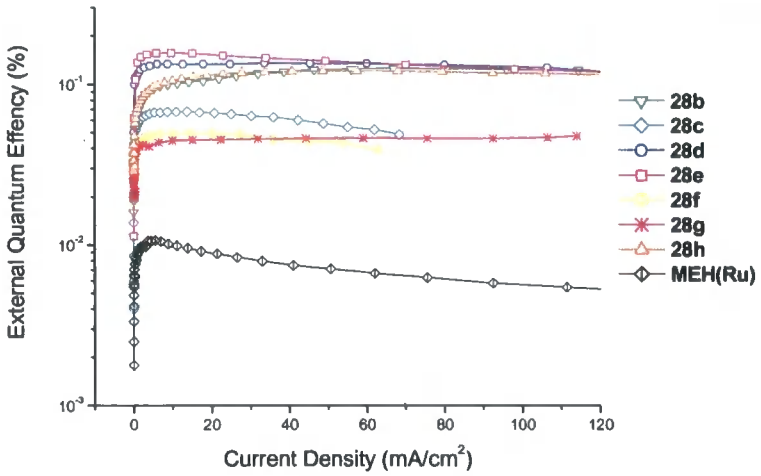

Figure 5: External quantum efficiencies versus current density relationships for the single layer and bilayer devices incorporating 1,3,4-oxadiazole hybrids 28b-h.[29d]

Further increases in EQE for this series of compounds have been observed by optimising the film thickness of both the MEH(Rubrene) and ETHB material. A maximum EQE of 0.7% was achieved for a device in the configuration ITO/[MEH(Rubrene)] (90 nm)/**28d** (55 nm)/Al.
The EL spectra of all the bilayer devices have essentially identical profiles with a peak at λ_{max} = 590 nm and a shoulder at *ca.* 630 nm, coincident with the EL emission of a single layer MEH-PPV device, indicating that charge recombination and subsequent light emission occurred exclusively within the MEH(Rubrene) layer.

1.4.2.1 Fluorene-OXD Hybrids

Antoniadis *et al.*[47] investigated the ETHB and EL properties of fluorene-oxadiazole hybrids **29**, **30a-c** and **31a-b** in multilayer vapour-deposited OLEDs combining the very efficient PL properties of fluorene with the good electron transport properties of 1,3,4-oxadiazole. These hybrids served as model compounds for blue emitting bipolar polymeric analogues as they comprise electron donating dimethylamine/diphenylamine and electron accepting oxadiazole moieties. LEDs were fabricated using an ITO anode onto which the starburst triphenylamine **32** was vapour deposited as a hole injecting buffer layer followed by a 2nd hole transport layer of TPD **6**. A layer of **29**, **30a-c** or **31a-b** was deposited as the electron transport and emissive layer, followed by a further electron transport layer of Alq_3 **3** to enhance adhesion to the Mg cathode.

The EL emission spectra of the device incorporating compound **29** showed a weak blue emission centred at 400 nm attributed to the intrinsic emission of **29**, with the majority of the emission shifted to longer wavelengths due to strong exciplex formation. For this device a maximum photometric efficiency of 0.6 cd A^{-1} was recorded, approximately 5 times smaller than the efficiency recorded for a TPD **6**/Alq_3 **3** device. Exciplex formation was suppressed using the bipolar compounds **30a-c** and **31a-b** with amine groups introduced to reduce the ionisation potential of the hybrid. Devices incorporating the dimethylamine-oxadiazole-fluorene hybrids **30a-b** showed photometric efficiencies up to 8.7 and 6.8 cd A^{-1}, respectively; they also displayed the lowest operating voltages in the series. The OLED comprising **30a** had a cyan (blue-green) colour with an emission centred at 495 nm. Luminances of 200-300 cd m^{-2} were achieved at as low as 6 V with corresponding photometric power efficiencies of 4.5 lm W^{-1} and 3.2 lm W^{-1} for devices incorporating **30a** and **30b**, respectively.

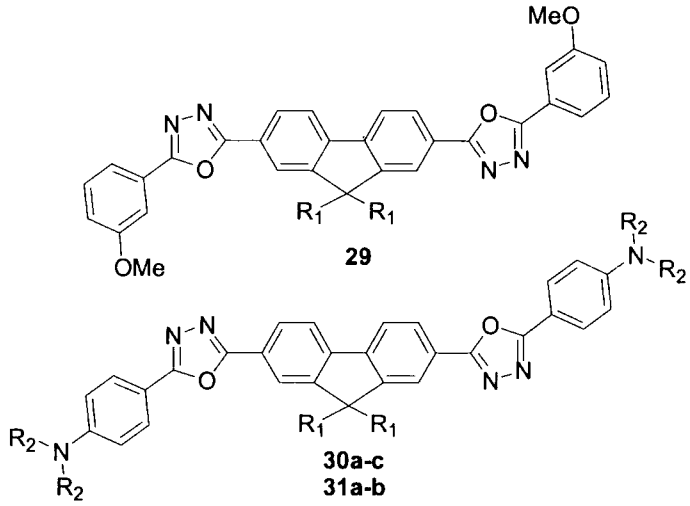

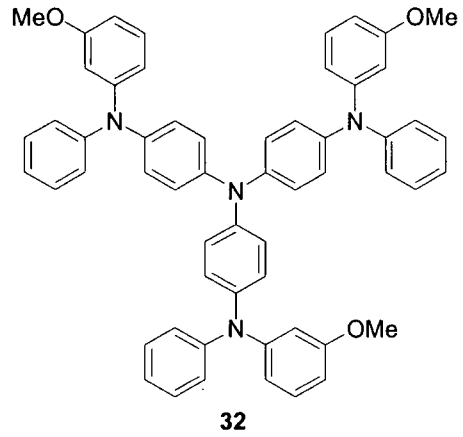

Compound	R_1	R_2
29	2-ethylhexyl	N/A
30a	2-ethylhexyl	methyl
30b	octyl	methyl
30c	4-methoxyphenyl	methyl
31a	octyl	phenyl
31b	4-methoxyphenyl	phenyl

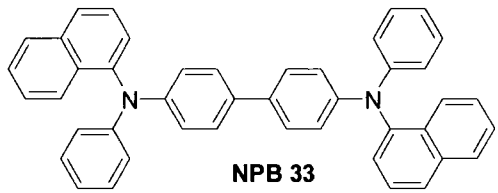

Scheme 9: Molecular structures of oxadiazole-fluorene hybrids 29, 30a-c and 31a-b along with hole transport materials 32 and 33 used in multilayer OLED studies by Antoniadis *et al.*[47]

Within the series of compounds **30a-c** and **31a-b** substituents R_1 were altered in an attempt to inhibit possible stacking and excimer formation of the fluorene molecule, and bulky diphenylamino groups were introduced at the R_2 position of **31a-b** to increase glass transition and melting temperatures (T_g) and (T_m), respectively. Difficulty arose in evaporation for compounds **31a-b** incorporating diphenylamino groups with temperatures as high as 350-390 °C needed for reasonable deposition rates. The devices incorporating **31a-b** also suffered from higher operating voltages (compared to **30a-b**), low efficiencies and lifetimes shorter than 100 s, attributed to possible destruction of their chemical structures during the heating process.

In an attempt to increase lifetimes, a series of devices incorporating **30a** was fabricated using the hole transport material NPB **33** instead of TPD **6** and copper phthalocyanine (CuPc) instead of the starburst triphenylamine **31,** due to the long lifetime characteristics and good thermal stability of these two hole transporting materials. In all cases the device lifetimes were not improved. The lifetime of two devices in the configuration ITO/CuPc/NPB/**30a**(x Å)/Alq_3(y Å)/Mg having different thickness ratios for **30a** and Alq_3 were also compared. Device A with a thin layer of **30a** (x = 30) and thick Alq_3 layer (y = 600) had a longer lifetime than device B, where (x = 500) and (y =100). For device A the emission

characteristics were dominated by the emission of Alq_3. In this device, the majority of the excitons are formed in the Alq_3 region, and only a small portion of the excitons are confined in the **30a** layer. Due to this the overall efficiency of device A (3.2 cd A^{-1}) is lower than that of device B (8.7 cd A^{-1}). The lifetimes of both devices were significantly improved but were still much shorter than expected for devices where **30a** is not included.[48] The possibility of instability of the 1,3,4-oxadiazole molecules when in the excited state as well as the likelihood of non-reversible reduction or oxidation processes may account for the poor performance of these materials in EL devices.

Tang *et al.*[49] used compound **30b** as an EL layer in a blue emitting OLED where a thin Al_2O_3 layer was inserted between the EL/Al cathode interface enhancing current injection, device efficiency and reduced driving voltage. These effects from the insertion of this layer were believed to result from the eliminated interaction between the EL layer and the Al cathode suspected of non-radiative singlet exciton quenching.

Wang,[50] working within our group, synthesised the related compound DFD **34**, which was used as an electron transport material blended over a range of compositions with the EL polymer MEH-PPV in a single-layer device. This configuration has the advantage of easy manufacture in terms of a single spin coating process. Light output from the blended OLEDs increased as the percentage of **34** in the blended layer increased from 20-70% by weight but decreased at higher percentage compositions. At an operating voltage of 25 V the EL of a 70% DFD device structure was 8 times that of a pure MEH-PPV layer reference device at the same voltage.

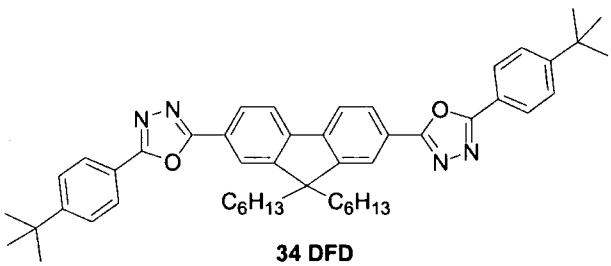

34 DFD

Scheme 10: Molecular structure of 34 DFD prepared by Wang.[50]

The brightness of this 70% blend device was 280 cd m^{-2} at a current density of 66 mA cm^{-2}. The increased light is indicative of efficient electron injection attributed to DFD. As concentrations of DFD increased from 20 to 40 to 70 and up to 95% the EQE increased accordingly with a maximum EQE of 0.1% for the 95% blend compared to that of the pure MEH-PPV reference device of 1 x 10^{-3}. The EL spectra of all of the blend devices were almost identical to that of the reference device with no emission evident from DFD, itself a

blue emitter, even at maximum concentrations of 95%. EL originated, therefore, exclusively from the MEH-PPV.

Preliminary optimisation of these devices included the incorporation of a hole transport layer poly(3,4-ethylenedioxythiophene) doped with polystyrene sulphonic acid [PEDOT:PSS] inserted between the anode and the blended film. The current and EL versus voltage behaviour of the OLEDs were similar to those without the PEDOT layer, however EQEs were all increased by a factor of approximately 3 independent of DFD concentrations. A maximum observed EQE of 0.3% was recorded for the optimised 95% DFD blend device.

Wu *et al.*[51] reported the synthesis and characterisation of efficient ET compounds **35a-c** where two identical ET OXD moieties were connected to a fluorene unit via the sp^3 C9 position to form a rigid 3-D structure. Increased glass transition temperatures relative to PBD **5** were observed for these compounds and attributed to the non-planar 3-D structure arising from the incorporation of the fluorene moiety.[52] Additionally **35a-c** displayed good film forming properties. The PL spectra of **35a** was almost superimposable on that of a model compound **36,** indicating that the tetrahedral C9 atom of **35a** effectively breaks any conjugation between the two OXD moieties.

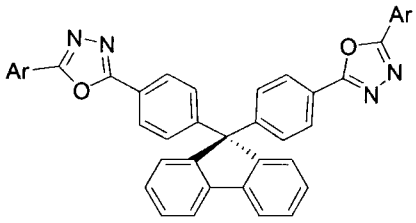

35a-c

a) Ar =

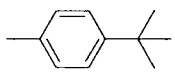

b) Ar =

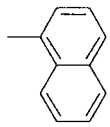

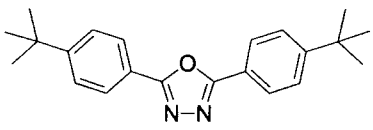

36

c) Ar =

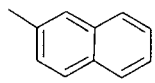

Scheme 11: Molecular structures of 35a-c and model compound 36.[51]

Bilayer devices incorporating **35a-c** as ETHB materials were fabricated in the configuration, ITO/NPB **33**/**35a-c**/Mg:Ag. Devices incorporating **35b** and **c** gave higher current densities than the device incorporating **35a**, with current densities of 500 mA cm^{-2} at a driving voltage of 10 V. EL spectra of all three devices had λ_{max} = 448 nm, identical to that observed from the PL of NPB **33**. This result indicates that holes are blocked by the ETHB materials because of the large energy barrier between the HOMO level of NPB **33** and those of **35a-c**. Also, the

small barrier between the LUMO of NPB **33** and those of **35a-c** results in the recombination zone being located within the NPB **33** layer.

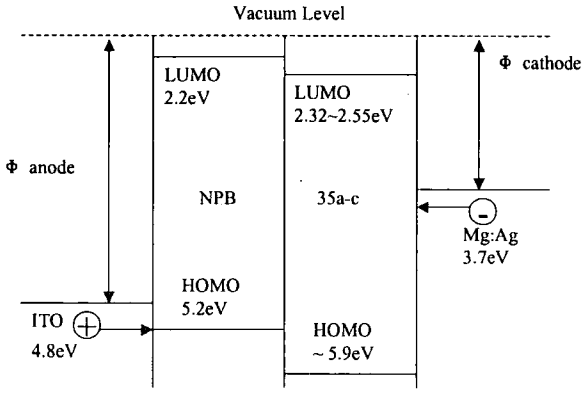

Figure 2b: Energy level diagram for compounds 35a-c.[51]

Unoptimised devices exhibited maximum brightness values between 450 and 1600 cd m^{-2}, and EQEs of 0.33, 0.20 and 0.25 for devices incorporating **35a-c**, respectively. Trilayer OLEDs were fabricated incorporating the blue dye PAP-NPA **37**[53] in the configuration ITO/NPB **33**/PAP-NPA **37**/**35a-c**/Mg:Ag. All three devices gave strong blue emission with λ_{max} = 454 nm resulting from the PAP-NPA. EQEs of the trilayer OLEDs incorporating **35a-c** and PAP-NPA **37** were recorded as 1.40, 1.54 and 1.75, respectively, with maximum brightnesses reaching *ca.* 5400-7000 cd m^{-2}.

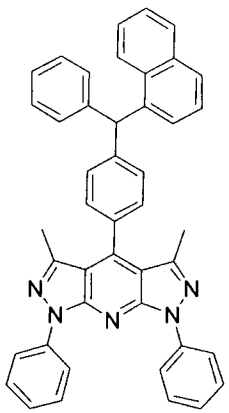

PAP-NPA 37

Scheme 12: Molecular structure of blue dye PAP-NPA 37.[53]

In an attempt to improve processability and morphological stability of 1,3,4-oxadiazole compounds, Salbeck and co-workers[54] synthesised **38**, a spiro linked molecule which essentially comprised two PBD **5** units orthogonal to each other.

It was shown by spin coating amorphous films of both PBD **5** and the spiro analogue **38** onto quartz substrates that recrystallisation of the amorphous PBD film, which occurred at

room temperature on standing for a period of 1 h, was eliminated for the film of **38** even at elevated temperatures. Recrystallisation of PBD **5** was detectable by the film becoming turbid and detection of a microcrystalline structure by scanning electron microscopy. The film of **38** remained amorphous and transparent throughout, with a smooth surface detected by electron tunnelling microscopy.

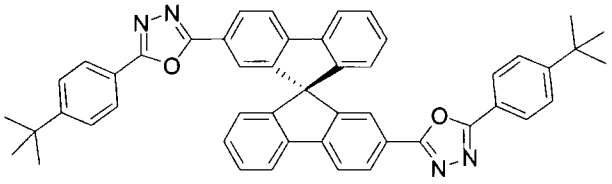

Spiro-PBD 38

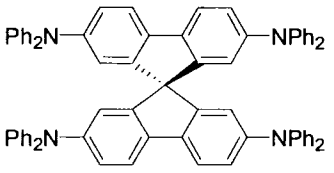

Spiro-TAD 39

Scheme 13: Molecular structures of spiro-PBD 38 and spiro-TAD 39 synthesised by Salbeck *et al.*[54]

The higher morphological stability of **38** was attributed to the steric demands of the spiro core. Also compound **38** has a higher stability than PBD with a melting point of 337 °C and a T_g of 163 °C compared to the melting point of PBD at 138 °C. The electronic properties of **38** are almost identical to the parent PBD compound although the emission maximum of compound **38** shows a 7 nm red shift compared to PBD attributed to the forced planarisation of the biphenyl units in the spirobifluorene core.

A blue light emitting bilayer OLED fabricated using a hole transporting aromatic amine (spiro-TAD) **39** and compound **38** in the configuration ITO/**39**/**38**/Al:Mg displayed a very low turn on voltage of 2.7 V, with a brightness of 500 cd m^{-2} measured at 5 V.[54]
Chien[55] reported the isomeric compound **40** with two 2-(4-*tert*-butylphenyl)-1,3,4-oxadiazole groups in the same plane attached to a spirobifluorene unit at the 2 and 7 positions. The bipolar analogue **41** was also reported, which incorporated two diphenylamine units orthogonal to the oxadiazole plane.

1.4.2.2 Bipolar OXD Materials

Bipolar compounds have received considerable attention in the context of advanced materials. In the context of this thesis the possibility of combining electron transport and hole transport moieties, as well as an emissive unit in some cases, in one molecule should allow easy fabrication of highly efficient single layer OLEDs. In the bipolar compound **41** the 1,3,4-oxadiazole conjugated oligoaryl system acts as the electron acceptor whilst the triarylamine moiety acts as the donor counterpart. Solvent polarity dependent fluorescence properties were observed for **41** due to the highly efficient photoinduced electron transfer reactions. OLED

work was not reported for **40** or **41**, although other groups have utilised bipolar compounds in OLEDs.

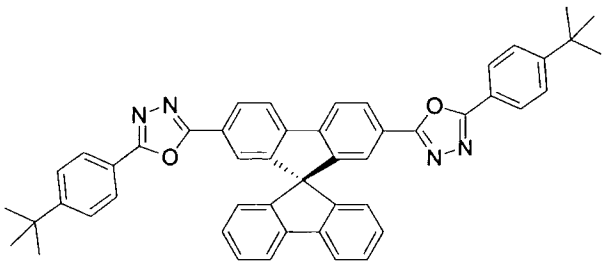

40

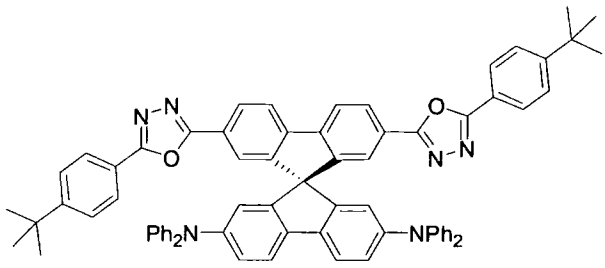

41

Scheme14: Molecular structure of compound 40 and the bipolar analogue 41.[55]

Hamada *et al.*[56] synthesised compound **42,** the bipolar analogue of OXD-7 **28c**, replacing the terminal *tert*-butyl groups of **28c** with electron donating dimethylamine groups and showed that this material was useful as a blue emitting layer (EML) instead of an ET layer due to the bipolar nature of the material, which offers good recombination sites for holes and electron charge carriers. Three different device configurations applying **42** as an EML were compared among which the double hetero (DH) structure, with the TPD **6** analogue **43** as the HTL, in the configuration of ITO/**43**/**42**/OXD-7 **28c** (ETL)/MgAg showed the best performance with a luminance of 1100 cd m^{-2} observed at a drive current density of 100 mA cm^{-2}. EL emission had λ_{max} = 475 nm corresponding well with the PL λ_{max} of the OXD dimer dye **42**.

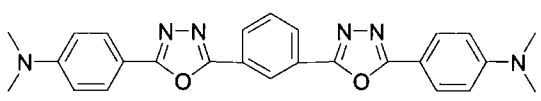

42

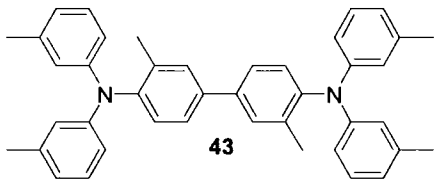

43

Scheme 15: Molecular structure of the bipolar compound 42 and HT material 43.[56]

Tamoto *et al.*[57] synthesised five new bipolar materials **44-48** for EML applications, replacing dimethylamine groups with triphenylamine units, which possess superior hole transport mobility.[58] It was postulated that higher charge carrier mobilities would reduce driving voltage and relieve exciplex formation, which usually takes place at the EML/transport layer interface. Compounds **44-48** have T_g values above 99 °C, with no clear crystallisation temperatures indicating that they form desirably stable amorphous films. Compound **48** showed a pronounced T_g of 166.5 °C possibly due to the starburst structure of the three triphenylamine units, also the hexafluoropropane linking unit of compound **44** is believed to enhance to the thermal stability.

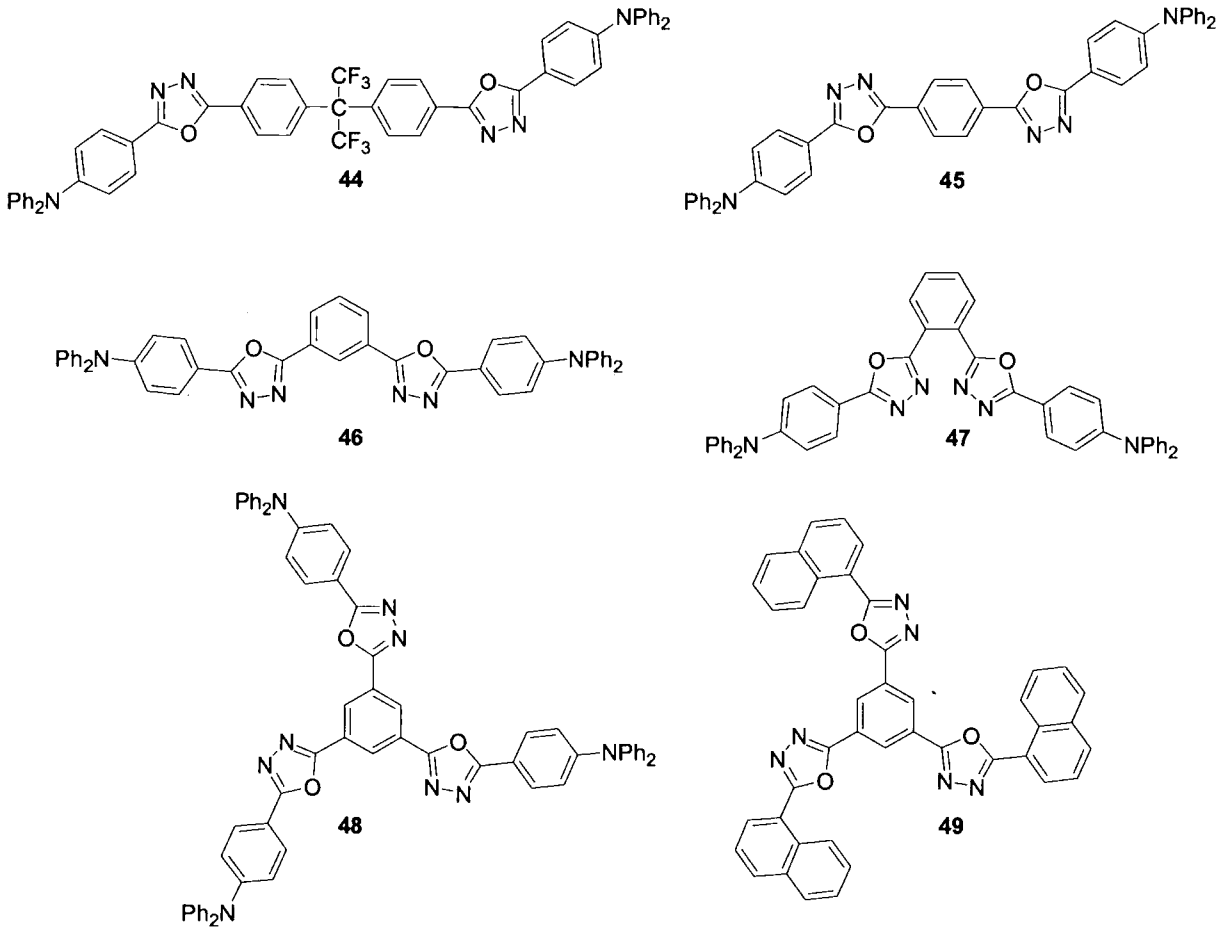

Scheme 16: Molecular structures of bipolar compounds 44-48 and ET material 49.[57]

For compounds **45-47** the bridging position of the disubstituted phenylene greatly influenced the thermal properties of the materials with the 1,4-disubstituted phenylene **45** displaying the highest thermal stability of all. Thin films of **44-48** all showed strong PL in the blue-green region with λ_{max} = 454, 489, 458, 469 and 487 nm, respectively. For compounds **44** and **46** the insulating nature of the hexafluoropropane unit, and the *m*-phenylene linkage, respectively, contributed to the blue emission. The *p*- and *o*- phenylene linkages of **45** and **47,** respectively, led to blue-green emission due to the extended conjugation. Comparison of **46** and **48** implied that trisubstitution slightly increased π conjugation.

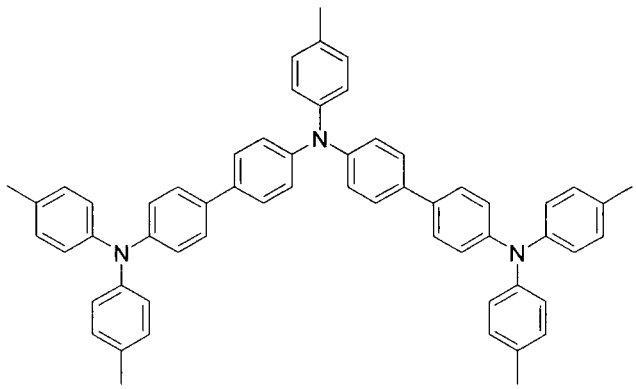

50

Scheme 17: Molecular structure of triphenylamine HT material 50.[57]

Multilayer devices were fabricated incorporating a triphenylamine based HT material **50**, EML **44-48**, compound **49** as an ETL and finally a further ETL of Alq_3 **3** in the configuration ITO/**50**/EML **42-46**/**49**/Alq_3/Mg:Ag. Each device showed good EL performances over a wide range of current densities. For the device incorporating compound **46** a maximum luminance of 6800 cd m^{-2} was recorded at a current density of 700 mA cm^{-2}. In contrast, the EL device incorporating compound **44** showed inferior characteristics.

Following this pioneering work, Justin Thomas *et al.*[59] synthesised multiply substituted carbazole derivatives **51-57** to combine the hole transporting carbazole unit with the OXD unit to provide balanced charge injection. All these materials were found to be amorphous with relatively high T_g's.

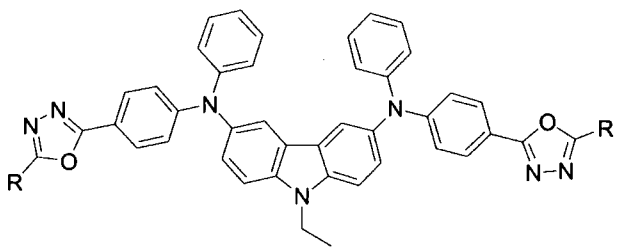

51 R = *p*-(*t*-butyl)phenyl
52 R = 9,9-di(*n*-butyl)-2-fluorenyl

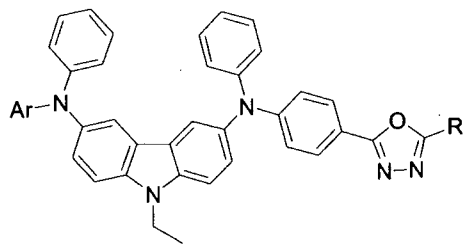

53 Ar = 1-naphthyl; R = 9,9-di(*n*-butyl)-2-fluorenyl
54 Ar = 1-pyrenyl; R = 9,9-di(*n*-butyl)-2-fluorenyl

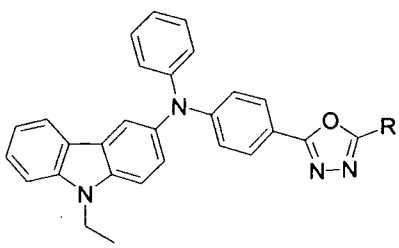

55 R = *p*-(*t*-butyl)phenyl
56 R = 9,9-di(*n*-butyl)-2-fluorenyl
57 R = 1-pyrenyl

Scheme 18: Molecular structure of carbazole-OXD compounds 51-57.[59]

Three device configurations incorporating compound **55** were compared to ascertain if this series of compounds were applicable as ET, HT or bifunctional materials. The device

incorporating **55** as a HT material, with the ET material TPBI **58,** in the configuration ITO/**55**/TPBI **58**/Mg:Ag was the only device to produce reasonable light output with bright blue-green EL, λ_{max} = 482 nm, very close to that observed for the film PL of **55** (λ_{max} = 490 nm), suggesting that these materials transport holes better than electrons. Therefore, devices incorporating **51-57** as hole transport materials were fabricated in the configuration ITO/**51-57**/TPBI **58**/Mg:Ag (Type 1), also, devices were fabricated incorporating Alq_3 **3** in the configuration ITO/**51-57**/Alq_3 **3**/Mg:Ag (Type 2). The type 2 device incorporating **55** displayed an emission maximum resembling that of Alq_3. Emission profiles of OXD derivatives can overlap with that of Alq_3 in general, therefore, determination of the contributions from each component is difficult. However, a larger fwhm (full-width at half-maximum) for EL from the Alq_3 devices means that mixing of profiles cannot be excluded.

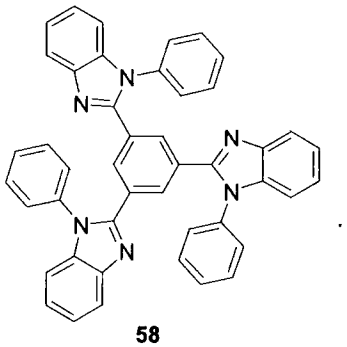

58

Scheme 19: Molecular structure of TPBI 58.[59]

Devices incorporating compounds **55** and **56** which contain only 1 OXD unit exhibited better performances compared to analogues with 2 OXD units (**51** and **52**). This suggests that interruption of the hole transport path by the hole blocking OXD moieties is more pronounced for the bis-OXD compounds.

The green emitting type 1 devices incorporating **55, 56** or **53** exhibited promising efficiencies with maximum EQEs of 5.2, 4.7 and 3.5%, respectively. Type 1 devices incorporating compounds **51, 53, 55** and **56** displayed superior brightnesses and efficiencies compared to type 2 devices incorporating these materials. Conversely, type 2 devices incorporating compounds **54** and **57** showed comparatively superior characteristics to the corresponding type 1 devices. This has been attributed to the differences of the LUMO positions between these two groups; for compounds **51, 53, 55** and **56** the LUMO resides above 2.2 eV, whilst compounds **54** and **57** possess LUMO levels lower than 2.2 eV; thus when the LUMO is lowered injection from the Alq_3 layer is enhanced, raising the device efficiency.

Justin Thomas *et al.*[60] synthesised compounds **59-63**, based on **55**, incorporating electron withdrawing groups such as CF_3 and C≡N. This series of carbazole-OXD analogues were incorporated into type 1 and 2 devices as HTLs with the electron transport materials TPBI and Alq_3, as before. EL spectra observed for the type 1 devices in general resembled the PL spectra of vapour deposited samples of the HTL materials, indicating that the excitons are effectively confined within the HTLs. However, a slight blue shift relative to the PL spectra was observed for devices incorporating the CF_3 analogues **59, 61** and **63**, which was possibly due to exciplex formation between the ETL and the HTL.

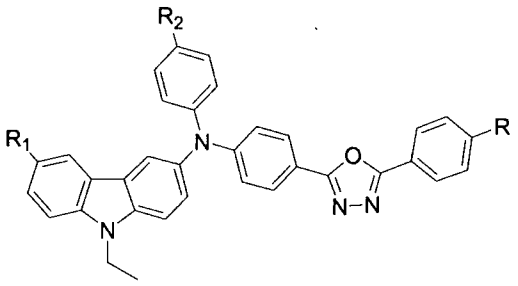

55, 59-63

	R	R_1	R_2
55	*t*-Bu	H	H
59	CF_3	H	H
60	*t*-Bu	H	Me
61	CF_3	H	Me
62	*t*-Bu	CN	H
63	CF_3	CN	H

Scheme 20: Molecular structure of carbazole-OXD compounds 55-and analogues 59-63.[60]

For type 1 devices the HOMO energy level difference (1.1-0.9 eV) between the HTL and ETL is significantly greater than the LUMO gap (0.5-0.3 eV), therefore holes can be effectively confined within the HTL. For type 2 devices HOMO (0.9-0.7 eV) and LUMO (1.1-0.9 eV) energy gaps between the HTL and ETL were very similar, consequently excitons can form within both the ETL and the HTL. In general, the CF_3 derivatives exhibited enhanced performances over the *t*-butyl derivatives. Compound **61** excelled in terms of maximum brightness (36,930 and 37,600 cd m^{-2}, for device types 1 and 2, respectively) and EQE (3.9 and 2.1 %; device types 1 and 2, respectively) possibly due to the ETHB properties imparted by the fluorine atoms.[61] Placement of the CF_3 on the OXD unit enhanced electron deficiency, whilst CN substitution on the carbazole nucleus decreased the donor strength of carbazole. This functional group positioning allows the fine-tuning of energy levels in these compounds.

Guan *et al.*[62] synthesised the thermally stable, highly efficient blue EL material CzOxa **64**. This bipolar material incorporating OXD and carbazole units was incorporated into bilayer and trilayer devices to investigate its EL properties using the HT material TPD **6** for the bilayer, and both TPD **6** and the ET material Alq_3 **3** for the trilayer device. The bilayer device ITO/TPD **6**/**64**/$Mg_{0.9}Ag_{0.1}$ exhibited onset voltages of 4 V with peak luminance efficiencies of 1.35 lm W^{-1} at a luminance of 524 cd m^{-2}. A maximum luminance of 9,200 cd m^{-2} at 15 V was observed for this device. In comparison, the device incorporating Alq_3

(ITO/TPD **6**/**64**/ $Alq_3/Mg_{0.9}Ag_{0.1}$) showed dramatic improvements in EL performance. The outstanding feature of this trilayer device is its blue colour purity (x = 0.14, y = 0.19) on a CIE (Commission International de l'Eclairage) 1931 chromaticity diagram, accompanied with a maximum luminance efficiency of 2.25 lm W^{-1} at a luminance of 2170 cd m^{-2} and a maximum luminance as high as 26200 cd m^{-2} at 15 V.

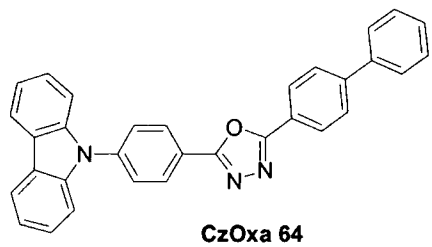

CzOxa 64

Scheme 21: Molecular structure of carbazole-OXD derivative CzOxa 64.[62]

EL spectra of the bilayer and trilayer devices are similar with λ_{max} = 470 nm and a shoulder at λ_{max} = 404 nm. No emission was evident from compound **64** (λ_{max} = 412 nm) and the shoulder was ascribed to TPD **6** (λ_{max} = 400 nm). The new peak at λ_{max} = 470 nm indicates that an exciplex is responsible for EL emission. To identify the emission origin from both devices the PL spectra of a molar equivalent mixture of TPD **6** and **64** spin coated onto a quartz substrate were obtained. Two emission bands were observed at λ_{max} = 400 and 470 nm. The disappearance of emission from **64** and the appearance of the new emission at λ_{max} = 470 nm implied that a new species is generated. The bipolar characteristics of **64** increase the number of holes and electrons injected into the layers, thereby favouring exciplex formation at the HTL/EML interface.

A series of novel carbazole dimers, trimers, fluorene and OXD hybrids was tested for their suitability for triplet emitters in OLEDs by Brunner *et al.*[63] Energies of the HOMO, singlet emission and triplet emission were recorded for a series of materials including compounds **65** and **66.** The combination of HT carbazole and ET OXD units for balancing charge transport was investigated in an attempt to establish a design rule for compounds with high triplet energies and suitable HOMO and LUMO levels for charge injection by commonly used injection layers. No OLED device data are currently available on compounds **65** and **66.**

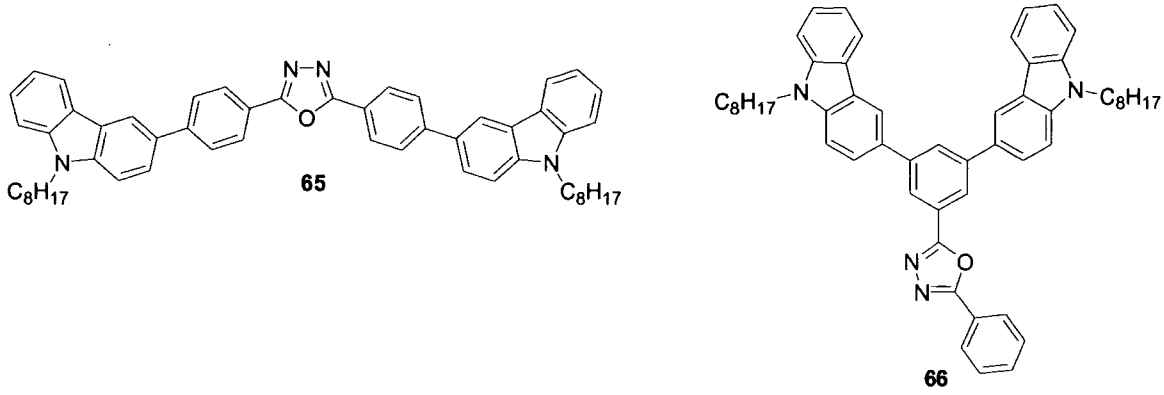

Scheme 22: Molecular structures of carbazole-OXD derivatives 65 and 66.

1.4.2.3 OXD Materials as Emitters in OLEDs

The fluorescent 1,8-naphthalimide-OXD hybrid molecule **67** was studied by Jiang and coworkers.[64] The oxadiazole moiety facilitates the injection of electrons from the cathode and the 1,8-naphthalimide moiety acts as an emitting centre. Two possible mechanisms for EL were proposed: the first involves intramolecular electron transfer from the π^*orbital of the oxadiazole moiety to the π^*orbital of the 1,8-naphthalimide moiety where recombination of the electrons and holes form excitons which then undergo radiative decay. The second involves intramolecular energy transfer. It was proposed that recombination occurs in the oxadiazole moiety, the energy of the excited oxadiazole is then transferred to the 1,8-naphthalimide moiety leading to EL characteristics only of the 1,8-naphthalimide moiety. Devices incorporating compound **67** displayed green-yellow EL at λ_{max} 532 nm, which reached a luminance of 225 cd m^{-2} at a voltage of 27 V. The maximum luminous efficiency of 0.43 lm W^{-1} at 19 V was achieved.

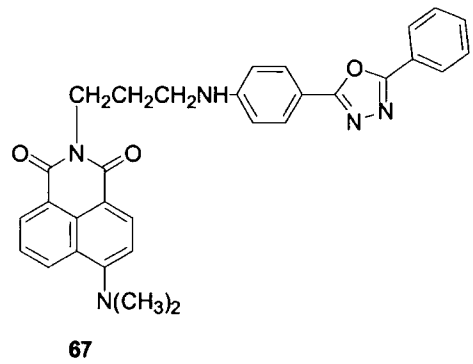

Scheme 23: Molecular structure of 1,8-naphthalimide-OXD hybrid 67.[64]

Liang *et al.* synthesised the blue light emitting ET complex 2-(5-phenyl-1,3,4-oxadiazolyl)phenolatolithium LiOXD **68**. OLEDs were fabricated incorporating TPD **6** as a

HT layer and **68** as the EML in the configuration ITO/TPD **6**/**68**/Al. A single layer device without TPD was shown to exhibit a low maximum luminance as well as a high turn on voltage. The bilayer device displayed blue emission at λ_{max} = 468 nm with a maximum luminance of 2900 cd m^{-2}. A maximum current efficiency of 3.9 cd A^{-1} and a luminance efficiency of 1.1 lm W^{-1} was obtained. A relatively high EQE value of 2.4 was recorded for this device. This impressive EL efficiency was attributed to i) the OXD segment in **68** has excellent ET ability and ii) the lithium salt is favourable for electron injection.

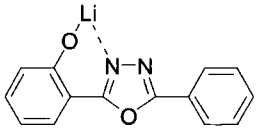

68

Scheme 24: Hydroxyphenyloxadiazole lithium complex 68.[65]

The efficiency of a device in the configuration ITO/NPB **33**/Alq_3/Al was significantly increased when a thin layer of complex **68** was inserted between the Alq_3 and aluminium electrode to act as an interface material. The performance of **68** as an interface material was directly related to the thickness of the complex. The optimum device specifications were as follows: ITO/NPB **33**(40 nm)/Alq_3 **3**(60 nm)/**68**(2 nm)/Al, which gave a maximum luminance of 18389 cd m^{-2} at a turn on voltage of 3.0 V. Furthermore, the device exhibited high current and power efficiencies of 5.21 cd m^{-2} and 2.4 lm W^{-1}, respectively.

1.4.2.4 EL OXD Complexes

Luminescent lanthanide complexes are good candidates for pure colour emission OLEDs, however the key problem is the very low efficiencies when incorporated into LEDs due to poor charge–carrier transporting ability. Liang *et al.*[65] synthesised a europium(III) complex **69** incorporating an oxadiazolyl moiety to improve the electron transport properties. The OXD moiety was attached through a flexible spacer to a 2-(2-pyridyl)-benzimidazole (PyBM) ligand, attached to the europium core, to improve the resulting solubility of the complex.

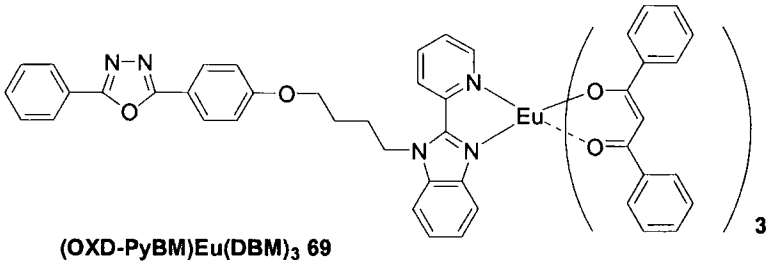

(OXD-PyBM)Eu(DBM)$_3$ **69**

Scheme 25: Molecular structure of the complex (OXD-PyBM)Eu(DBM)$_3$ 69.[65]

The oxadiazole moiety and the europium ion are expected to retain their own ET and EL properties, respectively, therefore, the complex was expected to exhibit the combined properties of efficient ET and highly efficient red EL. A bilayer device incorporating the complex **69** and the HT material TPD **6** in the configuration ITO/TPD **6**/**69**/LiF/Al emitted red light (λ_{max} = 612 nm) at driving voltages of 7.8 V, characteristic of the Eu^{3+} ion in the complex. For the bilayer device a maximum brightness of 322 cd m^{-2} at a driving voltage of 21 V and an EQE of 1.7% was achieved. A control device utilising (*N*-alkyl-substituted PyBM)Eu(DBM)$_3$ as an emitter exhibited poor performance, suggesting that the ET ability of **69** is significantly improved by the introduction of the OXD. Device fabrication is also simplified by the introduction of the OXD moiety in the complex.

Gong *et al.*[66] synthesised two novel, trifunctional, light emitting molecules based on rhenium(I) (Re^{I}) **70** and ruthenium(II) (Ru^{II}) **71** bipyridine complexes, where the ET OXD, HT triphenylamine and light emitting functional groups are incorporated into one molecule.

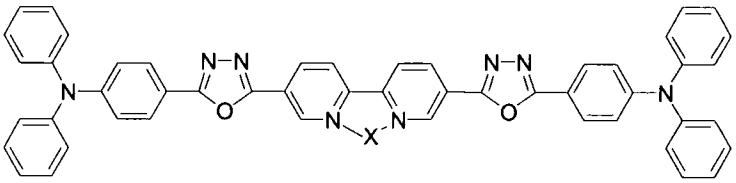

70: X = Re(CO)$_3$Cl

71: X = Ru(2,2'-bipyridine)$_2$ 2PF$_6^-$

Scheme 26: Re^{I} 70 and Ru^{II} 71 bipyridine complexes.

The complexes **70** and **71** were doped in different polymer hosts, polycarbonate (PC) and poly(vinyl alcohol) (PVOH), respectively, at a concentration of 40%-wt (**70** is a neutral compound, however **71** is an ionic metal complex). Two single layer devices in the configuration ITO/**70**:PC or **71**:PVOH/Al displayed low turn on voltages with estimated EQEs of ~0.1%. The metal complex/polymer systems exhibited EL spectra that were very similar to their corresponding PL spectra.

1.4.2.5 Highly Branched and Dendritic/Starburst OXD Materials

The amorphous films of low molecular weight OXDs can suffer from a lack of stability if crystallisation occurs during device fabrication, upon storage or with increased device operation temperature. Bulky substituents and non-planar dendritic/starburst molecular architectures are often adopted to enhance the solubility of the molecules by preventing the molecular stacking.[67] This reduction of intermolecular interactions in films of highly branched, dendritic/starburst compounds favour the formation of stable amorphous glassy materials and hence often increases device efficiency.

The zeroth-generation dendrimer and widely studied ET material 1,3,5-tris(4-*tert*-butylphenyl-1,3,4-oxadiazolyl)benzene (TPOB) **72a** was first described by Naito and Miura.[68] Bettenhausen and Strohriegl[69,70] later described the synthesis of starburst OXDs with benzene cores **72a-j** including TPOB **72a**, and triphenylbenzene, triethynylbenzene and triphenylamine cores **73-75**, respectively. Most of the starburst OXD compounds shown in Scheme **27** and **28** form amorphous glasses with high T_g's when cooled from the melt. However, they mostly crystallise on heating above their T_g. For compounds **72b-e** with small methyl, ethyl, or trifluoromethyl substituents no T_g's were observed; conversely, for compounds **72a,** and **72f-h** incorporating bulkier *tert*-butyl, ethoxy, *iso*-propyl and diethylamino groups, respectively, T_g's were observed ranging from 97 °C up to 142 °C for **72a.**

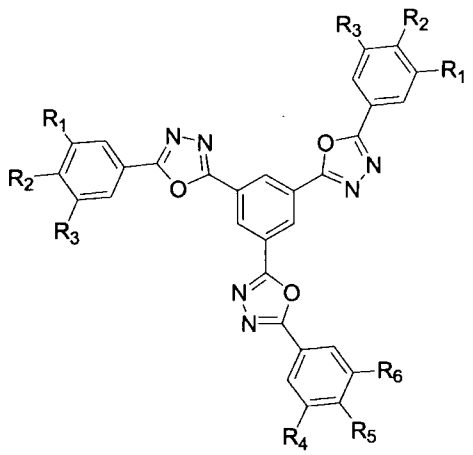

72	R_1	R_2	R_3	R_4	R_5	R_6
a	H	^{t}Bu	H	H	^{t}Bu	H
b	H	CH_3	H	H	CH_3	H
c	H	CH_3	CH_3	H	CH_3	CH_3
d	CF_3	H	CF_3	CF_3	H	CF_3
e	H	C_2H_5	H	H	C_2H_5	H
f	H	OC_2H_5	H	H	OC_2H_5	H
g	H	$CH(CH_3)_2$	H	H	$CH(CH_3)_2$	H
h	H	$N(C_2H_5)_2$	H	H	$N(C_2H_5)_2$	H
i	H	^{t}Bu	H	CF_3	H	CF_3
j	CF_3	H	CF_3	H	^{t}Bu	H

Scheme 27: Molecular structures of starburst OXD compound 72a TPOB and analogues 72b-j.[69]

In contrast to the symmetrically substituted OXD **72d** with six trifluoromethyl substituents, the two asymmetrically substituted OXDs **72i-j** form stable amorphous films with T_g's at 128 and 122 °C. Compounds **73** behaved similarly to **72a** with the most stable glasses formed by

75. Upon both heating and cooling, compound **75** displayed a T_g at 137 °C with neither crystallisation nor melting up to 350 °C. The morphological stability of **75** was attributed to its non-planar structure, whereby the three core phenyl rings are twisted out of the plane with respect to each other.[71] Compound **74** did not show reproducible DSC scans, which was attributed to thermal crosslinking of the triple bonds.[72]

Devices incorporating **72a** as an ETL in the configuration ITO/PPV/**72a**/Ag were comparable with devices incorporating PBD **5**, with EQEs of 0.1% and a brightness of several hundred cd m^{-2}.[73] Tokito *et al.*[74] also independently reported device studies on compound **72a.**

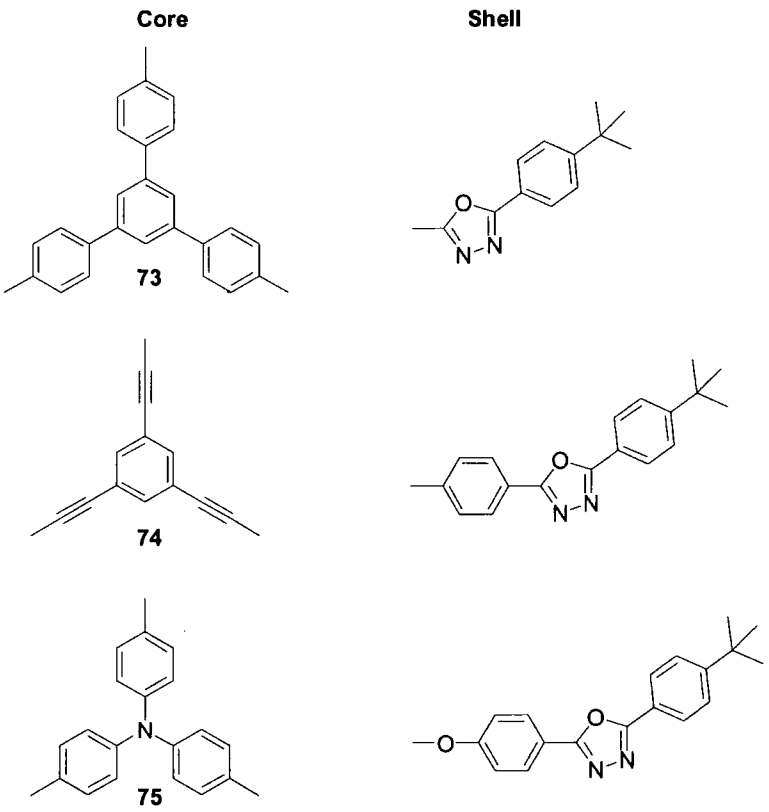

Scheme 28: Molecular structures of starburst OXD compound 73-75.[69]

Ogawa and co-workers[75] incorporated TPOB **72a** into bilayer devices of the configuration ITO/HTM/**72a**/MgAg with a series of amorphous triphenylamine HTMs to investigate exciplex formation at the interface between ET and HTLs, as a way of tuning the emission colour. EL Spectra for the series of devices did not correspond to the PL spectra of TPOB **72a** and displayed only weak emission bands corresponding to the HTMs. The strong peaks at λ_{max} =500-580 nm, were assigned to exciplex formation at the interface between the two transport layers. PL spectra of spin-coated films of equimolar mixtures of TPOB **72a** and each of the HTMs were in good agreement with the EL spectra of the devices, supporting the

exciplex formation theory. The emission colour of the devices resulting from exciplex formation was dependent on the ionisation potential of the HTMs. A plot of the energy of the EL spectral peaks for the devices versus the ionisation potential of the HTM gave a linear relationship. The emission colour of the OLEDs was tuned from greenish-blue to orange depending on the ionisation potential of the HT material used: a lower ionisation potential led to red-shifted emission.

Noda *et al.*[76] applied compound TPOB **72a** and Alq_3 **3** as ET materials in bilayer devices where the emitting layer is a p-dopable thiophene/oligothiophene system where n = 1-4 thiophene units end-capped with triarylamine substituents. These systems were based on 2,5-bis{4-[bis(4-methylphenyl)amino]phenyl}thiophene (n = 1), 2,2'-bithiophene (n = 2), 2,2':5',2''-terthiophene (n = 3) and 2,2':5',2'':5'',2'''-quarterthiophene (n = 4). Alq_3 was used for the devices incorporating the oligothiophene systems where n = 2-4; for these devices EL spectra were in agreement with the PL spectra of the emitting material. For the device incorporating the thiophene system, n = 1, emission was evident from the Alq_3 layer as well as the emissive material, therefore for this device, compound **72a** was used and the emission originated from the emitting material only. It was shown that by extending the thiophene chain from n = 1-4, and hence varying the conjugation length, the EL colour of the devices was tuned from light blue (n = 1) through to orange (n = 4). The bilayer devices incorporating both ET materials exhibited performances more than one order of magnitude higher than single layer devices of the EL material.

Electron transport dendrimers can be superior to comparable oligomers/polymers as the multiple branches of the dendritic structure increase the probability of charges finding an energetically favoured pathway when hopping from one molecule to another.[77]

To test this theory the 1st generation compound **76** was synthesised.[77] A further synthetic route to compound **76** was independently reported by Bettenhausen *et al.*[70] Dendrimer **76** formed stable amorphous glasses with a melting point of 407 °C during the first DSC heating cycle. No recrystallisation took place on cooling and in the second and third heating cycles a T_g at 222 °C was observed. This high T_g was comparable with that of thermally stable main chain polymers and was the first well-defined low molecular-weight OXD glass with a Tg above 200 °C.[70]

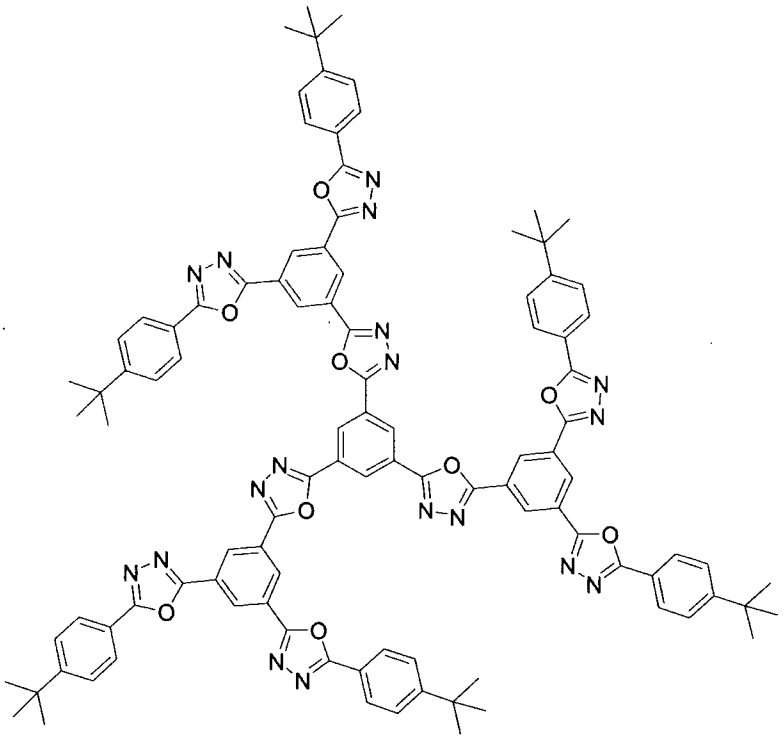

76

Scheme 29: Molecular structure of first generation OXD dendrimer 76.[70,77]

Device studies comparing the ET materials **76**, TPOB **72a**, PBD **5** (guest-host system in polystyrene) and the main-chain OXD polymer **77**[78] were carried out using PPV as the EML. All of the bilayer devices incorporating the ET materials showed considerable increase in the brightness and quantum efficiency compared to single layer PPV devices. In all cases the EL spectra of the bilayer devices were identical to that of the single layer PPV device. Threshold voltages for EL were only slightly increased from 2.5 to 3 V for devices incorporating **72a** and **76** compared to the single layer devices. In contrast, the devices incorporating PBD **5** in polystyrene or the main chain polymer **77** showed threshold voltages of 5 and 11 V, respectively. The best device results were obtained with the dendrimer **76**; for the device in the configuration ITO/PPV/**76**/Ag, EQE's of 0.4% were observed, a 4-fold increase compared to the devices incorporating TPOB **72a**. These results were the first hint that dendrimers possess enhanced carrier mobilities compared to linear low molecular-weight and polymeric counterparts,[73] as predicted in a previous theoretical paper.[79]

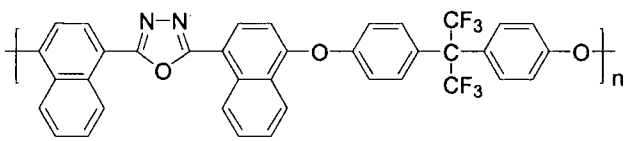

77

Scheme 30: Molecular structure of OXD main chain polymer 77.[78]

Compound **78** the triphenyl core analogue of dendrimer **76** was also investigated by Bettenhausen *et al.*[73] During the first DSC heating a melting point at 388 °C was observed with no recrystallisation on cooling. Further heating cycles displayed a T_g at 248 °C, 25 °C higher than that of compound **76** with the smaller phenyl core. In addition to the high T_g, compound **78** exhibited excellent film forming capabilities.

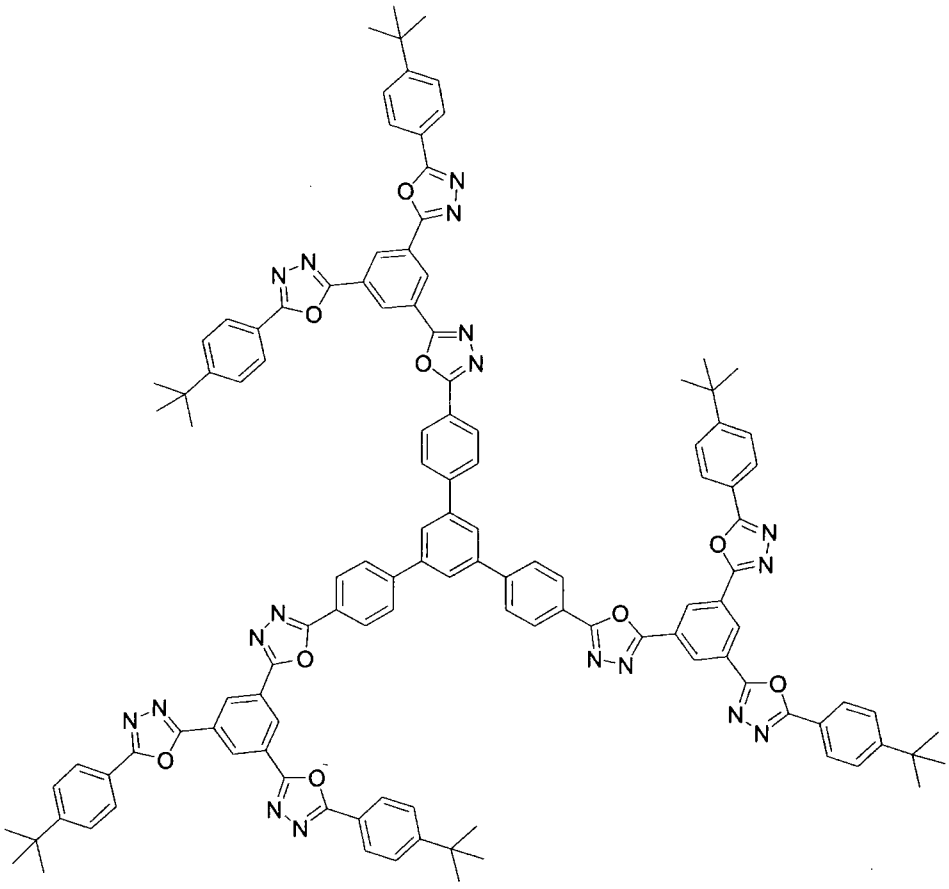

78

Scheme 31: Molecular structure of triphenyl core dendrimer 78.[73]

The X-shaped OXD compounds **79a-c** were also synthesised.[73] Compounds **79a** and **79c** exhibited similar behaviour in DSC experiments. In the first heating cycle melting points at 385 and 384 °C were observed. In the following cooling cycle no recrystallisation was observed. In the second heating cycle a T_g was detected at 186 °C for **79a** and 144 °C for **79c**, on further heating recrystallisation and melting occurred. For **79b** a melting point at 372 °C was observed in the first heating cycle. In all subsequent heating and cooling cycles no recrystallisation or melting was detected. A T_g at 152 °C was recorded for this compound.

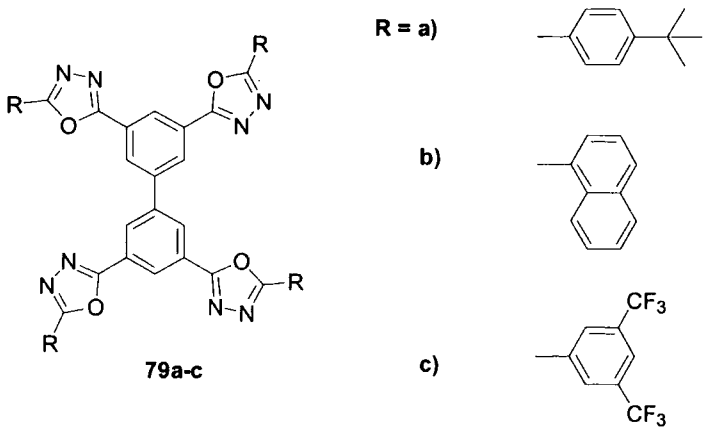

Scheme 32: Molecular structure of X-shaped OXD compounds 79a-c.[73]

The OXD functionality has been incorporated into various calamitic liquid crystalline systems, both as additives[80] and as mesogens.[81] Zhang *et al.*[82] synthesised a range of tris(oxadiazole) species **80** with benzene or triazine cores and three (trialkoxyaryl)oxadiazole arms including compound **80a,** 1,3,5-tris{5-[3,4,5-tris(octyloxy)phenyl]-1,3,4-oxadiazol-2-yl}benzene, which was studied in detail. This series of tris(OXD) species form columnar discotic liquid-crystalline mesophases rather than amorphous films.

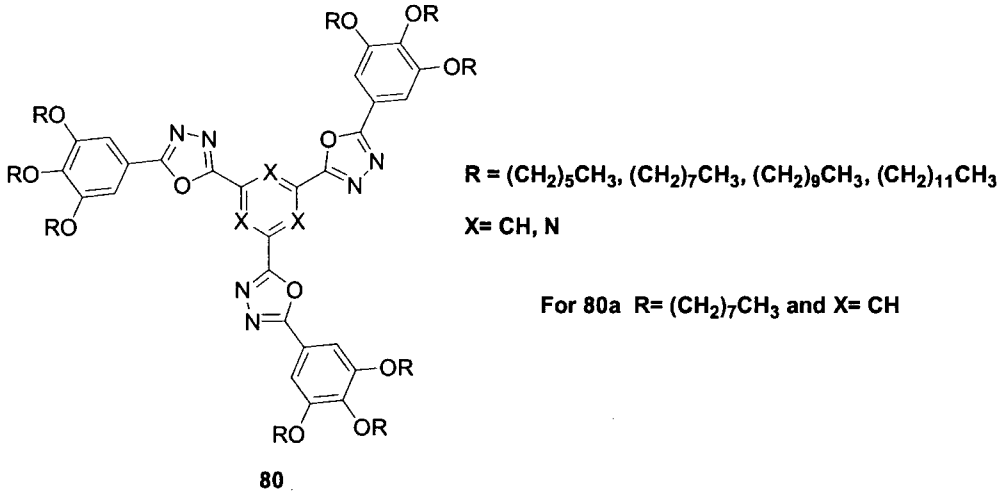

Scheme 33: Molecular structure of discoid tris(OXD) 80a synthesised by Zhang *et al.*[82]

Compound **80a** exhibited a columnar discotic liquid-crystalline mesophase between 38 and *ca.* 210 °C and possessed high electron mobility in the solid state. The electron mobility measurements were carried out without any attempt to align the directors of the columnar material. It is therefore anticipated that processing improvements, perhaps employing surface-modifying alignment agents, may lead to higher mobilities.[82]

Verheyde and Dehaen[83] prepared generation one (G_1) and generation two (G_2) OXD dendrons and using a tridirectional OXD core obtained $G_1$and G_2 dendrimers **81a** and **81b**, respectively. Compound **81b** contains three different OXD layers, which could be

advantageous as an ET material as the electrons have an enhanced probability of finding an energetically favourable pathway to hop from one site to another in the process of charge transport.

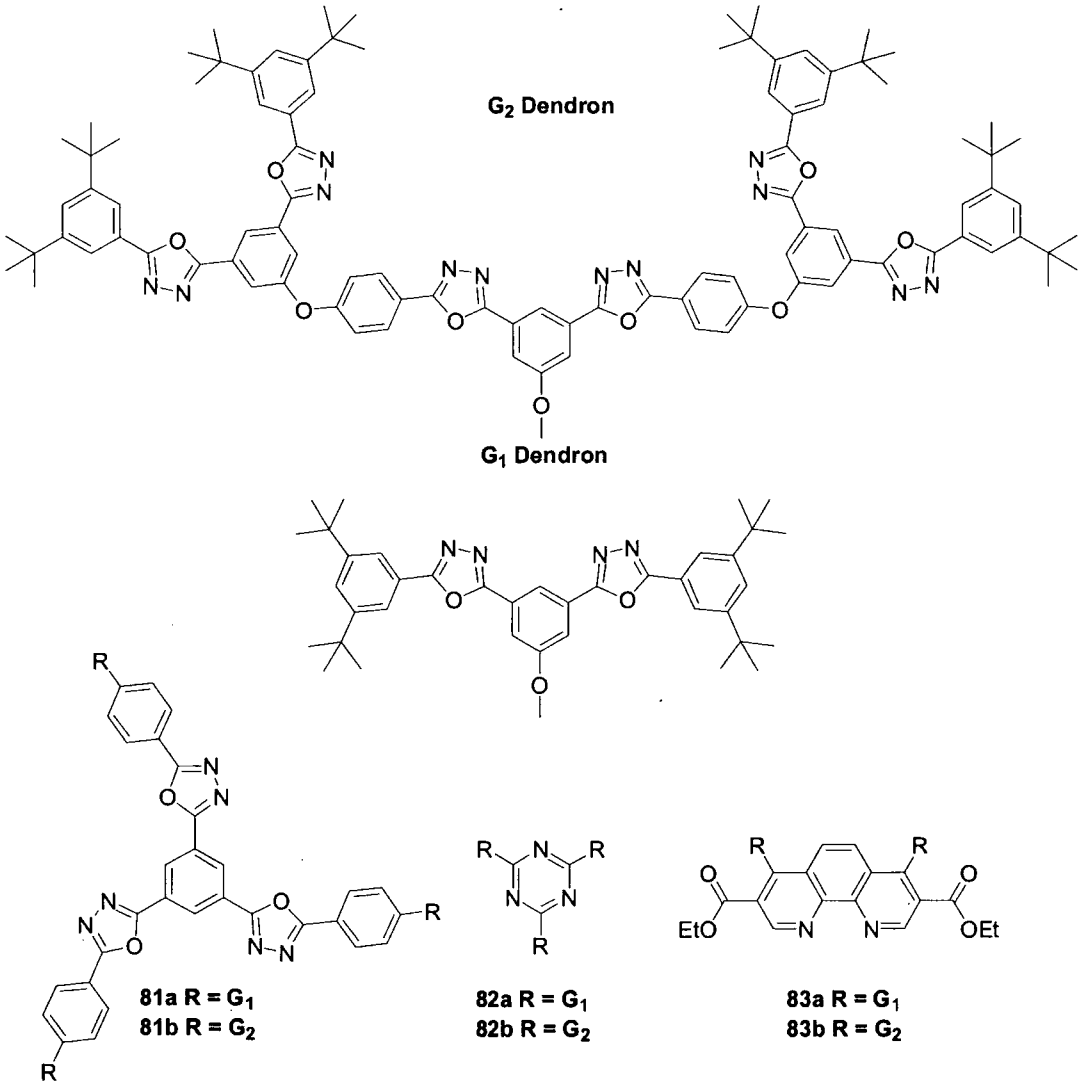

Scheme 34: Molecular structure of dendrimers 81-83.[83]

Compounds **82a-b** and **83a-b** with triazine and 1,10-phenanthroline cores, respectively, were also synthesised: no optoelectronic properties for **81-83** have been reported.

The rigid tetrahedral tetraphenylmethane skeleton is an effective core for stable amorphous phases of both molecular and oligomeric materials;[84] however, the EL properties of these materials have remained largely unexplored. Yeh *et al.*[67] established that compounds

84-88 form glassy films which serve as light emitting or charge transport materials.

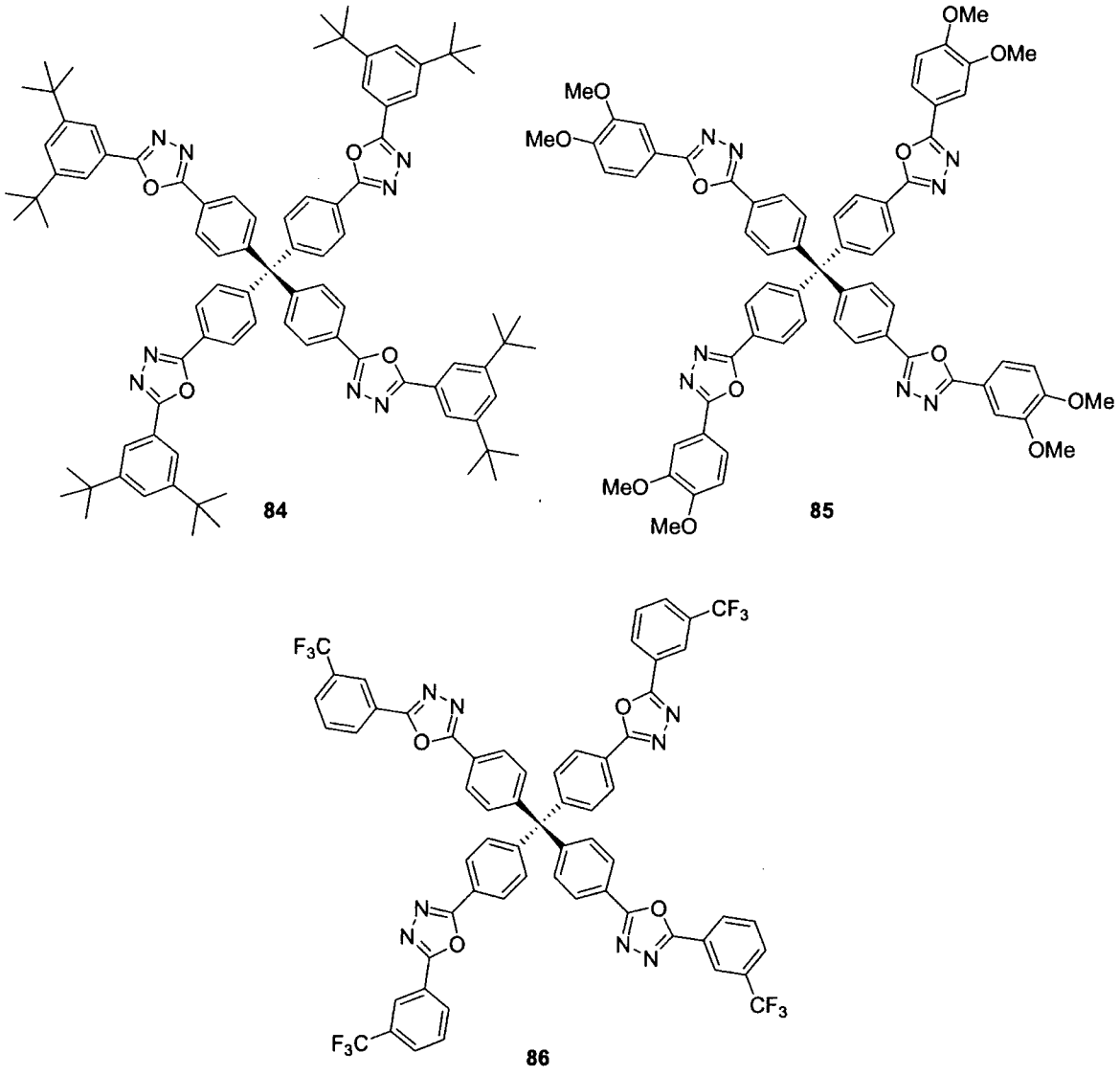

Scheme 35: Molecular structure of tetraphenylmethane-based OXD compounds 84-86.[67]

For compounds **84**, **85**, and **86** melting points were observed at 400, 337 and 270 °C and Tg's at 175, 97 and 125 °C, respectively. Exothermic crystallisation temperatures for the three compounds were observed between 200 and 220 °C. CV data implied that the tetraphenylmethane framework or peripheral substituents hardly altered the electron withdrawing ability of the oxadiazole ring in compounds **84-86** compared with that of PBD **5**. A three-layer device incorporating **86** in the configuration ITO/NPB **33**/Alq_3/**86** /MgAg was compared to a reference device incorporating PBD **5** in the configuration ITO/ **33**/Alq_3 **6**/**5**/MgAg. Compound **86** was chosen for device fabrication because of its acceptable volatility under high vacuum. Both devices had turn on voltages for EL at approximately 7-8 V, with EL characteristic of the Alq_3 at λ_{max} = 515 nm. At a drive voltage of 12 V the current

was three times lower in the **86** device than in the PBD device, and the **86** device was more than three times dimmer than the PBD device at the same driving voltage (10 V). With lower current density as well as lower EL the **86** device still has a comparable EQE of *ca.* 0.75% to that of the PBD device with an EQE of *ca.* 1%.

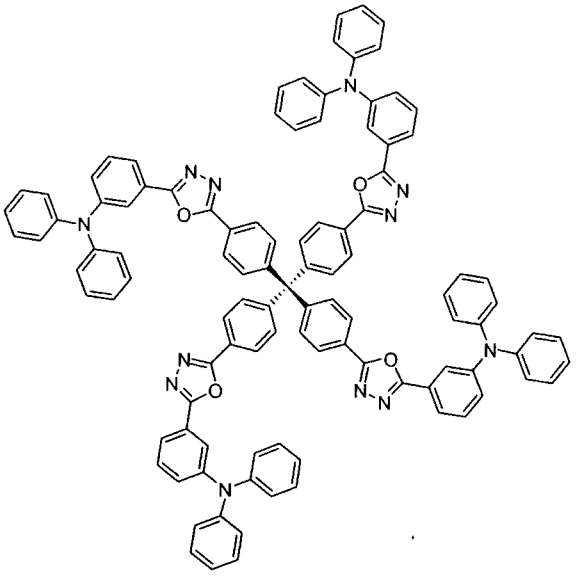

87

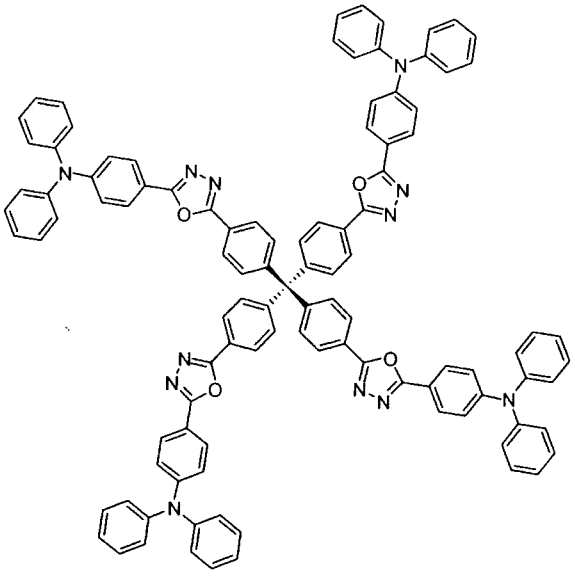

88

Scheme 36: Molecular structures of tetraphenylmethane-based OXD/TPA compounds 87 and 88.[67]

Bipolar compounds **87** and **88** possess peripheral diarylamine units (*meta-* and *para*-linked, respectively, to the OXD arms). T_g's were observed at 149 and 187 °C, respectively, with no melting point or recrystallisation temperatures observed. A single layer device in the configuration ITO/**88**/Ca/Ag showed blue emission at low applied voltages, which turned bluish white at elevated voltages. The device had a photometric efficiency of ~0.7 cd A^{-1} at a current density of ~10 mA cm^{-2}. The device brightness reached a maximum of 1690 cd m^{-2} at a driving voltage of ~14 V. Compound **88** behaves predominantly as an ET material, therefore a blended system containing both **88** and the HT material PVK **27** was constructed in an effort to provide a more efficient device. Doping of PVK with **88** in a 3:1 weight ratio for the device configuration ITO/PVK:**88**/Ca/Ag resulted in a slightly enhanced photometric efficiency of 0.8 cd A^{-1} with a current density of less than 8 mA cm^{-2}.

Two blue light emitting Y-shaped trimeric compounds having high T_g's have been synthesised by Cha and Jin.[85] Compound **89** incorporates three carbazole moieties for HT and compound **80** comprises three OXD moieties for effective ET. Both compounds exhibited high T_g's at 250 and 156 °C, respectively.

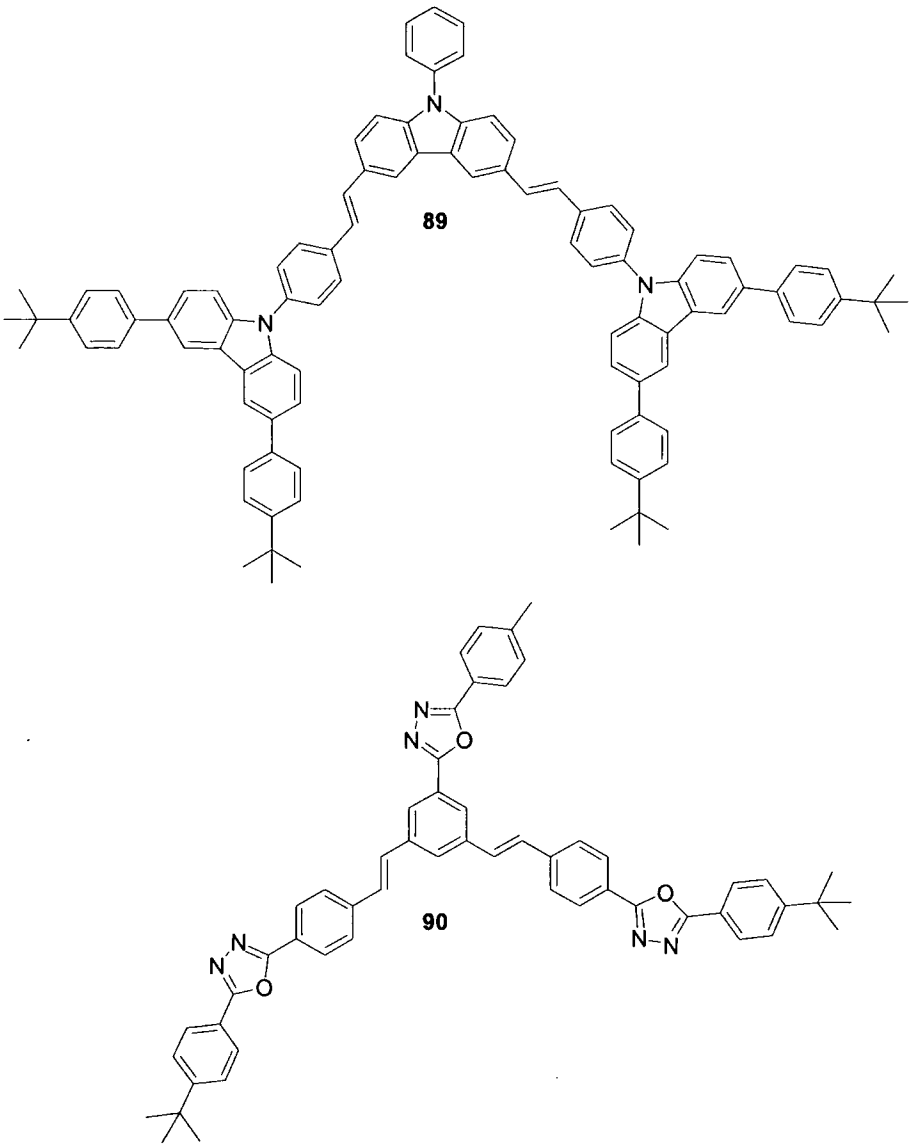

Scheme 37: Molecular structure of Y-shaped trimers 89 and 90.[85]

For a bilayer device incorporating **89** as both HT and EML, and **90** as ET and EML in the configuration ITO/**89**/**90**/LiAl, EL emission was dependent on the applied electric field and changed drastically when the applied voltage was higher than 2.5 mV cm^{-1}. At applied voltages of 1.5 and 1.83 mV cm^{-1} the device emitted between 400-550 nm with λ_{max} = 451 with a shoulder at 424 nm. Above 2.5 mV cm^{-1} the emission changed with the shoulder intensity greatly increasing so that λ_{max} = 424 nm. Emission was attributed to the excitons of both compounds with overlapping EL. Increasing the applied voltage again, resulted in two new peaks at λ_{max} = 526 and 592 nm in the green and red regions, respectively, in addition to the original blue emission. Above an applied field of 2.8 mV cm^{-1} the emitted light appeared to be white. The two new peaks were assigned to exciplexes formed at the interface of the organic layers. This study highlighted a novel method to design a white light source

employing a bilayer device consisting of electron donating and electron withdrawing layers both of which are blue-emitters, but are able to form green and red light emitting exciplexes. The intensity and efficiency of these devices, however, require further improvement for practical applications.

Cha *et al.*[29e] studied related branched compounds **91a-b** composed of a light-emitting core which defines the colour emission, surface groups controlling the processing properties and linkers allowing the transport of charges into the core unit. The 9,10-bis(phenylethynyl)anthracene core defines EL wavelength with ethynyl-OXD units acting as electron-transporting linkers between the conjugated sections of the molecule and the peripheral alkyl groups.

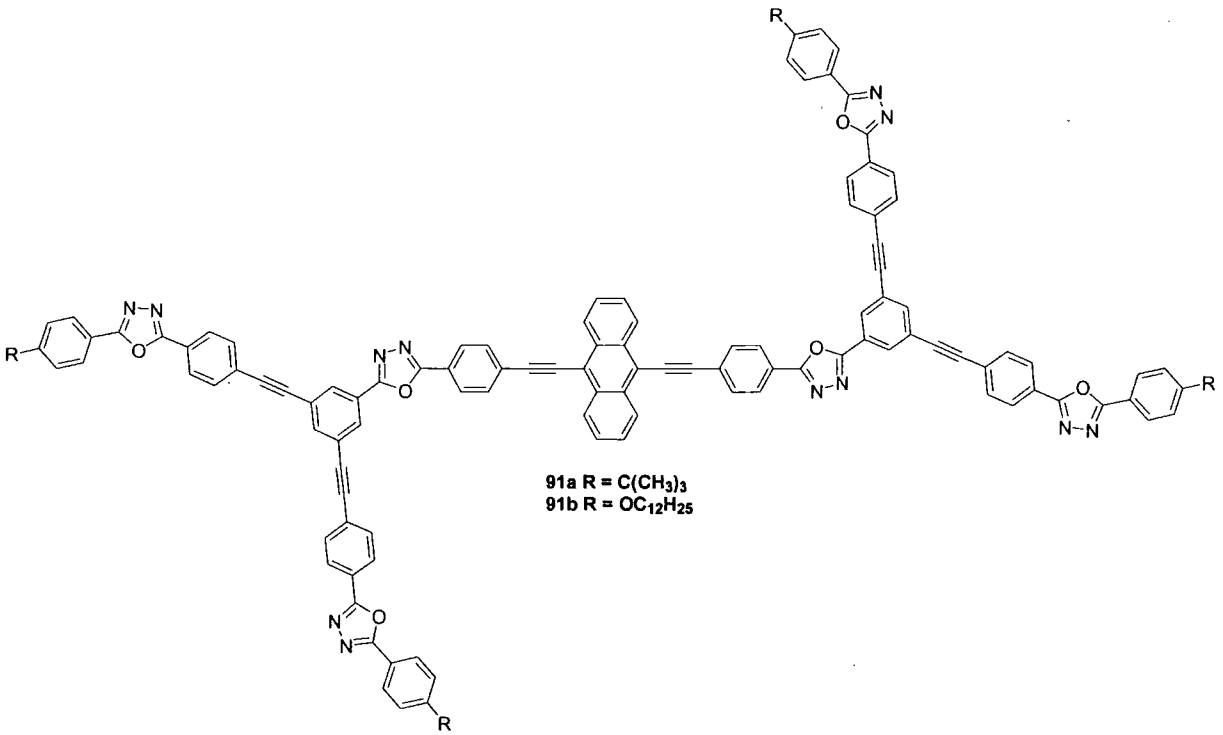

Scheme 38: Molecular structure of the four-armed conjugated compounds 91a and 91b.[29e]

Compound **91b** with dodecyloxy surface groups has a high T_g of 211 °C, exhibited good solubility in common organic solvents and formed good quality thin films by spin coating from solution. In contrast, compound **91a** with *tert*-butyl surface groups had low solubility and gave films of inferior quality. A device incorporating **91b** in the configuration ITO/PEDOT:PSS/**91b**/Li:Al emitted red light with an EQE of 0.02%, indicating that the oxadiazole moieties acted only as electron transporters as the core is the only red light emitting chromophore in the structure.

Chung *et al.*[86] synthesised the multibranched compound **92** which consists of two π-conjugated triphenylamino-OXD units connected to a central π–conjugated bis-2-

thienylethenylene bridging core. These two distinct chromophore units have different electronic excited-state energies as demonstrated by model compounds representing the arm and core structures. It was shown that the model arm unit is a higher energy band gap green emitting dye, whereas the model core is a lower energy red emitting dye. It was expected that these two chromophores built into one molecule **92**, would promote effective intrasystem excitation transport and conversion from the higher-energy state to the lower one. For compound **92** a very effective intramolecular energy transfer from the excited arm units to the π –conjugated bridge unit was observed; however no OLED applications of compound **92** have been reported.

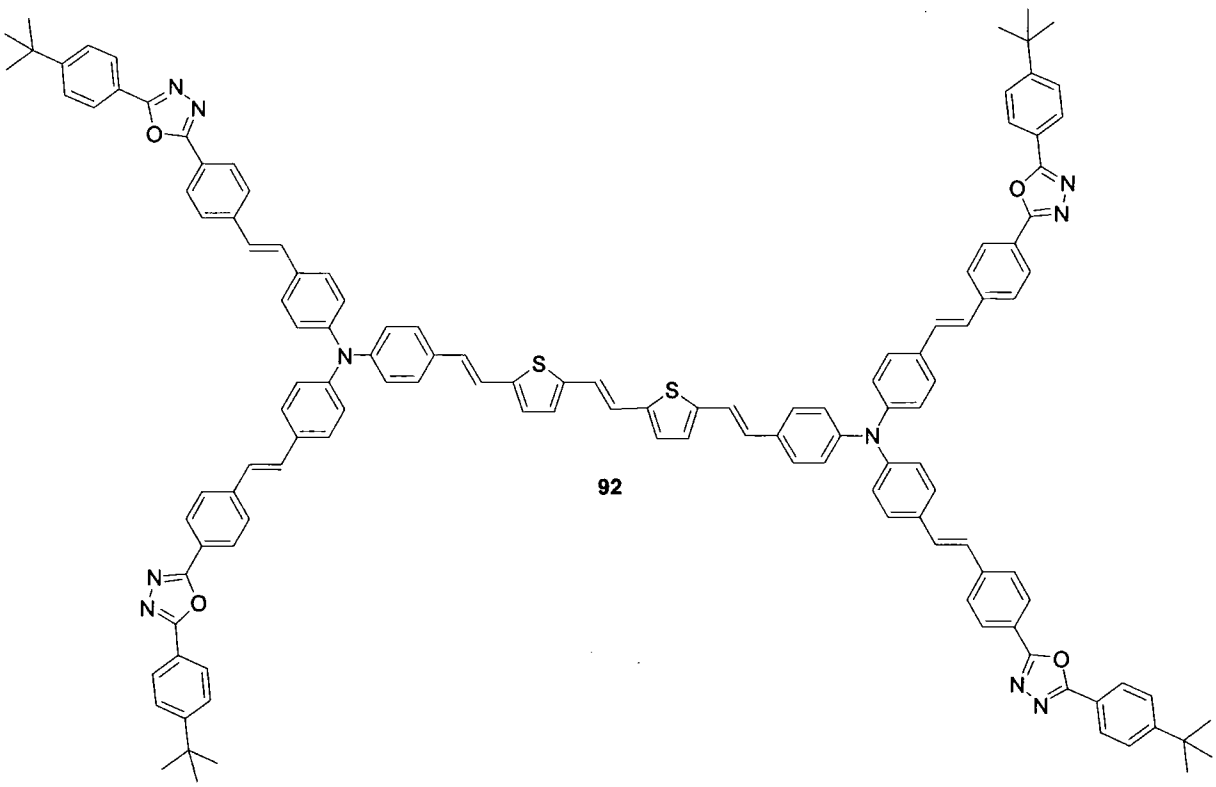

92

Scheme 39: Molecular structure of multibranched compound 92.[86]

1.4.2.6 Liquid Crystal OXD Materials

The introduction of a molecular orientation which promotes a large overlap of wavefunction of π-orbitals in conjugated materials would be expected to promote high charge carrier mobility.[87] This was seen for compound **80a** in the previous section and was the premise for the design of liquid crystal (LC) OXD materials **93-94** by Tokuhisa and co-workers[87,88] as high quality thin films of LC materials with a high degree of molecular orientation can be obtained.[89] The OXD chromophore served as a mesogenic unit in compound **93**. A large

enhancement of electron mobility due to a regulated molecular orientation was observed in the glassy LC film of **93**; however the azomethine linkage lacked thermal stability.

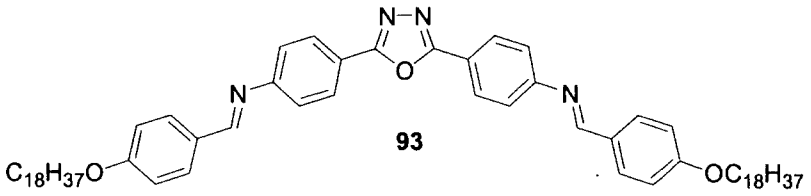

93

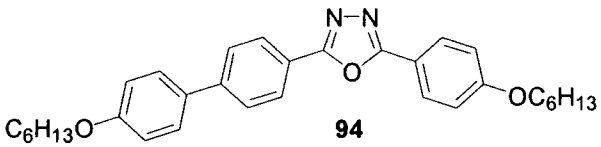

94

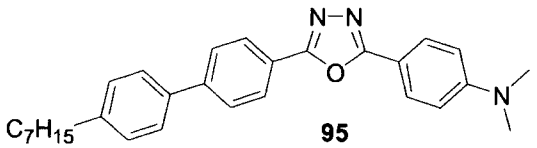

95

Scheme 40: Molecular structures of LC OXD materials 93-95.[87,88,91]

The LC material **94** in which the OXD chromophore is directly substituted with alkoxy groups exhibited very high electron mobilities, at a level of 10^{-3} cm^2 V^{-1} s^{-1}, in the smectic phase attributed to high intralayer molecular order. Compound **94** also exhibited strong PL in the LC phase, with emission highly polarised (order parameter S_{EL} = 0.32) along the rubbing direction of the ITO, and was therefore incorporated into OLEDs. A device in the configuration ITO/CuPc/**94**/Alq_3 **3**/Al exhibited linear polarised emission with EL corresponding to compound **94**; however, a low EQE of 2.8 x 10^{-5} was recorded for this device.[90]

Kawamoto *et al.*[91] synthesised the bipolar LC **95** incorporating an OXD moiety for ET, and an amine moiety as a HT unit, which exhibited LC behaviour and strong blue emission. Compound **95** was used as the EML in devices in the configuration ITO/**95**/MgAg, and ITO/PEDOT/**95**/MgAg, turn on voltages for current were observed at 12 and 8 V, respectively, and the values of luminance and current density of the bilayer device were ten and six times higher than those for the single layer device, respectively. For both devices EL was observed to originate from the LC **95**. Recently, achiral nematic LC materials based on OXDs have been reported by Görtz and Goodby.[92]

1.4.2.7 Electrochromic Device Applications of OXD Materials

Low molecular weight OXDs have been used in various other applications, Wang *et al.*[93] synthesised three new tetrathiafulvalene (TTF) derivatives **96-98** bearing OXD units as

chromophores and demonstrated that conjugation of the two moieties offered great potential for electrochromic devices (ECD)s.

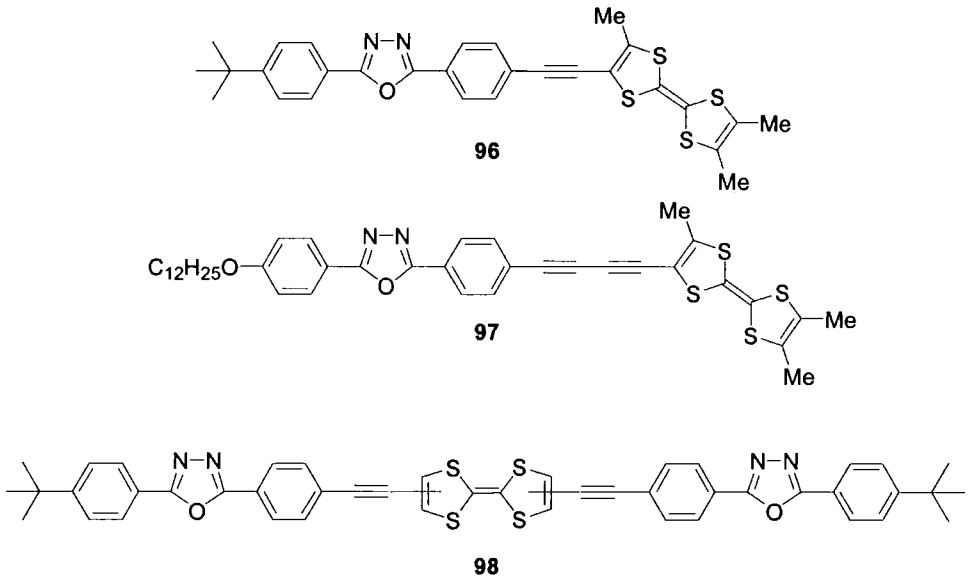

Scheme 41: Molecular structure of TTF-OXD materials 96-98.

The optical switching of **98** was realised, whilst applying electrical square waves across a spectroelectrochemical cell containing a solution **98** (in DCM), the optical absorption around the $\mathbf{98}^{+\cdot}$ λ_{max} peak was switched leading to a highly-reversible colouring (dark-green)/bleaching (orange) process.

1.4.2.8 Macrocyclic OXDs

Multidentate OXD, imine and phenol-containing macrocycles **99** and **100** were synthesised by Perez and Bermejo.[94] The two macrocycles can potentially co-ordinate two M(II) cations with electron neutrality after the deprotonation of the phenol group. However, both macrocycles were found to be insoluble in all common organic solvents.

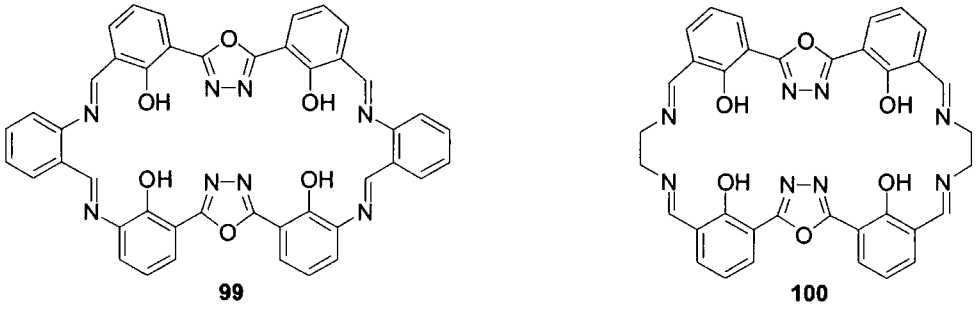

Scheme 42: Macrocycles 99 and 100.[94]

The use of azobenzene derivatives as an "on-off" switch to control chemical functions is of interest[95] and photochemically reversible switchable azomacrocycles have been prepared.[96] Zheng and co-workers[97] prepared azomacrocycle **101** containing two OXD moieties, but found difficulty in characterisation due to insolubity in all common organic solvents.

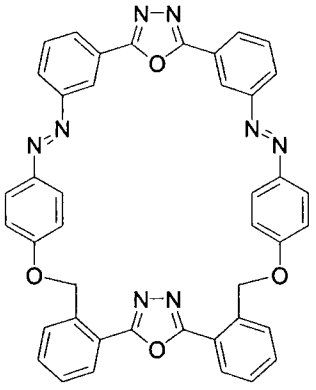

101

Scheme 43: Azomacrocycle 101.[97]

Du *et al.*[98] synthesised two macrocyclic phosphoramidate receptors **102** and **103** containing glycine ethyl ester and OXD units. From the P=O and N-H polar groups and the rigid aromatic units, hydrogen bonding and π -stacking may be present and result in self assembly or molecular recognition properties. The X-ray structure of the *trans* isomer **102** was reported.

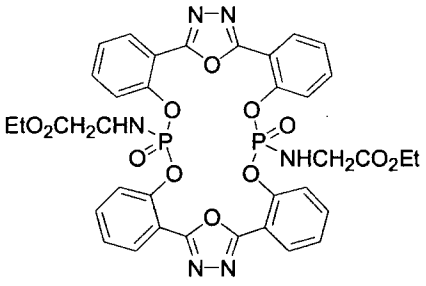

102

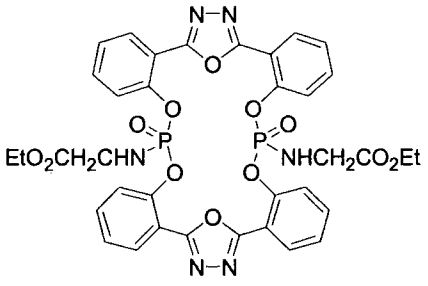

103

Scheme 44: macrocyclic phosphoramidate receptors 102 and 103.[98]

Macrocycles **102** and **103** are self associated by intermolecular N-H···O=P hydrogen bonds and intermolecular or intramolecular aromatic face-to-face π-π interactions.

1.4.3 Polymeric Oxadiazoles

Synthesis of π-conjugated polyoxadiazoles has been achieved by direct analogy with their low molecular weight counterparts via ring closure of polyhydrazides with reagents such as $POCl_3$ and polyphosphoric acid, or alternatively, by reaction of bis(tetrazole)s with bis(acid chloride)s. In addition, poly(oxadiazole ether)s can be prepared by activated nucleophilic polycondensation of oxadiazole difluorides with aromatic diols. The electron deficient OXD unit has been incorporated directly into the main chain or by attaching it as a pendant group to the polymeric aryl backbone.

Fully conjugated aromatic polyoxadiazoles usually exhibit low solubility in common organic solvents resulting in processability problems. To increase solubility and hence processability, without losing thermal stability, block copolymers containing flexible ethers[78,99,100] perfluoralkyl,[78,100,101] or diphenylsilyl[33,102] linkers have been developed as ETHB layers in polymer LEDs (PLED)s.[103,29a]

1.4.3.1 Main Chain OXD Polymers

Zheng *et al.*[104] synthesised a series of copolymers **105a-c** consisting of alternating blocks of rigid chromophores containing OXD units together with flexible spacer segments with the objective of raising the ET ability. The effect of the substituents on the optical properties of the copolymers was investigated.

Single layer devices incorporating the three OXD copolymers **105a-c** in the configuration ITO/**105a-c**/Ca/Al exhibited blue-green light, λ_{max} = 494, 509, 480 nm, respectively, compared to that of the reference copolymer **104** device which exhibited blue emission, λ_{max} = 477 nm. EL for **105a** and **105c** were similar to their PL spectra, indicating that EL and PL originate from the same excited state; however EL of **105b** (λ_{max} = 509 nm) was found to be significantly red shifted compared with its PL spectra (λ_{max} = 455 nm). Excimer emission could be responsible for this shift, although further investigations are required to fully understand this phenomena in these copolymer systems.

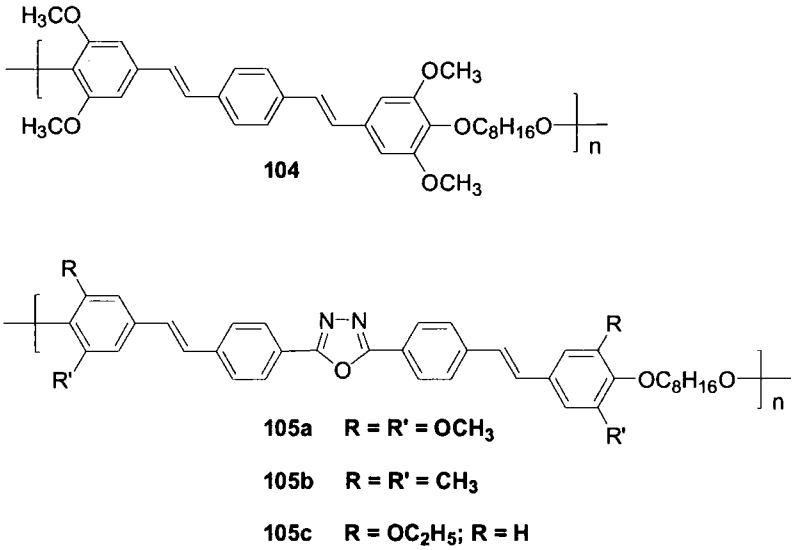

Scheme 45: Reference copolymer 104 and OXD copolymers 105a-c prepared by Zheng *et al.*[104]

The OXD copolymers were not only used as blue-green emitters but also as ET materials in bilayer devices. For the device incorporating **105c** and PPV as an emissive layer in the configuration ITO/PPV/**105c**/Ca/Al no emission from **105c** was observed indicating that **105c** acts as the ET material and PPV as the emitter. The brightness and efficiency of a single-layer PPV device ITO/PPV/Ca/Al was improved by a factor of $>10^3$ with the introduction of **105c**. The bilayer device had a brightness of 2,400 cd m^{-2} at 6.8 V with an EQE of 0.094%. This indicates the efficient ET ability for the OXD copolymer, moving the recombination zone away from the cathode interface and improving the probability of recombination in the PPV emitting layer.

Mikroyannidis and co-workers[105] synthesised two new PPV-type conjugated polymers **106-107** with OXD moieties in the backbone. Both polymers emitted greenish-blue light in solution with PL λ_{max} = 511 and 487 nm for **106** and **107,** respectively. The emission maximum for **106** red-shifted by 24 nm compared to that of **107** suggesting increased electron delocalisation along the backbone of polymer **106,** possibly due to the higher composition of electron donating dodecyloxy groups per repeat unit of **106** and/or a possible disruption of the conjugation along the backbone of **107** caused by the two OXD units. Therefore increasing the OXD composition in the polymer backbone of **107** did not extend the effective chromophore.

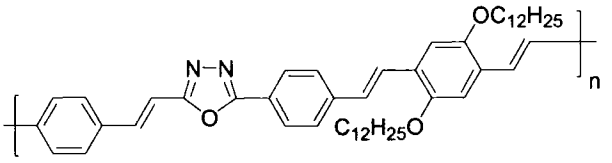

106

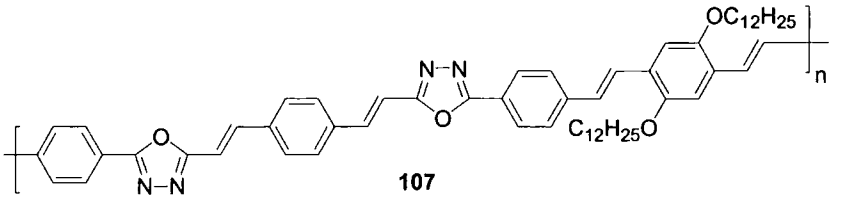

107

Scheme 46: PPV based OXD containing polymers 106-107.[105]

Bilayer devices incorporating polymer **106** in the configuration ITO/PEDOT/**106**/Al exhibited a maximum brightness of 23 cd m^{-2} and a low EQE of 0.002% at 16 V. EL spectra of this device displayed voltage tunable EL colors. At a turn on voltage of 9 V, the EL λ_{max} = 558 nm (yellow), however, the EL spectra gradually blue-shifted with an increase in applied bias, showing EL λ_{max} = 545 nm at 13.5 V, λ_{max} = 540 nm at 15 V and finally λ_{max} = 527 nm at 16 V. This trend was irreversible in that, for a device working at 16 V (λ_{max} = 527 nm), decreasing the applied bias back down to 9 V did not red-shift the EL to λ_{max} = 558 nm. This suggested that the application of higher electric fields and consequently greater local heating in the polymer films lead to changes in the conformation of the polymer backbone, leading to subtle variations in the electronic band structure.

To improve the device performance and efficiency, a blend of polymer **106** was made with a hole transport molecule, 6 wt % 1,1-bis(di-4-tolylaminophenyl)cyclohexane (TAPC). A maximum brightness of 70 cd m^{-2} and a maximum EQE of 0.01% at 17.5 V were achieved, representing a factor of 3-5 enhancement in performance over the device incorporating polymer **106** only. As before, EL spectra of this device displayed repeatable, irreversible voltage tunable EL. Devices incorporating polymer **107** did not show measurable EL properties, as the PL emission was very weak compared to polymer **106**.

The polymer **77**[78] described earlier (p. 35) was used as an ETHB material in PPV based devices and its ET properties evaluated against triazine and quinoxaline counterparts.[106] Polymer **77** forms stable glasses with a Tg of 220 °C, is readily soluble in common organic solvents and possesses excellent film forming capabilities. A bilayer device in the configuration ITO/PPV/**77**/Al demonstrated that **77** possessed hole-blocking capabilities, exhibiting increased operational performances in comparison to a reference single PPV layer device. A maximum brightness of 55 cd m^{-2} at a current density of 155 mA cm^{-2} was recorded

at an onset voltage of 7 V, compared to the reference device which gave a maximum brightness of 2 cd m^{-2} at a current density of 436 mA cm^{-2}, however, a lower onset voltage of 6 V was achieved. Applying polymer **77** in a device incorporating a Ca cathode in the configuration ITO/PPV/**77**/Ca, the EQE could be increased by one order of magnitude up to 0.2%.[78,99,107]

1.4.3.2 Fluorene-Oxadiazole Hybrid Main Chain Polymers

Ding *et al.*[108] synthesised a series of alternating copolymers with 9,9-dioctylfluorene and oxadiazole units. In the polymers the oxadiazole units were evenly dispersed in the main chain at every one, **108a** P(F_1-*alt*-Ox), three, **108b** P(F_3-*alt*-Ox), or four, **108c** P(F_4-*alt*-Ox), fluorene units. Another copolymer **109** with an asymmetric repeat unit structure P(F_3-Ox-F_1-Ox) was prepared for comparison. Electrochemical characterisation as well as photo- and electroluminescent studies demonstrated excellent stabilities of the majority of the copolymers at both positive and negative charged states and comparatively stable blue-light-emitting properties compared to polyfluorene.

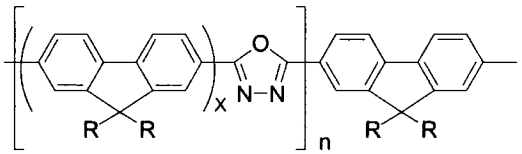

108a x = 1, P(F_1-*alt*-Ox)
108b x = 3, P(F_3-*alt*-Ox)
108c x = 4, P(F_4-*alt*-Ox)

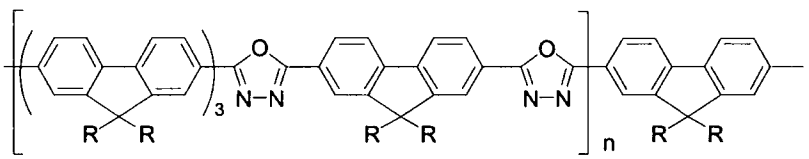

109 P(F_3-Ox-F_1-Ox)
R = n-C_8H_{17}

Scheme 47: Alternating fluorene-oxadiazole copolymers 108a-c and 109 prepared by Ding *et al.*[108]

Electrochemical studies also showed that the insertion of the oxadiazole moieties into the poly(fluorene) chain raised the electron affinities of the copolymers close to the work function of cathodes such as Ca and Mg. The UV-vis and PL spectra of the copolymers were very similar to those of poly(fluorene), except **108a**. It is apparent that as oxadiazole units are introduced into the poly(fluorene) conjugated chain, there is a 10-12 nm red-shift in the

absorption spectra and a 5-7 nm red-shift in the emission spectra. The extent of the red-shift was not affected by the oxadiazole content in the chain. This observation indicates that the oxadiazole unit does not interrupt the main chain conjugation, as suggested by Lee and Chen for PPV type copolymers.[100] Further work on these copolymers revealed that **108b** and **108c** have the highest electrochemical stability; therefore bilayer devices in the configuration ITO/HML/**108b-c**/Al were fabricated, where HML represents a non-emissive HTL. The two devices exhibited similar behaviour with relatively broad EL spectra almost identical to the PL spectra of the film. No additional bands were observed between 400 and 700 nm in the EL spectrum and this was maintained over a period of 12 h. Devices made from poly(fluorene) were found to emit blue light for only a few minutes at their original brightness before dimming quickly with a shift of the emitting wavelength from λ_{max} = 423 nm to λ_{max} = 510 nm.[109] It was therefore concluded that fluorene-oxadiazole copolymers have a high stability associated with their blue light-emitting properties and that they are good candidate materials for ET layers in PLEDs.

Ma and co-workers[110] reported the synthesis of the cationic conjugated alternating copolymer **110** (PFON$^+$(CH$_3$)$_3$I$^-$-PBD), comprising alternating fluorene and OXD in the main chain.

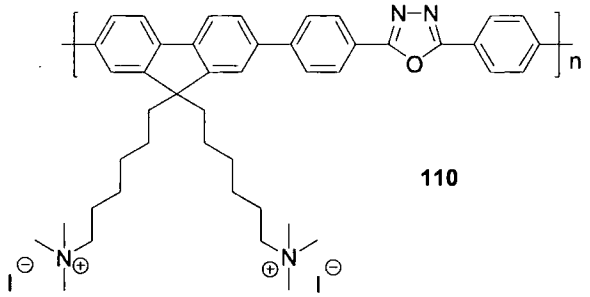

110

Scheme 48: Fluorene-OXD alternating cationic polymer 110.[110]

Multilayer PLEDs were fabricated using a light emitting polymer (cast from solution in an organic solvent) as an EML and the water-soluble (or methanol soluble) polymer **110** as an ET in the following configuration: ITO/PEDOT/emissive polymer/**110**/Ba/Al. Devices using poly(9,9-dioctylfluorenyl-2,7-diyl) (PFO) **132** as the EML were fabricated with and without the ETL **110**. The PFO/**110** device turned on at ~3 V, whereas for the PFO device without **110** the turn on voltage was ~ 5 V. At 6 V the luminance obtained from the PFO/**110** device was 3450 cd m^{-2}, compared to 30 cd m^{-2} for the device without **110**. For devices utilising MEH-PPV as the emissive material, again with and without the ET material, similar results were observed, with luminances of 5600 cd m^{-2} at 5 V compared to luminances of 3550 cd m^{-2} for

the device without the ETL. By casting the ETL **110** from solution in methanol and the emissive layer from solution in an organic solvent, interfacial mixing was avoided which facilitated fabrication methods. This demonstrated that high performance PLEDs can be fabricated by processing all layers from solution.

1.4.3.3 Bipolar Main Chain OXD Polymers

Meng *et al.*[111] synthesised the bipolar compound **111**, which emitted greenish-blue light in polymer films at λ_{max} = 475 nm. A device in the configuration ITO/**111**/Al emitted blue light at *ca.* 8 V with a current density of 1.14 mA cm^{-2}. When the forward bias was increased both the current and the light output increased rapidly after 6 V. These preliminary results suggest that polymer **111** could be a potential novel active material as it has a similar LUMO but higher HOMO compared to MEH-PPV, implying that it has a more balanced charge injection, which greatly enhances EQEs of PLEDs.

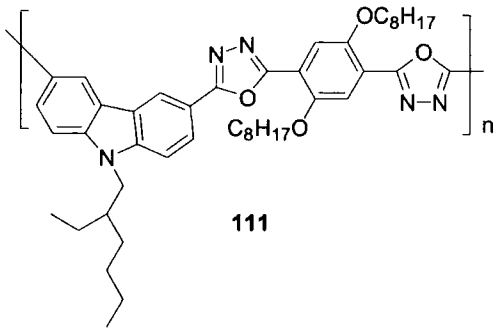

111

Scheme 49: Molecular structure of bipolar compound 111.[111]

Zhang and co-workers[112] reported the synthesis of the bipolar luminescent polymer **112** containing triphenylamine and OXD units in the main chain. The analogous polymer **113** without OXD units was also reported for comparison. UV-vis absorption spectra of thin films of the two polymers illustrated that the main absorption peak is red-shifted from λ_{max} = 470 nm (**113**) to λ_{max} = 495 nm (**112**) due to the inclusion of the OXD unit. A smaller red-shift was observed for the PL spectra, from λ_{max} = 545 nm (**113**) to λ_{max} = 555 nm (**112**). These data indicate that the effective conjugation length of the polymer is increased with the inclusion of the OXD unit.

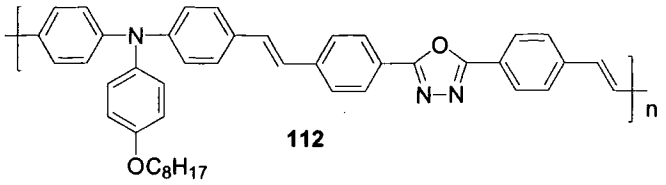

112

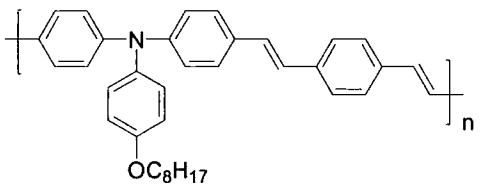

113

Scheme 50: Bipolar polymers 112 and 113 prepared by Zhang *et al.*[112]

Devices of the configuration ITO/PEDOT/**112** or **113**/CsF/Al gave blue EL. The device incorporating the bipolar polymer **112** exhibited a maximum brightness of 3600 cd m^{-2} and a maximum EL efficiency of 0.65 cd A^{-1}equating to an EQE of 0.3%. In contrast, the device incorporating the polymer **113** exhibited a significantly reduced maximum brightness of 284 cd m^{-2} and a lower EL efficiency of 0.042 cd A^{-1}. The devices incorporating the bipolar polymer **112** were observed to achieve brightnesses and efficiencies 15 times that of devices incorporating polymer **113**.

1.4.3.4 Pyridine-Oxadiazole Main Chain Polymers

In our group Wang *et al.*[113] synthesised the poly(alkoxyPBD) derivative **114** and its dipyridyl analogue **115** using Suzuki coupling methodology. Compound **114** was the first polymeric material based on the PBD structure **5** as the repeating unit.

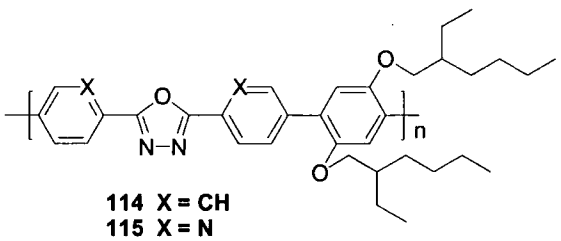

114 X = CH
115 X = N

Scheme 51: Poly(alkoxyPBD) derivative 114 and its dipyridyl analogue 115 prepared by Wang *et al.*[113]

Thermal gravimetric analysis (TGA) established that polymers **114** and **115** are highly stable up to 370 °C and 334 °C, respectively, and are amorphous with T_g's = 196 °C and 193 °C, respectively. Thin film PL spectra of **114** and **115** showed strong blue PL with λ_{max} = 444 nm and 475 nm, respectively. Polymer **114** was investigated as an ET polymer in bilayer LEDs

with MEH-PPV as the emissive layer. For the device ITO/PEDOT/MEH-PPV/**114**/Al an EQE of 0.26% and brightness of 800 cd m^{-2} was achieved, with emission solely from the MEH-PPV layer.

1.4.3.5 Side Chain OXD Polymers

Peng and Zhang[114] synthesised PPVs containing rigid OXD units as main chain substituents. Three polymers were synthesised, the homopolymers **116** and **118** and the random copolymer **117**, all of which are soluble in common organic solvents.

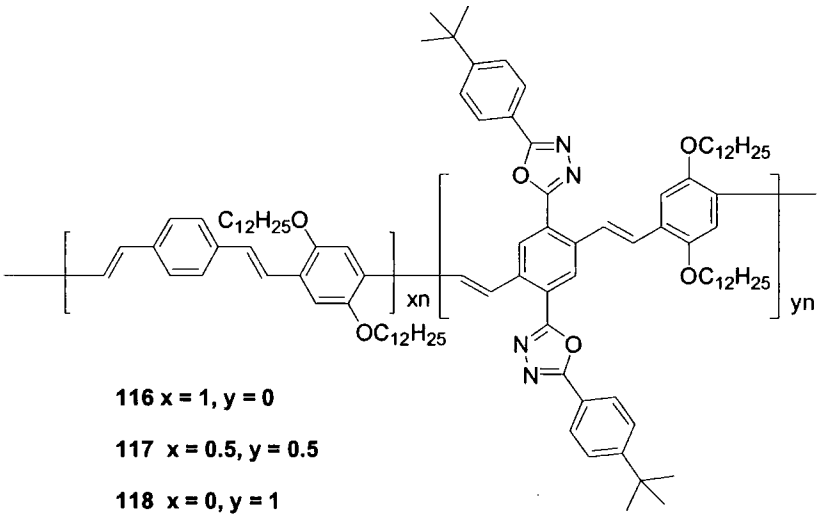

Scheme 52: Molecular structure of polymers 116-118 synthesised by Peng and Zhang.[114]

Single layer devices based on polymers **117** and **118** in the configurations ITO/polymer/Ca(Al) and ITO/polymer/Al displayed uniform red-orange EL identical to their PL spectra. For the devices incorporating **118** with Al as the cathode an EQE of 0.041% at a current density of 1 mA mm^{-2} was observed, which is 20 times higher than that of the devices incorporating the PPV type polymer **116**. Efficiency decreased slightly when the current density increased with the highest efficiency of 0.045% obtained at 0.3 mA mm^{-2}. The devices also showed similar turn-on voltages (8 V) for both the light and current, indicating a reasonably balanced charge injection. With Ca as the cathode, a higher efficiency of 0.066% and lower turn-on voltages were achieved. The EQE increased slightly when the current density increased, which is in contrast with the Al cathode devices. Polymer **117** which has half the OXD content of **118**, gave less efficient devices (0.018%) than **118** when Al was used as the cathode. However, this was still 1 order of magnitude greater than that of the PPV polymer **116**. Employing Ca as the cathode, polymer **117** showed the same efficiency as polymer **118**.

These results indicated that the electron injection properties are improved from polymer **116** to **117** and to **118**, also more balanced charge injection of both charge carriers has to be achieved, even for polymer **118**. Limited electronic interactions of the cross-conjugated OXD units with the conjugated backbone were thought to be a barrier to this. The LED efficiencies of **117** and **118** are higher than that of side chain OXD-PPVs prepared in previous work by Bao *et al.*[115] but lower than that of the main chain OXD-PPV polymer **119** prepared by Peng *et al.*[116] This seems consistent with the strength of electronic interactions between the OXD units and the conjugated backbone in these different OXD-PPV derivatives.

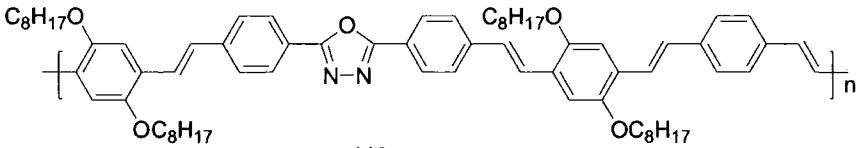

119

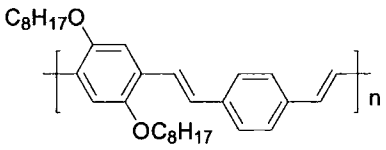

120

Scheme 53: Main chain OXD-PPV polymer 119 and reference polymer 120 prepared by Peng *et al.*[116]

For single layer devices in the configuration ITO/**119**/Al, EQEs of 0.15% were obtained, almost 40 times larger than that of devices incorporating PPV polymer **120**. The turn on voltages of 6 V for the polymer **119** devices were also much lower than that for the PPV polymer **120** devices (15 V).

In an attempt to ascertain if further improvement in device efficiency is possible, Peng and Zhang[117] synthesised the PPV based polymer **121** with OXD units incorporated into both the main chain and as side chain substituents. Single layer devices were fabricated in the configuration ITO/polymer/Al or Ca incorporating polymer **121** and compared to devices incorporating the PPV reference polymer **116**, the side chain OXD-PPV polymer **118** and the main chain OXD-PPV polymer **119**. Devices incorporating polymer **121** displayed uniform red-orange EL almost identical to its PL spectra with slight blue-shifting of its maximum by 20 nm compared to its PL spectra.

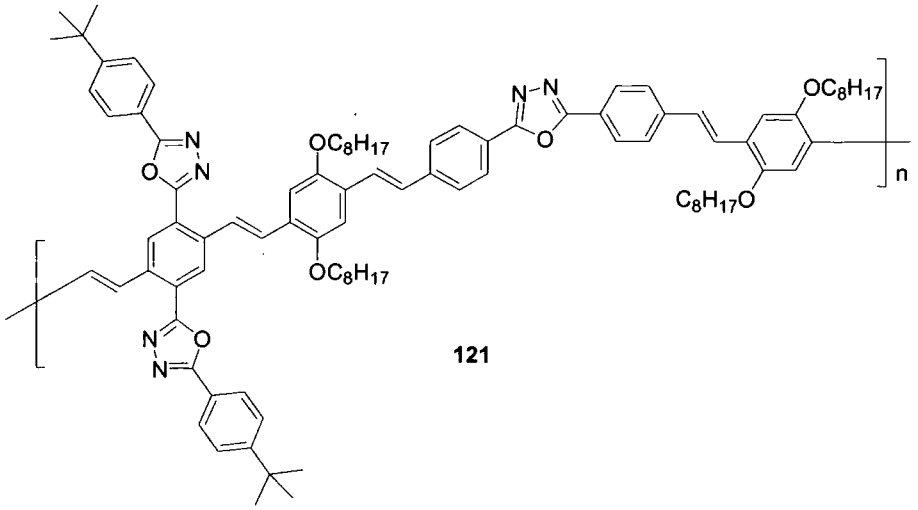

121

Scheme 54: Polymer 121 prepared by Peng *et al.*[117]

Polymer **121** devices with Al as the cathode showed EQE of 0.07%. This value is 30 times greater than for the reference PPV polymer **116** and more than twice that of polymer **118**, but lower than the main chain OXD-PPV polymer **119**. With Ca as the cathode, a higher EQE of *ca.* 0.15% and a lower turn-on voltage of 7 V compared to *ca.* 10 V for the Al device was achieved.

Chen *et al.*[118] prepared two PPV based polymers **122-123** functionalised with OXD side chains mimicking the chemical structure of PBD **5**.

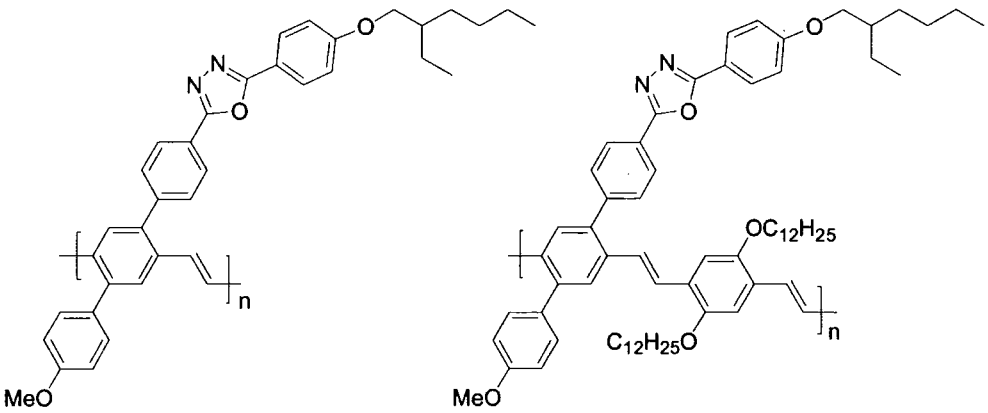

122 **123**

Scheme 55: OXD side chain PPV polymer 122 and 123.[118]

Polymer **122** could not be dissolved in any conventional solvents, therefore the 1:1 copolymer **123** was synthesised with a block containing two long alkoxy side chains. The copolymer **123** was soluble in common solvents and displayed high stability with an onset for degradation at 386 °C and a high T_g of 205 °C, which is rarely the case for PPV derivatives such as MEH-PPV. When excited at 426 nm, PL spectra of copolymer **123** showed λ_{max} = 560 nm, corresponding to orange-yellow light.

Bao *et al.*[115] synthesised the organic soluble polymer **124** bearing pendant OXD groups. Devices in the configuration ITO/**124**/Al exhibited EQEs of 0.2% at a current density of *ca.* 8 mA cm^{-2}.

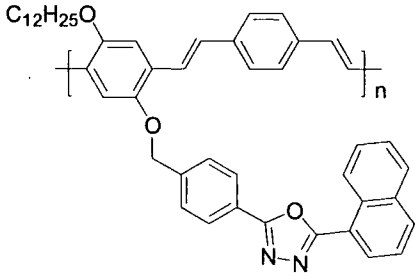

124

Scheme 56: Polymer 124 prepared by Bao *et al.*[115]

Lee *et al.*[119] reported the PPV derivatives **125** and **126**. The 2-ethylhexyloxy group of **126** may increase interchain distances.

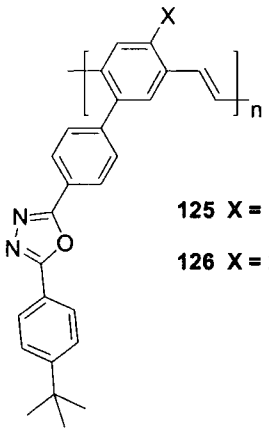

125 X = H

126 X = 2-Ethylhexyloxy

Scheme 57: Molecular structures of pendant OXD-PPV derivatives125-126.[119]

Excitation at 420 nm gave PL λ_{max} of 530 nm and 534 nm for polymer films of **125** and **126**, respectively, which are comparable with λ_{max} of 540 nm for films of PPV. Devices in the configuration ITO/**125** or **126**/Al displayed EL corresponding to their PL spectra and had EQEs 16 and 56 times greater, respectively, than that of PPV devices. In particular, the optimised device ITO/PEDOT:PSS/**126**/Al:Li revealed a maximum luminance of 1090 cd m^{-2} with an EQE of 0.045%. The presence of the bulky alkoxy pendant in polymer **126** increased device performance over polymer **125**. This was consistent with an earlier report, that long or bulky substituents enhance device efficiency by reducing the possibility of the formation of interchain polaron pairs.[120]

A new series of asymmetric PPV based homopolymers, as well as copolymers containing OXD pendant groups, were synthesised by Kim *et al.*[121] Bilayer devices incorporating polymers **127a-g** were fabricated in the configuration ITO/PEDOT:PSS/**127a-**

g/Al. Electrooptical properties and device performance could be adjusted by introducing the OXD-PPV content in the copolymers.

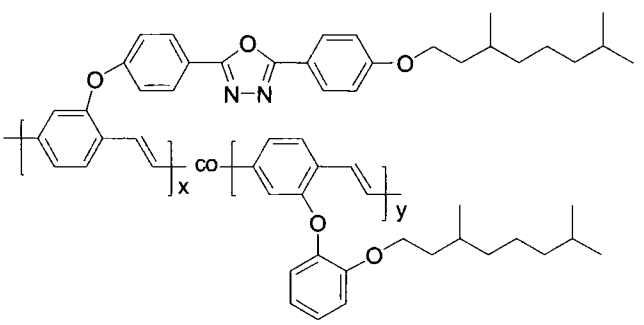

127 a: x = 100, y = 0
b: x = 84, y = 16
c: x = 64, y = 36
d: x = 51, y = 49
e: x = 28, y =72
f : x = 7, y =93
g: x = 0, y =100

Scheme 58: Homopolymers 127a, 127g and copolymers 127b-f prepared by Kim *et al.*[121]

As the OXD content in the copolymer increased from **127g** to **127a** the device performance was significantly increased. The luminance efficiency of the copolymer **127b** was 41 times higher than that of the homopolymer **127g**. The maximum brightness was achieved for the homopolymer **127a** and was found to be 19,395 cd m^{-2} at 14 V, the luminance efficiency was recorded at 21.1 cd A^{-1} at 5,930 cd m^{-2} and was 88 times higher than that of the homopolymer **127g.** The emission colours could be tuned from green to yellowish-orange from **127g-a** via intramolecular energy transfer.

The improved device performance of the PPV-OXD homopolymer **127a** over **127g** and the copolymers **127b-f** was attributed to better electron injection and charge balancing and also efficient intramolecular energy transfer from the OXD units to the PPV backbone. The maximum luminance efficiency of **127a** was ranked the highest value amongst PPV derivatives at the time of publishing.

Kim and co-workers[122] synthesised a novel highly efficient oxadiazole-PPV polymer **128** with oxadiazole units on the vinyl unit. Polymer **128** was expected to have highly twisted chain conformations because of the bulky oxadiazole units. Such chain conformations are expected to minimize chain interactions, which are well known to lower the efficiency of EL and PL.[123]

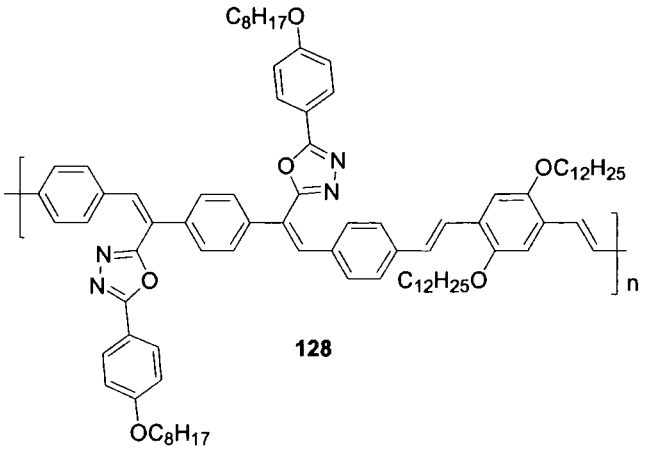

128

Scheme 59: Oxadiazole-PPV polymer 128 prepared by Kim and co-workers.[122]

Devices in the configuration ITO/PEDOT:PSS/**128**/Al displayed bright yellow emission with an EL maximum λ_{max} = 563 nm, which was almost identical to that of the PL maximum. Maximum EQEs of 0.34% at 11 V and 0.077A cm^{-2} and a maximum luminance of 1,457 cd m^{-2} at 13 V and 0.22 A cm^{-2} were recorded for this device. When the Al cathode was replaced with Ca a slight improvement in EL efficiency was observed with an EQE of 0.43% at 11 V (0.25 A cm^{-2}) and a maximum luminance of 5,140 cd m^{-2} at 12.5 V (0.61 A cm^{-2}).

1.4.3.6 Fluorene-Oxadiazole Hybrid Side Chain Polymers

Wu and co-workers[124] displayed further use of OXD pendant groups. Polymer **129** was synthesised by attaching two OXD groups onto the C-9 position of the alternating fluorene units. This 3-D structure was designed to restrict π-stacking between polymer chains and suppress the formation of excimers in the solid state.

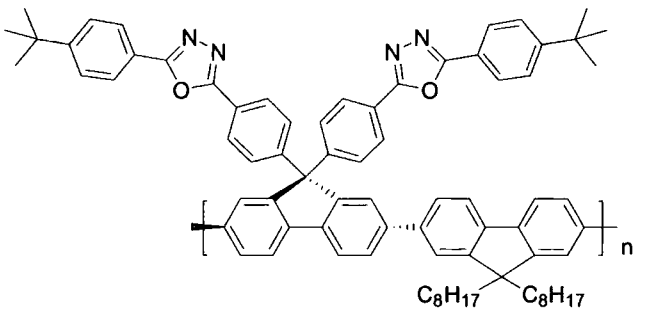

129

Scheme 60: Fluorene-OXD polymer 129 prepared by Wu and co-workers.[124]

Also the sp^3 carbon (C-9) serves as a spacer to effectively block the conjugation between the OXD side chains and the fluorene backbone, therefore maintaining the conjugation and integrity of the main chain polyfluorene emission spectrum.

The EL properties of polymer **129** were examined using the device configuration ITO/PEDOT:PSS/**129**/Ca/Ag. The EL at λ_{max} = 428 nm was identical to the PL spectrum. No undesirable excimer/aggregate/oxidation emission was observed at long wavelength which is a known problem with PFO **132** (Chapter 2). The device displays strong blue emission with a low turn-on voltage at 5.3 V and a high brightness of 2770 cd m^{-2} at 10.8 V. A maximum EQE of 0.52% at 537 cd m^{-2} at a voltage of 7.4 V was recorded. This device based on polymer **129** demonstrated a much higher brightness and efficiency than devices based on PFO **132**, which had a maximum brightness around 600 cd m^{-2} and an EQE of 0.2%.[125] This improved performance was due to increased electron injection and transport in polymer **129** and efficient energy transfer from the OXD side chains to the polyfluorene backbone.

A series of soluble alternating fluorene based copolymers, **130** and **131a-g**, containing symmetrical and asymmetrical OXD pendants with various terminal groups were synthesised by Sung and Lin.[126] A series of devices in the configuration ITO/PEDOT:PSS/polymer/Ca/Al were fabricated.

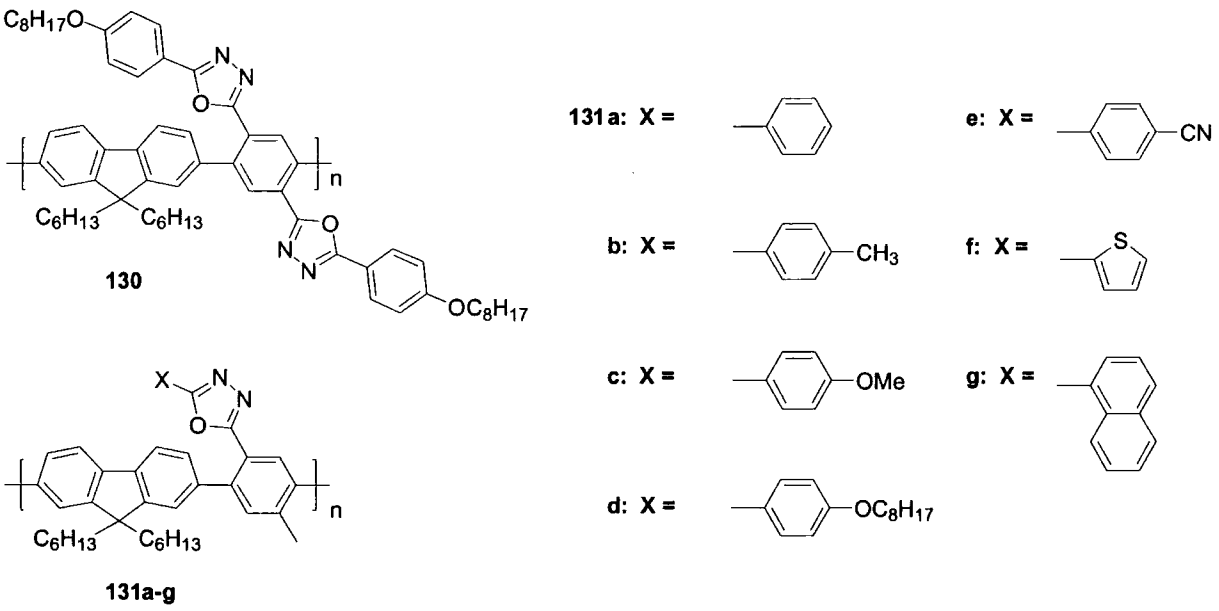

Scheme 61: Fluorene OXD polymers 130 and 131a-g synthesised by Sung and Lin.[126]

All of the devices show turn on voltages between 7 and 9 V; the maximum attainable luminance was 462 cd m^{-2} at 15 V with polymer **131g** as the emitter. All the asymmetrical OXD-substituted polymers **131a-g** displayed purple to blue emission with EL λ_{max} between 406 and 452 nm, which are well matched with their PL spectra. In contrast, the symmetrical polymer **130** displayed slight voltage dependent EL. Since the absorption and fluorescence data reveal that polymer **130** forms excimers due to aggregation in the solid film, the EL spectra of **130** is red-shifted and become broader by increasing the voltage. By comparison of

polymers **130** with **131d** it was observed that the asymmetrically substituted polymers possess better device properties (higher quantum yield and lower aggregation in the solid state) than the symmetrical substituted polymer **130**.

1.5 CONCLUSIONS

Since pioneering work employing PBD as an ETHB material in thin bilayer devices[12] and the discovery that organic conjugated polymers such as PPV could be used as emissive materials in OLEDs,[1] 1,3,4-oxadiazoles have been widely studied as ETHB materials in OLED applications. This chapter has reviewed and updated published work, although not exhaustively, on low molecular weight and polymeric 1,3,4-oxadiazoles demonstrating their wide functionalisation, molecular architecture and application in OLEDs, predominantly as ETHB materials but also as bipolar and emissive materials. Applications as liquid crystal and electrochromic materials have also been highlighted.

2 NEW 2,5-DIARYL-1,3,4-OXADIAZOLE-FLUORENE HYBRIDS

2.1 INTRODUCTION

As discussed in Chapter 1, 2,5-diaryl-1,3,4-oxadiazole derivatives have been widely studied in diverse areas of chemistry. In particular, owing to the electron deficient nature of the 1,3,4-oxadiazole ring, luminescent properties and excellent thermal and chemical stability, a range of OXD derivatives have been applied as emissive and/or ETHB materials in OLEDs.

At the outset of my work there were very few examples of covalent combinations of fluorene and OXD units. Therefore, it was timely in the search for new materials with balanced hole and electron transport properties to target novel fluorene-OXD hybrids. Many examples of such systems have been synthesised and their optoelectronic and OLED properties investigated.

2.1.1 Poly(fluorenes)

The first blue emitting PLED was made by Yoshino *et al.*[127] using poly(9,9-dihexylfluorenyl-2,7-diyl) **133**, since then poly(9,9-dialkyfluorene)s (PF)s have been widely studied as they are promising blue-light emitting materials for PLED applications due to their thermal stablity,[128] high PL quantum yields[129] and good charge transport properties.[130,131]

PFs are derivatives of poly(*para*-phenylene)s (PPP)s which fit into a class of rigid-rod blue light emitting polymers.[6,132] The extended conjugation characteristic of this class of materials enhances charge delocalisation by virtue of the greater molecular planarity attained along their rigid backbones. For PFs the bridging C-9 atom between the alternate pairs of phenyl rings rigidly planarises the biphenyl structure in the fluorene monomer. This delocalisation influences the polymer's physical properties including band gaps and emission quantum yields.[133] Also facile functionalistion at C-9 offers the ability of controlling polymer solubility, without significant effects on the electronic structure of the backbone,[134] and potential interchain interactions in films.[123,135]

The physical properties of PFs can be fine tuned through chemical structure modifications and copolymerisation, for example, to give EL emission across the full visible spectrum from blue to red, unlike the more widely studied PPVs.[134] A portfolio of fluorene copolymers that emit colours across the full visible spectrum has been prepared using Suzuki

couplings at Dow Chemical Company.[136] No other polymer class, to date, offers the full range of colours with high efficiency, low operating voltages and high device lifetime. Thus polyfluorene based molecules are amongst the most viable light emitting polymers (LEP)s for commercialisation.[137]

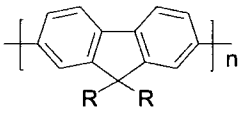

132 R = C_8H_{17} PFO
133 R = C_6H_{13}

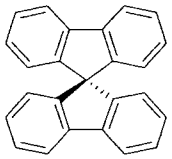

134

Scheme 62: Poly(9,9-dioctylfluorenyl-2,7-diyl) PFO 132, poly(9,9-dihexylfluorenyl-2,7-diyl) 133 and spirobifluorene 134.

However, PF based LEDs typically exhibit device degradation under operation with the emergence of a low-energy emission band (at ~2.2-2.4 eV). This longer wavelength band converts the desirable blue emission to greenish blue with an increase in broadband emission tailing.[138] Numerous groups have reported the appearance of this red-shifted component in the luminance spectra of a range of PF homo- and copolymer thin films.[128,131,139] The origin of this low energy emission band has been attributed to reordering of the polymer chains and subsequent aggregate or excimer formation.[109,125,135a,139e,140] However, recently several research groups[138,139g,141] have ascribed this emission to fluorenone defects produced by thermo-, photo-, or electro-oxidative degradation.[142] Sims *et al.*[134] concluded that whilst these fluorenone defects are necessary to activate the green band emission, they are not considered to be sufficient alone. The green band emission was attributed to fluorenone-based excimers. Although a number of possible mechanisms have been suggested, the origin of the longer wavelength band is the subject of ongoing study.

2.1.2 Spirobifluorene

An approach to improve the spectral stability of PFs is the introduction of a spiro structure. The tetrahedral bonding atom at the centre of **134** maintains a 90° angle between the connected biphenyl units via a σ-bonded network. It has been shown that the introduction of spiro linkages in low molecular weight organic materials (compound **38**) improves processability as well as morphological stability.[54] Also the bulky structure minimises the close packing of the spiro-annulated molecules in the solid state, therefore suppressing excimer formation in comparison with fluorene compounds.[143,144] Also this molecular

architecture is anticipated to reduce fluorenone defects as the susceptability for oxidation at the C-9 position of spirobifluorene should be decreased.

Kim *et al.*[145] reported a device incorporating 9,10-bis[(2,7-di-^{t}butyl)-9,9-spirobifluorenyl] anthracene as the EML which exhibited pure blue emission (x = 0.14, y = 0.08) at 300 cd m^{-2} in CIE chromaticity coordinates, which was the nearest to the National Television Standards Committee (NTSC) standard value reported at the time of publication. Also, no tailing in the longer wavelength region was observed. Wu *et al.*[146] reported devices incorporating a ter(spirobifluorene) compound that that did not exhibit any change in its EL spectra after continuous operation for 32 h. Similarly, Katsis and co-workers[147] observed no changes in morphology, emissive colour and PL quantum yield on heating spiro-oligo(fluorene) films.

Several groups have demonstrated that spirobifluorene-fluorene copolymers exhibited better colour stability than PFs with a reduction in longer wavelength emission following thermal treatment.[148] Also Wu *et al.*[149] reported a poly(spirobifluorene) which exhibited good luminescent stability with no green band emission observed in solid films after annealing for 3 h at 200 °C.

2.1.3 Fluorene-OXD Hybrids

The combination of poly(9,9-dihexylfluorene) **133** as an EML and an OXD derivative (PBD **5**) as an ETL was first described by Ohmori *et al.*[150] in a triple layer structure, also utilising TPD **6** as a HT material. Since then various fluorene-OXD small molecule[47,51,54,55] and polymeric[108,110,124,126] hybrids have been reported in the literature. Preliminary work within our group by Dr Wang[50] involved the synthesis of the fluorene-oxadiazole hybrid DFD **34** with a 1,3,4-oxadiazole moiety to confer electron injection and a fluorene moiety to provide blue emission. As stated in Chapter 1, it was established that DFD is an efficient ETHB material when used as a dopant in MEH-PPV in single layer devices.

Following these initial results we targeted a new series of fluorene-OXD hybrids and explored the effect of inserting additional phenyl rings into the backbone. We also investigated the effects of replacing the 9,9-dihexylfluorene core with spirobifluorene in an effort to eliminate the formation of fluorenone defects, which is a factor that can quench emission and impair device performance. Also further functionalisation of the OXD system has been carried out to afford the carbaldehyde compound **172**, which allowed further extension of these systems via Wittig chemistry. This chapter reports the synthesis of the

linearly extended conjugated ETHB compounds, namely **165**, the spirobifluorene analogue **171** and compound **177**, along with crystal structures of **165**, *ab initio* calculations, optical absorption, PL spectra, and OLED studies of compounds **165**, **171** and **177** blended with MEH-PPV to enhance electron injection.

2.2 RESULTS AND DISCUSSIONS

2.2.1 Synthesis

Our initial aim was to synthesise compound **140**, which from a synthetic viewpoint will offer excellent scope for functionalisation reactions which extend the π-conjugation leading to novel materials for ETHB applications.

The aroyl hydrazide **138** was prepared in high yields via the aminolysis of the commercially available methyl ester **137**.[151] Nucleophilic reaction of **138** with the acid chloride **136**, obtained from the corresponding benzoic acid **135**, yielded the diaroyl hydrazine **139**, which was not purified. The crude product **139** was cyclodehydrated using $POCl_3$[30] to give the 2,5-diaryl-1,3,4-oxadiazole **140** (76% yield). During the course of our work the preparation of **140** was described by other workers.[29e]

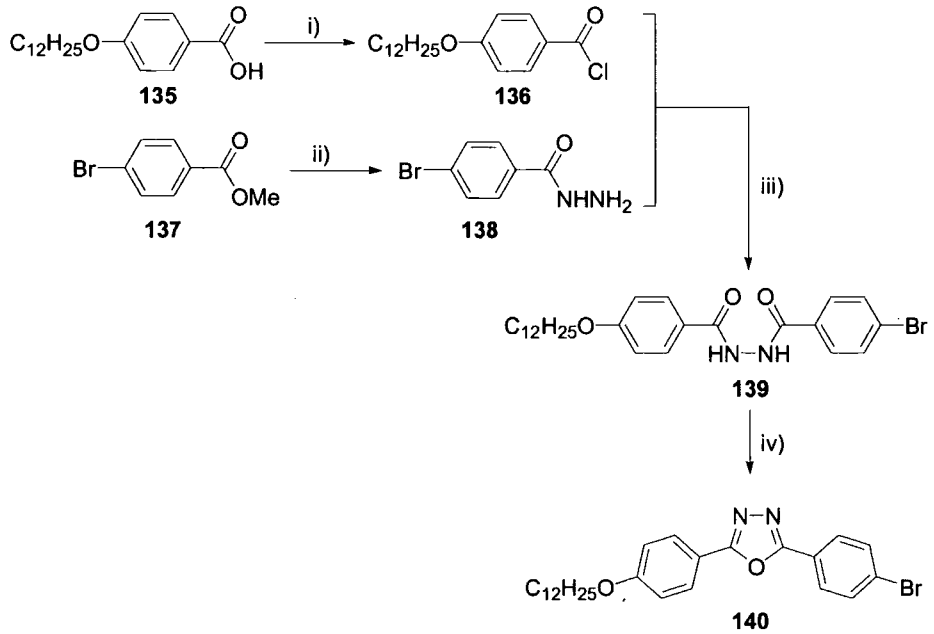

Scheme 63: Synthesis of 2-(4-bromophenyl)-5-(4-dodecyloxyphenyl)-1,3,4-oxadiazole 140: i) $SOCl_2$, Δ; ii) $NH_2NH_2.H_2O$, CH_3OH, Δ; iii) pyridine, 20 °C 0.5 h, Δ 0.5 h; iv) $POCl_3$, Δ.

The dodecyloxy chain of OXD **140** was attached to introduce solubility to the system for ease of purification and to allow further reactions to take place in common solvents. The bromine handle allows for further functionalisation via numerous aryl-coupling techniques.

It was initially attempted to convert the bromo substituted OXD **140** into the corresponding boronic acid **141** via lithiation at –78 °C, quenching with trialkyl borate and aqueous work up followed by acidification (Scheme 64).

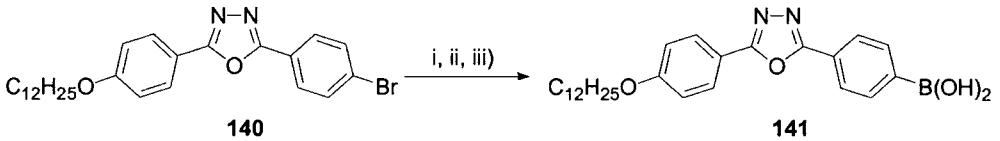

140 **141**

Scheme 64: Attempted synthesis of boronic acid analogue 141: i) *n*-BuLi, THF, -78 °C; ii) TIPB, -78 °C → 20 °C; iii) HBr/H_2O.

Although the ^{1}H NMR spectrum of the crude product showed a peak at *ca.* 9 ppm which disappeared on addition of D_2O (as would be expected for a boronic acid group), low yields were consistently obtained and further purification was not successful. In a revised procedure a suspension of **140** and *n*-BuLi in THF was maintained at -40 °C for 4 h in an attempt to drive lithiation to completion before quenching with triisopropyl borate (TIPB). This led to a darkening of solution, which was attributed to side reactions as no material precipitated out of the aqueous solution on acidification. Upon analysis it was observed that the organic layer contained starting material.

It was established that 1 mmol of compound **140** in 25 ml of THF would remain in solution at temperatures as low as -40 °C, but rapidly precipitated out of solution at lower temperatures; the above procedure was then repeated at -30 and -20 °C but again the reaction failed. Attempts using triethyl borate instead of TIPB at -78, -40, -30 and -20 °C were carried out, but as before, no material precipitated out of the aqueous solution on acidification and unreacted starting material was present in the organic layer.

The electron withdrawing effect of the oxadiazole unit could be the reason for lithiation problems; therefore, two methoxy groups *ortho* to the bromine were introduced into compound **145** to act as electron donors, to counter the electron withdrawing effect of the oxadiazole unit.

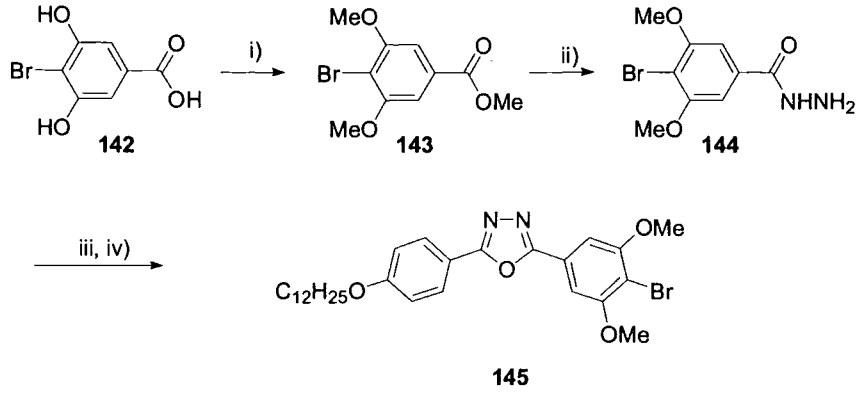

Scheme 65: Synthesis of dimethoxy analogue 145: i) K_2CO_3, dimethylsulphate, acetone, Δ; ii) $NH_2NH_2.H_2O$, CH_3OH, Δ; iii) 4-dodecyloxybenzoic acid chloride 136, pyridine, 20 °C 0.5 h, Δ 0.5 h; iv) $POCl_3$, Δ.

4-Bromo-3,5-dimethoxybenzoic acid methyl ester **143** was prepared in high yields (80%) via the methylation of 4-bromo-3,5-dihydroxybenzoic acid **142** with dimethylsulphate and K_2CO_3 in dry acetone.[152,153] Compound **143** was then converted to the hydrazide **144** (77%) via aminolysis with hydrazine monohydrate. Following the same procedure for the synthesis of **140**, compound **144** was dissolved in pyridine and reacted with the acid chloride **136.** The intermediate hydrazine was then cyclised with $POCl_3$ to give 2-(3,5-dimethoxy-4-bromophenyl)-5-(4-dodecyloxyphenyl)-1,3,4-oxadiazole **145** (73%).

Attempted boronic acid formation from **145** with *n*-BuLi, trialkylborate and HBr failed at -78, -40, -30 and -20 °C, as previously for **140**, with only starting material recovered from the organic layer. Trialkylborate was added before *n*-BuLi in one experiment to trap the lithiated species but this reaction also failed with only starting material recovered.

Although we were unable to prepare the boronic acid derivative of **145**, further functionalistion via a Suzuki coupling reaction with 4-formylbenzene boronic acid **146** was achieved, yielding compound **147**, which is expected to contain a highly twisted biaryl unit.[154]

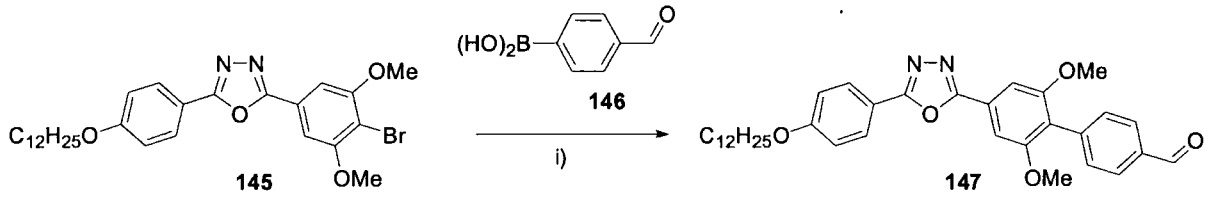

Scheme 66: Synthesis of compound 147: i) $Pd(PPh_3)_4$, Na_2CO_3, THF, Δ.

Following a literature preparation of the diphenyloxazole boronic acid derivative 5-(4-dimethylaminophenyl)-2-[4-(dihydroxyboranyl)phenyl]oxazole,[155] we attempted to synthesise the OXD-boronic ester derivative.

Compound **135** was converted into the corresponding methyl ester **148**[156] via acid-catalysed esterification in high yield (94%); this was then converted into the corresponding hydrazide **149**[157] (90%) as previously for compounds **138** and **144**.

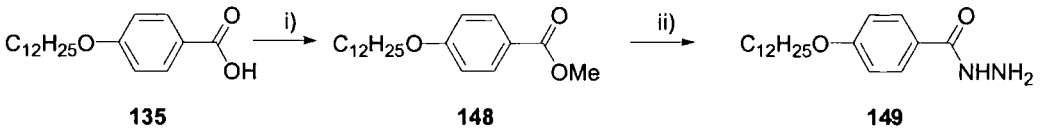

135 **148** **149**

Scheme 67: Synthesis of 4-dodecyloxybenzoic acid hydrazide 149: i) H_2SO_4, MeOH, Δ 12 h; ii) $NH_2NH_2.H_2O$, CH_3OH, Δ.

The commercially available 4-(4,4,5,5-tetramethyl-1,3,2-dioxaborolan-2-yl)benzoic acid **150** was treated with $SOCl_2$. The hydrazide **149** in pyridine was subsequently added. In the ^1H NMR spectrum of the product, no N-H protons were observed indicating that the reaction had possibly failed although peak broadening could not be ruled out. Attempted cyclisation carried out in $POCl_3$ established that the reaction had indeed failed.

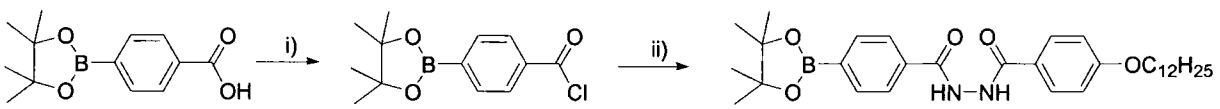

150 **151** **152**

Scheme 68: attempted synthesis of boronic ester 152: i) $SOCl_2$, ii) 4-dodecyloxybenzoic acid hydrazide 149, pyridine, 20 °C 0.5 h, Δ 0.5 h.

Although we were unable to prepare the OXD boronic acid analogue **141**, further functionalisation of the OXD system was readily achieved via Suzuki coupling with various aryl and heterocyclic boronic acids, demonstrating that compound **140** is a versatile reagent. Benzene boronic acid **153** and 3-methoxybenzene boronic acid **154** were coupled with OXD compound **140** under standard Suzuki conditions to give compounds **157** and **158** in 71 and 85% yields, respectively. Similarly, Suzuki couplings of compound **140** with the heterocyclic boronic acids, 2-furaldehyde-5-boronic acid **155**[158] and 2-methoxy-5-pyridyl boronic acid **156**[159] (both prepared by Dr Parry in our group) afforded compounds **159** and **160** in 28 and 68% yields, respectively.

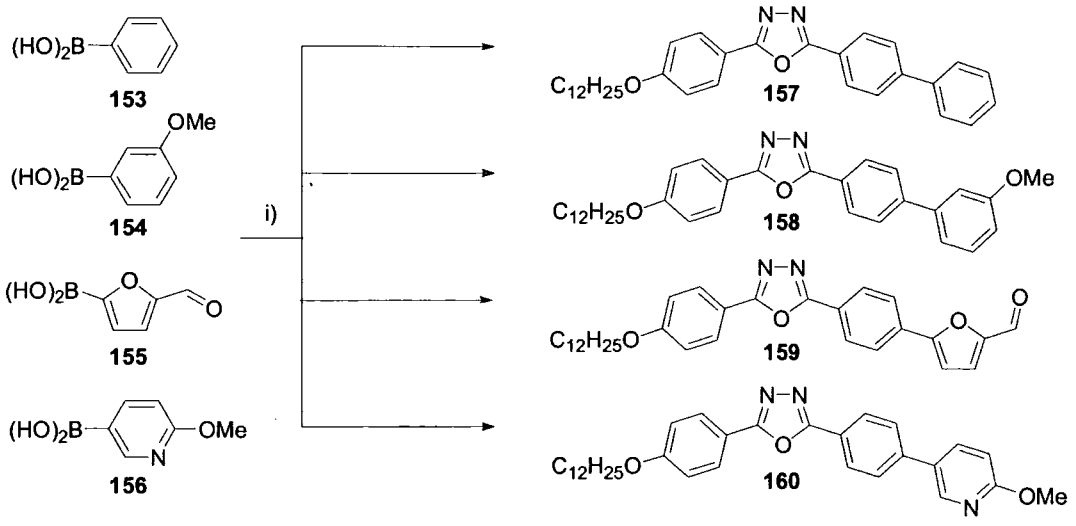

Scheme 69: Suzuki cross-coupling of compound 140: (i) 140, $Pd(PPh_3)_4$, Na_2CO_3, DMF/THF, Δ.

Having established suitable conditions for Suzuki couplings of **140**, our attention then turned to the synthesis of OXD-fluorene hybrids. 2,7-Dibromofluorene **162** was prepared in 65% yield from bromination of the commercially available fluorene **161** in an acetic/sulphuric acid mixture with an excess of bromine.[160] 9,9-Dihexyl-2,7-dibromofluorene **163** was then obtained in 82% yield from **162** by deprotonation with potassium *t*-butoxide followed by two-fold alkylation with bromohexane in THF.[161] This route was preferred to the protocol reported by several other groups[162] (*viz.* alkylation followed by bromination) as we prepared 2,7-dibromofluorene **162** on a large scale (1.5 mole) and subsequently alkylated smaller batches (50 mmol) when needed. This route also avoided possible bromination of the aliphatic chains, a difficulty in the alternative route.

9,9-Dihexylfluorene-2,7-diboronic acid **164,** a key reagent in the synthesis of fluorene based luminophores via Suzuki couplings, was obtained in 61% yield from **163** by reaction with *n*-BuLi and TIPB, followed by aqueous work up.[163,164]

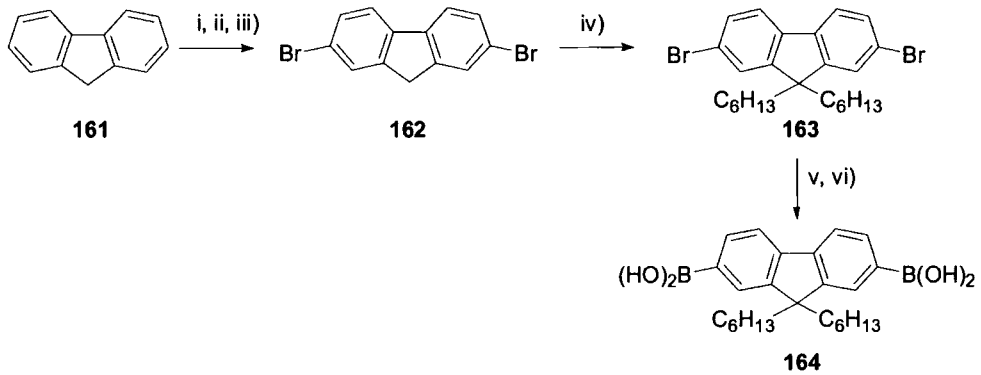

Scheme 70: Synthesis of 9,9-dihexylfluorene-2,7-diboronic acid 164: i) acetic acid/H_2SO_4; ii) bromine; iii) $KBrO_3$/acetic acid, T< 50 °C; iv) 1-bromohexane, *t*-BuOK, THF, 0 °C→ 20 °C; v) *n*-BuLi, THF, -78 °C; vi) TIPB, -78 °C → 20 °C, H_2O.

The two-fold reaction of compound **140** with 9,9-dihexylfluorene-2,7-diboronic acid **164** under standard palladium-catalysed Suzuki cross-coupling conditions afforded the linearly extended π-conjugated fluorene-OXD hybrid compound **165** in 44% yield.[27]

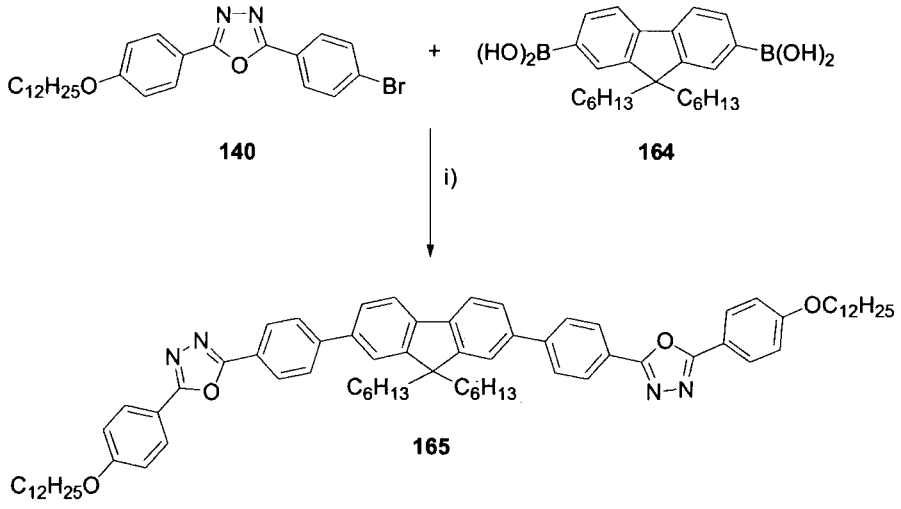

Scheme 71: Synthesis of 165: (i) $Pd(PPh_3)_4$, Na_2CO_3, THF, Δ.

We next targeted the spirobifluorene analogue of **165**. 9,9-Spirobifluorene was first synthesised by Clarkson and Gomberg[165] via Grignard reaction of 2-biphenylmagnesium iodide with fluorenone, yielding the tertiary alcohol, followed by a sulphuric acid promoted Friedel-Crafts cyclisation. Recently this method has been applied in the synthesis of 2-bromo- and 2,7-dibromospirobifluorene, via 2-bromo- and 2,7-dibromofluorenone.[166] This route was preferred to subsequent electrophilic bromination of spirobifluorene due to the purification problems of 2-bromospirobifluorene; also dibromination of spirobifluorene only occurs at the 2,2'-positions instead of the desired 2,7-positions.

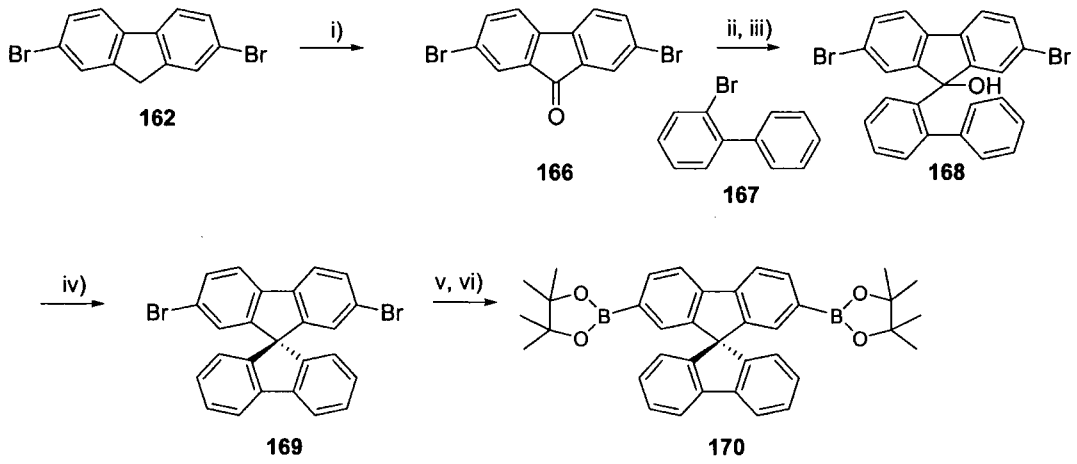

Scheme 72: Synthetic route to 2,7-di(4,4,5,5-tetramethyl-1,3,2-dioxaborolan-2-yl)spirobifluorene 170: (i) CrO_3, AcOH, Δ; (ii) 2-bromobiphenyl 167, *t*-BuLi, THF, -78 °C; (iii) 166, -78 °C→ 20 °C; (iv) HCl, AcOH, Δ; (v) *n*-BuLi, THF, -78 °C; (vi) 2-isopropoxy-4,4,5,5-tetramethyl-[1,3,2]-dioxaborolane -78 °C → 20 °C.

Instead of the Grignard route to **170**, we proposed to use lithium-halogen exchange of commercially available 2-bromobiphenyl **167** as described in the literature for 2-iodobiphenyl.[167] 2,7-Dibromofluorenone **166** was prepared in 79% yield by oxidation of 2,7 dibromofluorene **162** with chromium trioxide (Scheme 72).[168]

Lithium-halogen exchange of 2-bromobiphenyl **167** in THF was carried out via the addition of 2 equivalents of *t*-BuLi at -78 °C. The reaction was then quenched with 2,7-dibromofluorenone **166** to give carbinol **168**. Dehydrative cyclisation of **168** was then carried out with HCl in acetic acid yielding 2,7-dibromospirobifluorene **169** (72% yield). The dipinacolato boronic ester **170** was prepared in 58% yield via lithiation of **169** with *n*-BuLi, followed by quenching with 2-isopropoxy-4,4,5,5-tetramethyl-[1,3,2]-dioxaborolane.[166b]

The two-fold reaction of compound **140** with dipinacolato boronic ester **170** under palladium catalysed Suzuki cross-coupling conditions utilising tri-*t*-butyl phosphine afforded the spirobifluorene-OXD hybrid compound **171** in 40% yield.[27]

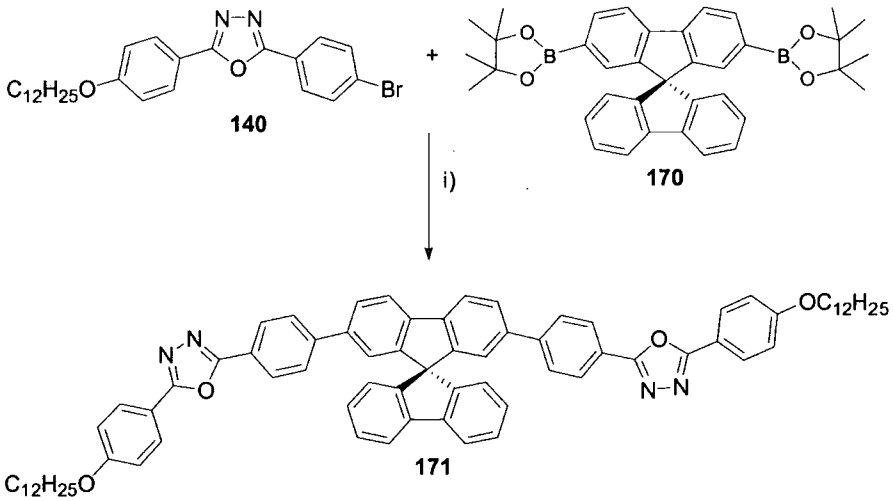

Scheme 73: Synthesis of compound 171: i) $Pd(PPh_3)_4$, PBu^t_3, K_2CO_3, Toluene, Δ.

As demonstrated in our exploratory Suzuki coupling studies (Scheme 69), a formyl group can be introduced onto the OXD unit (compound **159**), allowing for further functionalisation by Wittig chemistry. We, therefore, attached a *para*-formylphenyl unit via Suzuki coupling so that further extension of the conjugated system could be carried out. Compound **140** was coupled with 4-formylbenzene boronic acid **146** under standard palladium-catalysed Suzuki cross-coupling conditions to give 4'-[5-(4-dodecyloxyphenyl)-1,3,4-oxadiazol-2-yl]-biphenyl-4-carbaldehyde **172** in good yield (78%).

We initially tested compound **172** for its suitability in Wittig coupling with the simplest aryl triphenylphosphonium salt. The reaction between **172** and

benzyltriphenylphosphonium chloride employing NaOH as the base yielded 2-(4-dodecyloxyphenyl)-5-(4'-styryl-biphenyl-4-yl)-1,3,4-oxadiazole **173** (51%).

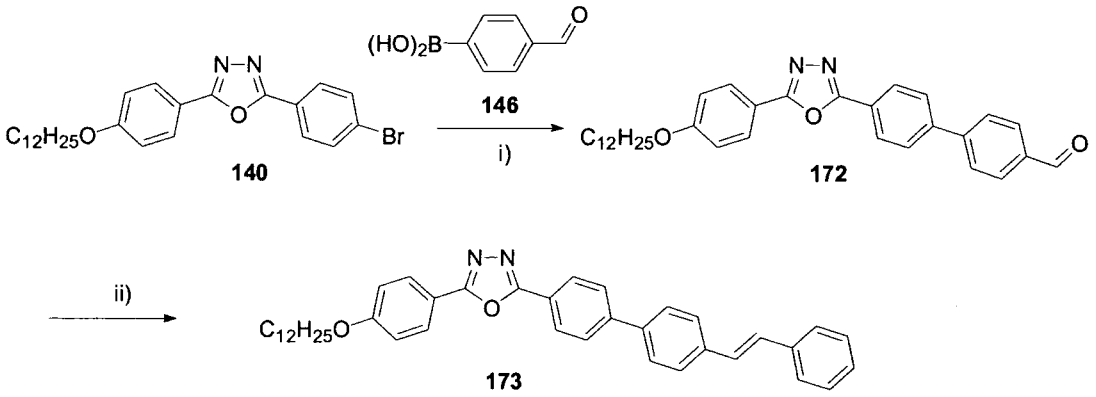

Scheme 74: Synthesis of compounds 172 and 173: (i) 146, $Pd[PPh_3]_4$, Na_2CO_3, THF, Δ; ii) benzyltriphenylphosphonium chloride, NaOH, THF.

To achieve further extension of the π-electron framework, compound **177** was prepared by two-fold Wittig reaction of compound **172** and the bis(triphenylphosphonium) salt **176**.[169] Compound **177** comprises two OXD moieties and a central fluorene moiety connected via phenylvinylene units.

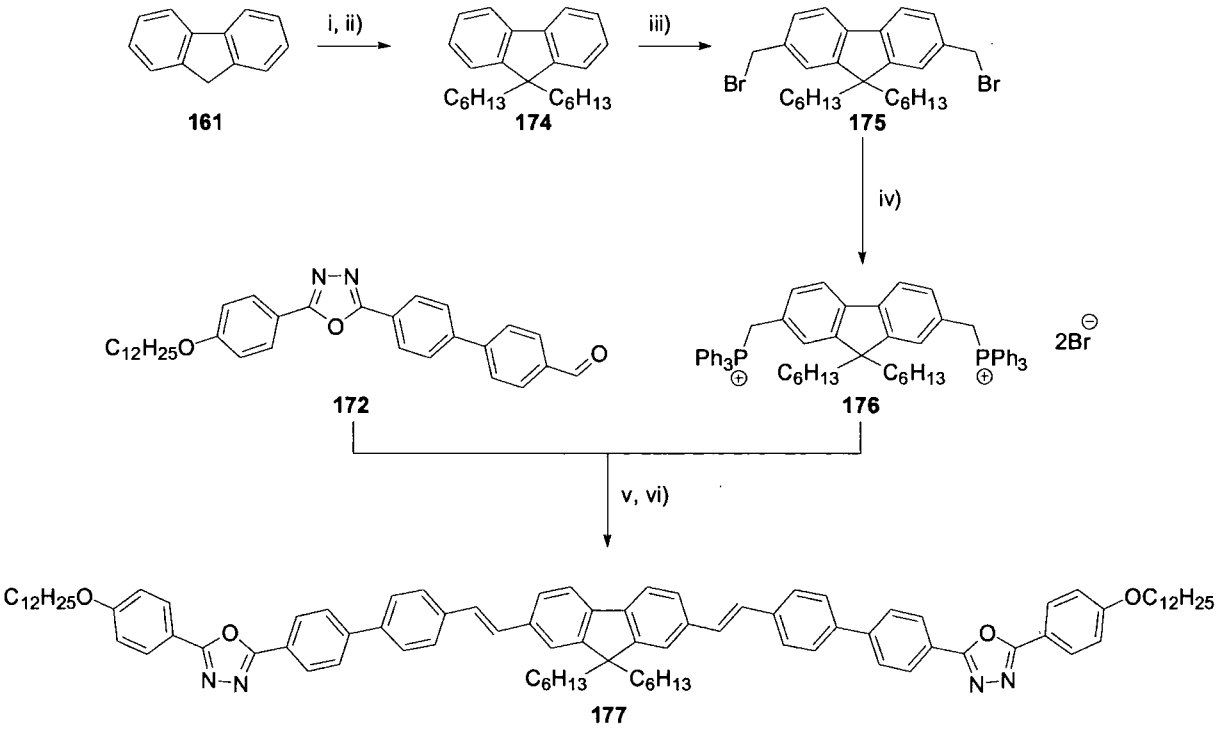

Scheme 75: Synthesis of the bis(triphenylphosphonium) salt 176 and compound 177: (i) *n*-BuLi, THF, -78 °C; (ii) bromohexane, -78 °C→ 20 °C; (iii) paraformaldehyde, HBr (33% in glacial acetic acid), Δ; (iv) triphenylphosphine, DMF, Δ; (v) NaOEt, EtOH/THF; (vi) HCl.

9,9-Dihexylfluorene **174** was synthesised according to the literature procedure.[170] The acidic protons at the 9-position of fluorene **161** were removed by lithiation with *n*-BuLi, followed by alkylation with 2 equivalents of bromohexane to give compound **174** (81%). Bromomethylation of **174** was carried out following the literature preparation[169] with paraformaldehyde and HBr in acetic acid to give 2,7-bis(bromomethyl)-9,9-dihexylfluorene **175** in 78% yield. The bis(triphenylphosphonium) salt **176** was prepared in 60% yield by treatment of 2,7-bis(bromomethyl)-9,9-dihexylfluorene **175** with triphenylphosphine in DMF. Finally the carbaldehyde **172** underwent two-fold Wittig reaction with the bis(triphenylphosphonium) salt **176** in freshly distilled dry ethanol and THF with sodium ethoxide as base to afford compound **177** (43%).

9,9-Dihexylfluorene-2,7-dicarbaldehyde[171] has been employed to introduce a fluorene moiety, *via* Wittig reaction, into copolymers, although the synthetic route to the dicarbaldehyde from fluorene involves 5 steps, compared to the bis(triphenylphosphonium) salt route used here (3 steps).

2.2.2 X-Ray Structure of Compound 165

The crystal structure of compound **165** was solved by Dr A. Batsanov. The asymmetric unit of **165** contains one molecule (Figure 6), which has neither crystallographic nor approximate symmetry. The fluorene moiety is planar within ±0.03 Å and forms dihedral angles of 21.9° and 30.3° with the adjacent benzene rings *i* and *iv*. On the contrary, the angles between the oxadiazole and adjacent benzene rings are small, viz. *i/ii* 5.0, *ii/iii* 6.7, *iv/v* 11.4, *v/vi* 9.5°, due to the absence of repulsion between peri-H atoms.

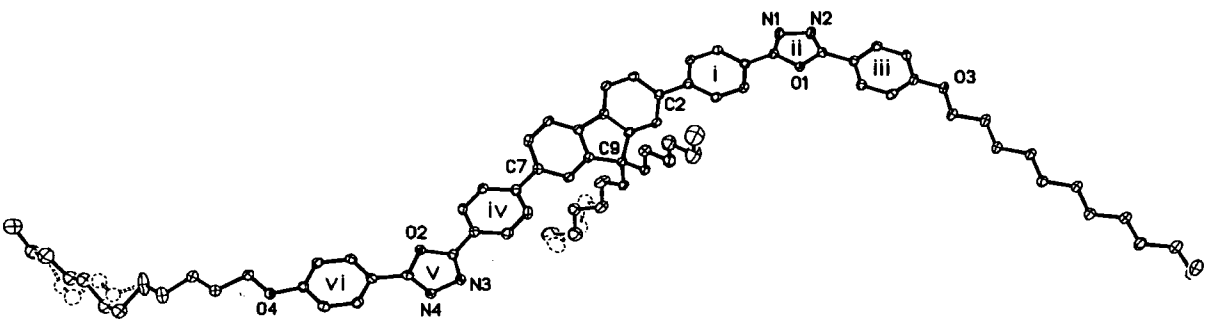

Figure 6: X-ray molecular structure of 165.

Of the two *n*-hexyl substituents at C(9), one is fully ordered and the other has two orientations, A and B. The C_{13} fragment [*n*-hexyl-C(9)-*n*-hexyl] adopts an all-*trans* conformation, except one terminal $CH_2CH_2CH_3$ moiety, which is disordered equally between

trans (A) and *gauche* (B) conformations. The *n*-dodecyl chain attached to O(3) adopts an all-*trans* conformation, except the terminal methyl group which has a *gauche* orientation. In the second *n*-dodecyl chain, four methylene groups are disordered between two positions; in each case one CCCC torsion angle corresponds to a *gauche* conformation and the rest to a *distorted trans* conformation [165.5(2)° to 179.4(4)°, average 171(4)°]. As a result, the former *n*-dodecyl chain is roughly coplanar with the polycyclic part of the molecule and the latter is bent out of this plane. The longest dimension of the molecule (in the crystal) is ca. 54 Å.

2.2.3 Quantum Chemical Calculations

Ab initio calculations were performed by Dr I. F. Perepichka in our group. Density functional theory (DFT) calculations investigated the geometry and the electronic structure of molecules **165, 171** and **177**. For comparison DFD **34** and the widely used ETHB material OXD-7 **28c** were also included.

To decrease the computational time we calculated the molecules **165a, 171a, 177a** (where index "**a**" means that in structures **165, 171** and **177** $C_{12}H_{25}O$ was replaced by CH_3O, and in structures **165** and **177** C_6H_{13} was replaced by C_2H_5; see Appendix 2.1) as well as compound **34a** (where C_6H_{13} was replaced by C_2H_5). Comparison of calculated LUMO energies for compounds **34a, 165a, 171a** and **177a** with that for OXD-7 **28c** shows that compounds **165a** and **171a** as acceptors match very well with **OXD-7** and compounds **34a** and **177a** are even better acceptors (by ca. 0.2 and 0.3 eV, respectively; Figure 7). So, from an energy point of view, compounds **34a, 165a, 171a** and **177a** are good alternatives to **OXD-7** as electron transport materials. On the other hand, all these compounds (**34a, 165a, 171a** and **177a**) have higher HOMO levels, so their function as hole blocking layers in OLEDs could be less efficient [although their HOMOs are still much lower than that of common EL polymers like MEH-PPV (~ –5.0 eV)].

Compound **177a** showed the smallest HOMO-LUMO gap (2.97 eV) and a feature is that its LUMO orbitals are delocalised between the central fluorene moiety and adjacent phenylene units (no LUMO population on the oxadiazole rings), whereas for all other oxadiazole derivatives (**34a, 165a, 171a** and **OXD-7**) substantial localisation of the LUMO is observed on the oxadiazole moieties (see Figure A6, Appendix 2.1).

The calculated HOMO energy for **OXD-7** (–6.27 eV) is quite close to its ionisation potential measured by photoemission studies ($I_p \approx 6.5$ eV, i.e. the difference is only ≈ 0.23

eV),[43] whereas the calculated LUMO energy (–2.03 eV) is higher than found experimentally (by subtraction of the optical gap energy: $E_A \approx I_p$ –3.7 eV ≈ 2.8 eV) by ca. 0.77 eV. In section 2.2.5 this difference between the experimental and calculated LUMO energies is used to moderate conduction band levels when discussing the energy diagram of OLEDs to compare LUMO levels of oxadiazole derivatives with that for MEH-PPV.

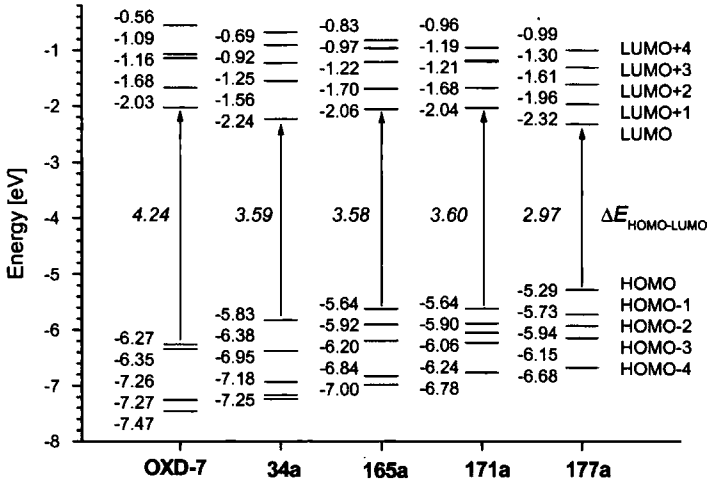

Figure 7: B3LYP/6-311G(2d,p)//B3LYP/6-31G(d) orbital energy level diagrams for compounds 34a, 165a, 171a and 177a in comparison with the ETHB material OXD-7 28c.

2.2.4 Optical Absorption and PL Properties

Solution UV-Vis absorption and photoluminescence (PL) spectra for compound **157**, **160**, **173**, **165**, **171** and **177** were recorded in DCM. The absorption spectra of **157** and **160** are very similar with λ_{max} =313-315 nm. The absorption of compound **173** is red shifted significantly with λ_{max} = 338 nm, which would be expected due to the extended conjugation of the extra phenylvinylene unit.

Compound	UV-Vis Absorption, λ_{max} / nm	PL, λ_{max} / nm
157	313	365, 378
160	315	364, 378
173	338	413
165	356	401, 422
171	356	399, 420
177	397	444, 468

Table 1: UV-Vis absorption and emission λ_{max} values for compound 157, 160, 173, 165, 171 and 177 in DCM, 20 °C.

The PL spectra of **157** and **160** are, as for the absorbance, very similar and are characterised by major peaks at 365 and 364 nm, respectively, and red shifted shoulders at λ_{max} = 378 nm for both compounds. The PL spectrum of **173** is red-shifted compared to **157** and **160** with a peak at λ_{max} = 413 nm, although blue-shifted shouldering is present.

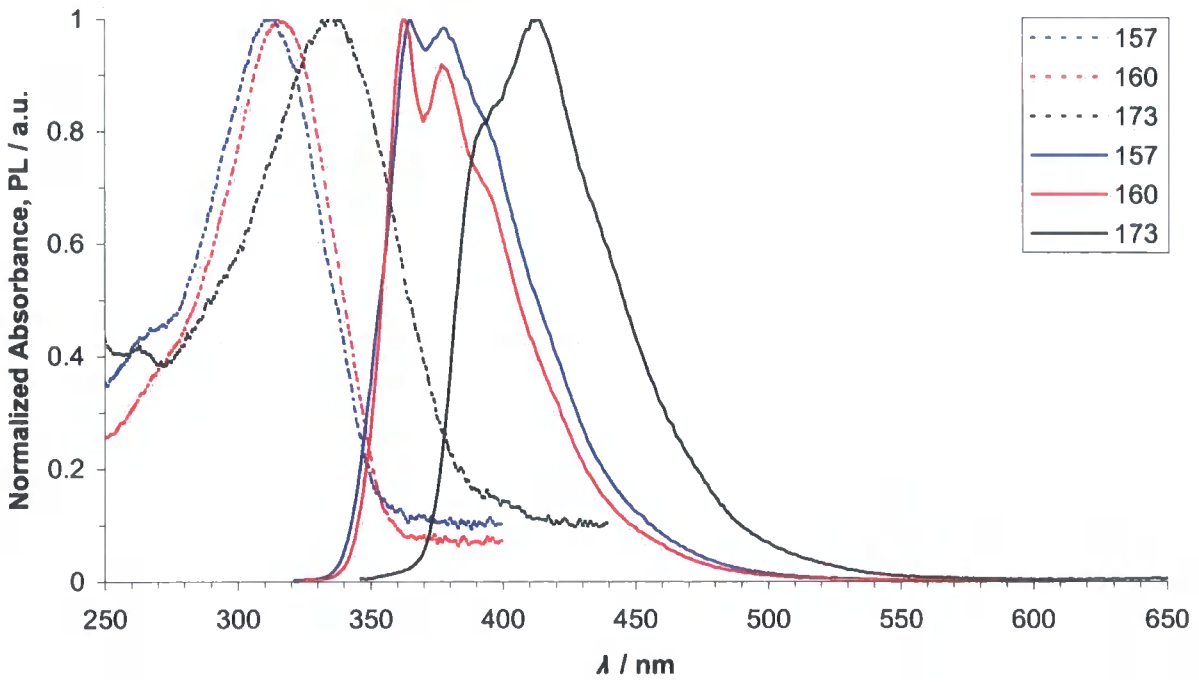

Figure 8: Normalized UV-Vis absorption (dashed lines) and PL (solid lines) spectra for compounds 157, 160 and 173 in DCM, 20 °C. Excitation wavelength corresponds to the maximum of absorption.

The absorption spectrum of **165** and **171** are identical with λ_{max} = 356 nm in both cases. For compound **177** the absorption is red shifted with λ_{max} = 397 nm; this can be explained due to

the further extension of conjugation in compound **177** and the lower calculated HOMO-LUMO gap compared to that of **165** and **171**.

The fluorescence spectra of **165** and **171** are again almost identical with main peaks at λ_{max} = 401 and 399 nm and smaller shoulders centred at λ_{max} = 422 and 420 nm, respectively. The PL spectrum of compound **177** displays a red-shifted broader emission than for compounds **165** and **171** with a peak observed at λ_{max} = 444 nm, accompanied with a smaller shoulder at λ_{max} = 468 nm.

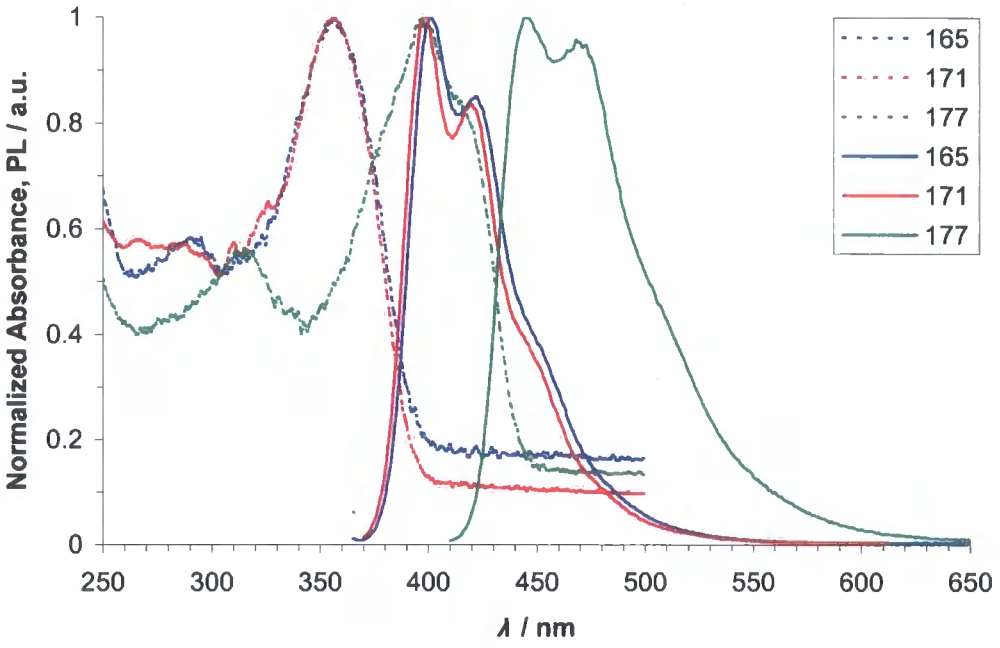

Figure 9: Normalized UV-Vis absorption (dashed lines) and PL (solid lines) spectra for compounds 165, 171 and 177 in DCM, 20 °C. Excitation wavelength corresponds to the maximum of absorption.

2.2.5 Optical Properties and Device Performance

As we have seen in the previous chapter the most widely studied emissive polymers, such as PPV and poly(fluorene) and their derivatives, are predominantly hole-transporting materials. For efficient EL, a means must be found to increase the number of electrons in the material. Ways of balancing charge injection that have met with notable success are as follows:

(i) A low work function metal, such as calcium, can be used as the cathode to lower the energy barrier to electron injection into the polymer film. The drawback of this strategy is that such metals are highly reactive and are unstable in the atmosphere.

(ii) Multilayer structures can be assembled with an ETHB layer placed on top of the emissive polymer film (by spin-coating or thermal evaporation) before deposition of the cathode. This approach requires more complex fabrication procedures than those used for single-layer devices.

(iii) Electron-deficient segments can be covalently bound to the emissive polymer, either by insertion into the main-chain, as end-capping groups, or as pendant side-groups. The synthesis of these polymers can be very challenging, often requiring multi-step routes and/or specific cross-coupling reactions.

(iv) ET materials can be blended into the emissive polymer prior to deposition. Single-layer devices of this type have the advantage that their manufacture requires only a single spin-coating process.[172]

Within our group single layer devices using blends of MEH-PPV and non-emissive, ETHB materials containing covalently linked OXD and pyridine units have previously been reported.[173] This section concerns the study of the new OXD-fluorene hybrids **165, 171** and **177** and their blends with MEH-PPV. Our strategy was to improve further the efficiency of the OLEDs through energy or charge transfer processes within the blended layer film.

All the OLEDs studied were fabricated by J. H. Ahn in Prof M. C. Petty's group in the School of Engineering, University of Durham. Initially devices in the configuration ITO/MEH-PPV:ETHB/Al were fabricated. The polymer blends all contained 70% electron transport materials by weight. The current density versus electric field (J–E) and light output versus electric field (L–E) characteristics of polymer blend devices using compound **34, 165, 171** and **177** are shown in Figure 10 (positive bias applied to the ITO electrode). The J–E and L–E characteristics of an OLED based on a pure (non-blended) MEH-PPV layer are also shown for comparison. For all the blended layer studies, the EL output was characteristic of MEH-PPV. It is evident that the EL emission from the blend devices was significantly greater than the light output of the pure MEH-PPV; at the same time, the current through the blend films was lower. However, within experimental errors, it was difficult to discern any particular trends between the different blended layers. The onset voltage for light emission for the blended devices was *ca.* 4.5 V, compared with *ca.* 6 V for the pure MEH-PPV device.

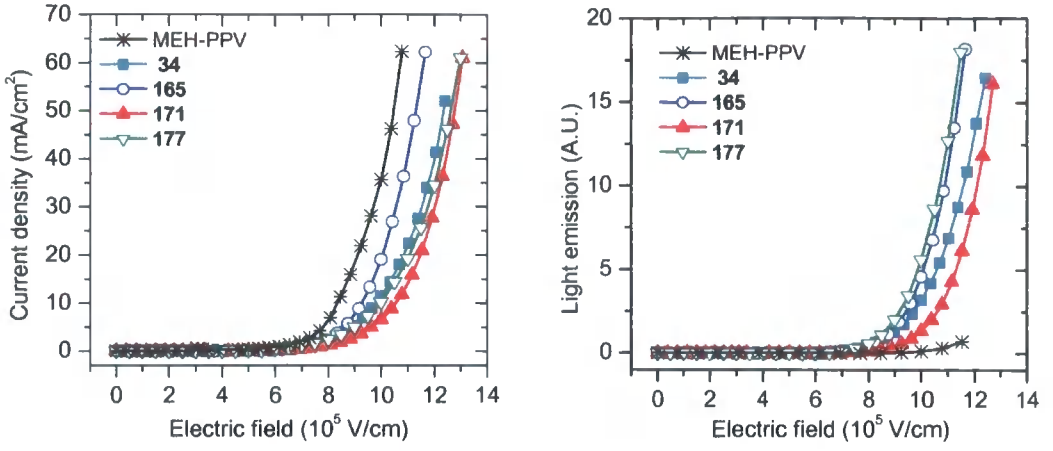

(a) (b)

Figure 10: (a) Current density *versus* electric field and (b) light output *versus* electric field characteristics for MEH-PPV polymer blend OLEDs incorporating 34, 165, 171 and 177. The polymer blends each contain 70% by weight of the electron transport materials. The data for a device based on pure MEH-PPV are shown for reference.

Figure 11 shows the external quantum efficiency of the devices whose optoelectrical behaviours are shown in Figure 10. The efficiency of the pure MEH-PPV device was about 0.001% while that of the blended devices (70% by weight) was about 0.05 %. The increase in the efficiency has resulted from both an increase in the light output as well as a decrease in the current; however, Figure 10 shows that the effect of the former is more significant.

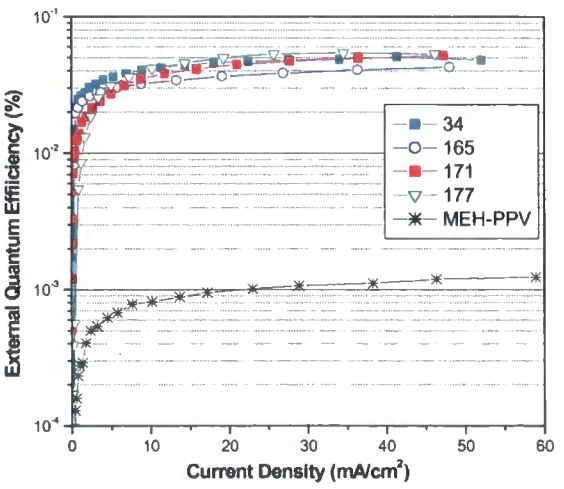

Figure 11: The external quantum efficiencies of MEH-PPV polymer blend OLEDs incorporating 70% by weight of 34, 165, 171 and 177. The data for a device based on pure MEH-PPV are shown for reference.

External quantum efficiencies of OLEDs containing different amounts of **171** are shown in Figure 12. These data are similar to those previously obtained by our group for blends incorporating **34**.[50] The device efficiency increased with the concentration of the electron transport material over the range of composition investigated. The efficiency for the 95% blend device was more than two orders of magnitude greater than that of the pure MEH-PPV device.

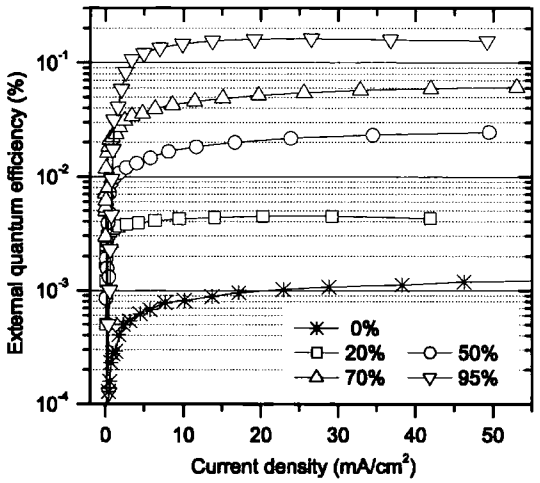

Figure 12: External quantum efficiency of blended MEH-PPV OLEDs incorporating compound 171. Data are shown for blend devices with 20%, 50%, 70%, and 95% of 171 by weight.

To investigate if this efficiency could be increased even further, a device incorporating 99.99% of **34** was fabricated. However, the EL emission was poor and the device quantum efficiency did not exceed 1×10^{-5} %, indicating an upper limit to the efficiency of our blended layer structures.

Despite the relatively high external quantum efficiencies of some of the blended layer OLEDs, the brightness and power efficiencies of the OLEDs are low compared to state-of-the-art polymer displays. For example, the brightness of a 70% blended device incorporating **165** was 210 cd m^{-2} at a current density of 62 mA cm^{-2}. However, it should be noted that our devices have not been optimised in any way, *e.g.* by use of a low work function cathode.

The HOMO and LUMO energy levels for MEH-PPV determined from oxidation and reduction potentials in CV experiments are $E_{HOMO} = -4.98$ eV and $E_{LUMO} = -2.89$ eV.[174a] This HOMO energy value is much higher than experimental I_p values for OXD-7 or calculated values for OXD-7, **34a**, **165a**, **171a**, and **177a** (Figure 7). Using the figure of 0.77 eV (the difference between the experimental value $E_A \approx 2.8$ eV and calculated HOMO energy level for OXD-7, and assuming that it is similar for other oxadiazole derivatives) we can estimate

LUMO energies for compounds **34**, **165**, **171** and **177** for direct comparison with the values for MEH-PPV (3.01, 2.83, 2.81 and 3.09 eV, respectively).

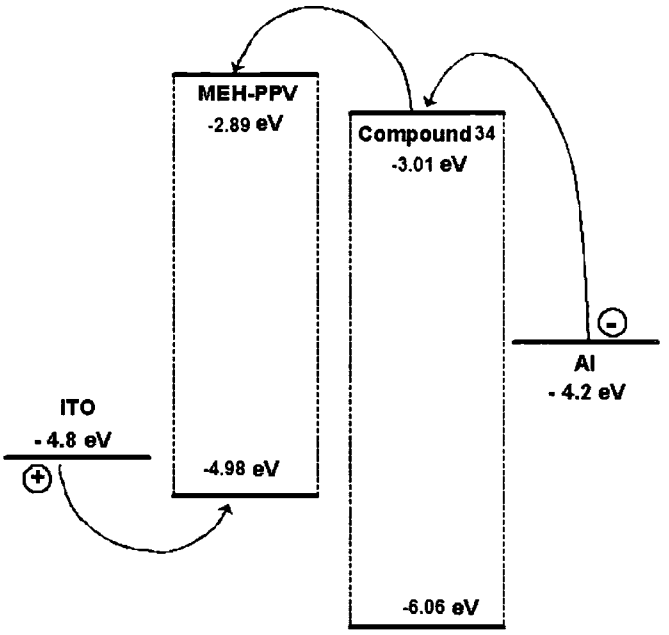

Figure 13: Energy band diagram of ITO, MEH-PPV, compound 34, and Al. For MEH-PPV, data are from Ref. 174a; for compound 34, the calculated energies of LUMO and HOMO levels for 34a have been corrected by adding the difference between the calculated and experimental values for OXD-7 (see Ref. 43) [$\Delta E^{calc\text{-}exp} \approx 0.77$ eV (LUMO), 0.23 eV (HOMO)].[i]

The LUMO levels for compounds **34** and **177** lie ~0.1–0.2 eV below that of MEH-PPV, whereas for compounds **165** and **171** they are comparable to that for MEH-PPV. Thus, holes are more likely to be transferred from the ITO anode to the MEH-PPV, (Figure 13) but electrons will move from the Al cathode to **34** or **177** more easily than to the MEH-PPV. The electrons can then easily move to the LUMO level of the host polymer, subsequently recombining with holes to produce EL characteristic of MEH-PPV. In the case of blends of MEH-PPV with compounds **165** and **171** electrons can also be injected directly into the LUMO of MEH-PPV as well as into the LUMO of oxadiazole derivatives (depending on the ratio in the blend). Nevertheless, in these cases EL also occurs only from MEH-PPV because of the substantial barrier for hole transfer from MEH-PPV into the HOMO of oxadiazoles.

When large amounts of **34** are blended with MEH-PPV it will become more difficult to inject holes (the majority carriers) from the ITO into the blended film and the device

[i] A more direct comparison of calculated energy levels for compounds **34**, **165**, **171** and **177** with ultraviolet photoelectron spectroscopy (UPS) calculated values could be applied. The UPS values for the HOMO and LUMO levels of MEH-PPV have been found to be 4.4 and 2.2 eV,[174b] however, these values are not a direct measurement and are determined in relation to the electrode material (gold).

current (majority carrier hole current) will decrease. In contrast, electron injection from the Al will increase, thereby increasing the EL. The light output will only decline when the supply of holes from the anode becomes limited. From experimental work with blended layers based on **171**, this seems to occur for concentrations of the electron transport material greater than 95% by weight.

The EL emission from OLEDs depends on the injection and transport of carriers, the generation of singlet excitons and their survival from non-radiative deactivation. For the blend devices in this work, the electron injection and transport are increased as noted previously. A 'dilution' effect may also be a contributory factor to the increase in our OLED efficiencies with increasing electron transport material concentration. As the polymer molecules become separated by the electron transporting molecules, concentration quenching - intermolecular non-radiative decay of singlet excitons - will be reduced resulting in an enhanced light output.

Kang *et al.*[175] have previously noted that the external quantum efficiency increased over seven times when MEH-PPV was blended with 90 wt% poly(methyl methacrylate) (PMMA), an electro-optically inert material. A much larger increase in efficiency (almost 500 times) was noted by mixing the MEH-PPV with another electroactive polymer. In our own studies, no improvement in the OLED efficiency was found using a 90% PMMA and MEH-PPV blend. An increase in the photoluminescence (PL) efficiency was noted in some of the films formed from mixtures of MEH-PPV with the electron transport compounds. For example, the PL efficiency of blends based on **34** increased by a factor of three as the concentration of **34** was increased from 20% to 90% by weight. Over the same composition range, the EL efficiency increased by a factor of 40, suggesting that dilution effects do not play a major role in determining the efficiency of our blended layer OLEDs.

The external quantum efficiency of our blend devices could be increased further by incorporating a PEDOT:PSS layer between the ITO and the blend film. The external quantum efficiency of the blend devices was increased two to three times regardless of the composition. The external quantum efficiency of 95% blend devices using a PEDOT layer was about 0.4%. Table 2 shows the external quantum efficiencies of OLEDs based on **34** and **171**. It is also expected that thermal annealing[50] could be used to extend the efficiencies of these devices.

Compound **34**			Compound **171**		
wt%	Without PEDOT	With PEDOT	wt%	Without PEDOT	With PEDOT
40%	0.01%	0.04%	50%	0.02%	0.08%
70%	0.03%	0.10%	70%	0.06%	0.15%
95%	0.11% (6.7)	0.31% (12.7)	95%	0.16%	0.38%

Table 2: External quantum efficiencies of MEH-PPV polymer blend OLEDs incorporating compound 34 and compound 171, with and without a PEDOT:PSS layer. The current density was 30 mA cm^{-2} unless designated in parentheses.

For all the electron transport compounds studied, the EL spectra were found to be independent of the blend composition. Figure 14 compares the EL spectra of a pure MEH-PPV device with blended devices, 50% by weight, incorporating **34**, **165**, and **177**: the emission of all the blend devices corresponded to that from MEH-PPV.

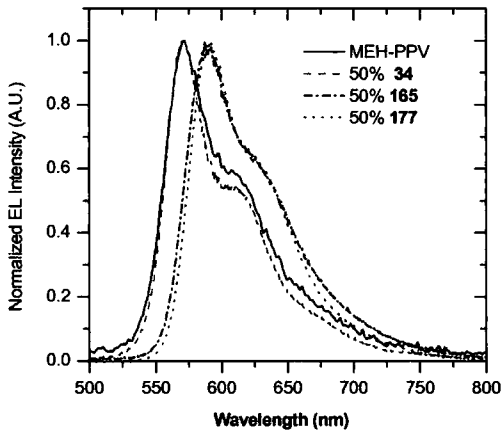

Figure 14: The EL spectra of a pure MEH-PPV OLED and blended layer devices incorporating compounds 34, 165, and 177. The composition of all the blends was 50% by weight.

No emission was evident from the electron transport materials, all of which are blue emitters. The OLED incorporating a blend of compound **34** possessed a main peak at 570 nm, exactly the same as that of the pure MEH-PPV device. However, the spectra of the devices incorporating **165** and **177** were red-shifted relative to pure MEH-PPV, with the main EL peak located at 590 nm. Blended devices based on **171** also exhibited a red-shifted EL spectrum (data not shown).

It is interesting to note that the three compounds exhibiting red-shifted EL spectra (**165**, **171** and **175**) have dodecyloxy terminal groups. These groups are replaced by *tert*-butyl

groups in the case of compound **34**. To study the influence of the terminal groups on the EL spectrum, a further compound, **178** was synthesised by G. Hughes in our laboratory.[176]

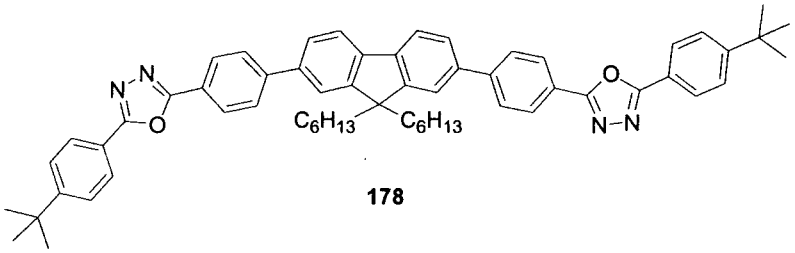

178

Scheme 76: Molecular structure of compound 178.

This has basically the same chemical structure as **165**, but with *tert*-butyl terminal groups instead of dodecyloxy groups. The EL spectra for blended layer OLEDs incorporating **178** and **165** (both 50% compositions by weight) are contrasted in Figure 15. The EL output of the device based on **178** peaks at the same wavelength as the pure MEH-PPV device, providing very strong evidence that the red-shifts noted in our studies are associated with the dodecyloxy chains interacting with the emissive MEH-PPV.

It is known that the emission of conjugated polymers such as MEH-PPV can be changed by varying the chain conformation. Schwartz and co-workers reported that the photoluminescence of MEH-PPV solutions varies according to the polarity of the solvents.[177] These workers noted that MEH-PPV chains in non-polar solvents such as chlorobenzene are more extended than in polar solvents such as tetrahydrofuran. This results in a red-shift of the PL spectrum of the chlorobenzene solution relative to the tetrahydrofuran solution. The same group demonstrated red shifts for MEH-PPV oriented on silica porous composite materials, in which the energy initially located on randomly oriented polymer segments exterior to the pores was driven to the aligned segments in the channel interior where the PL emission occurred.[178] In a similar way, the MEH-PPV molecules in our blend films may adopt different conformations depending on the properties of the other component of the blend and consequently the emission from MEH-PPV varies.[179]

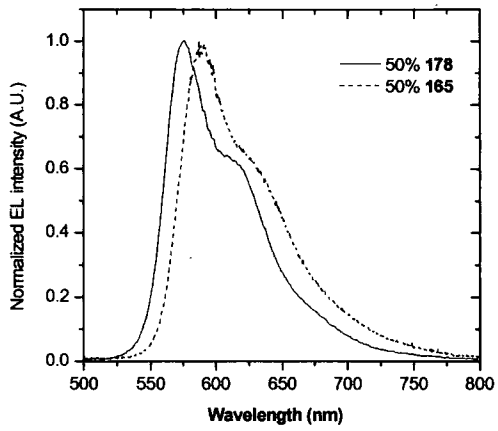

Figure 15: EL spectra of blended layer MEH-PPV OLEDs incorporating compounds 165 and 178. The composition of both blends was 50% by weight.

The results described above suggest a good mixing of the MEH-PPV with the electron transport compounds. No sign of phase separation was evident using atomic force microscopy, although this is not a definitive method of determining the distribution of the two components. The fact that no direct EL from the electron transport materials could be measured, even at high concentration (up to 95%), implies that the molecules of these materials are well distributed among the MEH-PPV polymer chains. Strong evidence for intimate mixing was also provided by the red-shifted EL curves for devices incorporating **165**, **171** and **177**. For these OLEDs, no unshifted MEH-PPV spectrum was detected, supporting the view that the MEH-PPV is able to interact with the electron transport compounds.

Devices were fabricated utilising the ETHB materials **165**, **171** and **177** as emitting material without MEH-PPV in the configuration ITO/PEDOT:PSS/ETHB/Al. The current density versus electric field (J–E) and light output versus electric field (L–E) characteristics of pure devices using compound **165**, **171** and **177** are shown in Figure 16 (positive bias applied to the ITO electrode).

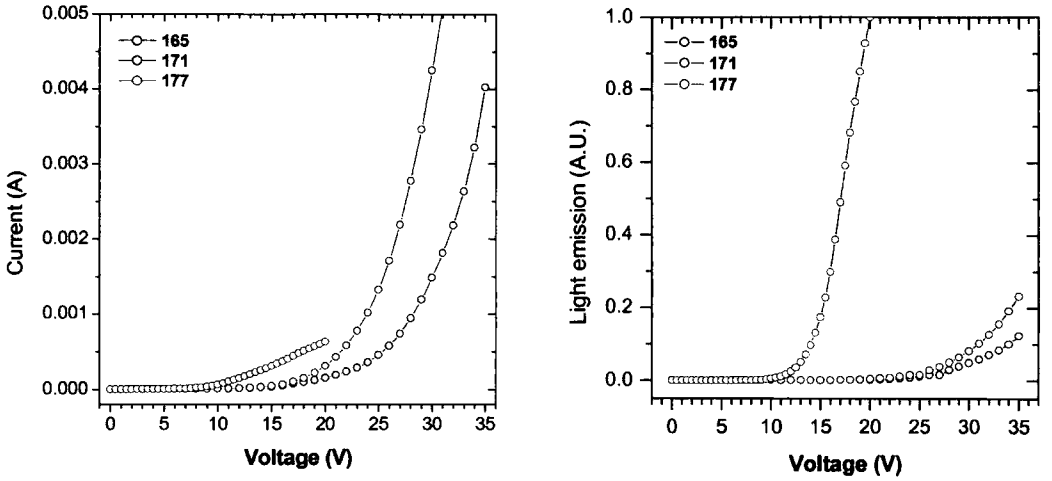

(a) (b)

Figure 16: (a) Current density *versus* electric field and (b) light output *versus* electric field characteristics for OLEDs incorporating 165, 171 and 177, in the configuration ITO/PEDOT:PSS/ETHB/Al.

The onset voltage for light emission was relatively high, 10 V, for the device incorporating **177** and *ca.* 25 V for the pure **165** and **171** devices. The device incorporating pure ETHB material **177** was the only device to show promise as an emitting material with an EQE of *ca.* 0.02%, compared to EQEs of *ca.* 0.001% recorded for devices incorporating **165** and **171**.

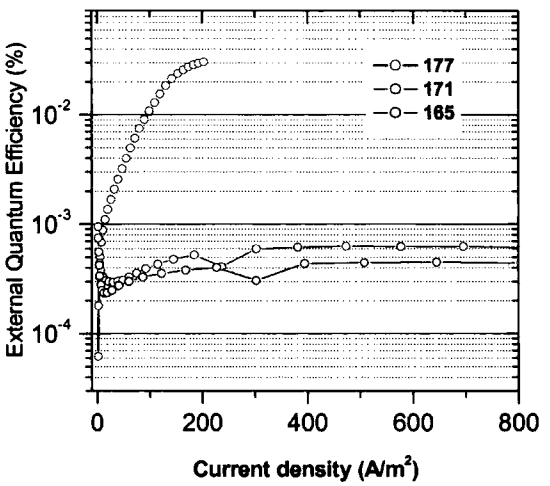

Figure 17: The external quantum efficiencies of OLEDs incorporating 165, 171 and 177, in the configuration ITO/PEDOT:PSS/ETHB/Al.

From the EL spectra of the pure compound devices for **165**, **171** and **177**, λ_{max} = 430, 433 and 487 nm, respectively. The EL λ_{max} is *ca.* 30-40 nm red-shifted compared to the PL λ_{max} for compounds **165**, **171** and **177**.

The EL spectra of the pure devices demonstrates a more intense blue emission for compound **171** comprising the spiro architecture compared to that of compound **165**, comprising dihexyl chains at the C-9 position. A slight reduction in the low energy tailing is also observed for the spiro analogue **171** compared to **165**, although this is not as significant as would be expected.

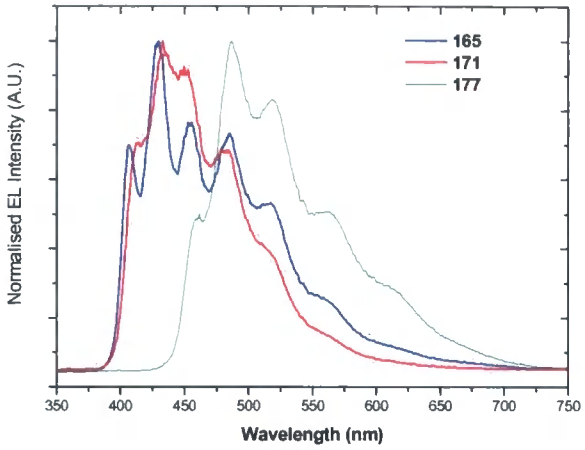

Figure 18: The EL spectra of OLEDs incorporating 165, 171 and 177, in the configuration ITO/PEDOT:PSS/ETHB/Al.

The CIE coordinates calculated from the respective EL spectra of the devices incorporating pure compounds **165**, **171** and **177** were (x = 0.19, y = 0.23), (x = 0.17, y = 0.15) and (x = 0.28, y = 0.43), respectively. This again illustrates the purer blue emission of the spiro analogue **171** over that of compound **165**.

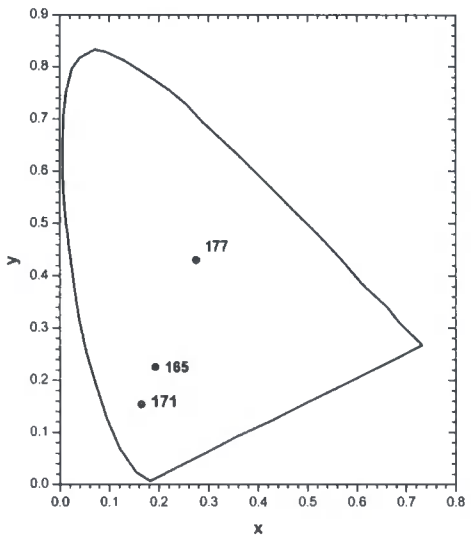

Figure 19: The CIE chromaticity coordinates of OLEDs incorporating 165, 171 and 178, in the configuration ITO/PEDOT:PSS/ETHB/Al (calculated from the EL spectra).

2.3 CONCLUSIONS

We have synthesised the OXD derivative **140** and achieved further functionalisation by Suzuki cross-coupling reactions to yield the linearly extended fluorene-OXD hybrid **165** and the spirobifluorene-OXD analogue **171**. Wittig chemistry has also been used to extend the conjugation via the carbaldehyde substituted OXD **172** to yield compound **177**. Spectroscopic studies in solution have established that the spirobifluorene architecture of **164** has no electronic effect on the OXD-fluorene backbone, as identical UV-Vis absorption and PL spectra were obtained for compounds **165** and **171**.

The OLED performance of the ETHB materials **165**, **171** and **177** blended with MEH-PPV has been investigated. The EQE of blended-layer devices containing the ETHB materials increased significantly compared to those fabricated using pure MEH-PPV. A striking feature of this work is that EL originates exclusively from the MEH-PPV material, even when the ET material is 95% by weight of the blend. The EL spectra of devices incorporating compounds **165**, **171** and **177**, which all bear terminal dodecyloxy groups, are red shifted by *ca.* 20 nm compared to the devices with compounds **34** and **178** which have terminal *tert*-butyl groups. This provides evidence for intimate mixing of the polymer and ET compounds. Further improvements have been achieved by incorporating a layer of PEDOT:PSS, with efficiencies reaching *ca.* 0.4% at 30 mA cm^{-2} for a device in the configuration ITO/PEDOT:PSS/MEH-PPV–**171** (95% by weight)/Al.

Devices comprising pure **165**, **171** and **177** as the emitting material were fabricated. compound **177** was the only ET material to show promise as an emitting material, with devices incorporating **177** displaying EQEs 20 times that of devices incorporating compounds **165** and **171**. The EL spectrum and CIE coordinates of the spiro analogue **171** demonstrated a more intense pure blue colour compared to that of **165**. This may be attributed to the reduction in fluorenone defects for compound **171**.

3 NEW OXD–FLUORENE HYBRIDS INCORPORATING PYRIDINE AND THIOPHENE UNITS

3.1 INTRODUCTION

Pyridine is an electron-deficient heterocycle, so its presence in OXD systems is expected to increase the electron affinity compared to the OXD compounds **165** and **171** described in Chapter 2. The synthesis of the symmetrical 2,5-di-(3-pyridyl)-1,3,4-oxadiazole has been reported[180] along with the corresponding symmetrical 2,5-di-(2-pyridyl)-1,3,4-oxadiazole and 2,5-di-(4-pyridyl)-1,3,4-oxadiazole, for which a crystal structure was obtained.[181]

The effect of combining the two electron deficient heterocycles on the ETHB properties of the pyridine-1,3,4-oxadiazole hybrid PDPyDP **28d** was studied within our group.[44] Following on from this work, our strategy was to combine the strong ET ability of the 2-phenyl-5-pyridyl-1,3,4-oxadiazole (PyOXD) units with a 9,9-dihexylfluorene core to provide blue emission and to utilise energy- or charge-transfer processes within blended layer films to improve further the efficiency of the OLEDs.

In this chapter we report the synthesis of the novel 2-phenyl-5-pyridyl-1,3,4-oxadiazole ring system **183** and describe Suzuki cross-coupling reactions to obtain **184** and the spirobifluorene analogue **185**. The 1,4-di(2-ethylhexoxy)-bis-2,5-PyOXD **187** was synthesised to ascertain if the absence of the planarising fluorene unit and the introduction of electron-donating alkoxy groups induce steric twisting in these systems which would influence the UV-absorption and PL spectra compared to compounds **184** and **185**.

Polymers with covalently linked thiophene and 1,3,4-oxadiazole units have been synthesised and used in the fabrication of blue OLEDs as functional materials.[182] The oligothiophene blocks exhibit high π-electron density, while the oxadiazole blocks show high electron affinity. Varying the length of the oligothiophene block provided a means of tuning the luminescence of these polymers, whereas the oxadiazole units facilitated ET in the polymers. The emission tuning of a series of thiophene-oxadiazole polymers has been attributed to the remarkable difference in HOMO-LUMO band gap between the two heterocycles.[182d] Goddard synthesised the OXD derivative 5-(5-phenyl-1,3,4-oxadiazol-2-yl)-2-thiophenecarboxylic acid, incorporating a thiophene unit[183] and Mitschke *et al.*[184] synthesised oligoheterocycles incorporating thiophene and oxadiazole moieties. Predictably, the introduction of the oxadiazole unit into the conjugated π-systems led to enhanced electron

acceptor characteristics compared to analogous oligothiophenes. We therefore synthesised compound **189**, namely a thiophene-OXD-fluorene system. The crystal structure of **189**, *ab initio* calculations of **184** and **185**, and OLED studies on compounds **184** and **185** blended with MEH-PPV have been carried out. Optical absorption and PL spectra of compounds **184**, **185**, **187** and **189** are compared with those of **165** and **171** to evaluate the effect of replacing a phenyl unit with pyridyl and thienyl moieties.

3.2 RESULTS AND DISCUSSIONS

3.2.1 Synthesis

The initial aim was to synthesise the pyridine analogue of compound **140** and via Suzuki coupling reactions synthesise PyOXD-fluorene analogues of compounds **165** and **171**. DFT calculations (Section 3.2.4) established that compound **184a**, with the pyridyl nitrogen adjacent to the fluorene, is a stronger electron acceptor than its isomer **184-iso** which has the pyridyl nitrogen adjacent to the oxadiazole ring. Therefore, we chose the former system as our synthetic target. The route to compound **183** is shown in Scheme 77. 6-Bromonicotinic acid **180** was synthesised from 2-bromo-5-methylpyridine **179** following the literature procedure.[185] The reaction of compound **180** with thionyl chloride at reflux gave 2-chloropyridine-4-carbonyl chloride, which was reacted directly with 4-dodecyloxybenzoic acid hydrazide **149** in pyridine to give the intermediate dihydrazide, which was not purified. *In situ* dehydrative cyclisation in refluxing phosphorus oxychloride,[30] followed by reaction with HBr in glacial acetic acid (to convert the 2-chloro substituent to 2-bromo) gave the functionalised 2-phenyl-5-pyridyl-1,3,4-oxadiazole reagent **183** in 37% yield from **180**.

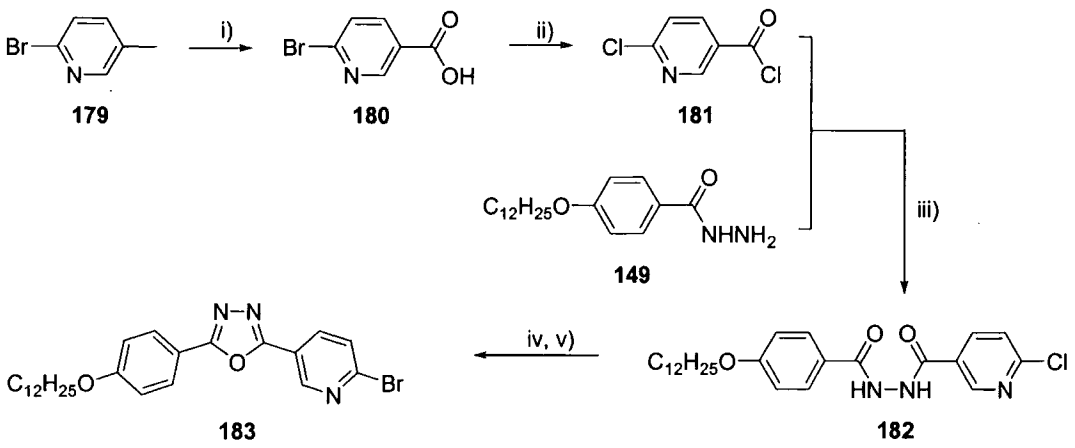

Scheme 77: Synthesis of 2[5-(2-bromopyridyl)]-5-(4-dodecyloxyphenyl)-1,3,4-oxadiazole 183: i) $KMnO_4$, H_2O, aliquat 336, Δ; ii) $SOCl_2$, Δ; iii) pyridine, 20 °C 1 h, Δ 2 h; iv) $POCl_3$, Δ; v) DCM, HBr (33% in glacial acetic acid).

Other methods of bromination were applied, including the use of phosphorus tribromide, which has been used in the conversion of 6-chloronicotinonitrile to 6-bromonicotinonitrile,[186] although very low yields of compound **183** were obtained.

Bromination of the chloro substituent was carried out, as at the time of synthesis, there were very few reports of efficient palladium-catalysed Suzuki couplings of aryl chlorides. With hindsight it is likely that the chloro-substituted analogue of compound **183** should undergo successful Suzuki coupling reactions due to the electron deficient nature of the pyridine and oxadiazole rings.[187] Chloro-substituted pyridines have been shown to be suitable substrates for room temperature Suzuki reactions.[188]

Two-fold reactions of **183** with 9,9-dihexylfluorene-2,7-diboronic acid **164**[163] and the dipinacolboronate reagent **170**[166b] under palladium-catalysed Suzuki-Miyaura conditions gave the target compounds **184** and **185**, respectively, in 35% and 56% yields.

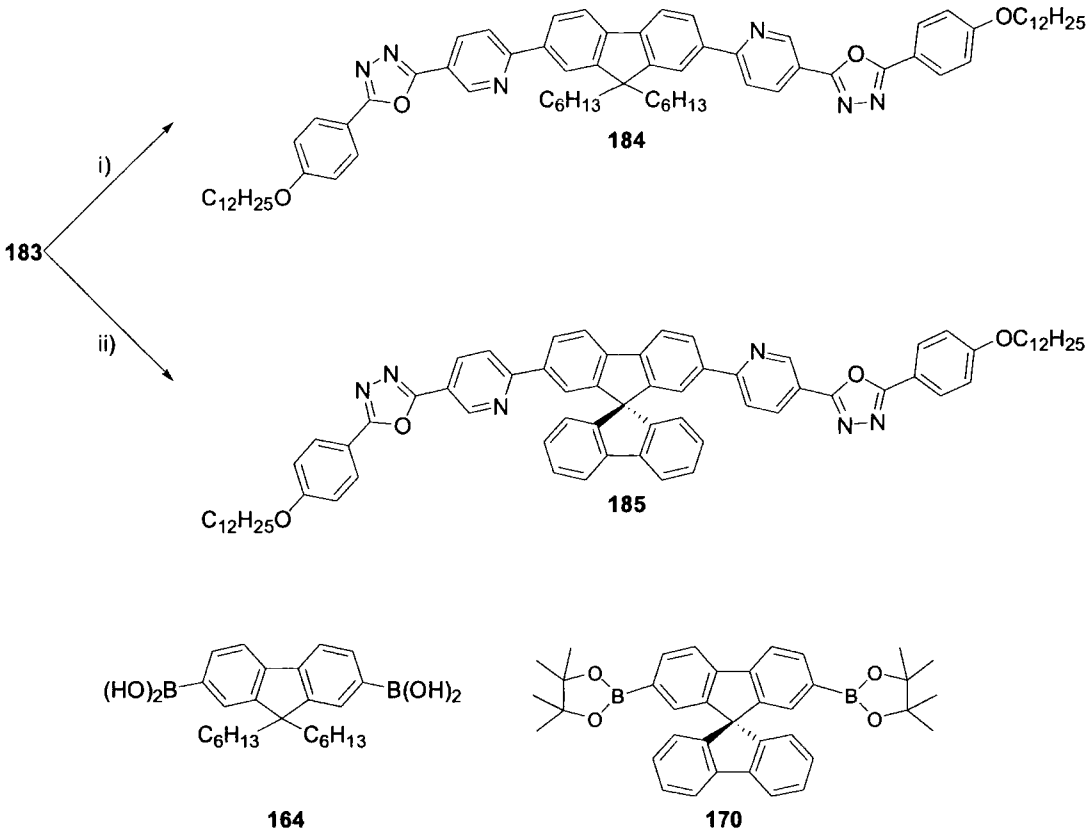

164 **170**

Scheme 78: Synthesis of compound 184 and 185: (i) 164, $Pd[PPh_3]_4$, Na_2CO_3, THF, Δ; (ii) 170, $Pd[PPh_3]_4$, PBu^t_3, K_2CO_3, toluene, Δ.

Further Suzuki coupling of compound **183** with 1,4-bis(2-ethylhexyloxy)benzene-2,5-diboronic acid **186,**[189] which was available within our group, yielded compound **187** in 41% yield.

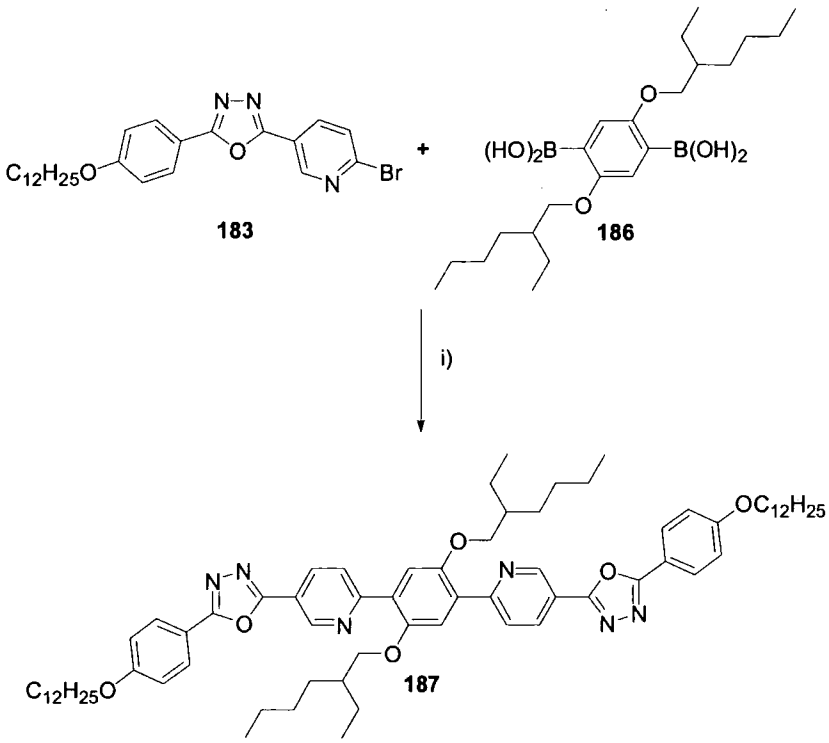

Scheme 79: Synthesis of compound 187: i) $Pd(PPh_3)_2Cl_2$, PBu^t_3, Na_2CO_3, THF, Δ.

The effect of replacing the phenyl and pyridyl moiety in compounds **165** and **184**, respectively, with a thienyl moiety was investigated by coupling the thienyl analogue of **140**, 2-(4-*tert*-butylphenyl)-5-[2-(5-iodothienyl)]-1,3,4 oxadiazole **188**,[190] which was synthesised within our group, with the boronic acid **164** to yield the thienyl-OXD-fluorene hybrid **189** in 42% yield. The replacement of the dodecyloxy chains with *tert*-butyl groups in compound **189** is not anticipated to have a significant effect on the spectroscopic characteristics of **189** with respect to **165** and **184**.

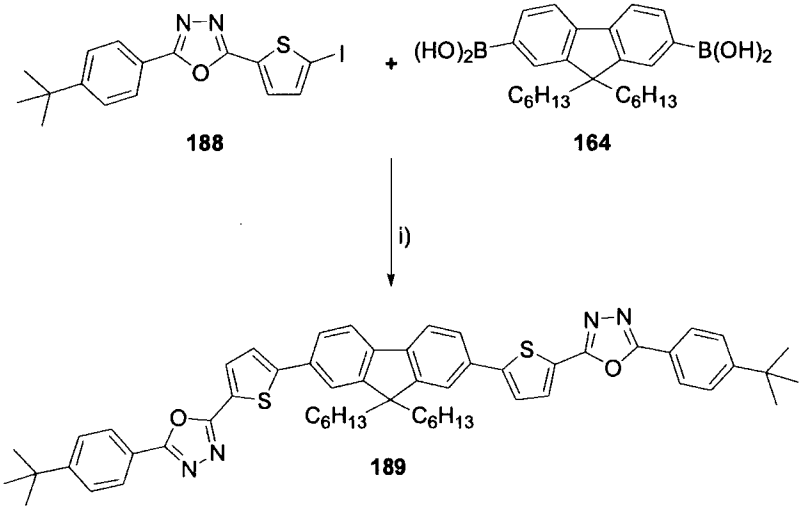

Scheme 80: Synthesis of compound 189: i) $Pd(PPh_3)_2Cl_2$, PBu^t_3, Na_2CO_3, THF, Δ.

3.2.2 X-ray Crystal Structure of 189

The crystal structure of compound **189** was solved by Dr A. Batsanov. The asymmetric unit of **189** comprises two molecules, **189A** and **189B**, each having one *t*-Bu and one *n*-hexyl group conformationally disordered (Figure 20). The conformations of the molecular 'rod' are somewhat different. In molecule **189B**, as in **165**, the central fluorene moiety is planar with the mean deviation δ=0.013 Å (max. δ=0.025 Å), whilst in molecule **189A** it is substantially puckered (mean δ=0.08, max. 0.16 Å). The interplanar angles between the fluorene moiety (or rather its outer 6-membered rings, i and v) and the adjacent thiophene rings ii and vi varies from 4.6 to 36.4°, but on average are smaller than the corresponding angles in **165**, which has benzene rings instead of thiophene. In both molecules of **189**, the mutual orientation of the two thiophene rings is *transoid*, that of oxadiazole rings also *transoid*, and each adjacent pair of thiophene and oxadiazole rings has the S and O atoms in *trans*-positions relative to the connecting C-C bond. The dihedral angles between these and other rings along the chain are also mostly small. Overall, the 'rod' acquires some out-of-plane bending. Thus, the two outlying C(benzene)–C(*t*-Bu) bonds deviate from the fluorene mean plane by ca. 1° and 22° in molecule **189A**, 17° and 25° in **189B**.

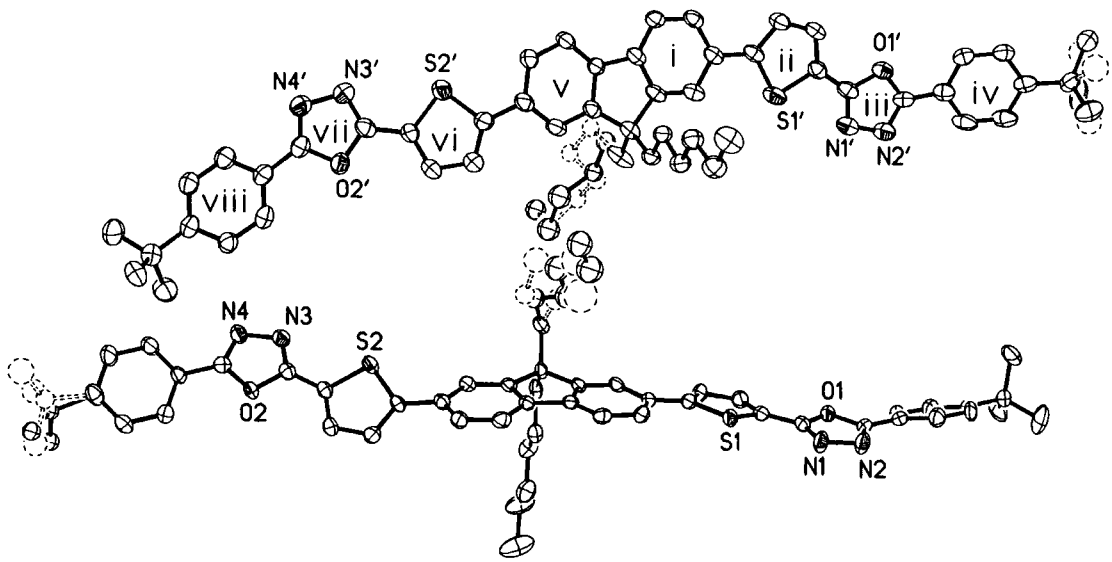

Figure 20: X-ray structure of compound 189.

3.2.3 Optical Absorption and Emission Properties

Solution UV-Vis absorption and photoluminescence (PL) spectra for compound **184**, **185**, **187** and **189** were recorded in DCM and are collated in Table 3. The Stokes shifts in λ_{max} values for compounds **184**, **185** and **189** are in the range 50-80 nm, which agrees with known OXD

derivatives.[191] Compound **187** has a Stokes shift of *ca.* 130 nm, which would indicate a relatively larger conformational change upon photoexcitation than for compounds **184**, **185** and **189**.

Compound	UV-Vis Absorption, λ_{max} / nm	PL, λ_{max} / nm
184	372	411, 431
185	371	407, 430
187	327, 380	460
189	394	439, 466

Table 3: UV-Vis absorption and emission λ_{max} values for compound 184, 185, 187 and 189 in DCM, 20 °C.

The absorption and PL spectra of **184** and **185** (Figure 21) are almost identical, the PL structure consisting of a major peak and a red-shifted shoulder, by analogy with their phenyl analogues **165** and **171.** The λ_{max} of compound **184** is slightly red-shifted compared to **185**.

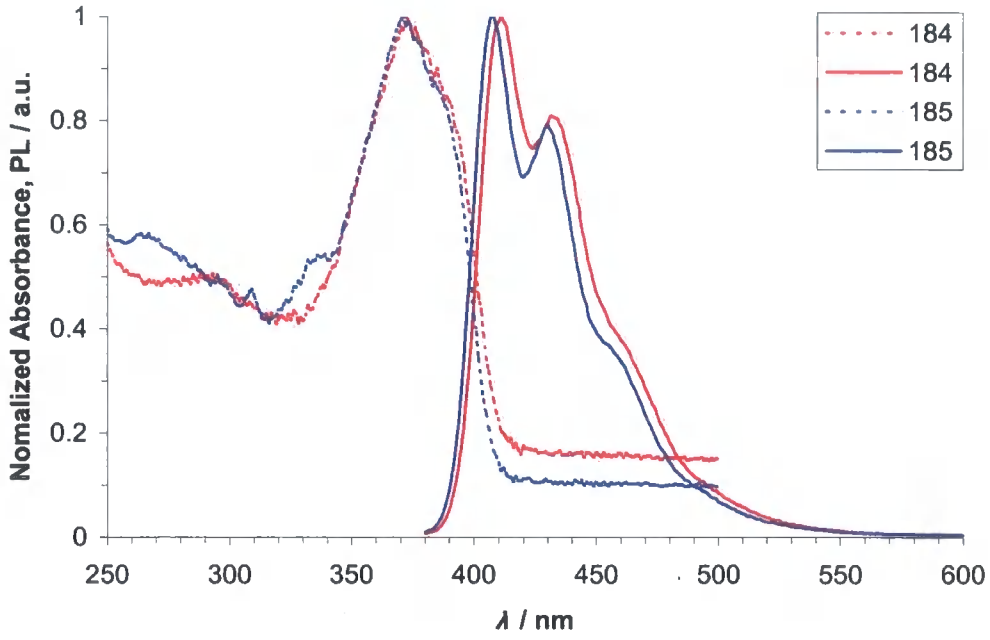

Figure 21: Normalized UV-Vis absorption (dashed lines) and PL (solid lines) spectra for compounds 184 and 185 in DCM, 20 °C. Excitation wavelengths correspond to the maximum of absorption.

The absorption spectrum of **187** displays a major peak at λ_{max} = 327 nm and a shoulder at λ_{max} = 380 nm. The PL spectrum has one broad peak with λ_{max} = 460 nm, which is red-shifted, compared to the **184**, **185** and **189**. The large Stokes shift, indicating larger relative conformational change upon photoexcitation of **187** compared to the fluorene systems **184**,

185 and **189**, could be attributed to the increased ability for the molecule to twist due to the absence of the conformationally restricting fluorene core.

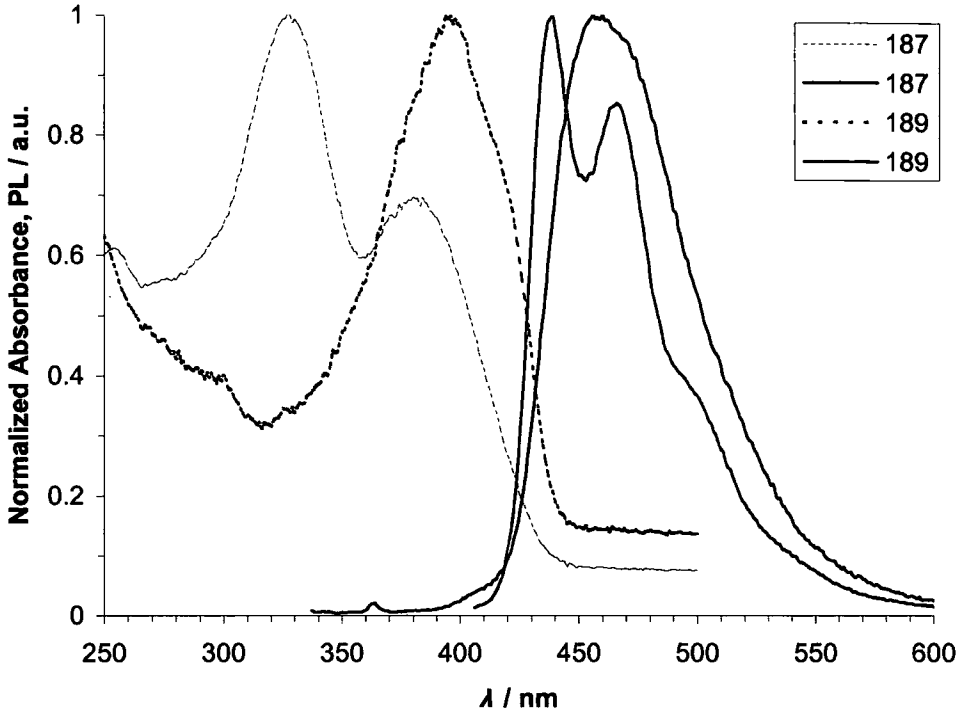

Figure 22: Normalized UV-Vis absorption (dashed lines) and PL (solid lines) spectra for compounds 187 and 189 in DCM, 20 °C. Excitation wavelengths correspond to the maximum of absorption.

The absorption and emission peaks of **184** and **185** are red-shifted compared with their phenyl analogues **165** (abs: 16 nm, PL: *ca.* 10 nm) and **171** (abs: 15 nm, PL: *ca.* 9 nm), respectively. Figure 23 shows the gradual red-shift in PL from the spirobifluorene phenyl analogue **171** to the 9,9-dihexylfluorenepyridyl analogue **184**.

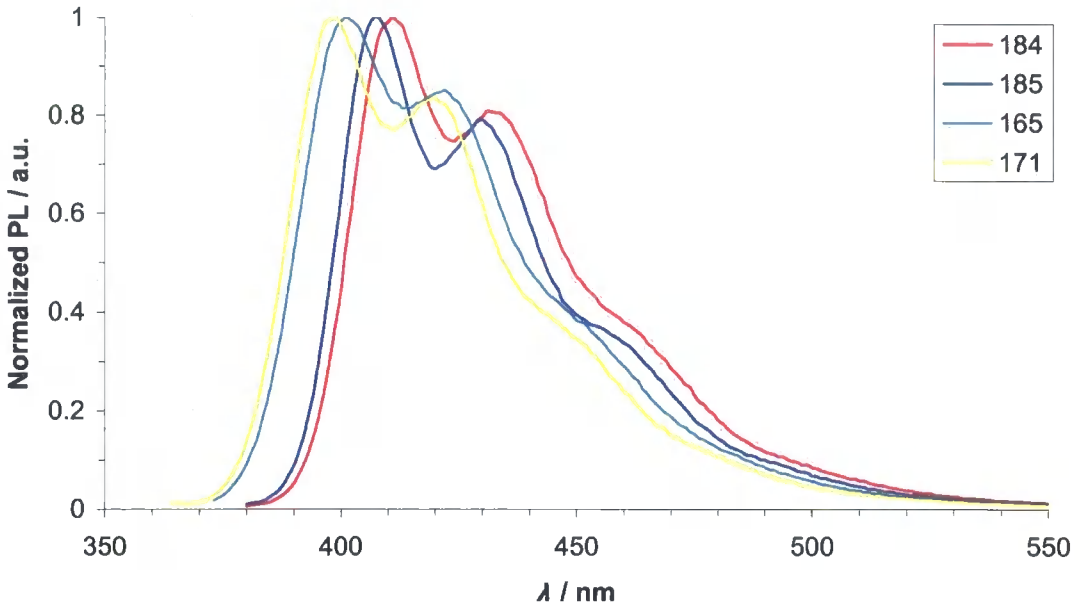

Figure 23: Normalized UV-Vis PL spectra for compounds 165, 171, 184 and 185 in DCM, 20 °C. Excitation wavelength corresponds to the maximum of absorption.

The absorption spectra of the series of OXD-fluorene compounds with phenyl, pyridyl and thienyl substituents **165**, **184** and **189**, respectively, are shown in Figure 24. The structure of the PL spectra for compounds **165**, **184** and **189** (Figure 25) are all similar in shape with a main peak followed by a shoulder red-shifted by *ca.* 20 nm for **165** and **84**, and by 27 nm for **189**. For this series of compounds the absorption and PL λ_{max} is red shifted going from phenyl **165** to the pyridyl analogue **184** (abs: 16 nm, PL: *ca.* 10 nm) and from **165** to the thienyl analogue **189** (abs: 38 nm, PL: *ca.* 40 nm).

The absorption maximum for compound **187** shows a main peak at lower wavelength than **165** and a further peak at 380 nm, comparable with **184**. This blue-shifted peak is expected, as compound **187** will be highly twisted due to the 2-ethylhexyloxy groups, leading to a reduction in conjugation. The PL spectra of **187** λ_{max} is red-shifted compared to compound **184** by *ca.* 40 nm. This is possibly due to the electron donating characteristics of the 2-ethylhexyloxy groups.

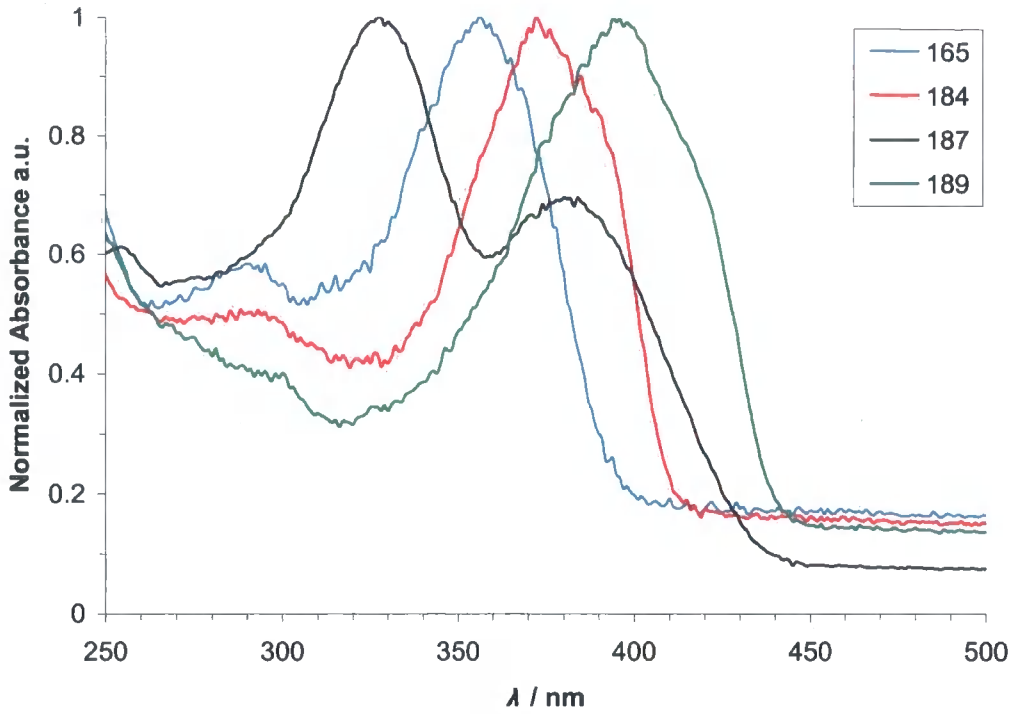

Figure 24: Normalized UV-Vis absorption spectra for compounds 165, 184, 187 and 189 in DCM, 20 °C.

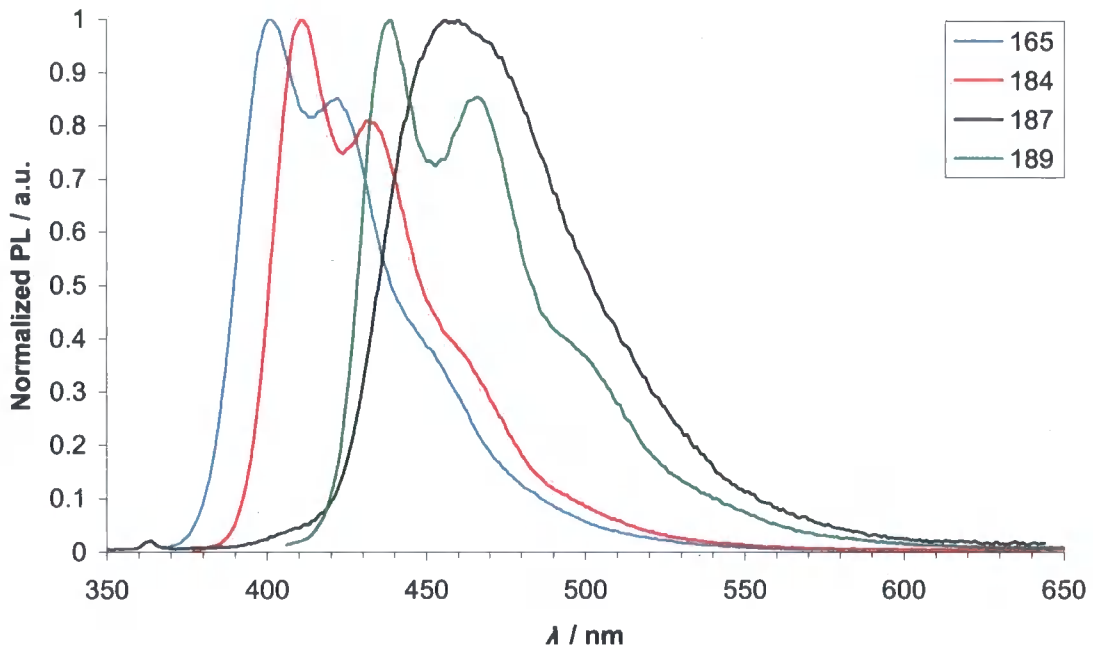

Figure 25: Normalized PL spectra for compounds 165, 184, 187 and 189 in DCM, 20 °C. Excitation wavelength corresponds to the maximum of absorption.

The red-shift in absorption and PL spectra with the replacement of phenyl ring (**165** and **171**) by the pyridyl ring (**184** and **185**) is in agreement with the calculated electronic states of these compounds (Section 3.2.4), where a decrease in the HOMO-LUMO energy gap by *ca.* 0.23

eV for both **184** and **185**, with respect to **165** and **171** is observed, originating from the electron deficient character of the pyridine ring.

The replacement of the phenyl ring (**165**) by the thienyl ring (**189**) leads to a larger red-shift in both absorption and emission spectra. This can be explained by a "push-pull effect" of the conjugated electron donating thiophene ring and the electron accepting oxadiazole ring lowering the HOMO-LUMO gap.[192] Also, compound **189** possesses an increased planarity compared to **165** (observed from the X-ray structure of **189**, Section 3.2.2) this increase in conjugation will also contribute to a red-shift in absorption and PL spectra. Within our group investigations into the replacement of a phenyl ring with thienyl in alkyne substituted OXDs also lead to a red-shift in the absorbance and PL spectra.[190]

3.2.4 Quantum Chemical Calculations

Ab initio calculations were performed by Dr I. F. Perepichka in our group. DFT calculations were performed to elucidate the geometry and the electronic state of the new pyridyl-containing derivatives **184** and **185** in comparison with **165** and **171**. As previously (Chapter 2), to decrease the computational time calculations were performed on molecules **184a** and **185a** (Appendix 2.2). Calculations were also performed on the geometrical isomers of compounds **184a** and **185a**, with different substitution positions at the pyridine rings (compounds **184a-iso** and **185a-iso**), which have not been synthesised.

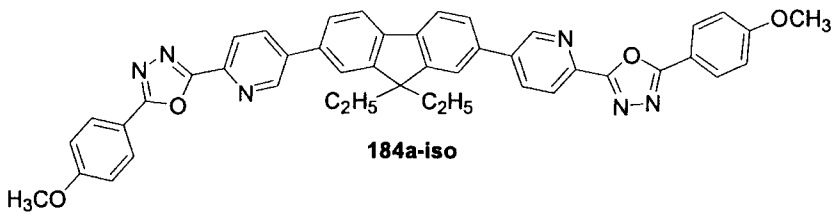

184a-iso

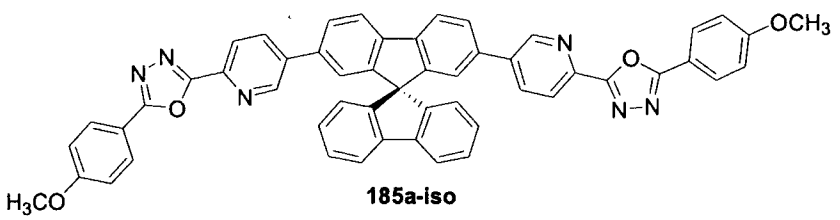

185a-iso

Scheme 81: Molecular structures of 184a-iso and 185a-iso.

The optimised geometries of compounds **184a-iso** and **185a-iso** are generally similar to the previously reported benzene analogues **165a** and **171a**, whereas the reduced steric hindrance

between the pyridine and fluorene rings in **184a** and **185a** results in substantial planarisation of the system and consequently an increase in the conjugation (Figure A9, Appendix 2.2). Thus, the dihedral angles between the pyridine and fluorene rings in compounds **184a** and **185a** are 15.5° and 16.3°, respectively, whereas these angles in **184a-iso** and **185a-iso** are 36.4° and 36.5°, respectively, which are similar to those between the fluorene and adjacent benzene rings in **165a** and **171a**, *viz.* 35.9° and 36.3°, respectively. All these six structures show planarity at the oxadiazole site; the dihedral angles between the oxadiazole moiety and the adjacent benzene and pyridine rings are less than 1°.

The localisation of the HOMO and LUMO orbital coefficients for compounds with different substituents at position 9 of the fluorene moiety is quite similar for both series, i.e. **184a/185a** and **184a-iso/185a-iso**. The main population of the HOMO is on the central aromatic fluorene moiety with some extension onto the pyridine and oxadiazole moieties, and quinoidal character of the LUMO orbital (see Figures A10 and A11, Appendix 2.2). Comparison of the two isomers, **184a** and **184a-iso**, demonstrates some differences in the occupancy of their HOMOs. In the case of **184a**, better planarity and consequently increased conjugation between the pyridine and fluorene rings, results in increased population on the central fluorene ring, whereas for the isomer **184a-iso** the HOMO is more delocalised over the molecule even extending onto the terminal alkoxyphenyl moieties (Figure 26).

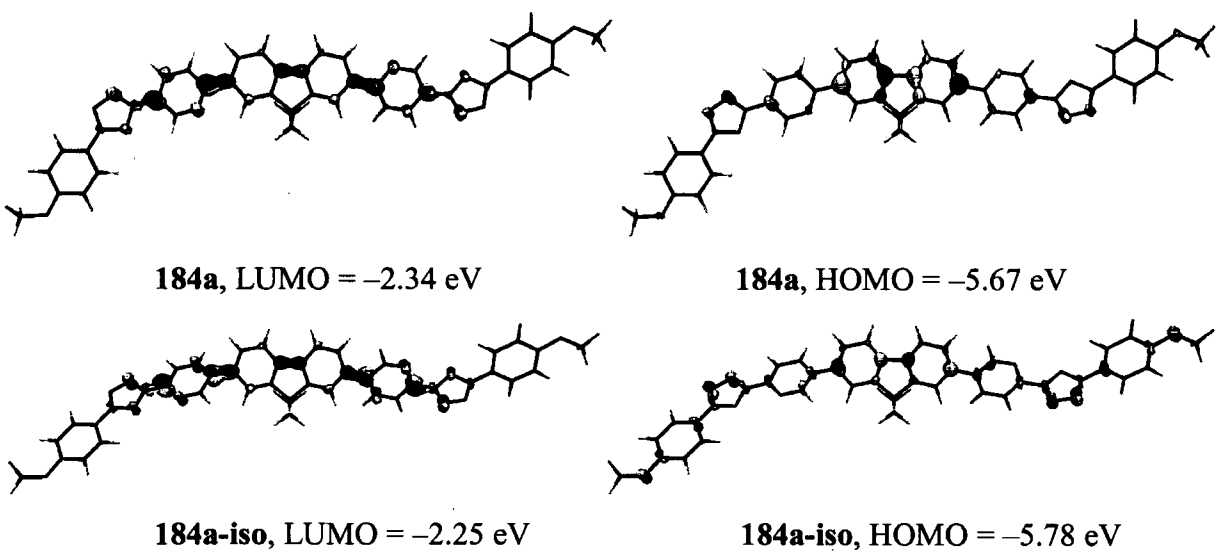

Figure 26: B3LYP/6-311G(2d,p)//B3LYP6-31G(d) frontier orbitals of compounds 184a and 184a-iso.

The most interesting feature of the electronic structure of the new compounds **184** and **185**, compared to their benzene analogues **165** and **171**, is the difference in the frontier orbital energies (Figure 27). Whereas the HOMO energies for both series of compounds are almost the same (the difference is only ≈0.03–0.04 eV), a pronounced decrease in the LUMO

energies by 0.28 eV is observed when the benzene rings in **165a** and **171a** are replaced by pyridine rings (**184a** and **185a**) (Figure 27). Substitution of the phenyl rings in **165a** and **171a** by isomeric pyridine rings (compounds **184a-iso** and **185a-iso**) results in a decrease in HOMO energy levels by 0.14 eV (in contrast to **184a** and **185a**) whereas the decrease in their LUMO energies is less pronounced (0.19 eV), so the isomers **184a-iso** and **185a-iso** are expected to be weaker electron acceptors than **184a** and **185a** (although still stronger acceptors compared to **165** and **171**). Similar results were obtained from the comparative orbital analysis of compounds **184a**, **185a**, **165a** and **171a** at the B3LYP/6-31G(d) level of theory (very similar HOMO orbital energies and a decrease in LUMO energies upon replacing the benzene rings by pyridine rings; see Figure A8, Appendix 2.2. This pronounced decrease in LUMO orbital energies in compounds **184a** and **185a** originates from the electron-deficient character of the pyridine rings and their orientation with respect to the fluorene moiety; this makes them stronger electron acceptors and on this basis increased ET properties and improved performance of OLEDs would be expected from compounds **184** and **185**.

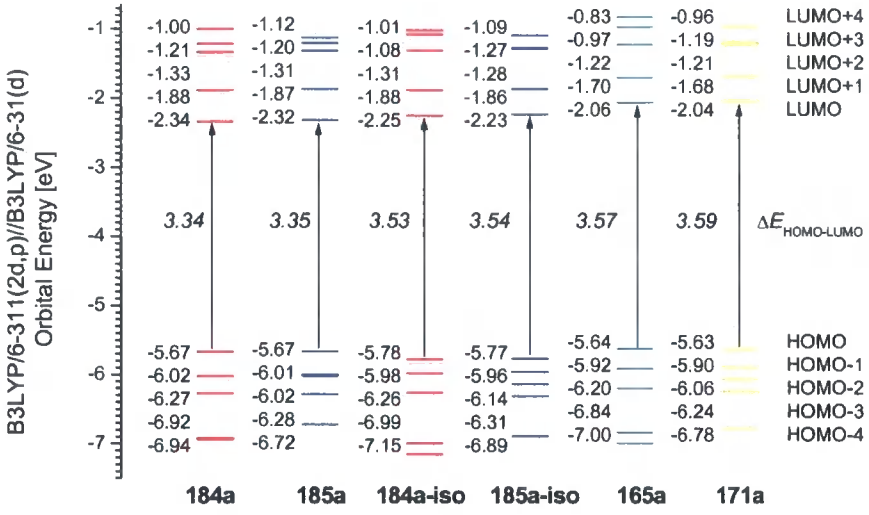

Figure 27: B3LYP/6-311G(2d,p)//B3LYP/6-31G(d) orbital energy level diagrams for compounds 184a, 185a compared with isomers 184a-iso and 185a-iso, and benzene analogues 165a and 171a.

3.2.5 Optical Properties and Device Performance

All the OLEDs were fabricated by J. H. Ahn in collaboration with Prof M. C. Petty's group in the School of Engineering, University of Durham. The current versus voltage (I–V) and light output versus voltage (L–V) characteristics of single-layer polymer blend devices using **184**,

185, **165** and **171** are shown in Figure 28 (positive bias applied to the ITO electrode). The device configuration was ITO/MEH-PPV:ETHB/Al and the polymer blends all contained 70% of the electron transport materials by weight. While the current density was similar for all the devices investigated, the electroluminescent output varied considerably. The light outputs from derivatives **184** and **185** were significantly higher than for compounds **165** and **171**. For example, at 10×10^5 V cm^{-1}, the light emission from blended devices containing **184** and **185** was about 2.5 and 10 times higher, respectively, than from the device incorporating **165**.

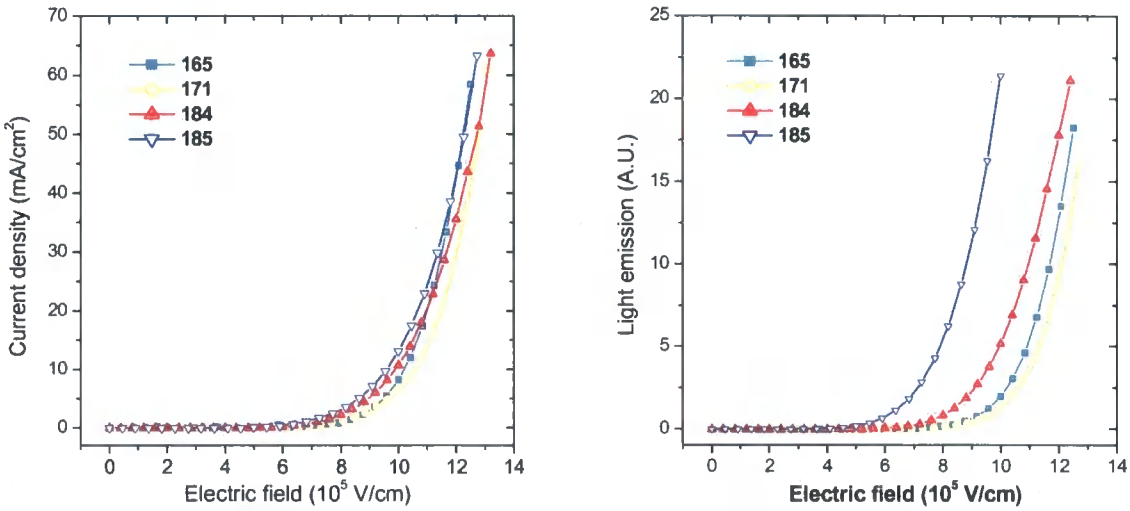

(a) **(b)**

Figure 28: (a) Current density versus electric field and (b) light output versus electric field characteristics for MEH-PPV polymer blend OLEDs incorporating 184, 185, 165 and 171. The polymer blends each contain 70% by weight of the electron transport materials. Device configuration: ITO/MEH-PPV:ETHB/Al.

Figure 29 shows the external quantum efficiencies of the OLEDs (data calculated from the optoelectronic characteristics of Figure 28). The efficiency of devices based on 70% blends of **184** and **185** was *ca.* 0.08% and 0.25%, respectively. In comparison, the efficiency of blend devices incorporating 70% of **165** and **171** was *ca.* 0.05%, while that of a pure MEH-PPV reference device was 10^{-3}%, and for OLEDs based on pure **185** less than 10^{-3}%. The increase in the external quantum efficiency of an OLED can result from either an increase in the light emission or a decrease in the current (or both). From Figure 28, it is evident that the improvement in the efficiencies of the devices containing **184** and **185** is due to increased

light emission. This can almost certainly be attributed to an enhanced electron (minority carrier) injection from the top aluminium cathode.

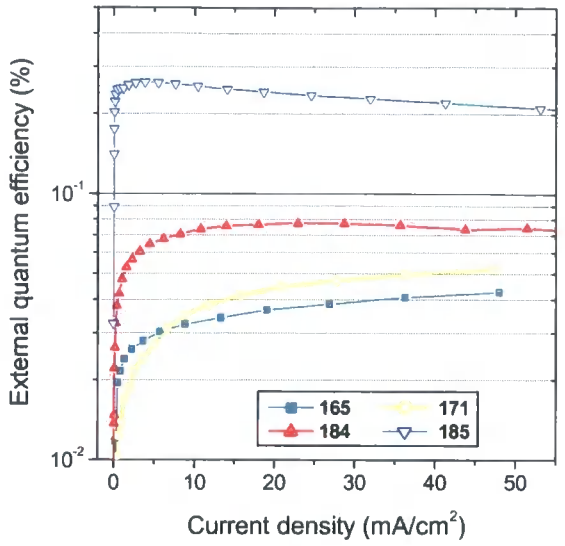

Figure 29: The external quantum efficiencies of MEH-PPV polymer blend OLEDs incorporating 70% by weight of 184, 185, 165 and 171. Device configuration: ITO/MEH-PPV:ETHB/Al.

The variation of quantum efficiency with the blend composition is depicted in Figure 30. While the efficiency for **165**-containing OLEDs increased with concentration over the range of composition investigated, the efficiencies of devices incorporating compounds **184** and **185** appeared to saturate (in the case of **184**) or even reduce (**185**) for devices containing high concentrations of the ET materials. The diminished efficiency of OLEDs containing compound **185** is probably related to a decrease in the light emission at high concentrations (95%) as the hole current is expected to reduce for blends consisting predominantly of the ET compound. The maximum external quantum efficiency that could be achieved from the blended-layer devices was 0.24% for the OLED containing 70% of compound **185**. This efficiency is over 200 times higher than that for pure MEH-PPV devices and about twice the highest values achieved with blended-layer devices incorporating OXD–fluorene hybrids **165** and **171**. It is also significant that the **185** blended-layer devices were more efficient than OLEDs incorporating compound **184** throughout the concentration range investigated. There are other examples in the literature where the spiro-bifluorene system enhances efficiency compared to the 9,9-dialkylfluorene analogues, which can yield fluorenone defects that quench the emission.[193]

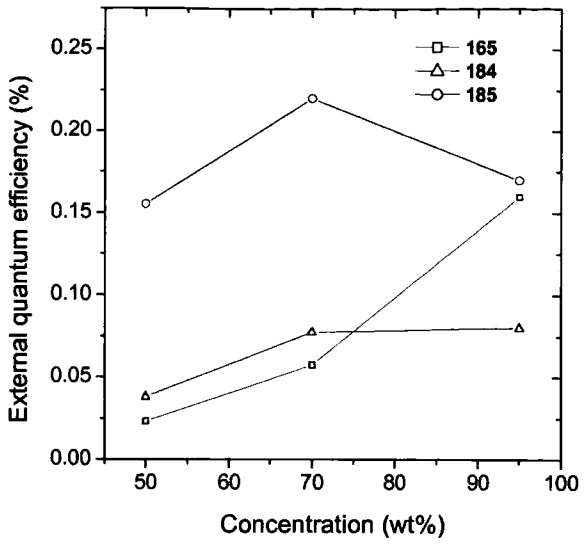

Figure 30. External quantum efficiency of blended MEH-PPV OLEDs incorporating 184, 185 and 165. Data are shown for blend devices with 50%, 70%, and 95% by weight.

The external quantum efficiency of our OLEDs could be increased further by using a layer of PEDOT:PSS between the ITO and the blended-layer film.[194] This resulted in an efficiency increase of 2–3 times, regardless of the composition and material. A 70% compound **185**-containing blend device with PEDOT exhibited an external quantum efficiency of 0.5% and a luminous efficiency of 0.93 cd A^{-1} at 9.5 V and a luminance of 100 cd m^{-2}. When the Al cathode was replaced by Ca/Al (thermally evaporated), the efficiency values for the 70% **185**-based device increased further to 0.6% and 1.2 cd A^{-1} at 10.5 V.

This result is interesting as the use of Ca might be expected to increase significantly the blend efficiency, as it does with pure MEH-PPV (at 5 V and 100 cd A^{-1} the EQE and the luminous efficiency for an ITO/PEDOT/MEH-PPV/Ca/Al device were 0.42% and 0.72 cd A^{-1}, respectively). However, only a very modest increase was observed. This suggests that the two methods of enhancing the electron injection into the emissive polymer are mutually exclusive, *i.e.* one can either use a low work function metal such as Ca, or exploit a blended-layer structure. For the latter devices, it appears that there is not much further gain in then adding Ca as a top electrode. Indeed, the use of blended layers with an Al cathode offers a distinct advantage in terms of environmental stability and ease of handling, as Ca electrodes are highly reactive and unstable in the atmosphere.

Figure 31 contrasts the EL spectrum of a pure MEH-PPV device with the spectra from 50% **165**, 50% **185** and 70% **184** blended-layer OLEDs. The emission from all these devices was from MEH-PPV. No EL could be detected from the ET materials, which are all blue

emitters. The pure MEH-PPV device exhibited a main peak at 570 nm while the spectra of the blended-layer devices were red-shifted, with the main peaks located at *ca.* 590 nm. As suggested in Chapter 2 it is believed that these long terminal groups are responsible for the red shift. It is known that the emission of conjugated polymers such as MEH-PPV can be changed by varying its chain conformation. This, in turn, is affected by the polarity of the solvent or by the spin casting speed.[177,195]

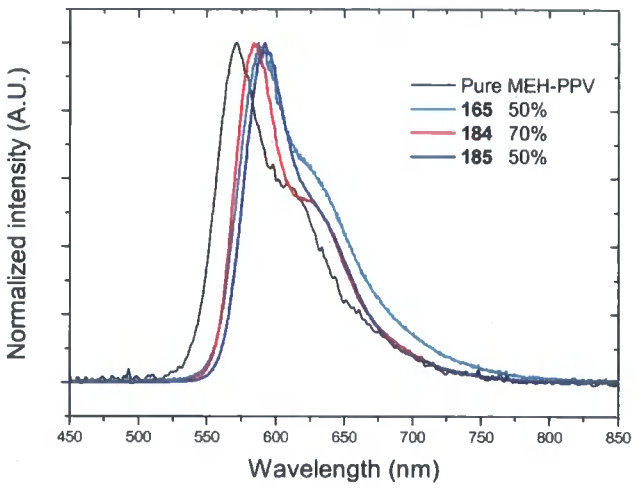

Figure 31: The EL spectra of a pure MEH-PPV OLED and blended-layer devices incorporating compounds 50% 165, 70% 184, and 50% 185 by weight.

The implication of this is that the components of the blended layers (polymer and ET material) are intimately mixed. The fact that no direct EL from the ET materials could be measured, even at high concentration (up to 95%), implies that the molecules of these materials are well-distributed among the MEH-PPV polymer chains. Under certain conditions, however, we found that phase separation could be observed for blended-layer devices based on **184** and **185**; for example, by using films that were spin-cast from solutions of a mixed solvent. Figure 32 shows atomic force microscope (AFM) images of 70% **184** (a) and 50% **185** (b) blended-layer films spin-cast from the mixed solution using chloroform as the solvent; and 50% **184** (c) and 50% **185** (d) films formed using a mixed solvent system, *viz.* chloroform and *p*-xylene (3:1 v/v). There is no notable morphology in the blend films spin-coated from the pure chloroform solution (the micron-size particles evident in Figures 32a and 32b are thought to originate from environmental contamination during processing). However, a needle-like phase is clearly visible in both the blended-layer films formed from the mixed solvent. The phase separation was particularly acute in the films containing compound **185**. This is probably related to the presence of the bulky spiro unit at the centre of

the molecule, which inhibits mixing with the chains of the MEH-PPV. (This solvent effect was not observed in comparable experiments using ET materials **165** and **171**). The microstructure and crystallinity of MEH-PPV films are known to vary depending on the solvents from which the film has been cast.[196]

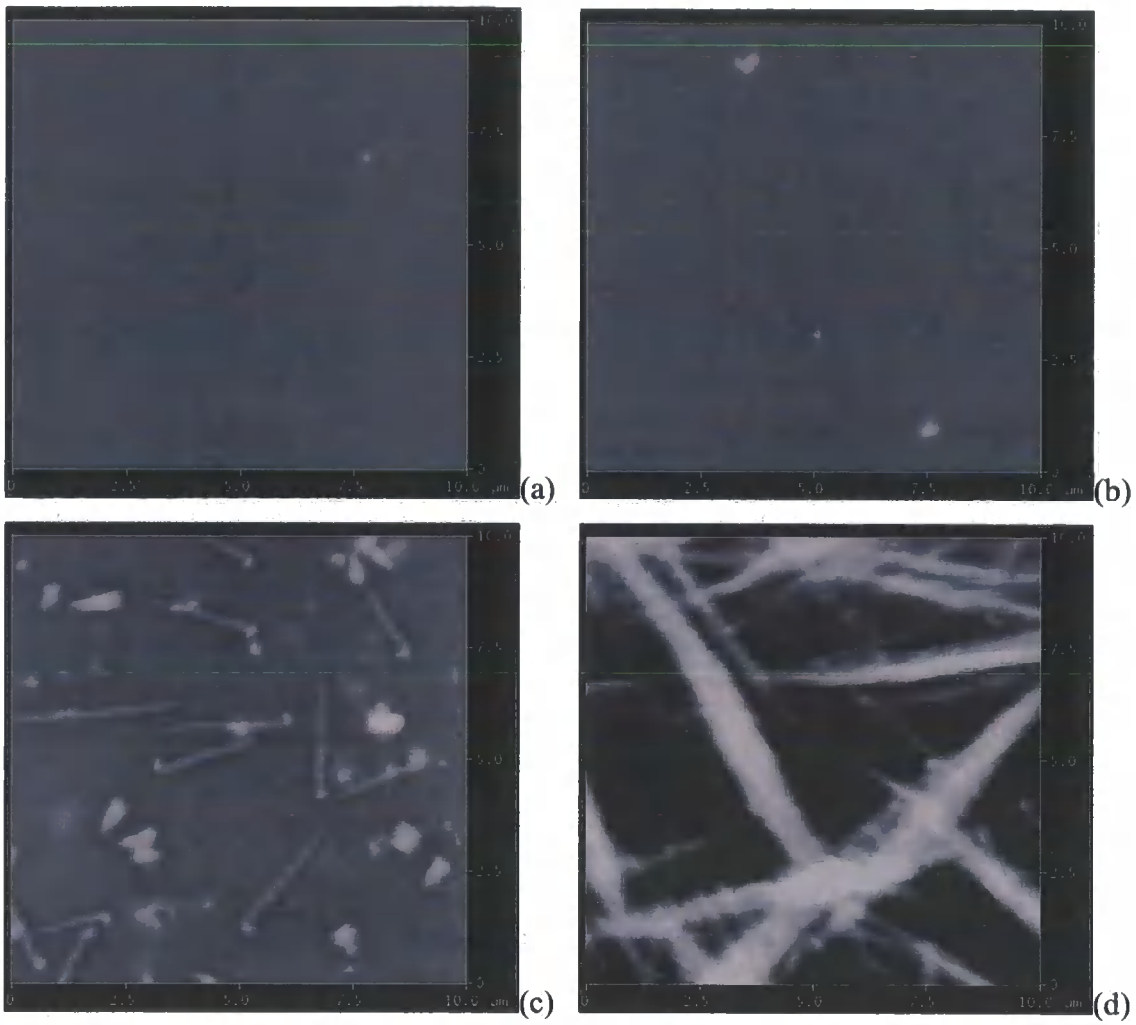

Figure 32: AFM images of the 70% 184 (a) and 50% 185 (b) blend films spin-cast from the blend solution using chloroform as the solvent; 50% 184 (c) and 50% 185 (d) blend films from the blend solutions using the mixture of chloroform and *p*-xylene (3:1 v/v).

In contrast to the results from Figure 31, EL from the ET compounds was evident in OLEDs incorporating phase-separated layers. Figure 33 compares the EL spectra of a 70% **185** blended-layer device formed from pure chloroform with 70% **184** and 70% **185** blended-layer devices formed using the mixed solvent. Small shoulders in the 420–520 nm region can be seen in the spectra for the OLEDs fabricated using the mixed solvent; this is more evident for the device containing compound **185**. These peaks coincide with the emission from devices based on the pure ET compounds **184** and **185**. The phase separation also affected the external quantum efficiencies of the devices. The efficiency of all these devices decreased as the blend

composition exceeded 50% of the ET material and was less than 0.1%. The interface between the separated phase and the matrix can act as a quenching site where non-radiative singlet-exciton decay takes place, consequently reducing the light emission and the efficiency. Another reason for the efficiency decrease with the concentration can be that more light will be emitted from clusters of **185**.

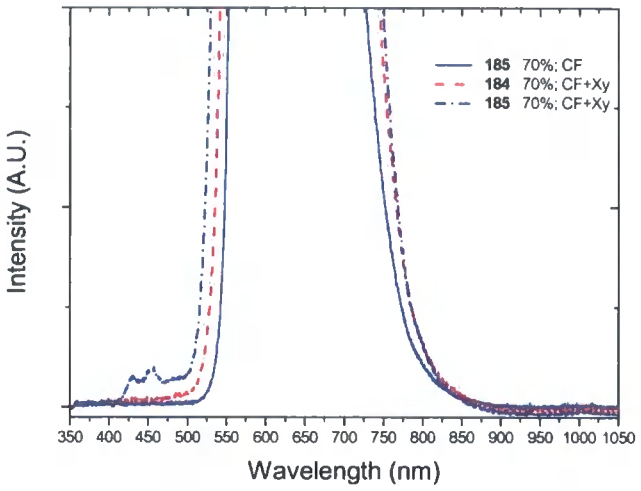

Figure 33. The EL spectra of 70% 185 devices spin-cast from chloroform solution; 70% 184 and 185 device from the solution using a mixture of chloroform (CF) and *p*-xylene (Xy) solvent.

3.3 CONCLUSIONS

We have synthesised the 2-phenyl-5-pyridyl-1,3,4-oxadiazole ring system **183** and described Suzuki cross-coupling reactions to obtain the first OXD–fluorene hybrids which incorporate pyridine (**184** and **185**) within the linearly-extended π-electron system. The first OXD–fluorene hybrid that incorporates a thienyl unit (**189**) was also synthesised. X-ray structure analyses of **189** revealed that two molecular configurations of **189** are present in the unit cell.

Spectroscopic studies in solution establish that replacement of the phenyl ring in compounds **165** and **171** by a pyridine ring (**184** and **185**, respectively) leads to a significant red-shift in both the absorption (*ca.* 16 nm) and emission spectra (*ca.* 10 nm). Further red-shift in absorption (*ca.* 38 nm) and emission spectra (*ca.* 40 nm) are observed when the phenyl ring (**165**) is replaced with a thienyl ring (**189**).

We have shown that the introduction of the pyridyl unit into OXD-fluorene systems significantly increases the ETHB properties of the materials. Single-layer OLEDs were fabricated by spin-coating blends of MEH-PPV as the emissive material with added ET

compounds **184** or **185**. The external quantum efficiencies of the devices were greatly enhanced compared to pure MEH-PPV reference devices, with EQEs of (based on 70% blends) **184** and **185** of *ca.* 0.08 % and 0.25 %, respectively. In comparison, the efficiency of blend devices incorporating 70% of **165** and **171** was *ca.* 0.05 %, while that of a pure MEH-PPV reference device was 10^{-3}%.

Further improvements in efficiency were realised by incorporating PEDOT:PSS. The EQE for the device ITO/PEDOT:PSS/MEH-PPV–**185** (30:70% by weight)/Al reached 0.5% and a luminous efficiency of 1.1 cd A^{-1} at 11 V and a luminance of 100 cd m^{-2} was achieved. Replacing the Al cathode with Ca/Al gave only a modest increase in efficiency (EQE 0.6 % and 1.3 cd A^{-1} at 9.3 V) unlike the pure MEH-PPV reference device where a far greater increase in efficiency occurs. This leads to the important conclusion that electron injection into the MEH-PPV emitter can be enhanced *either* by using a low work function metal such as Ca, *or* by exploiting a blended-layer structure.

4 A NEW OXD-FLUORENE COPOLYMER

4.1 INTRODUCTION

Having successfully achieved the synthesis of OXD-fluorene hybrid materials (**165** and **171**) which met with success as ETHB materials, we therefore turned our attention to polymeric OXD-fluorene hybrids for use in OLEDs as emissive materials with electron transport characteristics.

OXD-fluorene main chain[110] and side chain polymers[124,126] have been synthesised and applied in PLEDs. In our group Wang *et al.*[113] synthesised the poly(alkoxyPBD) derivative **114** using Suzuki coupling methodology. Following on from this work, our strategy was to combine the OXD units with a spirobifluorene core to provide blue emission and minimise the formation of fluorenone defects. Ethylhexoxy units were introduced into the system to increase solubility and hence processability.

In this chapter we report the synthesis of the OXD-fluorene copolymer **191** via Suzuki coupling methodology along with solution and solid-state optical absorption and PL spectra. The synthesis of the monomer **196,** an analogue of **165,** which was achieved via a tetrazole route, is also described.

4.2 RESULTS AND DISCUSSIONS

4.2.1 Synthesis

Initially we synthesised polymer **191** via Suzuki-type co-polymerisation of an equimolar mixture of the OXD derivative **190,** which was synthesised by C. Wang in our laboratory, and the dipinacolboronate reagent **170**[166b] with $Pd(PPh_3)_4$ as the catalyst in THF. This yielded the target copolymer **191** in a 7% yield. The polymer was subjected to GPC analysis in THF solution using a refractive index detector. Molecular weights were calculated from a calibration curve created with polystyrene standards, and so are approximate values. The polymer synthesised under these initial conditions (i) had a number average molecular weight (*Mn*) of *ca.* 3.8×10^3 g mol^{-1}, with a polydispersity (pd) index of 2.0. Due to the low yield of polymer **191** under this first set of conditions, we repeated the synthesis under the second set

of conditions (ii). The $Pd(PPh_3)_4$-catalysed Suzuki coupling reaction of dipinacolboronate reagent **170** and monomer **190** was accomplished in toluene solution by adding a catalytic amount of bulky tri-*tert*-butylphosphine as a promoter.[166b] This revised set of conditions (ii) yielded the polymer in an increased yield of 48%. GPC analysis was carried out, as previously, and revealed that polymer **191** synthesised under conditions (ii) had an increased *Mn* of *ca.* 5.8 x 10^3 g mol^{-1} and a pd of 2.35.

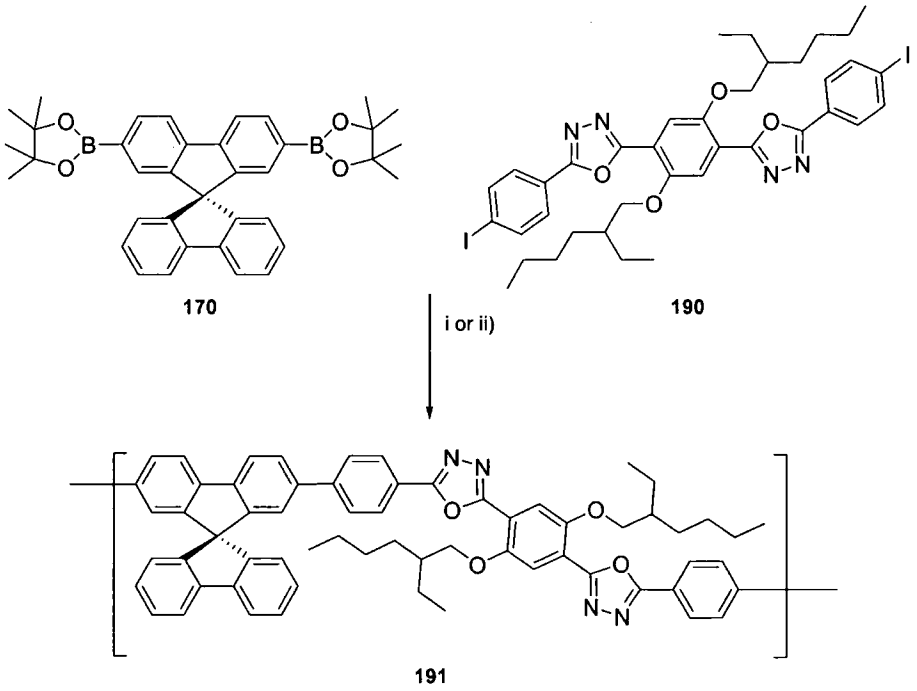

Scheme 82: Synthesis of polymer 191 (i) $Pd[PPh_3]_4$, Na_2CO_3, THF, Δ; (ii) $Pd[PPh_3]_4$, PBu^t_3, K_2CO_3, toluene, Δ.

Polymer **191** exhibited good solubility in a range of common organic solvents. Differential scanning calorimetry (DSC) was carried out at a heating rate of 10.0 °C min^{-1} in the temperature range from 25 to 300 °C. For polymer **191** no phase transitions were observable.

The synthesis of monomer **196** was achieved via a tetrazole route.[36] 2,7-Bis(4-cyanophenyl)-9,9-dihexylfluorene **193** was synthesised in 47% yield via Suzuki coupling of 9,9-dihexyl-2,7-dibromofluorene **163** and the commercially available 4-cyanophenyl boronic acid **192**.[197] Compound **193** was converted into the corresponding tetrazole **194** in 82% yield, via the reaction of sodium azide and ammonium chloride in DMF.[55] Tetrazole **194** was then treated with 4-iodobenzoyl chloride **195** in pyridine to yield the monomer **196** in 75 % yield.[55]

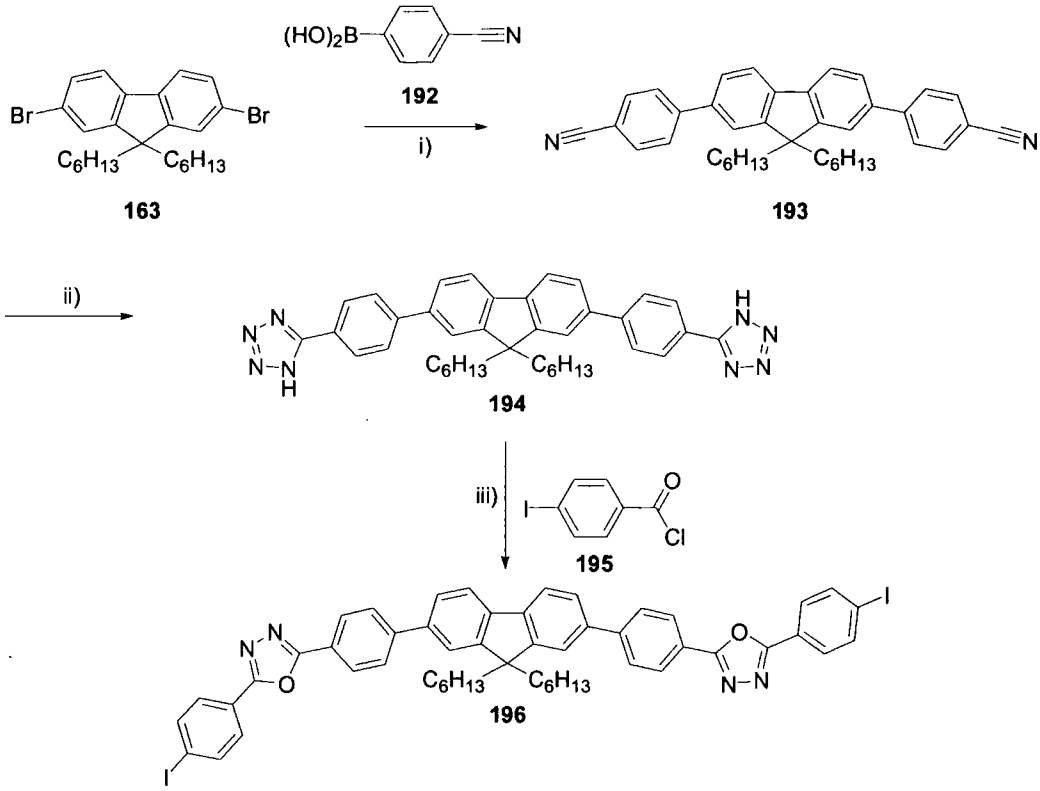

Scheme 83: Synthesis of compound 196 (i) $Pd[PPh_3]_2Cl_2$, PBu^t_3, Na_2CO_3, THF, Δ; (ii) NaN_3, NH_4Cl, DMF, Δ; (iii) pyridine, Δ.

4.2.2 Optical Absorption and Emission Properties

Solution UV-Vis absorption and PL spectra for polymer **191** were recorded in DCM. A broad absorption was observed for the polymer with λ_{max} of 380 nm. The PL spectrum consisted of a major peak at λ_{max} = 415 nm and a red-shifted shoulder at λ_{max} = 436 nm.

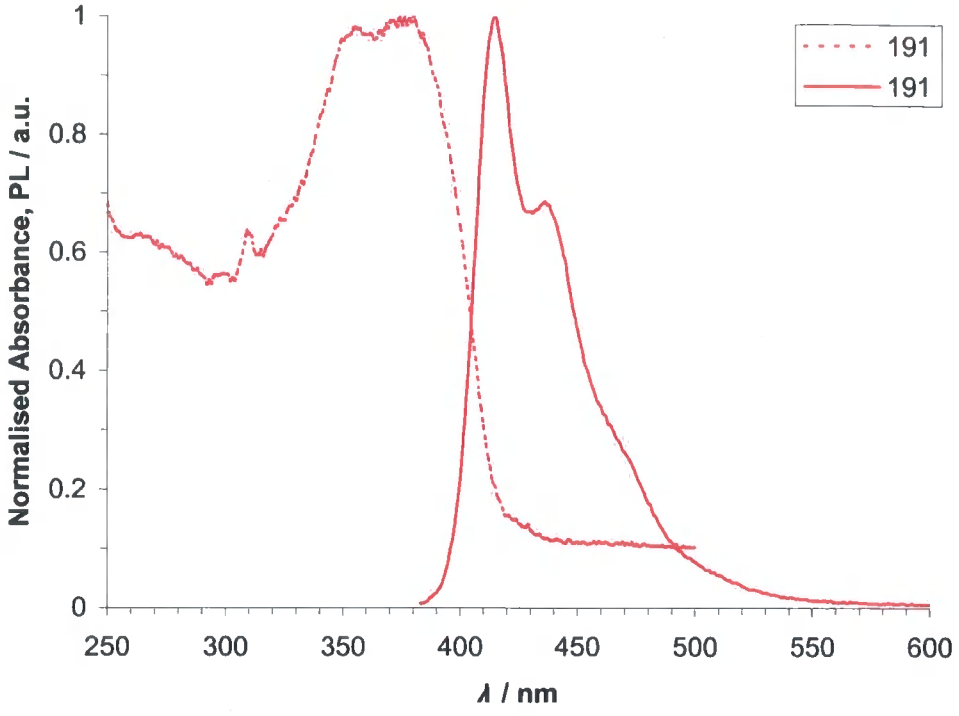

Figure 34: Normalized UV-Vis absorption (dashed line) and PL (solid line) spectra for polymer 191 in DCM, 20 °C. Excitation wavelengths correspond to the maximum of absorption.

Photoluminescence quantum yields (PLQY) measurements were undertaken by S. King in collaboration with Prof A. P. Monkman's group in the Department of Physics, University of Durham. Solution PLQY measurements were undertaken in toluene using diphenylanthracene (DPA) as a standard. For polymer **191** a solution PLQY of 77% was calculated from integration of the PL of polymer **191** in comparison with that of the DPA standard (Figure 35).

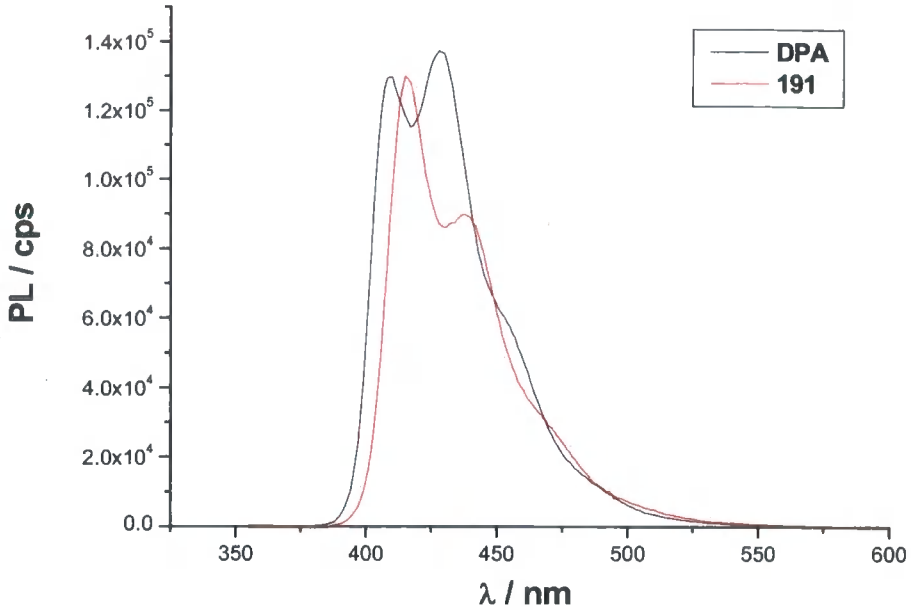

Figure 35: UV-Vis PL spectra for polymer 191 and DPA in toluene, 20 °C. Excitation wavelengths correspond to the maximum of absorption.

Solid state PLQY measurements of thin films of polymer **191** were carried out using a fluorimeter in combination with an integrating sphere.[198] Polymer **191** was spin-coated onto a sapphire substrate from chlorobenzene. The calibrated PL was calculated from the measured spectra by subtracting the spectral response of the sphere (Figure 36).

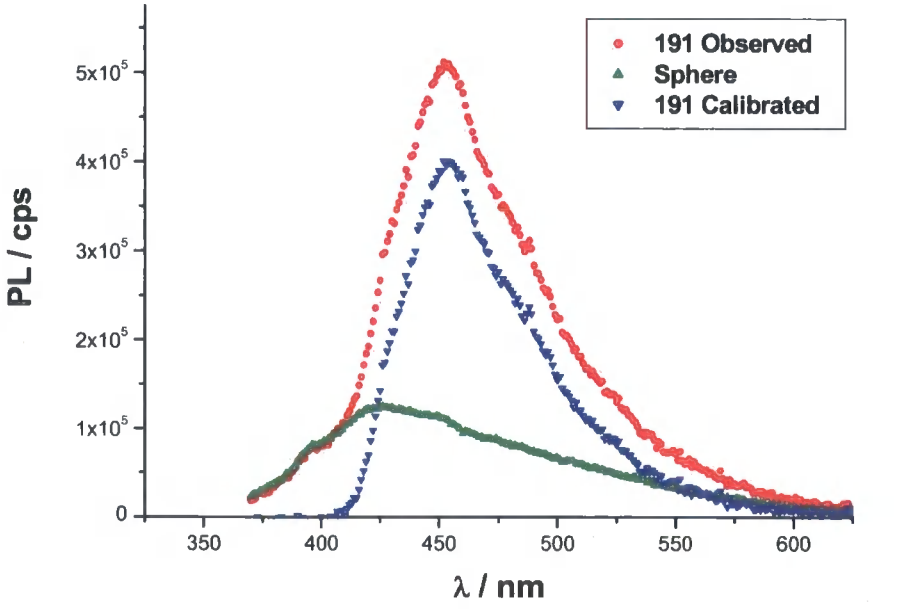

Figure 36: PL spectra of thin films of polymer 191 and calibrated spectra used in PLQY measurements.

The calculated PLQY for the thin film of polymer **191** was only *ca.* 1%, which is significantly diminished, compared to the solution state PLQY. There is precedent for this reduction in PL efficiency in related systems, as Morgado *et al.* found that the PL efficiency of a series of fluorene-thiophene copolymers was strongly reduced on going from solution to the solid state, which was attributed to the quenching effects associated with the interchain interactions.[199] Given this low PLQY for films of **191**, device studies were not pursued.

4.3 CONCLUSIONS

We have synthesised the fluorene-OXD copolymer **191** and the monomer **196**. No further studies were carried out on copolymer **191** due to the strong reduction in PLQY in the solid state compared to solution measurements, which is severely detrimental for OLED applications. The monomer **196** was prepared via a tetrazole route but was not taken any further. This compound is the analogue of **165** and could be a key reagent in future OXD-fluorene co-polymer studies within our laboratory.

5 EXPERIMENTAL PROCEDURES

This chapter details the experimental procedures and analytical data for each of the novel compounds presented in this thesis. This chapter also includes the experimental procedures for some compounds which were already known in the literature that were used in the course of this work.

5.1 GENERAL METHODS

All reactions that required inert or dry atmospheres were carried out under a blanket of argon, which was dried by passage through a column of phosphorus pentoxide. All reagents employed were of standard reagent grade and purchased from Aldrich, Lancaster, Avocado, Fluka or Merck and used without further purification unless otherwise stated. The following solvents were dried and distilled immediately prior to use: acetone, over Drierite ($CaSO_4$), acetonitrile and dichloromethane over calcium hydride, diethyl ether and toluene over sodium metal, tetrahydrofuran over potassium metal. *N,N*-Dimethylformamide was dried by standing over 4 Å molecular sieves for at least 48 h and was not distilled prior to use. Ethanol and methanol were dried and distilled over magnesium turnings and stored under dry argon over 3 Å molecular sieves. Pyridine was dried by standing over potassium hydroxide overnight followed by vacuum distillation and stored under dry argon over 3 Å molecular sieves. Chlorobenzene, cyclohexane, ethyl acetate, hexane and petroleum ether were used without prior purification.

Column chromatography was carried out using Prolabo silica (70-230 mesh). Solvents used for chromatography were distilled prior to use, with the exception of dichloromethane, chloroform and petroleum ether, which were used as supplied. Analytical Thin Layer Chromatography (tlc) was performed on Merck DC-Alufolien Silica gel, 60 F_{254} 0.2 mm thickness or Merck DC-Alufolien oxide neutral (Type E), 60 F_{254} 0.2 mm thickness precoated tlc plates.

UV-Vis spectra were recorded using a Varian Cary 5 spectrophotometer at ambient temperatures. Photoluminescence spectra were recorded using a Jobin-Yvon Horiba Flurolog 3-22 Tau-3 spectrofluorimeter with a 0.5-2 nm bandpass using a Xenon lamp. Spectra were recorded using conventional 90 ° geometry with an excitation at the maximum absorbance recorded for the specific compound. PLQY of thin films were measured using a Jobin-Yvon Fluromax spectrofluorimeter equipped with integrating sphere.[198]

For the fabrication of OLEDs, MEH-PPV was purchased from Aldrich and blended with the ET materials described in Chapters 2 and 3. Indium-tin-oxide (ITO) coated glass from Merck with sheet resistance of 9 Ω $\square^{-1}$ was used as the anode. This was cleaned by ultrasonication in acetone and isopropyl alcohol for 30 min each and dried with a nitrogen gun. The polymer and ET materials were dissolved in chloroform or in a mixture of chloroform and *p*-xylene (3:1 v/v) to provide the blend solution, which was spin-coated onto the ITO. The concentration of ET material was changed from 20% to 95% for compounds **165**, **171** and **177** and 50 % to 95 % for compound **184** and **185**, of the total weight. Following the spin-coating, Al or Ca/Al top electrodes, in the form of dots (radius 1 mm; thickness 150 nm) were thermally evaporated at a pressure of about 10^{-6} mbar. In some cases PEDOT:PSS, purchased from Bayer AG, was spin-coated onto the ITO prior to the deposition of the polymer blend. These PEDOT layers (40 nm in thickness) were dried for 12 h in nitrogen at room temperature to remove residual solvent.

Electrical measurements were undertaken in a vacuum chamber (10^{-1} mbar). The d.c. bias was applied and the current measured by a Keithley 2400 Source Meter. The light emitted from the device was collected by a large area photodiode (1.5 cm diameter) connected to a Keithley 485 Digital Picoammeter. For external quantum efficiency measurements, the light power was calculated using the photocurrent and the conversion factor (wavelength dependent) of the photodiode (ampere/watt). Electroluminescence (EL) spectra were measured using an Ocean Optics USB2000 Miniature Fibre Optic Spectrometer. The surface morphologies of the blend films were observed using a Digital Instrument NanoScope E atomic force microscope.

Solution ^{1}H NMR and ^{13}C NMR spectra were recorded on Mercury 200, Varian Unity 300, Bruker Avance 400 and Varian Inova 500 spectrometers operating at (^{1}H) 199.99, 299.91, 400.13, 499.99 and (^{13}C) 50.29, 75.42, 100.62, 124.99 MHz, respectively. Chemical shifts are reported in ppm downfield of tetramethylsilane (TMS), using TMS or the residual solvent as internal reference. The following abbreviations are used in listing NMR spectra: s = singlet, d = doublet, dd = doublet of doublets, dt = doublet of triplets, t = triplet, m = multiplet and br = broad.

Mass spectra were obtained on a VG7070E instrument operating in EI mode at 70 eV. Electrospray high resolution mass spectra were obtained on a Micromass LCT (TOF). MALDI-TOF spectra were obtained on an Applied Biosystems Voyager-DE STR operating in reflector mode.

Elemental analyses were obtained on a Carlo-Erba Strumentazione instrument. Melting points were determined in open-end capillaries using a Stuart Scientific melting point apparatus SMP3 at a ramp rate of 2.5 °C min^{-1} without calibration.

Single-crystal X-ray diffraction experiments were carried out on a Bruker SMART 3-circle diffractometer with an APEX CCD area detector, using graphite monochromated Mo-K_α radiation ($\overline{\lambda}$ =0.71073 Å) from 60W Mo-target microfocus Bede Microsource® X-ray generator with glass polycapillary X-ray optics and a Cryostream-Plus open-flow N_2 cryostat. The structure was solved by direct methods and refined by full-matrix least squares against F^2 of all reflections, using SHELXTL 6.14 software (Bruker-Nonius AXS, Madison, WI, USA, 2003).

5.2 Experimental Procedures of Chapter 2

5.2.1 Suzuki Cross-Coupling: General Procedure

The halide, the boronic acid and the catalyst (5 mol% relative to the boronic acid) were added sequentially to degassed THF/ DMF/ toluene, in the absence of light. The reaction mixture was stirred at 20 °C for 0.5 h. Degassed aqueous Na_2CO_3/K_2CO_3 solution was added and the reaction mixture was heated at reflux under Ar until tlc monitoring showed that the reaction was complete (48–96 h). Solvent was evaporated *in vacuo* and the crude products were extracted into organic solvent. The organic layer was washed with H_2O, separated and dried over $MgSO_4$. Products were purified by column chromatography.

5.2.2 4-Bromo-benzoic acid hydrazide 138

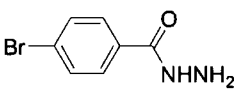

Methyl-4-bromobenzoate **137** (10.75 g, 50 mmol) was dissolved in ethanol (70 cm^3) with heating. Hydrazine monohydrate (7.27 cm^3, 150 mmol) was added and the mixture was refluxed for 12 h. The solution was then cooled to rt and the white crystalline solid collected by suction filtration and washed with cold ethanol. The product was then dried under high vacuum for 24 h yielding compound **138** (9.68 g, 90%), mp: 167.8-168.1 °C, (lit.[151] 163-165 °C). δ_H (DMSO-d_6, 400 MHz) 9.84 (s, 1H), 7.75 (d, *J* 8, 2H), 7.64 (d, *J* 8, 2H), 4.49 (s, 2H). δ_C (DMSO-d_6, 100 MHz) 165.57, 133.07, 132.03, 129.74, 125.46.

5.2.3 2-(4-Bromophenyl)-5-(4-dodecyloxyphenyl)-1,3,4-oxadiazole 140

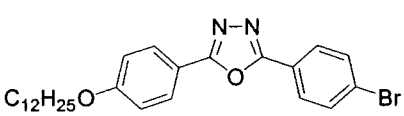

4-*n*-Dodecyloxybenzoic acid (3.07 g, 10 mmol) **135** was refluxed in thionyl chloride ($SOCl_2$) (15 cm^3) for 12 h under argon to obtain a clear orange solution. The excess $SOCl_2$ was then removed by vacuum distillation to yield an orange residue. Dry toluene (30 cm^3) was then added and distilled off at

reduced pressure to remove any remaining $SOCl_2$. After cooling to rt, 4-bromobenzoic acid hydrazide **138** (2.15 g, 10 mmol) dissolved in pyridine (20 cm^3) was added via syringe. The solution was stirred for 0.5 h at rt and then for a further 0.5 h at 110 °C. Pyridine was removed by vacuum distillation. After cooling to rt, methanol (100 cm^3) was then added and the suspension was heated at reflux for 15 min, cooled and the white solid obtained by vacuum filtration. The crude intermediate product was dried for 12 h under high vacuum and then refluxed with phosphorus oxychloride ($POCl_3$) (25 cm^3) for 5 h after which time the $POCl_3$ was removed by vacuum distillation yielding a cream solid. Methanol (100 cm^3) was then added and the suspension was heated at reflux for 15 min, cooled and the solid obtained by vacuum filtration. The crude product was then purified by column chromatography (eluent: DCM-EtOAc 19:1 v/v) and crystallisation (ethanol) to yield white crystals of compound **140** (3.7 g, 76%), mp: 101.5-102 °C (lit.[29e] 101 °C). MS (EI) *m/z* 486 (M^+, ^{81}Br, 100%), 484 (M^+, ^{79}Br, 98%). Anal. Calcd for $C_{26}H_{33}BrN_2O_2$: C, 64.33; H, 6.85; N, 5.77. Found: C, 64.09; H, 6.89; N, 5.60. δ_H ($CDCl_3$, 400 MHz) 8.04 (d, *J* 9, 2H), 7.98 (d, *J* 8.8, 2H), 7.66 (d, *J* 8.8, 2H), 7.01 (d, *J* 8.8, 2H), 4.03 (t, *J* 6.6, 2H), 1.81 (m, 2H), 1.26 (m, 18H), 0.87 (t, *J* 6.5, 3H). δ_C ($CDCl_3$, 100 MHz) 167.31, 163.60, 162.32, 132.61, 128.95, 128.43, 126.37, 123.25, 116.23, 115.23, 68.53, 32.151, 29.87, 29.80, 29.59, 29.34, 26.23, 24.68, 24.53, 22.93, 21.31, 14.37.

5.2.4 Attempted synthesis of 2-(4-benzene boronic acid)-5-(4-dodecyloxyphenyl)-[1,3,4] oxadiazole 141

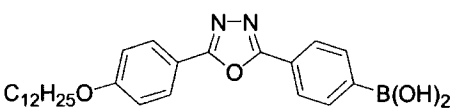

To a solution of 2-(4-bromophenyl)-5-(dodecyloxyphenyl)-1,3,4-oxadiazole **140** (1.0 g, 2.1 mmol) in dry THF (40 cm^3) was added *n*BuLi solution in hexane (1.6 M, 1.6 cm^3) drop wise at –78 °C under argon. The mixture was stirred at –78 °C for 6 h to give a dense white suspension. Triisopropyl borate (TIPB) (1.0 cm^3, 4.3 mmol) was syringed in quickly at –78 °C and the mixture was stirred for 12 h with a cooling bath allowing the temperature to rise gradually to 20 °C yielding a bright yellow solution. The suspension was quenched with H_2O to give a cloudy cream suspension, which was stirred for a further 0.5 h. THF was evaporated under *vacuo* and NaOH (5% soln) was added until a pH of 10 was achieved. The organic material was then extracted with an ether/hexane (4:1) mixture and the aqueous layer was acidified with aqueous HBr (48%) giving a white precipitate. Crystallisation of the crude

product from a H_2O / EtOH mixture yielded a white solid (0.05g, 5%). δ_H (DMSO-d_6, 300 MHz) 8.29 (s, 2H), 8.02 (m, 6H), 7.16 (d, *J* 7.5, 2H), 4.01 (m, 2H), 1.7 (m, 2H), 1.06 (m, 18H), 0.81 (m, 3H). The peak at 8.29 ppm disappeared on addition of D_2O (as would be expected for a boronic acid group). However, impurities in the ^1H and ^{13}C NMR spectra, incorrect elemental analysis and decomposition at 189.1-193 °C rather than a clean sharp melting point were obtained. Low yields were consistently obtained and further purification proved difficult making it impossible for satisfactory identification of the product. Further modifications to this procedure carried out as described on page 66 did not yield compound **141**.

5.2.5 Methyl-4-bromo-3,5-dimethoxybenzoate 143

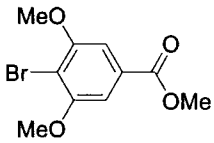

4-Bromo-3,5-dihydroxybenzoic acid **142** (7.0 g, 30 mmol), potassium carbonate (12.44 g, 90 mmol) and dimethylsulphate (8.52 cm^3, 90 mmol) in dry acetone (75 cm^3) under argon were stirred at rt for 20 min and then refluxed for 8 h. After cooling the salts were filtered off and the solvent evaporated under vacuo. The crude product was dissolved in diethylether and washed sequentially with H_2O, NaOH (5% soln.), H_2O, ammonium hydroxide (conc.), H_2O, HCl (dil.), and finally H_2O. The washed solution was dried over Na_2SO_4 and evaporated under vacuo to give a white solid, which was recrystallised from ethanol to yield white crystals of compound **143** (6.59 g, 80%), mp: 121.6-122.6 °C (Lit.[200] 121-122 °C). δ_H (DMSO-d_6, 200 MHz) 7.19 (s, 2H), 3.88 (s, 6H), 3.86 (s, 3H). δ_C (DMSO-d_6, 100 MHz) 166.30, 157.24, 130.67, 106.20, 105.77, 57.22, 53.20.

5.2.6 4-Bromo-3,5-dimethoxybenzoic acid hydrazide 144

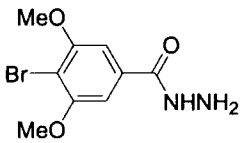

Methyl-4-bromo-3,5-dimethoxybenzoate **143** (6.0 g, 21.8 mmol) was dissolved in ethanol (20 cm^3) with heating. Hydrazine monohydrate (10 cm^3, 206 mmol) was added and the solution was refluxed for 12 h. The solution was then cooled to rt and suspended in an ice bath. The cream crystalline solid was then collected by vacuum filtration and washed with ice cold ethanol. The product was then dried under high vacuum for 24 h to yield compound **144** (3.8 g, 63%), mp: 212.7-213.5 °C.

MS (EI) *m/z* 276 (M^+, ^{81}Br, 3%), 274 (M^+, ^{79}Br, 3%). Anal. Calcd for $C_9H_{11}BrN_2O_3$: C, 39.29; H, 4.03; N, 10.18. Found: C, 39.27; H, 4.07; N, 10.36. δ_H (DMSO-d_6, 200 MHz) 9.88 (s, 1H), 7.16 (s, 2H), 4.53 (s, 2H), 3.87 (s, 6H). δ_C (DMSO-d_6, 100 MHz) 165.59, 157.03, 134.35, 104.15, 103.33, 57.17.

5.2.7 2-(3,5-Dimethoxy-4-bromophenyl)-5-(4-dodecyloxyphenyl)-1,3,4-oxadiazole 145

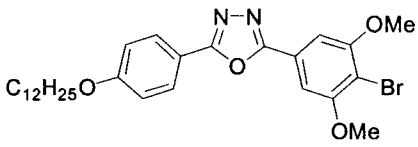

4-*n*-Dodecyloxybenzoic acid **135** (3.07g, 10.0 mmol) was refluxed in $SOCl_2$ (15 cm^3) for 12 h under argon. The excess $SOCl_2$ was then removed by vacuum distillation. Dry toluene (30 cm^3) was then added and distilled off at reduced pressure to remove any remaining $SOCl_2$. After cooling to rt, 4-bromo-3,5-dimethoxybenzoic acid hydrazide **144** (2.75 g, 10 mmol) dissolved in pyridine (20 cm^3) was added via syringe. The solution was stirred for 0.5 h at rt and then for a further 0.5 h at 110 °C. Pyridine was removed by vacuum distillation. After cooling to rt, H_2O (100 cm^3) was then added and the suspension was heated at reflux for 15 min, cooled and the cream solid obtained by vacuum filtration. The crude intermediate product was dried for 12 h under high vacuum and then refluxed with $POCl_3$ (25 cm^3) for 5 h after which time the $POCl_3$ was removed by vacuum distillation yielding a cream solid. H_2O (100 cm^3) was then added and the suspension was heated at reflux for 15 min, cooled and the solid obtained by vacuum filtration. The crude product was then purified by column chromatography (eluent: DCM-EtOAc 9:1 v/v) and crystallisation (ethanol) to yield white crystals of compound **145** (3.97 g, 73%), mp: 116.5-117.3 °C. MS (EI) *m/z* 546 (M^+, ^{81}Br, 51%), 544 (M^+, ^{79}Br, 51%). Anal. Calcd for $C_{28}H_{37}BrN_2O_2$: C, 61.65; H, 6.84; N, 5.14. Found: C, 62.11; H, 6.97; N, 4.98. δ_H (DMSO-d_6, 200 MHz) 8.04 (d, *J* 8.6, 2H), 7.36 (s, 2H), 7.11 (d, *J* 8.6, 2H), 4.06 (t, *J* 6.3, 2H), 3.96 (s, 6H), 1.72 (m, 2H), 1.23 (m, 18H), 0.83 (t, *J* 6.6, 3H). δ_C ($CDCl_3$, 100 MHz) 164.82, 163.74, 162.16, 157.65, 128.78, 124.03, 115.93, 115.03, 105.06, 102.95, 68.35, 56.80, 31.91, 29.64, 29.62, 29.58, 29.55, 29.36, 29.33, 29.13, 26.00, 22.67, 14.08.

5.2.8 2-(3,5-Dimethoxy-4-(4-benzaldehyde)-phenyl)-5-(4-dodecyloxyphenyl)-1,3,4-oxadiazole 147

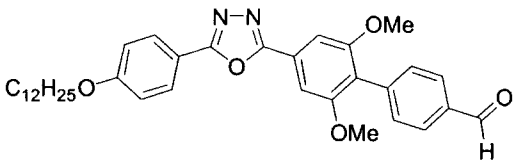

In accordance with the general method for Suzuki cross-coupling reactions, compound **145** (1.64 g, 3 mmol), 4-formylbenzene boronic acid **146** (0.57 g, 3.8 mmol), $Pd(PPh_3)_4$ (230 mg, 0.19 mmol), THF (40 cm^3) and Na_2CO_3 (2 M, 9.75 cm^3); reaction time 96 h; extracted with diethyl ether. Chromatography eluent: DCM–EtOAc (17:3 v/v), followed by recrystallisation from ethanol gave **147** as a white solid (0.82 g, 48%), mp: 103.5-104.0 °C. MS (EI) *m/z* 570 (M^+, 100%). Anal. Calcd. for $C_{35}H_{42}N_2O_5$: C, 73.66; H, 7.42; N, 4.91. Found: C, 73.17; H, 7.42; N, 4.90. δ_H ($CDCl_3$, 400 MHz) 10.07 (s, 1H), 8.10 (d, *J* 8.8, 2H), 7.95 (d, *J* 8.4, 2H), 7.56 (d, *J* 8.4, 2H), 7.42 (s, 2H), 7.04 (d, *J* 8.8, 2H), 4.06 (t, *J* 6.6, 2H), 3.88 (s, 6H), 1.83 (m, 2H), 1.28 (m, 18H), 0.89 (t, *J* 7.2, 3H). δ_C ($CDCl_3$, 100 MHz) 192.05, 164.81, 163.98, 162.15, 157.87, 140.09, 135.21, 131.59, 129.10, 128.79, 125.06, 121.41, 116.03, 115.05, 102.81, 68.36, 56.24, 31.91, 29.65, 29.62, 29.58, 29.56, 29.37, 29.33, 29.14, 26.00, 22.67, 14.09.

5.2.9 4-Dodecyloxybenzoic acid methyl ester 148

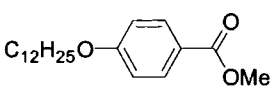

4-*n*-Dodecyloxybenzoic acid **135** (6.13 g, 20 mmol) was dissolved in methanol (50 cm^3). Conc. H_2SO_4 (1.0 cm^3) was added and the solution was refluxed for 12 h. The solution was then cooled to rt and the white precipitate collected by suction filtration and washed with water and cold methanol. Recrystallisation of the solid from methanol afforded compound **148** as white needles (6.04 g, 94%), mp: 55.0-55.9 °C (lit.[156] 57-58 °C). δ_H ($CDCl_3$, 400 MHz) 8.0 (d, *J* 8.8, 2H), 6.9 (d, *J* 8.8, 2H), 4.0 (t, *J* 6.5, 2H), 3.9 (s, 3H), 1.8 (m, 2H), 1.3 (m, 18H), 0.9 (t, *J* 6.8, 3H). δ_C ($CDCl_3$, 100 MHz) δ 167.17, 163.18, 131.78, 122.50, 114.27, 68.42, 52.07, 32.15, 29.89, 29.87, 29.82, 29.79, 29.59, 29.57, 29.34, 26.21, 22.93, 14.36.

5.2.10 4-Dodecyloxybenzoic acid hydrazide 149

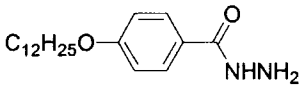

4-*n*-Dodecyloxybenzoic acid methyl ester **148** (5.8 g, 18.1 mmol) was dissolved in methanol (50 ml) with heating. Hydrazine monohydrate (8.7 cm^3, 180 mmol) was added and the mixture was refluxed for 12 h. The solution was then cooled to rt and the white precipitate collected by suction filtration and washed with water and cold methanol. Recrystallisation of the solid from ethyl acetate afforded compound **149** as a white solid (5.2 g, 90%), mp: 95.3-96 °C (lit.[157] 94-96 °C). MS (EI) *m/z* 320 (M^+, 100%). δ_H ($CDCl_3$ 200 MHz) 7.7 (d, *J* 8.8, 2H), 7.5 (br, 1H), 6.9 (d, *J* 8.8, 2H), 4.0 (t, *J* 6.6, 2H), 3.4 (br, 2H), 1.8 (m, 2H), 1.3 (m, 18H), 0.9 (t, *J* 6.2, 3H).

5.2.11 Attempted synthesis of 152

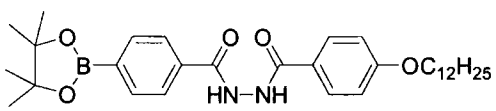

Compound **150** (1.24 g, 5.0 mmol) was refluxed in $SOCl_2$ (15 cm^3) for 12 h under argon. The excess $SOCl_2$ was then removed by vacuum distillation. Dry toluene (30 cm^3) was added and distilled off at reduced pressure to remove any remaining $SOCl_2$. After cooling to rt, 4-dodecyloxybenzoic acid hydrazide **149** (1.60 g, 5 mmol) dissolved in pyridine (20 cm^3) was added via syringe. The solution was stirred for 0.5 h at rt and then for a further 0.5 h at 110 °C. Pyridine was removed by vacuum distillation. After cooling to rt, H_2O (100 cm^3) was then added and the suspension was heated at reflux for 15 min, cooled and the cream solid obtained by vacuum filtration. From ^1H NMR analysis of the crude intermediate product **152**, no N-H peaks were observed indicating the reaction had possibly failed. The intermediate **152** was dried for 12 h under high vacuum and then refluxed with $POCl_3$ (25 cm^3) for 5 h after which time the $POCl_3$ was removed by vacuum distillation. H_2O (100 cm^3) was then added and the suspension was heated at reflux for 15 min, cooled and the solid obtained by vacuum filtration. ^1H NMR analysis of the crude product showed no identifiable features. Further purification proved difficult making it impossible for satisfactory identification of the crude product.

5.2.12 2-Biphenyl-4-yl-5-(dodecyloxyphenyl)-1,3,4-oxadiazole 157

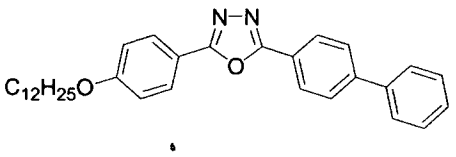

By analogy with the synthesis of **147**, compound **140** (1.0 g, 2.1 mmol), benzeneboronic acid **153** (0.30 g, 2.5 mmol), $Pd(PPh_3)_4$ (144 mg, 0.13 mmol), DMF (30 cm^3) and Na_2CO_3 (1 M, 6.2 cm^3); reaction time 96 h; extracted with DCM. Chromatography eluent: DCM–EtOAc (9:1 v/v), followed by recrystallisation from cyclohexane gave **157** as a white crystalline solid (0.72 g, 71%), mp: 115.4–116.4 °C. MS (EI) *m/z* 482 (M^+, 72%). Anal. Calcd. for $C_{32}H_{38}N_2O_2$: C, 79.63; H, 7.94; N, 5.80. Found: C, 79.36; H, 7.88; N, 5.75. δ_H ($CDCl_3$, 200 MHz) 8.21 (d, *J* 8.2, 2H), 8.09 (d, *J* 8.2, 2H), 7.74 (d, *J* 6.8, 2H), 7.60 (d, *J* 8.2, 2H), 7.51 (t, *J* 7.2, 1H), 7.40 (t, *J* 7.2, 2H), 7.02 (d, *J* 8.6, 2H), 4.04 (t, *J* 6.6, 2H), 1.8 (m, 2H), 1.3 (m, 18H), 0.88 (t, *J* 6.6, 3H). δ_C ($CDCl_3$, 100 MHz) 164.31, 164.01, 162.25, 141.63, 144.41, 129.22, 128.93, 128.37, 127.91, 127.51, 127.40, 123.10, 117.22, 115.22, 68.52, 32.16, 29.90, 29.88, 29.83, 29.81, 29.61, 29.59, 29.37, 26.24, 22.93, 14.38. UV-Vis (DCM) λ_{max} 313 nm, PL (DCM) λ_{max} 365, 378 nm.

5.2.13 2-(4-Dodecyloxyphenyl)-5-(3-methoxybiphenyl-4-yl)-1,3,4-oxadiazole 158

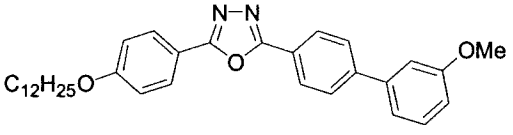

By analogy with the synthesis of **147**, compound **140** (0.51 g, 1.1 mmol), 3-methoxybenzene boronic acid **154** (0.23 g, 1.5 mmol), $Pd(PPh_3)_4$ (85 mg, 0.07 mmol), THF (20 cm^3) and Na_2CO_3 (2 M, 2.2 cm^3); reaction time 72 h; extracted with DCM. Chromatography eluent: DCM–EtOAc (9:1 v/v), followed by recrystallisation from ethanol gave **158** as a white crystalline solid (0.46 g, 85%), mp: 99.1–99.7 °C. MS (EI) *m/z* 512 (M^+, 86%). Anal. Calcd. for $C_{33}H_{40}N_2O_3$: C, 77.31; H, 7.86; N, 5.46. Found: C, 77.74; H, 7.86; N, 5.34. δ_H ($CDCl_3$, 200 MHz) 8.18 (d, *J* 8.2, 2H), 8.08 (d, *J* 8.2, 2H), 7.74 (d, *J* 8.2, 2H), 7.40 (t, *J* 7.8, 1H), 7.26 (s, 1H), 7.19 (d, *J* 8.8, 1H), 7.02 (d, *J* 8.8, 2H), 6.96 (d, *J* 8.2, 1H), 4.04 (t, *J* 6.6, 2H), 3.89 (s, 3H), 1.82 (m, 2H), 1.28 (m, 18H), 0.88 (t, *J* 6.6, 3H). δ_C ($CDCl_3$, 100 MHz) 179.89, 164.21, 162.22, 160.29, 144.33, 141.61, 130.25, 128.93, 127.97, 127.47, 123.23, 119.88, 116.37, 115.21, 113.68, 113.16, 68.52, 55.62, 32.20, 29.90, 29.88, 29.83, 29.81, 29.62, 29.60, 29.37, 26.23, 22.93, 14.38.

5.2.14 5-{4-[5-(4-Dodecyloxyphenyl)-1,3,4-oxadiazol-2-yl]-phenyl}-furan-2-carbaldehyde 159

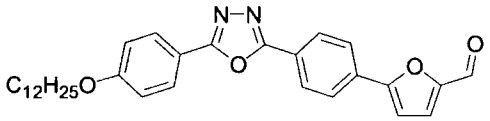

By analogy with the synthesis of **147**, compound **140** (0.24 g, 0.50 mmol), 2-furaldehyde-5-boronic acid **155** (0.10 g, 0.72 mmol), $Pd(PPh_3)_4$ (42 mg, 0.04 mmol), THF (20 cm^3) and Na_2CO_3 (2 M, 1.1 cm^3); reaction time 96 h; extracted with EtOAc. Chromatography eluent: DCM–EtOAc (9:1 v/v), followed by recrystallisation from ethanol gave **159** as a pale pink solid (0.07 g, 28%), mp: 167.5-168.1 °C. MS (EI) *m/z* 500 (M^+, 62%). Anal. Calcd. for $C_{31}H_{36}N_2O_4$: C, 74.37; H, 7.25; N, 5.60. Found: C, 74.04; H, 7.32; N, 5.58. δ_H ($CDCl_3$, 200 MHz) 9.63 (s, 1H), 8.12 (d, *J* 8.2, 2H), 8.05 (d, *J* 8.4, 2H), 7.89 (d, *J* 8.2, 2H), 7.29 (d, *J* 3.8, 1H), 6.98 (d, *J* 8.4, 2H), 6.90 (d, *J* 3.8, 1H), 3.97 (t, *J* 6.6, 2H), 1.80 (m, 2H), 1.20 (m, 18H), 0.81 (t, *J* 6.6, 3H). δ_C ($CDCl_3$, 100 MHz) 177.65, 165.10, 162.37, 158.13, 152.70, 136.61, 131.75, 129.01, 127.58, 125.96, 124.97, 117.65, 116.11, 115.20, 109.40, 68.54, 32.14, 29.86, 29.82, 29.83, 29.63, 29.61, 29.59, 29.34, 26.22, 22.92, 14.36.

5.2.15 5-{4-[5-(4-Dodecyloxyphenyl)-1,3,4-oxadiazol-2-yl]-phenyl}-2-methoxypyridine 160

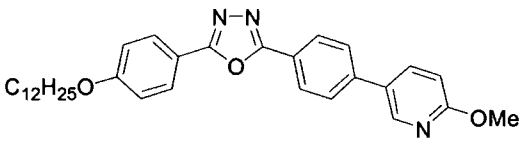

By analogy with the synthesis of **147**, compound **140** (0.49 g, 1.0 mmol), 2-methoxypyridine-5-boronic acid **156** (0.23 g, 1.5 mmol), $Pd(PPh_3)_4$ (87 mg, 0.08 mmol), THF (20 cm^3) and Na_2CO_3 (2 M, 2.25 cm^3); reaction time 72 h; extracted with EtOAc. Chromatography eluent: DCM–EtOAc (17:3 v/v), followed by recrystallisation from ethanol gave **160** as a cream/white crystalline solid (0.35 g, 68%), mp: 145.1-145.7 °C. MS (EI) *m/z* 513 (M^+, 11%). Anal. Calcd. for $C_{32}H_{39}N_3O_3$: C, 74.82; H, 7.65; N, 8.18. Found: C, 74.74; H, 7.71; N, 8.23. δ_H ($CDCl_3$, 200 MHz) 8.47 (d, *J* 2.5, 1H), 8.19 (d, *J* 8.5, 2H), 8.07 (d, *J* 9, 2H), 7.85 (dd, J_{ab} 6.4, J_{ac} 2.5, 1H), 7.68 (d, *J* 8.4, 2H), 7.02 (d, *J* 9, 2H), 6.95 (d, *J* 8.6, 1H), 4.0 (m, 5H), 1.82 (m, 2H), 1.26 (m, 18H), 0.87 (t, *J* 6.6, 3H). δ_C ($CDCl_3$, 100 MHz) 164.90, 164.09, 162.24, 164.34, 145.44, 141.19, 137.44, 129.04, 128.93, 127.69, 127.32, 123.15, 116.33, 115.22, 111.36, 68.53, 53.93, 32.16, 29.90, 29.88, 29.83, 29.80, 29.61, 29.59, 29.36, 26.23, 22.93, 14.37. UV-Vis (DCM) λ_{max} 315 nm, PL (DCM) λ_{max} 364, 378 nm.

5.2.16 2,7-Dibromofluorene 162

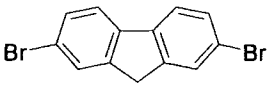

Fluorene **161** (250.0 g, 1.5 mol) was dissolved in acetic acid (2000 cm^3) at 70 °C and H_2SO_4 (98%, 25 cm^3) was added slowly to the solution. The reaction mixture was allowed to cool to *ca.* 50 °C with stirring, and a solution of Br_2 (100 cm^3) in acetic acid (200 cm^3) was then added dropwise with stirring, keeping the temperature at 40-55 °C to avoid crystallisation of the fluorene. When *ca.* half of the Br_2 had been added, 2,7-dibromofluorene started to crystallise. When this was observed, the remaining Br_2 was added simultaneously with $KBrO_3$ (100 g) in acetic acid (400 cm^3) in small portions whilst cooling the flask in an ice bath and ensuring the reaction solution did not exceed 55 °C. The reaction was stirred for 3-4 h at rt and then cooled in an ice bath. The precipitate was collected via vacuum filtration, washed with acetic acid and H_2O 1:1 (v/v) and then H_2O before drying to yield compound **162** (316.8 g, 65%), mp: 163-164 °C (lit.[201] 163.5-165.5 °C). MS (EI) *m/z* 325 (M^+, ^{81}Br, ^{81}Br, 58%), 323 (M^+, ^{79}Br, ^{81}Br, 63%), 321 (M^+, ^{79}Br, ^{79}Br, 59%). Anal. Calcd. for $C_{13}H_8Br_2$: C, 48.19; H, 2.49. Found: C, 47.87; H, 2.48. δ_H ($CDCl_3$, 400 MHz) 7.65 (s, 2H), 7.58 (d, *J* 8, 2H), 7.49 (d, *J* 8, 2H), 3.84 (s, 2H). δ_C ($CDCl_3$, 400 MHz) δ 144.79, 139.69, 130.15, 128.31, 121.19, 120.94, 36.56.

5.2.17 2,7-Dibromo-9,9-dihexylfluorene 163

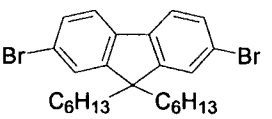

Potassium *tert*-butoxide (1.0 M in THF, 46 cm^3) was added over a period of 0.5 h to a solution of 2,7-dibromofluorene **162** (15 g, 46 mmol) and bromohexane (32.4 cm^3, 0.23 mol) in THF (250 cm^3) at 0 °C, resulting in a red suspension. After stirring for 1 h a second portion of potassium *tert*-butoxide (1.0 M in THF, 46 cm^3) was added dropwise and the suspension stirred for 12 h at rt. THF was removed under *vacuo*, dry DCM (100 cm^3) was added and the purple suspension was then filtered removing inorganic salts. The filtrate was concentrated and purified by column chromatography (silica, eluent: hexane) and recrystallised from ethanol to yield white plates of compound **163** (18.5 g, 82%), mp: 71.2-72.0 °C (lit.[163] 72-73 °C). MS (EI) *m/z* 494 (M^+, ^{81}Br, ^{81}Br, 23%), 492 (M^+, ^{79}Br, ^{81}Br, 44%), 490 (M^+, ^{79}Br, ^{79}Br, 22%). Anal. Calcd. for $C_{25}H_{32}Br_2$: C, 60.99; H, 6.55. Found: C, 60.87; H, 6.54. δ_H ($CDCl_3$, 300 MHz) 7.51-7.54 (m, 2H), 7.45-7.48 (m, 4H), 1.92 (t, *J* 8.4, 4H), 1.04 (m, 12H), 0.79 (t, *J* 6.9, 6H), 0.54 (m, 4H). δ_C

($CDCl_3$, 100 MHz) δ 152.51, 139.01, 130.11, 126.13, 121.43, 121.09, 55.65, 40.18, 31.44, 29.56, 23.62, 22.56, 13.99.

5.2.18 9,9-Dihexylfluorene-2,7-diboronic acid 164

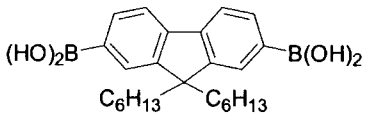

^{n}Butyllithium (2.5 M, 17.7 cm^3, 44.3 mmol) was added dropwise to a stirred solution of 2,7-dibromo-9,9-dihexylfluorene **163** (10.8 g, 21.9 mmol) in THF (100 cm^3) at -78 °C. After 5 h stirring at -78 °C, TIPB (15.2 cm^3, 66 mmol) was added to the white suspension in one portion. The suspension was stirred for 12 h with a cooling bath allowing the temperature to rise gradually to rt. The reaction was quenched with H_2O (100 cm^3) and the mixture stirred for a further 4 h. THF was then removed under *vacuo* and the remaining mixture acidified slowly with HBr (48%) to pH 5. The crude product was then extracted into diethyl ether (3 x 50 cm^3), dried over $MgSO_4$ and the diethyl ether removed under *vacuo*. The white solid was then recrystallised from acetonitrile to yield a white crystalline solid **164** (5.7 g, 61%), mp: 298.0-299.0 °C (lit.[163] 297-298 °C). Anal. Calcd for $C_{25}H_{36}B_2O_4$: C, 71.12; H, 8.60. Found: C, 71.33; H, 8.64. δ_H (DMSO-d_6, 400 MHz) 8.06 (s, 4H), 7.88 (s, 2H), 7.77-7.78 (m, 4H), 1.92 (m, 4H), 1.05 (m, 12H), 0.75 (t, *J* 7.2, 6H), 0.4 (m, 4H). δ_C (DMSO-d_6, 100 MHz) 149.37, 142.30, 132.87, 128.37, 118.96, 54.15, 30.88, 28.96, 23.39, 21.89, 13.71.

5.2.19 2,7-Bis{4-[2-(4-dodecyloxyphenyl)-1,3,4-oxadiazol-5-yl]phenyl}-9,9-dihexylfluorene 165

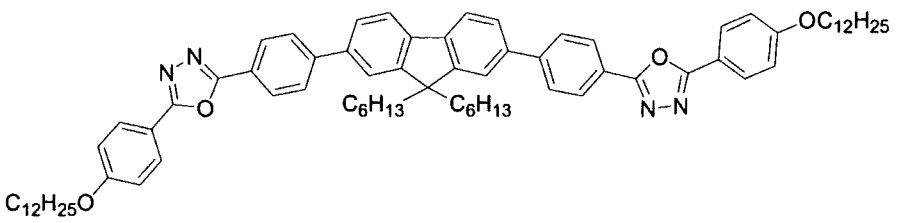

By analogy with the synthesis of **147**, compound **140** (0.44 g, 0.91 mmol), compound **164** (0.23 g, 0.54 mmol), $Pd(PPh_3)_4$ (63 mg, 0.05 mmol), THF (20 cm^3) and Na_2CO_3 (2 M, 0.82 cm^3); reaction time 96 h; extracted with ethyl acetate. Chromatography eluent: DCM–EtOAc (24:1 v/v), followed by recrystallisation from cyclohexane gave **165** as a white solid (0.27 g, 44%), mp: 161.5-162.0 °C. MS (MALDI-TOF) *m/z* Calcd. for $C_{77}H_{98}N_4O_4$: 1143.63

(M^+). Found 1143.74. Anal. Calcd. for $C_{77}H_{98}N_4O_4$: C, 80.87; H, 8.64; N, 4.90. Found: C, 80.59; H, 8.60; N, 4.77. δ_H ($CDCl_3$, 300 MHz) 8.2 (d, *J* 8.4, 4H), 8.0 (d, *J* 8.7, 4H), 7.8 (m, 6H), 7.6 (d, *J* 7.8, 2H), 7.5 (s, 2H), 7.0 (d, *J* 8.7, 4H), 4.0 (t, *J* 6.6, 4H), 2.0 (m, 4H), 1.8 (m, 4H), 1.3 - 1.2 (m, 36H), 1.0 (m, 12H), 0.8 (t, *J* 6.9, 6H), 0.7 (m, 10H). δ_C ($CDCl_3$, 100 MHz) 164.87, 164.28, 162.23, 152.23, 144.84, 140.92, 139.19, 128.94, 127.34, 127.52, 126.50, 122.94, 121.69, 120.64, 116.40, 115.225, 68.53, 55.71, 40.63, 32.16, 31.70, 30.01, 29.91, 29.88, 29.84, 29.81, 29.62, 29.60, 29.37, 26.25, 24.05, 22.94, 22.81, 14.38, 14.25. A crystal for X-ray analysis was grown from hexane / DCM mixture. UV-Vis (DCM) λ_{max} 356 nm, PL (DCM) λ_{max} 401, 422 nm.

5.2.20 2,7-Dibromofluorenone 166

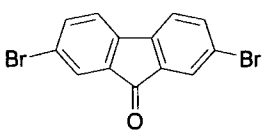

2,7 Dibromofluorene **162** (160 g, 0.49 mol) was dissolved in acetic acid (1400 cm^3) with heating at 95-110 °C. A solution of CrO_3 (122.8 g) in H_2O (100 cm^3) and acetic acid (400 cm^3) was added dropwise with stirring at 95-110 °C. After complete addition the reaction mixture was stirred for 2 h and then allowed to cool to rt with continuous stirring. The yellow solid was then collected, washed sequentially with acetic acid, then acidified H_2O (98%, 30 cm^3 HCl: 700 cm^3 H_2O), to remove chromium salts, and finally H_2O until neutral. The crude product was recrystallised from toluene to give the yellow solid **166** (130.8 g, 79%), mp: 208.1-209.0 °C (lit.[202] 205-209 °C). MS (EI) *m/z* 339 (M^+, ^{81}Br, ^{81}Br, 50%), 337 (M^+, ^{79}Br, ^{81}Br, 100%), 335 (M^+, ^{79}Br, ^{79}Br, 52%). Anal. Calcd for $C_{13}H_6Br_2O$: C, 46.20; H, 1.79. Found: C, 46.15; H, 1.74. δ_H ($CDCl_3$, 400 MHz) 7.76 (d, *J* 2, 2H), 7.63 (dd, J_{ab} 8, J_{ac} 2, 2H), 7.38 (d, *J* 8, 2H), δ_C ($CDCl_3$, 100 MHz) δ 190.92, 142.25, 137.47, 135.27, 127.85, 123.32, 121.84.

5.2.21 2,7- Dibromospirobifluorene 169

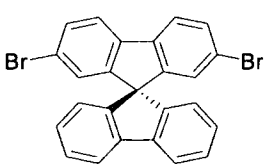

^{t}Butyllithium (1.7 M, 29.4 cm^3, 50 mmol) was added dropwise to a stirred solution of 2-bromobiphenyl **167** (3.45 cm^3, 20 mmol) in THF (30 cm^3) at -78 °C. After 3 h stirring at -78 °C a solution of 2,7-dibromofluorenone **166** (6.76 g, 20 mmol) dissolved in THF (50 cm^3) was added over a

period of 0.5 h. The reaction was stirred for a further 2 h and allowed to warm to rt. The reaction was quenched with H_2O and the THF removed under *vacuo*. The crude product was extracted twice with diethylether, dried over $MgSO_4$ and the diethylether removed under *vacuo*. The crude product was dissolved in acetic acid (20 cm^3) with the addition of HCl (98%, 1 cm^3), the solution was then refluxed for 0.5 h, allowed to cool and then quenched with H_2O. The precipitate was then filtered and washed with H_2O before being dissolved into chloroform and dried over $MgSO_4$. The chloroform was then removed under *vacuo* and the crude product was purified by column chromatography (eluent: chloroform-hexane 1:1 v/v) and recrystallised from chloroform / ethanol to yield a white solid **169** (6.8 g, 72 %), mp: >305 °C (decomp.). MS (EI) *m/z* 475 (M^+, ^{81}Br, ^{81}Br, 52%), 473 (M^+, ^{79}Br, ^{81}Br, 100%), 471 (M^+, ^{79}Br, ^{79}Br, 52%). Anal. Calcd for $C_{25}H_{14}Br_2$: C, 63.32; H, 2.98. Found: C, 63.11, H, 2.90. δ_H ($CDCl_3$, 400 MHz) 7.86 (d, *J* 8, 2H), 7.68 (d, *J* 8, 2H), 7.50 (dd, J_{ab} 8, J_{ac} 2, 2H), 7.42 (td, J_{ab} 7.6, J_{ac} 1.2, 2H), 7.16 (td, J_{ab} 7.6, J_{ac} 1.2, 2H), 6.85 (d, *J* 2, 2h), 6.74 (d, *J* 8, 2H), δ_C ($CDCl_3$, 100 MHz) δ 150.55, 147.07, 141.7, 139.64, 131.13, 128.29, 128.09, 127.34, 124.06, 121.89, 121.39, 120.28, 65.61.

5.2.22 2,7-Di (4,4,5,5-tetramethyl-1,3,2 dioxaborolan-2-yl) spirobifluorene 170

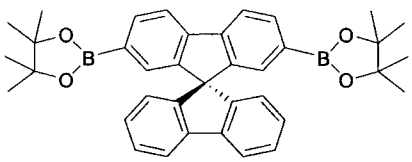

^{n}Butyllithium (1.6 M, 15 cm^3, 25.5 mmol) was added dropwise to a stirred solution of 2,7-dibromospirobifluorene **169** (2.5 g, 5.2 mmol) in THF (100 cm^3) at -78 °C. After 2 h stirring at -78 °C, 2-isopropoxy-4,4,5,5-tetramethyl-[1,3,2]-dioxaborolane (5.31 cm^3, 26 mmol) was added in one portion. The suspension was stirred for a further 2 h and allowed to warm to rt. The reaction was quenched with H_2O and the THF removed under *vacuo*. The crude product was extracted twice with diethylether, dried over $MgSO_4$ and the diethylether removed under *vacuo*. The crude product was then recrystallised from toluene / hexane to give a white solid **170** (1.69 g, 58 %), mp: 320-321 °C (lit.[166b] 321-322 °C). MS (EI) *m/z* 568 (M^+, 100%). Anal. Calcd for $C_{37}H_{38}B_2O_4$: C, 78.20; H, 6.74. Found: C, 77.77, H, 6.68. δ_H ($CDCl_3$, 400 MHz) 7.88-7.85 (m, 6H), 7.37 (td, J_{ab} 7.5, J_{ac} 1.2, 2H), 7.15 (s, 2H), 7.10 (td, J_{ab} 7.5, J_{ac} 1.2, 2H), 6.70 (d, *J* 7.6, 2H), 1.26 (s, 24H), δ_C ($CDCl_3$, 100 MHz) 148.8, 148.6, 144.7, 142.3, 134.9, 130.4, 127.9, 127.8, 124.5, 120.3, 119.9, 83.9, 66.1, 25.0.

5.2.23 2,7-Bis{4-[2-(4-dodecyloxyphenyl)-1,3,4-oxadiazol-5-yl]phenyl}spirobifluorene 171

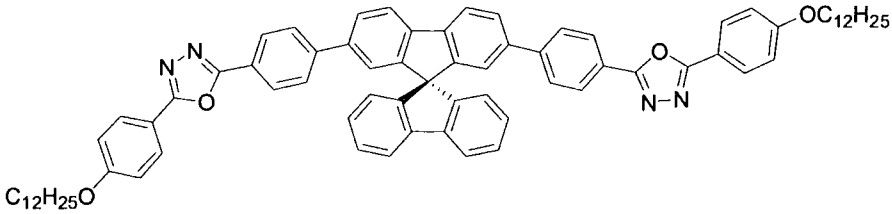

By analogy with the synthesis of **147**, compound **140** (0.40 g, 0.82 mmol), compound **170** (0.23 g, 0.4 mmol), $Pd(PPh_3)_4$ (58 mg, 0.05 mmol), tri-*tert*-butylphosphine (0.02 g, 0.1 mmol), toluene (10 cm^3) and K_2CO_3 (2 M, 2.17 cm^3); reaction time 48 h; extracted with chloroform. Chromatography eluent: DCM-EtOAc (19:1 v/v) followed by recrystallisation from cyclohexane / ethanol mixture gave compound **171** as a white solid (0.18 g, 40%), mp: 138.4-139.6 °C. MS (MALDI-TOF) *m/z* Calcd. for $C_{77}H_{80}N_4O_4$: 1125.48 (M^+). Found 1125.66; Anal. calcd. for $C_{77}H_{80}N_4O_4$: C, 82.17; H, 7.16; N, 4.98. Found: C, 81.71; H, 7.28; N, 4.96. δ_H ($CDCl_3$, 400 MHz) 8.08-8.04 (m, 8H), 8.00 (d, *J* 8, 2H), 7.93 (d, *J* 8, 2H), 7.72 (dd, J_{ab} 8, J_{ac} 1.6, 2H), 7.60 (d, *J* 8, 4H), 7.44 (td, J_{ab} 7.6, J_{ac} 0.8, 2H), 7.17 (td, J_{ab} 7.6, J_{ac} 0.8, 2H), 7.03-7.01 (m, 6H), 6.86 (d, *J* 7.6, 2H), 4.04 (t, *J* 6.8, 4H), 1.83 (m, 4H), 1.5-1.3 (m, 36H), 0.89 (t, *J* 6.8, 6H). δ_C ($CDCl_3$, 100 MHz) δ 164.51, 163.93, 161.98, 150.21, 148.29, 147.51, 143.83, 141.88, 141.25, 139.84, 128.69, 128.05, 127.60, 127.17, 127.09, 124.22, 122.78, 122.64, 120.73, 120.25, 116.16, 114.98, 68.30, 66.14, 31.93, 29.67, 29.64, 29.60, 29.57, 29.38, 29.36, 29.14, 26.00, 22.70, 14.13. UV-Vis (DCM) λ_{max} 356 nm, PL (DCM) λ_{max} 399, 420 nm.

5.2.24 4'-[5-(4-Dodecyloxyphenyl)-1,3,4-oxadiazol-2-yl]-biphenyl-4-carbaldehyde 172

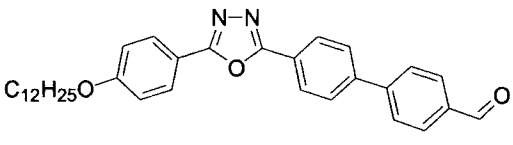

By analogy with the synthesis of **47**, compound **140** (1.46 g, 3.0 mmol), 4-formylbenzene boronic acid **146** (0.58 g, 3.9 mmol), $Pd(PPh_3)_4$ (0.23 g, 0.2 mmol), THF (25 cm^3) and Na_2CO_3 (1 M, 12 cm^3); reaction time 96 h; extracted with chloroform. Chromatography eluent: $CHCl_3$-EtOAc (9:1 v/v) and recrystallisation from $CHCl_3$ / ethanol gave compound **172** as a white solid (1.19 g, 78 %), mp: 211.9-212.7 °C. MS (EI): *m/z* 510 (M^+, 55%); Anal. Calcd. for $C_{33}H_{38}N_2O_3$: C, 77.61; H, 7.50; N, 5.49. Found: C, 77.15; H, 7.34; N, 5.40. δ_H ($CDCl_3$, 200 MHz) 10.10 (s, 1H), 8.25 (d, *J* 7.8, 2H), 8.09 (d, *J*

8.0, 2H), 8.01 (d, *J* 7.8, 2H), 7.80-7.84 (m, 4H), 7.04 (d, *J* 8.0, 2H), 4.05 (t, *J* 6.2, 2H), 1.83 (m, 2H), 1.28 (m, 18H), 0.89 (t, *J* 6.4, 3H). δ_C ($CDCl_3$, 100 MHz) 191.70, 162.12, 145.74, 142.64, 141.47, 135.81, 130.37, 128.75, 127.98, 127.78, 127.44, 124.06, 116.07, 115.05, 99.99, 68.34, 31.91, 29.65, 29.63, 29.58, 29.56, 29.37, 29.34, 29.13, 26.00, 22.68, 14.10.

5.2.25 2-(4-Dodecyloxyphenyl)-5-(4'-styryl-biphenyl-4-yl)-1,3,4-oxadiazole 173

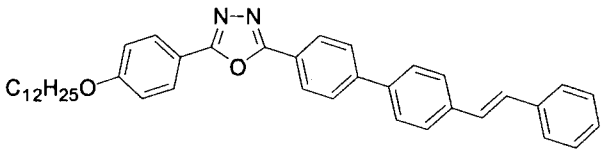

Compound **172** (0.26 g, 0.5 mmol) and benzyltriphenylphosphonium chloride (0.29 g, 0.5 mmol) were dissolved in THF (15 cm^3). NaOH (50% soln. 2.0 cm^3) was then added dropwise over 0.5 h. The reaction was stirred for 8 h. The solvent was removed in *vacuo* and the crude product was extracted with toluene, washed with water and dried over $MgSO_4$. After removal of toluene under *vacuo* the crude product was recrystallised from cyclohexane yielding a yellow solid **173** (0.15 g, 51%), mp: 131.5-132.0 °C. MS (ES) *m/z* 585 (M^+, H^+); Anal. calcd. for $C_{40}H_{44}N_2O_2$: C, 82.15; H, 7.58; N, 4.79. Found: C, 81.94; H, 7.49; N, 4.84. δ_H ($CDCl_3$, 400 MHz) 8.18 (d, *J* 8.4, 2H), 8.08 (d, *J* 8.8, 2H), 7.75 (d, *J* 8.4, 2H), 7.54 (d, *J* 8.0, 2H), 7.37 (d, *J* 8.4, 2H), 7.31 (m, 5H), 7.03 (d, *J* 8.8, 2H), 6.66 (d, *J* 7.6, 2H), 4.05 (t, *J* 6.6, 2H), 1.83 (m, 2H), 1.28 (m, 18H), 0.89 (t, *J* 6.0, 3H). δ_C ($CDCl_3$, 100 MHz) 162.02, 137.21, 130.94, 129.55, 128.62, 128.69, 128.73, 128.32, 127.37, 127.26, 127.10, 126.84, 126.59, 123.59, 122.87, 116.23, 115.02, 109.99, 90.19, 68.33, 31.91, 29.65, 29.63, 29.58, 29.56, 29.37, 29.34, 29.14, 26.00, 22.68, 14.09.

5.2.26 9,9-Dihexylfluorene 174

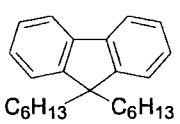

^{n}Butyllithium (1.6 M, 31.3 cm^3, 50 mmol) was added dropwise to a stirred solution of fluorene **161** (3.3 g, 20 mmol) in THF (50 cm^3) at -78 °C. After stirring for 1 h at -78 °C, bromohexane (8.2 cm^3, 60 mmol) was added. The reaction was stirred for 2 h and allowed to warm to rt. The reaction was quenched with H_2O and the THF removed under *vacuo*. The crude product was extracted twice with diethylether, dried over $MgSO_4$ and the diethylether removed under *vacuo* to yield the white deliquescent solid **174** (5.40 g, 81%). MS (EI): *m/z* 334 (M^+, 66%); Anal. Calcd. for $C_{25}H_{34}$: C, 89.76; H,

10.24. Found: C, 89.49; H, 10.20. δ_H ($CDCl_3$, 400 MHz) 7.71 (d, *J* 8, 2H), 7.35 (d, *J* 8.4, 2H), 7.29-7.33 (m, 4H), 1.89-1.85 (m, 4H), 1.02-0.93 (m, 12H), 0.67 (t, *J* 6.8, 6H), 0.54 (m, 4H), δ_C ($CDCl_3$, 100 MHz) 150.71, 141.15, 126.99, 126.70, 122.85, 119.65, 55.04, 40.44, 31.52, 29.75, 23.75, 22.60, 14.10.

5.2.27 2,7-Bis(bromomethyl)-9,9-di-*n*-hexylfluorene 175

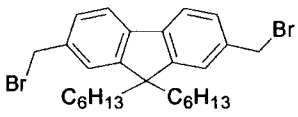

A mixture of 9,9-dihexylfluorene **174** (5.00 g, 15 mmol) and paraformaldehyde (6 g, 200 mmol) in HBr (in acetic acid, 33%) (42 cm^3) was stirred at 60 °C for 24 h. The reaction was cooled to rt and H_2O (100 cm^3) added. The crude product was extracted with DCM (3 x 50 cm^3), washed sequentially with saturated $NaHCO_3$, NaCl and H_2O then dried over $MgSO_4$. After removal of DCM under *vacuo* the crude product was purified by column chromatography (eluent: hexane-ethyl acetate 9:1 v/v) to give the colourless viscous liquid **175** (6.1 g, 78 %). MS (EI) *m/z* 522 (M^+, ^{81}Br, ^{81}Br, 3%), 520 (M^+, ^{79}Br, ^{81}Br, 5%), 518 (M^+, ^{79}Br, ^{79}Br, 3%). δ_H ($CDCl_3$, 400 MHz) 7.44-7.74 (m, 6H), 4.81 (s, 4H), 1.99 (m, 4H), 1.00 (m, 12H), 0.73 (m, 6H), 0.52 (m, 4H). δ_C ($CDCl_3$, 400 MHz) 171.89, 162.88, 150.39, 139.80, 129.45, 119.75, 84.00, 54.85, 40.37, 31.25, 29.56, 23.57, 22.50, 14.02

5.2.28 2,7-Bis(bromomethyl)-9,9-dihexylfluorene triphenylphosphonium dibromide salt 176

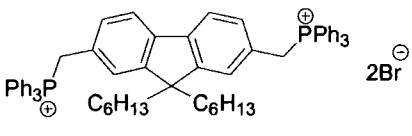

A mixture of 2,7-bis(bromomethyl)-9,9-dihexylfluorene (6.0 g, 11.5 mmol) **175** and triphenyphosphine (10.74 g, 40.95 mmol) in DMF (120 cm^3) was refluxed for 12 h. The cooled solution was then added slowly to diethyl ether (500 cm^3) with vigorous stirring. The white salt, which precipitated, was then filtered, washed with ether and dried under high vacuum for 24 h giving compound **176** (7.2 g, 60 %). δ_H ($CDCl_3$, 400 MHz) 7.78-7.62 (m, 30H), 7.35 (d, *J* 7.6, 2H), 7.07 (d, *J* 7.6, 2H), 6.95 (s, 2H), 5.42 (d, *J* 14, 4H), 1.46 (t, *J* 8.4, 4H), 1.08 (m, 4H), 0.83 (m, 8H), 0.76 (t, *J* 7, 6H), 0.19 (m, 4H). δ_P ($CDCl_3$, 121 MHz) 23.63. δ_C ($CDCl_3$,

100 MHz) 151.24, 140.40, 134.97, 134.99, 134.33, 134.23, 130.15, 130.03, 126.14, 118.14, 117.29, 54.86, 39.96, 31.60, 29.52, 23.79, 22.57, 13.96

5.2.29 Compound 177

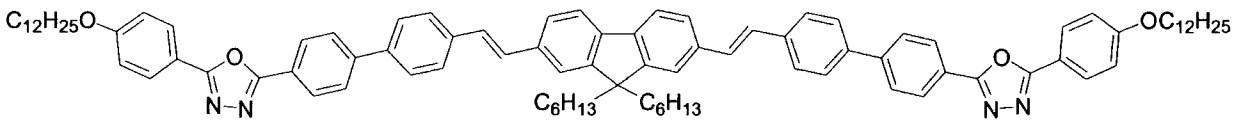

Compound **172** (0.28 g, 0.55 mmol) and compound **176** (0.28 g, 0.27 mmol) were dissolved in a mixture of distilled anhydrous ethanol (30 cm^3) and THF (15 cm^3). Sodium metal (0.03 g) in anhydrous ethanol (15 cm^3) was then added dropwise over 0.5 h. The reaction was stirred for 12 h and then HCl (0.1 M, 1 cm^3) was added. The solvents were removed in *vacuo* and the crude product was extracted with toluene, washed with H_2O and dried over $MgSO_4$. After removal of toluene in *vacuo* the crude product was purified by column chromatography (eluent: $CHCl_3$-diethylether 11.5:1 v/v) and recrystallised from $CHCl_3$ / ethanol to yield compound **177** as a yellow solid (0.16 g, 43%). mp: 171.3-172.7 °C. MS (MALDI-TOF) *m/z* Calcd. for $C_{93}H_{110}N_4O_4$: 1347.89 (M^+). Found 1347.76; Anal. calcd. for $C_{93}H_{110}N_4O_4$: C, 82.87; H, 8.23; N, 4.16. Found: C, 82.38; H, 8.23; N, 4.05. δ_H ($CDCl_3$, 400 MHz) 8.21 (d, *J* 7.2, 4H), 8.10 (d, *J* 7.6, 4H), 7.73 (d, *J* 7.6, 4H), 7.70 (m, 10H), 7.52-7.56 (m, 4H), 7.25-7.29 (m, 4H), 7.04 (d, *J* 7.6, 4H), 4.05 (t, *J* 6.6, 4H), 2.05 (m, 4H), 1.83 (t, *J* 8.1, 4H), 1.28 (m, 36H), 1.09-1.13 (m, 12H), 0.89 (t, *J* 6.0, 6H), 0.71-0.78 (m, 10H). δ_C ($CDCl_3$, 100 MHz) 164.62, 164.00, 162.02, 156.66, 151.66, 143.61, 140.82, 138.64, 137.53, 136.22, 129.97, 128.70, 127.36, 127.32, 127.22, 127.05, 125.82, 122.87, 120.89, 120.02, 116.21, 115.01, 68.32, 55.05, 40.57, 31.92, 31.53, 29.77, 29.67, 29.64, 29.60, 29.57, 29.38, 29.35, 29.15, 26.00, 23.83, 22.68, 22.60, 14.11, 14.01. UV-Vis (DCM) λ_{max} 397 nm, PL (DCM) λ_{max} 444, 468 nm.

5.3 Experimental Procedures of Chapter 3

5.3.1 6-Bromonicotinic acid 180

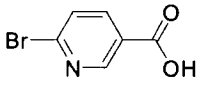

2-Bromo-5-methylpyridine **179** (17.2 g, 100 mmol) and phase transfer agent Aliquat-336 (0.5 cm^3) in H_2O (350 cm^3) were heated at 70 °C. Powdered $KMnO_4$ (44 g, 0.28 mol) was added carefully in small portions over a period of 3 h. The mixture was then refluxed for a further 1.5 h. After cooling, the solid was filtered off, washed with hot water and the combined filtrates were concentrated to *ca.* 150 cm^3, then acidified with HBr (48%) and cooled in an ice bath. The precipitate was then filtered off, washed with H_2O, recrystallised from H_2O and dried to yield **180** as colourless plates (10.1 g, 50%), mp: 194.5–195.0 °C (lit.[185] 195 °C). Anal. Calcd. for $C_6H_4BrNO_2$: C, 35.67; H, 2.00; N, 6.93. Found: C, 35.61; H, 1.99; N, 6.95. δ_H (DMSO-d_6, 400 MHz) 8.87 (d, *J* 2, 1H), 8.16 (dd, J_{ab} 8.2, J_{ac} 2, 1H), 7.80 (d, *J* 8.2, 1H). δ_C ($CDCl_3$, 100 MHz) 165.51, 151.12, 145.54, 139.86, 128.23, 126.42.

5.3.2 2-[5-(2-Bromopyridyl)]-5-(4-dodecyloxyphenyl)-1,3,4-oxadiazole 183

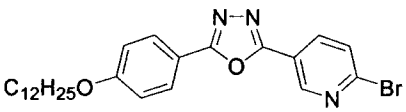

6-Bromonicotinic acid **180** (6.6 g, 32.7 mmol) was refluxed in thionyl chloride (40 cm^3) for 12 h under nitrogen. The excess thionyl chloride was then removed by vacuum distillation. Dry toluene (30 cm^3) was then added and distilled off at reduced pressure to remove any remaining thionyl chloride. After cooling to rt, 4-dodecyloxybenzoic acid hydrazide **149** (10.58 g, 33 mmol) dissolved in pyridine (50 cm^3) was added via a syringe. The solution was stirred for 1 h at rt and then for a further 2 h at 110 °C. Pyridine was removed by vacuum distillation. After cooling to rt, methanol (50 cm^3) was then added and the suspension was heated at reflux for 15 min, cooled and a solid obtained by vacuum filtration. The crude intermediate product was dried for 12 h under high vacuum and then refluxed with $POCl_3$ (40 cm^3) for 12 h after which time the $POCl_3$ was removed by vacuum distillation yielding a cream solid. Methanol (50 cm^3) was

then added and the suspension was heated at reflux for 15 min, cooled and the solid obtained by vacuum filtration. The crude product was dried for 12 h under high vacuum and then dissolved in a minimum amount of dichloromethane. HBr (in glacial acetic acid, 33%) (20 cm^3) was then added and the suspension was stirred at rt for 96 h. The suspension was then diluted with H_2O (20 cm^3) and neutralised with Na_2CO_3 (2 M). The mixture was extracted with DCM, washed with NaOH and then H_2O and filtered through celite before drying with $MgSO_4$ and filtering. The solution was concentrated *in vacuo* and the crude product was then purified by column chromatography (eluent: $CHCl_3$–EtOAc 19:1 v/v) and crystallisation (ethanol) to yield white crystals of compound **183** (5.9 g, 37%), mp: 144–144.5 °C. MS (EI) *m/z* 487 (M^+, ^{81}Br, 20%), 485 (M^+, ^{79}Br, 20%). Anal. Calcd for $C_{25}H_{32}BrN_3O_2$: C, 61.73; H, 6.63; N, 8.64. Found: C, 61.58; H, 6.63; N, 8.43. δ_H ($CDCl_3$, 400 MHz) 9.08 (d, *J* 2.4, 1H), 8.28 (dd, J_{ab} 8.4, J_{ac} 2.4, 1H), 8.07 (d, *J* 8.8, 2H), 7.69 (d, *J* 8.4, 1H), 7.04 (d, *J* 8.8, 2H), 4.05 (t, *J* 6.8, 2H), 1.83 (m, 2H), 1.28 (m, 18H), 0.89 (t, *J* 6, 3H), δ_C ($CDCl_3$, 100 MHz) 165.30, 162.40, 160.00, 154.21, 147.68, 136.50, 128.89, 128.54, 119.63, 115.50, 115.14, 68.38, 31.91, 29.64, 29.62, 29.58, 29.55, 29.35, 29.33, 29.11, 25.99, 22.67, 14.09.

5.3.3 2,7-Bis{5-[2-(4-dodecyloxyphenyl)-1,3,4-oxadiazol-5-yl]-2-pyridyl}-9,9-dihexylfluorene 184

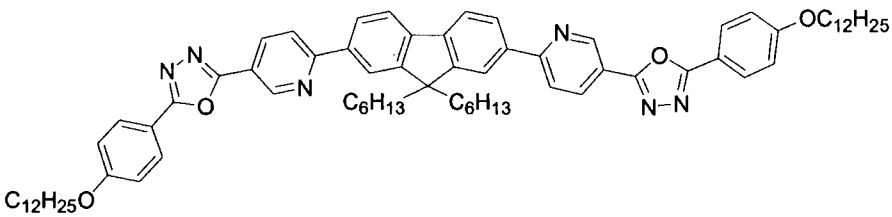

In accordance with the general method for Suzuki cross-coupling reactions, compound **183** (0.196 g, 0.4 mmol), compound **164** (0.077 g, 0.18 mmol), $Pd(PPh_3)_4$ (23 mg, 0.02 mmol), THF (25 cm^3) and Na_2CO_3 (2 M, 0.6 cm^3); reaction time 48 h; extracted with DCM. Chromatography eluent: DCM–EtOAc (19:1 v/v) followed by DCM–EtOAc (9:1 v/v) and recrystallisation from ethanol gave **184** as a white solid (0.073 g, 35%), mp: 166.7–167.5 °C. MS (MALDI-TOF) *m/z* Calcd. for $C_{75}H_{96}N_6O_4$: 1145.76. Found 1145.73 (M^+); Anal. Calcd. for $C_{75}H_{96}N_6O_4$: C, 78.63; H, 8.45; N, 7.34. Found: C, 78.99; H, 8.51; N, 6.94. δ_H ($CDCl_3$, 400 MHz) 9.44 (d, *J* 2, 2H), 8.51 (dd, J_{ab} 8, J_{ac} 2, 2H), 8.14 (m, 4H), 8.12 (d, *J* 8.8, 4H), 8.02 (d, *J* 8, 2H), 7.9 (d, *J* 8, 2H), 7.06 (d, *J* 8.8, 4H), 4.06 (t, *J* 6.4, 4H), 2.17 (m, 4H), 1.84 (m, 4H), 1.5-1.3 (m, 36H), 1.1 (m, 12H), 0.9 (t, *J* 6.4, 6H), 0.74 (m, 10H). δ_C ($CDCl_3$, 100 MHz)

165.02, 162.25, 159.81, 152.33, 147.66, 142.40, 134.80, 134.78, 128.84, 126.43, 121.59, 120.64, 120.44, 120.41, 118.62, 115.86, 115.12, 68.37, 55.70, 53.39, 40.38, 31.91, 31.50, 29.65, 29.63, 29.59, 29.56, 29.37, 29.34, 29.13, 26.00, 23.88, 22.68, 22.56, 14.10, 13.95. UV-Vis (DCM) λ_{max} 372 nm, PL (DCM) λ_{max} 411, 431 nm.

5.3.4 2,7-Bis{5-[2-(4-dodecyloxyphenyl)-1,3,4-oxadiazol-5-yl]-2-pyridyl}spirobifluorene 185

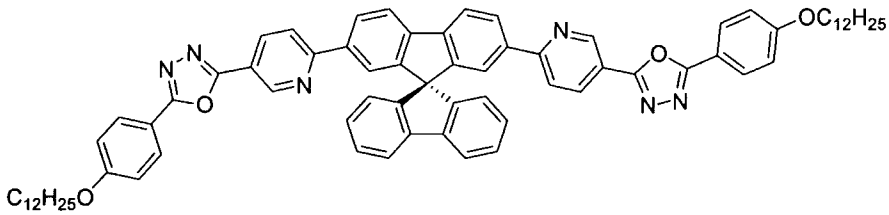

By analogy with the synthesis of **184**, compound **183** (0.486 g, 1 mmol), compound **170** (0.284 g, 0.5 mmol), $Pd(PPh_3)_4$ (58 mg, 0.05 mmol), tri-*tert*-butylphosphine (0.02 g, 0.1 mmol), toluene (20 cm^3) and K_2CO_3 (2 M, 2.5 cm^3); reaction time 48 h; extracted with chloroform. Chromatography eluent: $CHCl_3$–EtOAc (17:3 v/v) followed by recrystallisation from a toluene/ethanol mixture gave compound **185** as a yellow solid (0.32 g, 56%), mp: 203.0–203.4 °C. MS (MALDI-TOF) *m/z* Calcd. for $C_{75}H_{78}N_6O_4$: 1127.62. Found 1127.65 (M^+); Anal. calcd. for $C_{75}H_{78}N_6O_4$: C, 79.90; H, 6.97; N, 7.45. Found: C, 79.70; H, 7.00; N, 7.26. δ_H ($CDCl_3$, 400 MHz) 9.27 (s, 2H), 8.33 (d, *J* 8.4, 2H), 8.23 (d, *J* 8, 2H), 8.04 (m, 6H), 7.94 (d, *J* 8, 2H), 7.72 (d, *J* 8.4, 2H), 7.43 (m, 4H), 7.15 (t, *J* 7.6, 2H), 7.02 (d, *J* 8.4, 4H), 6.84 (d, *J* 7.6, 2H), 4.04 (t, *J* 6, 4H), 1.82 (m, 4H), 1.5-1.3 (m, 36H), 0.89 (t, *J* 6.4, 6H). δ_C ($CDCl_3$, 100 MHz) 164.95, 162.19, 162.09, 159.13, 150.4, 147.98, 147.45, 142.85, 142.0, 138.30, 134.57, 128.81, 128.10, 127.48, 127.17, 124.25, 122.72, 121.00, 120.43, 120.30, 118.62, 115.76, 115.06, 68.33, 66.15, 31.92, 29.66, 29.64, 29.59, 29.57, 29.39, 29.37, 29.12, 25.99, 22.70, 14.13. UV-Vis (DCM) λ_{max} 371 nm, PL (DCM) λ_{max} 407, 430 nm.

5.3.5 1,4-Bis{5-[2-(4-dodecyloxyphenyl)-1,3,4-oxadiazol-5-yl]-2-pyridyl}-2,5-(2-ethylhexoxy) phenyl 187

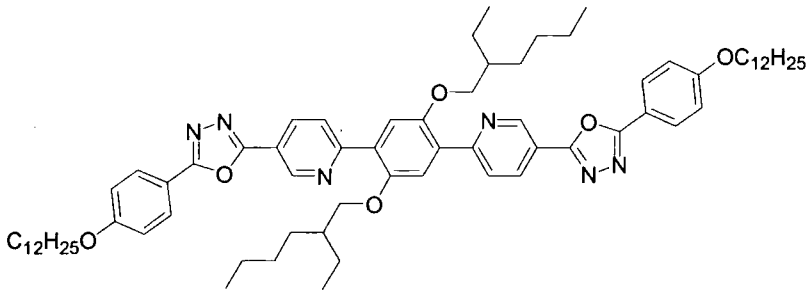

By analogy with the synthesis of **184**, compound **183** (0.69 g, 1.4 mmol), compound **186** (0.30 g, 0.71 mmol), $Pd(PPh_3)_2Cl_2$ (52 mg, 0.07 mmol), tri-*tert*-butylphosphine (0.02 g, 0.1 mmol), THF (50 cm^3) and Na_2CO_3 (2 M, 2.8 cm^3); reaction time 96 h; extracted with toluene. Chromatography eluent: DCM–EtOAc (11.5:1 v/v) followed by recrystallisation from ethanol gave compound **187** as a yellow solid (0.33 g, 41%), mp: 144.5-145.2 °C. MS (MALDI-TOF) *m/z* Calcd. for $C_{72}H_{100}N_6O_6$: 1145.71. Found 1145.77 (M^+); Anal. calcd. for $C_{72}H_{100}N_6O_6$: C, 75.49; H, 8.80; N, 7.34. Found: C, 74.99; H, 8.76; N, 7.37. δ_H ($CDCl_3$, 400 MHz) 9.45 (d, *J* 2.4, 2H), 8.43 (dd, J_{ab} 8.4, J_{ac} 2.4, 2H), 8.28 (d, *J* 8.4, 2H), 8.11 (d, *J* 8.8, 4H), 7.76 (s, 2H), 7.06 (d, *J* 8.8, 4H), 4.07 (m, 8H), 1.85 (m, 6H), 1.5-1.3 (m, 52H), 0.89 (m, 18H). δ_C ($CDCl_3$, 100 MHz) 165.00, 162.29, 162.24, 157.65, 151.54, 147.20, 133.55, 129.46 128.83, 125.55, 118.50, 115.88, 115.37, 115.11, 71.64, 68.36, 39.70, 31.91, 30.83, 29.65, 29.62, 29.85, 29.55, 29.36, 29.33, 29.13, 29.10, 26.00, 24.23, 23.02, 22.67, 14.09, 14.03, 11.23. UV-Vis (DCM) λ_{max} 327, 380 nm, PL (DCM) λ_{max} 460 nm.

5.3.6 2,7-Bis{5-[5-(4-*tert*-butylphenyl)-1,3,4-oxadiazol-2-yl]-thien-2-yl}-9,9-dihexylfluorene 189

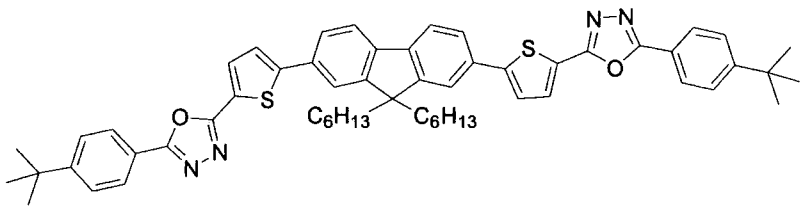

By analogy with the synthesis of **184**, compound **188** (0.3 g, 0.73 mmol), compound **164** (0.17 g, 0.40 mmol), $Pd(PPh_3)_2Cl_2$ (29 mg, 0.04 mmol), tri-*tert*-butylphosphine (0.01 cm^3, 0.1 mmol), THF (50 cm^3) and Na_2CO_3 (2 M, 1.0 cm^3); reaction time 96 h; extracted with toluene. Chromatography

eluent: DCM–EtOAc (32.3:1 v/v) followed by DCM–EtOAc (9:1 v/v) and recrystallisation from toluene / ethanol gave yellow needles of **189** (0.15 g, 42%), mp: 252.6-253.0 °C. MS (EI) *m/z* 898 (M^+, 100%). Anal. calcd. for $C_{57}H_{62}N_4O_2S_2$: C, 76.13; H, 6.95; N, 6.23. Found: C, 75.73; H, 6.89; N, 5.91. δ_H ($CDCl_3$, 400 MHz) 8.08 (d, *J* 8.4, 4H), 7.84 (d, *J* 4, 2H), 7.78 (d, *J* 8.0, 2H), 6.70 (d, *J* 8.0, 2H), 7.65 (s, 2H), 7.57 (d, *J* 8.4, 4H), 7.47 (d, *J* 4, 2H), 2.07 (m, 4H), 1.40 (s, 18H), 1.11 (m, 12H), 0.77 (m, 10H). δ_C ($CDCl_3$, 100 MHz) 164.12, 160.93, 155.43, 152.16, 149.75, 141.11, 132.39, 130.54, 128.81, 126.08, 125.34, 123.85, 123.75, 120.94, 120.61, 120.41, 55.53, 40.35, 35.12, 31.43, 31.13, 29.62, 23.79, 22.54, 13.96. UV-Vis (DCM) λ_{max} 394 nm, PL λ_{max} (DCM) 439, 466 nm.

5.4 EXPERIMENTAL PROCEDURES OF CHAPTER 4

5.4.1 Polymer 191 (Method 1)

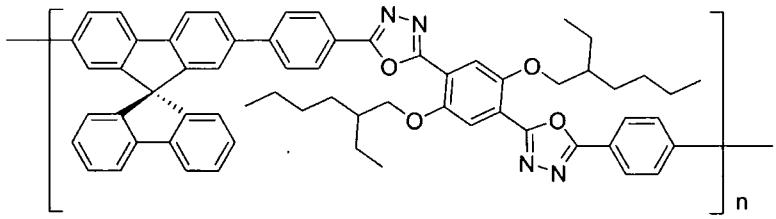

In accordance with the general method for Suzuki cross-coupling reactions, compound **190** (0.87 g, 1.0 mmol), compound **170** (0.57 g, 1.0 mmol), $Pd(PPh_3)_4$ (115 mg, 0.1 mmol), THF (50 cm^3) and Na_2CO_3 (2 M, 5 cm^3); reaction time 96 h; extracted with $CHCl_3$. The organic solution was then washed with H_2O, dried and filtered through a celite column. The filtrate was concentrated in *vacuo* to afford a viscous solution that was added dropwise into vigorously stirring ethanol (150 cm^3) and the resulting mixture was stirred at rt for 12 h. The resulting pale yellow solid was filtered, washed with ethanol and dried for 48 h under high vacuum giving polymer **191** (0.1 g, 7%), M_n: 9970, Pd: 1.11 (polystyrene standard). δ_H ($CDCl_3$, 400 MHz) 8.13-7.45 (m, 18H), 7.19-6.80 (m, 6H), 4.07 (m, 4H), 1.84 (m, 2H), 1.5-1.3 (m, 16H), 0.94-0.82 (m, 12H). UV-Vis (DCM) λ_{max} 380 nm, PL (DCM) λ_{max} 415, 436 nm.

5.4.2 Polymer 191 (Method 2)

By analogy with method 1, compound **190** (0.79 g, 0.9 mmol), compound **170** (0.52 g, 0.9 mmol), $Pd(PPh_3)_4$ (104 mg, 0.09 mmol), tri-*tert*-butylphosphine (0.01 cm^3, 0.1 mmol), toluene (50 cm^3) and K_2CO_3 (1 M, 10 cm^3); reaction time 96 h; extracted with $CHCl_3$. The organic solution was then washed with H_2O, dried and filtered through a celite column. The filtrate was concentrated in *vacuo* to afford a viscous solution that was added dropwise into vigorously stirring ethanol (150 cm^3) and the resulting mixture was stirred at rt for 12h. The resulting pale yellow solid was filtered, washed with ethanol and dried for 48 h under high vacuum giving polymer **191** (0.64 g, 48%), M_n: 35000, Pd: 1.02 (polystyrene standard). Spectroscopic data were identical to those obtained by method 1.

5.4.3 2,7-Bis(4-cyanophenyl)-9,9-dihexylfluorene 193

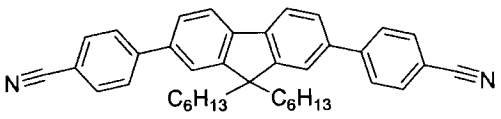

In accordance with the general method for Suzuki cross-coupling reactions, compound **163** (4.9 g, 10.0 mmol), 4-cyanophenyl boronic acid **192** (3.08 g, 21.0 mmol), $Pd(PPh_3)_2Cl_2$ (1.52 g, 2.1 mmol), tri-*tert*-butylphosphine (0.2 cm^3, 1.0 mmol), THF (50 cm^3) and Na_2CO_3 (2 M, 42.0 cm^3); reaction time 72 h; extracted with DCM. Chromatography eluent, hexane–EtOAc (9:1 v/v) followed by recrystallisation from ethanol gave compound **193** (2.5 g, 47%), mp: 114.2-115.1 °C (lit.[197] 113-115 °C), MS (EI) *m/z* 536 (M^+, 100%). Anal. calcd. for $C_{39}H_{40}N_2$: C, 87.27; H, 7.51; N, 5.22. Found: C, 87.25; H, 7.52; N, 5.21. δ_H ($CDCl_3$, 400 MHz) 7.84 (d, *J* 7.6, 2H), 7.78 (m, 8H), 7.62 (d, *J* 8.0, 2H), 7.58 (s, 2H), 2.07 (m, 4H), 1.06 (m, 12H), 0.77 (m, 10H). δ_C ($CDCl_3$, 100 MHz) 152.14, 145.96, 140.98, 138.45, 132.61, 127.77, 126.44, 121.59, 120.63, 118.98, 110.80, 55.55, 40.32, 31.42, 29.60, 23.80, 22.51, 13.93.

5.4.4 2,7-Bis[4-(5-1*H*-tetrazole)phenyl]-9,9-dihexylfluorene 194

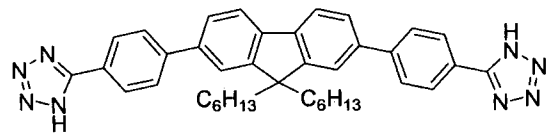

A mixture of 2,7-bis(4-cyanophenyl)-9,9-dihexylfluorene **193** (0.54 g, 1 mmol), NaN_3 (0.16 g, 2.5 mmol) and NH_4Cl (0.13 g, 2.5 mmol) in degassed DMF (15 ml) was refluxed for 24 h. The reaction mixture was then cooled to rt and HCl (5 cm^3) in H_2O (30 ml) was added slowly. The green precipitate was then filtered, washed with H_2O and dried for 48 h under high vacuum giving compound **194** (0.51 g, 82%), mp: >250 °C (decomp.), MS (EI) *m/z* 622 (M^+). Anal. calcd. for $C_{39}H_{42}N_8$: C, 75.21; H, 6.80; N, 17.99. Found: C, 74.77; H, 6.80; N, 17.56. δ_H (DMSO-d_6, 400 MHz) 8.21 (d, *J* 8.4, 4H), 8.06 (d, *J* 8.4, 4H), 8.02 (d, *J* 8.0, 2H), 7.95 (s, 2H), 7.83 (d, *J* 8, 2H), 2.2 (m, 4H), 1.05 (m, 12H), 0.71 (m, 10H). δ_C (DMSO-d_6, 100 MHz) 151.58, 142.91, 140.23, 137.96, 127.58, 127.49, 125.90, 122.92, 121.17, 120.67, 55.14, 31.49, 29.57, 24.12, 22.61, 14.46.

5.4.5 2,7-Bis{4-[2-(4-iodophenyl)-1,3,4-oxadiazol-5-yl]phenyl}-9,9-dihexylfluorene 196

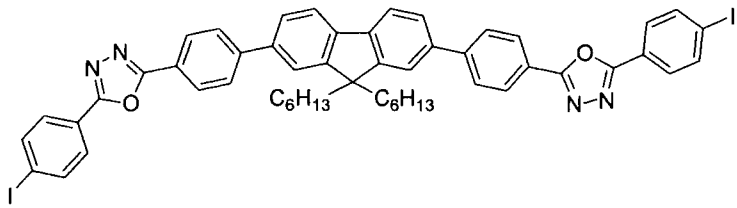

4-Iodobenzoyl chloride **195** (1.07 g, 4 mmol), dissolved in pyridine (5 cm^3) was added dropwise to a solution of 2,7-bis[4-(5-1*H*-tetrazole)phenyl]-9,9-dihexylfluorene **194** (0.50 g, 0.8 mmol) in pyridine (15 cm^3) and the mixture was refluxed for 3 h. Pyridine was removed by vacuum distillation. After cooling to rt, methanol (30 cm^3) was added and the suspension was heated at reflux for 15 min, cooled and the white solid obtained by vacuum filtration. The crude product was then purified by column chromatography (eluent: DCM-EtOAc 24:1 v/v) and recrystallised from toluene to yield white crystals of compound **196** (0.62 g, 75%), mp: 253.8-254.5 °C. MS (MALDI-TOF) *m/z* Calcd. for $C_{53}H_{48}I_2N_4O_2$: 1027.19. Found 1027.20 (M^+). Anal. Calcd for $C_{53}H_{48}I_2N_4O_2$: C, 62.00; H, 4.71; N, 5.46. Found: C, 61.77; H, 4.72; N, 5.39. δ_H ($CDCl_3$, 400 MHz) 8.24 (d, *J* 8.4, 4H), 7.92 (m, 8H), 7.87 (m, 6H), 7.68 (d, *J* 8, 2H), 7.65 (s, 2H), 2.09 (m, 4H), 1.09 (m, 12H), 0.77 (m, 10H). δ_C ($CDCl_3$, 100 MHz) 164.76, 164.06, 152.05, 145.03, 140.78, 138.90, 138.42, 128.29, 127.78, 127.47, 126.32, 123.46, 122.36, 121.51, 120.45, 98.55, 55.52, 40.37, 31.45, 29.65, 23.83, 22.54, 13.97.

6 REFERENCES

[1] J. H. Burroughes, D. D. C. Bradley, A. R. Brown, R. N. Marks, K. Mackay, R. H. Friend, P. L. Burn and A. B. Holmes, *Nature,* 1990, **347**, 539.

[2] C. K. Chiang, C. R. Fincher, Y. W. Park, A. J. Heeger, H. Shirakawa, E. J. Louis, S. C. Gau and A. G. MacDiarmid, *Phys. Rev. Lett.*, 1977, **39**, 1098.

[3] R. Kiebooms, R. Menon, K. Lee and H. S. Nalwa (Ed.), *Handbook of Advanced Electronic and Photonic Materials and Devices*, 2001, Academic Press, San Diego, Vol **8**, p. 6.

[4] C. W. Tang and S. A. VanSlyke, *Appl. Phys. Lett.*, 1987, **51**, 913.

[5] S. W. Depp and W. E. Howard, *Sci. Am.*, 1995, **6**, 70.

[6] A. Kraft, A. C. Grimsdale and A. B. Holmes, *Angew. Chem. Int. Ed.,* 1998, **37**, 402.

[7] O. Gelsing, *Chem. & Ind.*, 2003, **17**, 19.

[8] J. K. Borchardt, *Materials Today*, Sept. 2004, 42.

[9] M. Pope, H. P. Kallman and P. Magnante, *J. Chem. Phys.*, 1963, **38**, 2042.

[10] W. Helfrich and W. G. Schneider, *Phys. Rev. Lett.,* 1965, **14**, 229.

[11] P. S. Vincett, W. A. Barlow, R. A. Hann and G. G. Roberts, *Thin Solid Films,* 1982, **94**, 171.

[12] C. Adachi, T. Tsutsui and S. Saito, *Appl. Phys. Lett.*, 1989, **55**, 1489.

[13] R. N. McDonald and T. W. Campbell, *J. Am. Chem. Soc.,* 1960, **82**, 4669.

[14] A. Greiner and W. Heitz, *Makromol. Chem., Rapid Commun.,* 1988, **9**, 581.

[15] R. A. Wessling and R. G. Zimmerman (Dow Chemical), US-B 3401152, 1968 [*Chem. Abstr.,* 1968, **69**, 87735q].

[16] R. A. Wessling, *J. Polym. Sci. Symp.,* 1985, **72**, 55.

[17] D. A. Halliday, P. L. Burn, R. H. Friend, D. D. C. Bradley and A. B. Holmes, *Synth. Met.,* 1993, **55**, 902.

[18] S. Doi, M. Kuwabara, T. Noguchi and T. Ohnishi, *Synth. Met.,* 1993, **57**, 4174.

[19] D. Braun and A. J. Heeger, *Appl. Phys. Lett.*, 1991, **58**, 1982.

[20] D. Braun, A. J. Heeger and H. Kroemer, *J. Electron. Mater.*, 1991, **20**, 945.

[21] A. J. Heeger and D. Braun (UNIAX), WO-B 92/16023, 1992 [*Chem. Abstr.*, 1993, **118**, 157401j].

[22] a) F. Wudl, P. M. Allemand, G. Srdanov, Z. Ni and D. McBranch, *ACS Symp. Ser.,* 1991, **455**, 683; (b) F. Wudl (University of California), US-B 5189136, 1990 [*Chem. Abstr.,*

1993, **118**, 255575p].

[23] H. G. Gilch and W. L. Wheelwright, *J. Polym. Sci. A1,* 1966, **4**, 1337.

[24] C. Wang, M. Kilitziraki, J. A. H. MacBride, M. R. Bryce, L. E. Horsburgh, A. K. Sheridan, A. P. Monkman and I. D. W. Samuel, *Adv. Mater.*, 2000, **12**, 217.

[25] S. M. Kelly, *Flat Panel Displays*, Royal Society of Chemistry, Cambridge, 2000, 139.

[26] For a discussion on the different ways of measuring the efficiency of OLEDs see: S. R. Forrest, D. D. C. Bradley and M. E. Thompson, *Adv. Mater.,* 2003, **15**, 1043.

[27] S. Oyston, C. Wang, G. Hughes, A. S. Batsanov, I. F. Perepichka, M. R. Bryce, J. H. Ahn, C. Pearson and M. C. Petty, *J. Mater. Chem.,* 2005, **15**, 194.

[28] For a review of ETHB materials see: G. Hughes and M. R. Bryce, *J. Mater. Chem.,* 2005, **15**, 94.

[29] *a*) B. Schultz, M. Bruma and L. Brehmer, *Adv. Mater.*, 1997, **9**, 601; (*b*) M. Thelakkat and H.-W. Schmidt, *Polym. Adv. Technol.*, 1998, **9**, 429; (*c*) K. Chondroudis and D. B. Mitzi, *Chem. Mater.*, 1999, **11**, 3028; (*d*) C. Wang, G.-Y. Jung, A. S. Batsanov, M. R. Bryce and M. C. Petty, *J. Mater. Chem.*, 2002, **12**, 173; (*e*) S. W. Cha, S.-H. Choi, K. Kim and J.-I. Jin, *J. Mater. Chem.*, 2003, **13**, 1900.

[30] F. N. Hayes, B. S. Rogers and D. J. Ott, *J. Am. Chem. Soc.*, 1955, **77**, 1850.

[31] J. B. Birks, *Photophysics of Aromatic Molecules,* Inter-Science, London, 1970, 134.

[32] C. J. Abshire and C. S. Marvel, *Makromol. Chem.,* 1961, **44**, 388.

[33] S. Janietz, A. Wedal and R. Friedrich, *Synth. Met.,* 1997, **84**, 381.

[34] R. Cervini, X. –C. Li, G. W. C. Spencer, A. B. Holmes, S. C. Moratti and R. H. Friend, *Synth. Met.,* 1997, **84**, 359.

[35] G. Lussem and J. H. Wendorff, *Polym. Adv. Technol.,* 1998, **9**, 443.

[36] R. Huigsen, J. Sauer, H. J. Sturm and J. H. Markgraf, *Chem. Ber.,* 1960, **93**, 2106.

[37] W. G. Finnegan, R. A. Henry and R. Lofquist, *J. Am. Chem. Soc.,* 1958, **80**, 3908.

[38] T. Tsutsui, E. Aminaka, Y. Fujita, Y. Hamada and S. Saito, *Synth. Met.,* 1993, **55-57**, 4157.

[39] P. May, *Phys. World*, 1995, **8**, 52.

[40] A. R. Brown, D. D. C. Bradley, J. H. Burroughes, R. H. Friend, N. C. Greenham, P. L Burn, A. B. Holmes and A. Kraft, *Appl. Phys. Lett.*, 1992, **61**, 2793.

[41] X. Gong, J. C. Ostrowski, D. Moses, G. C. Bazan and A. J. Heeger, *Adv. Funct. Mater.*, 2003, **13**, 439.

[42] J. Kido, K. Hongawa, K. Okuyama and K. Nagai, *Appl. Phys. Lett.,* 1993, **63**, 2627.

[43] D. O'Brien, A. Bleyer, D. G. Lidzey, D. D. C. Bradley and T. J. Tsutsui, *J. Appl. Phys.*, 1997, **82**, 2662.

[44] C. Wang, G.-Y. Jung, Y. Hua, C. Pearson, M. R. Bryce, M. C. Petty, A. S. Batsanov, A. E. Goeta and J. A. K. Howard, *Chem. Mater.*, 2001, **13**, 1167.

[45] J. K. Kim, J. W. Yu, J. M. Hong, H. N. Cho, D. Y. Kim and C. Y. Kim, *J. Mater. Chem.*, 1999, **9**, 2165.

[46] G.-Y. Jung, *Ph.D. Thesis*, University of Durham, 2001.

[47] H. Antoniadis, M. Inbasekaran and E. P. Woo, *Appl. Phys. Lett.*, 1998, **73**, 3055.

[48] S. A. VanSlyke, C. H. Chen and C. W. Tang, *Appl. Phys. Lett.*, 1996, **69**, 2160.

[49] H. Tang, F. Li and J. Shinar, *Appl. Phys. Lett.*, 1997, **71**, 2560.

[50] J. H. Ahn, C. Wang, C. Pearson, M. R. Bryce and M. C. Petty, *Appl. Phys. Lett.*, 2004, **85**, 1283.

[51] F. I. Wu, C. F. Shu, C. H. Chien and Y. T. Tao, *Synth. Met.*, 2005, **148**, 133.

[52] a) K. T. Wong, Z. J. Wang, Y. Y. Chien and C. L. Wang, *Org. Lett.*, 2001, **3**, 2285; b) C. W. Ko and Y. T. Tao, *Synth. Met.*, 2002, **126**, 37.

[53] Y. T. Tao, C. H. Chuen, C. W. Ko and J. W. Peng, *Chem. Mater.*, 2002, **14**, 4256.

[54] J. Salbeck, N. Yu, J. Bauer, F. Weissortel and H. Bestgen, *Synth. Met.*, 1997, **91**, 209.

[55] Y.-Y. Chien, K.-T. Wong, P.-T. Chou and Y.-M. Cheng, *Chem. Commun.*, 2002, 2874.

[56] Y. Hamada, C. Adachi, T. Tsutsui and S. Saito, *Jpn. J. Appl. Phys.*, 1992, **31**, 1812.

[57] N. Tamoto, C. Adachi and K. Nagai, *Chem. Mater.*, 1997, **9**, 1077.

[58] M. Stolka, J. Yanus and D. Pai, *J. Phys. Chem.*, 1984, **88**, 4707.

[59] K. R. Justin Thomas, J. T. Lin, Y. T. Tao and C. H. Chuen, *Chem. Mater.*, 2002, **14**, 3852.

[60] K. R. Justin Thomas, J. T. Lin, Y. T. Tao and C. H. Chuen, *Chem. Mater.*, 2004, **16**, 5437.

[61] K. Okumoto and Y. Shirota, *Chem. Mater.*, 2003, **15**, 699.

[62] M. Guan, Z. Q. Bian, Y. F. Zhou, F. Y. Li, Z. J. Li and C. H. Huang, *Chem. Commun.*, 2003, 2708.

[63] K. Brunner, A. Dijken, H. Borner, J. J. A. M. Bastiaansen, N. M. M. Kiggen and B. M. W. Langeveld, *J. Am. Chem. Soc.*, 2004, **126**, 6035.

[64] X. Jiang, Y. Liu, H. Tian, W. Qui, X. Song and D. Zhu, *J. Mater. Chem.*, 1997, **7**, 1395.

[65] F. Liang, Q. Zhou, Y. Cheng, L. Wang, D. Ma, X. Jing and F. Wang, *Chem. Mater.*, 2003, **15**, 1935.

[66] X. Gong, P. K. Ng and W. K. Chan, *Adv. Mater.*, 1998, **10**, 1337.

[67] H.-C. Yeh, R.-H. Lee, L.-H. Chan, T.-Y. J. Lin, C.-T. Chen, E. Balasubramaniam and Y.-T. Tao, *Chem. Mater.*, 2001, **13**, 2788.

[68] K. Naito and A. Miura, *J. Chem. Phys.*, 1993, **97**, 6240.

[69] J. Bettenhausen and P. Strohriegl, *Adv. Mater.*, 1996, **8**, 507.

[70] J. Bettenhausen and P. Strohriegl, *Macromol. Rapid Commun.*, 1996, **17**, 623.

[71] J. V. Grazulevicius, P. Strohriegl and H. S. Nalwa (Ed.), *Handbook of Advanced Electronic and Photonic Materials and Devices*, 2001, Academic Press, San Diego, Vol **10**, p. 265.

[72] S.-C. Lin and E. M. Pearce, *High-Performance Thermosets—Chemistry, Properties, Applications,* Carls Hanser Verlag, Munich 1994, p.137.

[73] J. Bettenhausen, M. Greczmiel, M. Jandke and P. Strohriegl, *Synth. Met.*, 1997, **91**, 223.

[74] S. Tokito, H. Tanaka, K. Noda, A. Okada and Y. Taga, *Macromol. Symp.*, 1997, **125**, 181.

[75] H. Ogawa, R. Okuda and Y. Shirota, *Appl. Phys. A,* 1998, **67**, 599.

[76] a) T. Noda, H. Ogawa, N. Noma and Y. Shirota, *Adv. Mater.*, 1997, **9**, 720; (b) T. Noda, H. Ogawa, N. Noma and Y. Shirota, *J. Mater. Chem.*, 1999, **9**, 2177.

[77] A. Kraft, *Chem. Commun.*, 1996, 77.

[78] E. Buchwald, M. Meier, S. Karg, W. Rieß, M. Schwoerer, P. Posch, H.-W. Schmidt and P. Strohriegl, *Adv. Mater.*, 1995, **7**, 839.

[79] S. M. Risser, D. N. Beratan and J. N. Onuchic, *J. Phys. Chem.*, 1993, **97**, 4523.

[80] H. Mochizuki, T. Hasui, O. Tsutsumi, A. Kanazawa, T. Shiono, T. Ikeda, C. Adachi, Y. Taniguchi and Y. Shirota, *Mol. Cryst. Liq. Cryst.*, 2001, **365**, 129.

[81] a) H. Tokuhisa, M. Era and T. Tsutsui, *Adv. Mater.*, 1998, **10**, 404; (b) H. Tokuhisa, M. Era and T. Tsutsui, *Chem. Lett.*, 1997, 303; (c) H. Tokuhisa, M. Era and T. Tsutsui, *Appl. Phys. Lett.*, 1998, **72**, 2639; (d) H. Mochizuki, T. Hasui, M. Kawamoto, T. Shiono, T. Ikeda, C. Adachi, Y. Taniguchi and Y. Shirota, *Chem. Commun.*, 2000, 1923.

[82] Y.-D. Zhang, K. G. Jespersen, M. Kempe, J. A. Kornfield, S. Barlow, B. Kippelen and S. R. Marder, *Langmuir,* 2003, **19**, 6534.

[83] B. Verheyde and W. Dehaen, *J. Org. Chem.*, 2001, **66**, 4062.

[84] a) S. Wang, W. J. Jr. Oldham, R. A. Hudack and G. C. Bazan, *J. Am. Chem. Soc.*, 2000, **122**, 5695; (b) C.-T. Chen, T.-Y. J. Lin, L.-H. Jan, H.-C. Yeh, E. Balasubramaniam and Y.-T. Tao, *Mater. Res. Soc. Proc.*, 2000, **598**, BB3.5.1.

[85] S. W. Cha and J. I. Jin, *J. Mater. Chem.*, 2003, **13**, 479.

[86] S.-J. Chung, T.-C. Lin, K.-S. Kim, G. S. He, J. Swiatkiewicz, P. N. Prasad, G. A. Baker and F. V. Bright, *Chem. Mater.*, 2001, **13**, 4071.

[87] H. Tokuhisa, M. Era and T. Tsutsui, *Adv. Mater.*, 1998, **10**, 404.

[88] H. Tokuhisa, M. Era and T. Tsutsui, *Chem. Lett.*, 1997, 303.

[89] D. Adam, P. Schumacher, J. Simmerer, L. Haessling, K. Siemensmeyer, K. H. Etzbach, H. Ringsdorf and D. Haarer, *Nature*, 1994, **371**, 141.

[90] H. Tokuhisa, M. Era and T. Tsutsui, *Appl. Phys. Lett.*, 1998, **72**, 2639.

[91] M. Kawamoto, H. Mochizuki and T. Ikeda, *J. Appl. Phys.*, 2003, **94**, 6442.

[92] V. Görtz and J. W. Goodby, *Chem. Commun.*, 2005, 3262.

[93] C. Wang, A. S. Batsanov and M. R. Bryce, *Chem. Commun.*, 2004, 578.

[94] M. Perez and J. Bermejo, *J. Org. Chem.*, 1993, **58**, 2628.

[95] a) S. Shinkai, T. Nakaji, T. Ogawa and O. Manabe, *J. Am. Chem. Soc.*, 1980, **102**, 5860; (b) Z. F. Liu, K. Hashimoto and A. Fujishima, *Nature*, 1990, **347**, 685.

[96] H. W. Losensky, H. Spelthann, A. Ehlen, F. Voegtle and J. Bargon, *Angew. Chem. Int. Ed. Engl.*, 1988, **27**, 1189.

[97] S. Zheng, S. Wang and W. Hua, *J. Heterocycl. Chem.*, 1998, **35**, 275.

[98] D.-M. Du, W.-T. Hua and X.-L. Jin, *J. Mol. Struct.*, 2001, **561**, 145.

[99] W. Rieβ, *Polym. Adv. Technol.*, 1997, **8**, 381.

[100] Y.-Z. Lee and S.-A. Chen, *Synth. Met.*, 1999, **105**, 185.

[101] S. T. Kim, D.-H. Hwang, X. C. Li, J. Gruner, R. H. Friend, A. B. Holmes and H. K. Shim, *Adv. Mater.*, 1996, **8**, 979.

[102] B. Schulz, Y. Kaminorz and L. Brehmer, *Synth. Met.*, 1997, **84**, 449.

[103] U. Mitschke and P. Bauerle, *J. Mater. Chem.*, 2000, **10**, 1471.

[104] M. Zheng, L. Ding, E. E. Gurel, P. M. Lahti and F. E. Karasz, *Macromolecules*, 2001, **34**, 4124.

[105] J. A. Mikroyannidis, I. K. Spiliopoulos, T. S. Kasimis, A. P. Kulkarni and S. A. Jenekhe, *Macromolecules*, 2003, **36**, 9295.

[106] P. Pösch, R. Fink, M. Thelakkat and H.-W. Schmidt, *Acta Polym.*, 1998, **49**, 487.

[107] R. Brütting, P. Pösch, P. Ströhriegl, E. Buchwald, W. Brütting and M. Schwoerer, *Macromol. Chem. Phys.*, 1997, **198**, 2743.

[108] a) J. Ding, M. Day, G. Robertson and J. Roovers, *Macromolecules*, 2002, **35**, 3474; (b) J. Ding, Y. Tao, M. Day, J. Roovers and M. D'Iorio, *J. Opt. A: Pure Appl. Opt.*, 2002, **4**,

5267.

[109] K.-H. Weinfurtner, H. Fujikawa, S. Tokito and Y. Taga, *Appl. Phys. Lett.*, 2000, **76**, 2502.

[110] W. Ma, P. K. Iyer, X. Gong, B. Liu, D. Moses, G. C. Bazan and A. J. Heeger, *Adv. Mater.*, 2005, **17**, 274.

[111] H. Meng, Z.-K. Chen, X.-L. Liu, Y.-H. Lai, S.-J. Chua and W. Huang, *Phys. Chem. Chem. Phys.*, 1999, **1**, 3123.

[112] Y. Zhang, Y. Hu, H. Li, L. Wang, X. Jing, F. Wang and D. Ma, *J. Mater. Chem.*, 2003, **13**, 773.

[113] C. Wang, M. Kilitziraki, L.-O. Pålsson, M. R. Bryce, A. P. Monkman and I. D. W. Samuel, *Adv. Funct. Mater.*, 2001, **11**, 47.

[114] Z. Peng and J. Zhang, *Chem. Mater.*, 1999, **11**, 1138.

[115] Z. Bao, Z. Peng, M. E. Galvin and E. A. Chandross, *Chem. Mater.*, 1998, **10**, 1201.

[116] Z. Peng, Z. Bao and M. E. Galvin, *Adv. Mater.*, 1998, **10**, 680.

[117] Z. Peng and J. Zhang, *Synth. Met.*, 1999, **105**, 73.

[118] Z.-K. Chen, H. Meng, Y.-H. Lai and W. Huang, *Macromolecules,* 1999, **32**, 4351.

[119] D. W. Lee, K.-Y. Kwon, J.-I. Jin, Y. Park, Y.-R. Kim and I.-W. Hwang, *Chem. Mater.*, 2001, **13**, 565.

[120] F. Wudl, P. M. Allemand, G. Srdanov, Z. Ni and D. Mcbranch, *ACS Symp. Ser.*, 1991, **455**, 683.

[121] S.-H. Jin, M.-Y. Kim, J. Y. Kim, K. Lee and Y.-S. Gal, *J. Am. Chem. Soc.*, 2004, **126**, 2474.

[122] J. H. Kim, J. H. Park and H. Lee, *Chem. Mater.*, 2003, **15**, 3414.

[123] S. A. Jenekhe and J. A. Osaheni, *Science,* 1994, **265**, 765.

[124] F.-I. Wu, D. S. Reddy, C.-F. Shu, M. S. Liu and A. K.-Y. Jen, *Chem. Mater.*, 2003, **15**, 269.

[125] A. W. Grice, D. D. C. Bradley, M. T. Bernius, M. Inbasekaran, W. W. Wu and E. P. Woo, *Appl. Phys. Lett.*, 1998, **73**, 629.

[126] H.-H. Sung and H.-C. Lin, *Macromolecules,* 2004, **37**, 7945.

[127] Y. Ohmori, M. Uchida, K. Muro and K. Yoshino, *Jpn. J. Appl. Phys.*, 1991, **30**, L1941.

[128] M. Kreyenschmidt, G. Klaerner, T. Fuhrer, J. Ashenhurst, S. Karg, W. D. Chen, V. Y. Lee, J. C. Scott and R. D. Miller, *Macromolecules,* 1998, **31**, 1099.

[129] Y. Yang and Q. Pei, *Appl. Phys. Lett.*, 1997, **81**, 3294.

[130] M. Redecker, D. D. C. Bradley, M. Inbasekaran and E. P. Woo, *Appl. Phys. Lett.*, 1999,

74, 1400.

[131] Q. Pei and Y. Yang, *J. Am. Chem. Soc.*, 1996, **118**, 7416.

[132] J. Teetsov and A. Fox, *J. Mater. Chem.*, 1999, **9**, 2117.

[133] A. J. Heeger, F. Hide, B. Schwartz and M. A. Diaz-Garcia, *Chem. Phys. Lett.*, 1996, **256**, 424.

[134] M. Sims, D. D. C. Bradley, M. Ariu, M. Koeberg, A. Asimakis, M. Grell and D. G. Lidzey, *Adv. Funct. Mater.*, 2004, **14**, 765.

[135] a) U. Lemmer, S. Heun, R. F. Mahrt, U. Scherf, M. Hopmeir, U. Siegner, R. O. Göbel, K. Mullen and H. Bassler, *Chem. Phys. Lett.*, 1995, **240**, 373; (b) J. Grüner, H. F. Whittmann, P. J. Hamer, R. H. Friend, J. Huber, U. Scherf, K. Müllen, S. C. Moratti and A. B. Holmes, *Synth. Met.*, 1994, **67**, 181.

[136] M. T. Bernius, M. Inbasekaran, E. Woo, W. Wu and L. Wujkowski, *J. Mater. Sci. Mater. Electron.*, 2000, **11**, 111.

[137] M. T. Bernius, M. Inbasekaran, J. O'Brien and W. Wu, *Adv. Mater.*, 2000, **12**, 1737.

[138] X. Gong, P. K. Iyer, D. Moses, G. C. Bazan, A. J. Heeger and S. S. Xiao, *Adv. Funct. Mater.*, 2003, **13**, 325.

[139] a) D. D. C. Bradley, M. Grell, X. Long, H. Mellor and A. Grice, *SPIE Proc. Int. Soc. Opt. Eng.*, 1997, **3145**, 245; (b) X. Long, M. Grell, A. Malinowski, D. D. C. Bradley, M. Inbasekaran and E. P. Woo, *Opt. Mater.*, 1998, **9**, 70; (c) J.-I. Lee, G. Klärner and R. D. Miller, *Synth. Met.*, 1999, **101**, 126; (d) L.-O. Pålsson, C. Wang, A. P. Monkman, M. R. Bryce, G. Rumbles and I. D. W. Samuel, *Synth. Met.*, 2001, **119**, 627; (e) V. N. Bliznyuk, S.A. Carter, J. C. Scott, G. Klärner, R. D. Miller and D. C. Miller, *Macromolecules,* 1999, **32**, 361; (f) M. Gaal, E. J. W. List and U. Scherf, *Macromolecules,* 2003, **36**, 4236; (g) E. J. W. List, R. Guentner, P. S. de Freitas and U. Scherf, *Adv. Mater.*, 2002, **14**, 374.

[140] a) E. Conwell, *Trends Polym. Sci.*, 1997, **11**, 671; (b) M. Grell, D. D. C. Bradley, G. Ungar, J. Hill and K. S. Whitehead, *Macromolecules,* 1999, **32**, 5810; (c) D. Sainova, T. Miteva, H. G. Nothofer, U. Scherf, I. Glowacki, J. Ulanski, H. Fujikawa and D. Neher, *Appl. Phys. Lett.*, 2000, 76, 1810.

[141] a) U. Scherf and E. J. W. List, *Adv. Mater.*, 2002, **14**, 477; (b) J. M. Lupton, M. R. Craig and E. W. Meijer, *Appl. Phys. Lett.*, 2002, **80**, 4489; (c) W. Zhou, T. Cao and J. M. White, *Adv. Funct. Mater.*, 2004, **14**, 783; (d) L. Romaner, A. Pogantsch, P. S. de Freitas, U. Scherf, M. Gaal, E. Zojer and E. J. W. List, *Adv. Funct. Mater.*, 2003, **13**, 597.

[142] D. Vak, C. Chun, C. L. Lee, J.-J. Kim and D.-Y. Kim, *J. Mater. Chem.*, 2004, **14**, 1342.

[143] R. Pudzich and J. Salbeck, *Synth. Met.*, 2003, **138**, 21.

[144] H. Lee, J. Oh, H. Y. Chu, J.-I. Lee, S. H. Kim, Y. S. Yang, G. H. Kim, L.-M. Do, T. Zyung, J. Lee and Y. Park, *Tetrahedron*, 2003, **59**, 2773.

[145] Y.-H. Kim, D.-C. Shin, S.-H. Kim, C.-H. Ko, H.-S. Yu, Y.-S. Chae and S.-K. Kwon, *Adv. Mater.*, 2001, **13**, 1690.

[146] C.-C. Wu, Y.-T. Lin, K.-T. Wong, R.-T. Chen and Y.-Y. Chien, *Adv. Mater.*, 2004, **16**, 61.

[147] D. Katsis, Y. H. Geng, J. J. Ou, S. W. Culligan, A. Trajkovska, S. H. Chen and L. J. Rothberg, *Chem. Mater.*, 2002, **14**, 1332.

[148] a) W.-L. Yu, J. Pei, W. Huang and A. J. Heeger, *Adv. Mater.*, 2000, **12**, 828; (b) G. Zeng, W.-L. Yu, S.-J. Chua and W. Huang, *Macromolecules,* 2002, **35**, 6907; (c) S. Gamerith, M. Gaal, L. Romaner, H.-G. Nothofer, R. Günter, P. S. de Freitas, U. Scherf and E. W. J. List, *Synth. Met.*, 2003, **139**, 855.

[149] Y. Wu, J. Li, Y. Fu and Z. Bo, *Org. Lett.*, 2004, **6**, 3485.

[150] Y. Ohmori, M. Uchida, C. Morishima, A. Fuji and K. Yoshino, *Jpn. J. Appl. Phys.*, 1993, Part 2 **32**, L1663.

[151] L. C. Tavares, T. C. V. Penna and A. T. Amoral, *Bull. Chim. Pharm.*, 1997, **136**, 244.

[152] J. R. Cannon, T. M. Cresp, B. W. Metcalf, M. V. Sargent, G. Vinciguerra and J. A. Elix, *J. Chem. Soc. (C),* 1971, 3495.

[153] Following a route to the analogous 4-bromo-3,5-diethoxybenzoic acid ethyl ester; M. Linderberg, S. Hellberg, S. Björk, B. Gotthammar, T. Högberg, K. Persson, R. Schwarcz, J. Luthman and R. Johansson, *Eur. J. Med. Chem.*, 1999, **34**, 729.

[154] For discussion on the preparation of hindered biphenyls via Suzuki reactions see; M. G. Johnson and R. J. Foglesong, *Tetrahedron Lett.*, 1997, **38**, 7001.

[155] N. DiCesare and J. R. Lakowicz, *Chem. Commun.*, 2001, 2022.

[156] A. Lesac, D. Moslavac-Forjan, D. W. Bruce and V. Sunjic, *Helv. Chim. Acta,* 1999, **82**, 1707.

[157] X. Zhao, X.-Z. Wang, X.-K. Jiang, Y.-Q. Chen, Z.-T. Li and G.-J. Chen, *J. Am. Chem. Soc.*, 2003, **125**, 15128.

[158] P. R. Parry, M. R. Bryce and B. Tarbit, *Org. Biomol. Chem.*, 2003, **1**, 1447.

[159] P. R. Parry, C. Wang, A. S. Batsanov, M. R. Bryce and B. Tarbit, *J. Org. Chem.*, 2002, **67**, 7541.

[160] I. I. Perepichka, I. F. Perepichka, M. R. Bryce and L.-O. Pålsson, *Chem. Commun.*, 2005,

3397.

[161] For alternative procedures for alkylation of 2,7-dibromofluorene **162** to yield **163** see: (a) W.-Y. Wong, K.-H. Choi, G.-L. Lu, J.-X. Shi, P.-Y. Lai and S.-M. Chan, *Organometallics*, 2001, **20**, 5446; (b) S.-H. Lee and T. Tsutsui, *Thin Solid Films,* 2000, **363**, 76; (c) W.-L. Yu, J. Pei, Y. Cao, W. Huang and A. J. Heeger, *Chem. Commun.*, 1999, 1837; (d) M. Ranger and M. Leclerc, *Chem. Commun.,* 1997, 1597.

[162] a) S. Destri, M. Pasini, C. Botta, W. Porzio, F. Bertini and L. Marchio, *J. Mater. Chem.,* 2002, **12**, 924; (b) S. W. Chang, J.-M. Hong, J. W. Hong and H. N. Choi, *Polym. Bull.,* 2001, **47**, 231; (c) S. Beaupré, M. Ranger and M. Leclerc, *Macromol. Rapid Commun.,* 2000, **21**, 1013; (d) H. N. Cho, J. K. Kim, D. Y. Kim, C. Y. Kim, N. W. Song and D. Kim, *Macromolecules,* 1999, **32**, 1476; (e) M. Ranger, M. Rondeau and M. Leclerc, *Macromolecules,* 1997, **30**, 7686.

[163] G. Hughes, C. Wang, A. S. Batsanov, M. Fearn, S. Frank, M. R. Bryce, I. F. Perepichka, A. P. Monkman and B. P. Lyons, *Org. Biomol. Chem.,* 2003, **1**, 3069.

[164] For alternative procedures of obtaining compound **164** from **163** see: (a) Ref. 161c.; (b) B. Liu, W.-L. Yu, Y.-H. Lai and W. Huang, *Macromolecules,* 2000, **33**, 8945; (c) X. Zhan, Y. Liu, D. Zhu, W. Huang and Q. Gong, *Chem. Mater.,* 2001, **13**, 1540.

[165] R. G. Clarkson and M. Gomberg, *J. Am. Chem. Soc.,* 1930, **52**, 2881.

[166] a) J. Pei, J. Ni, X.-H. Zhou, X.-Y. Cao and Y.-H. Lai, *J. Org. Chem.,* 2002, **67**, 4924; (b) K.-T. Wong, Y.-Y. Chien, R.-T. Chen, C.-F. Wang, Y.-T. Lin, H.-H. Chiang, P.-Y. Hsieh, C.-C. Wu, C.-H. Chou, Y. O. Su, G.-H. Lee and S.-M. Peng, *J. Am. Chem. Soc.,* 2002, **124**, 11576.

[167] J. M. Tour, R. Wu and J. S. Schumm, *J. Am. Chem. Soc.,* 1990, **112**, 5662.

[168] E. Bergman and J. Hervey, *Chem. Ber.,* 1929, **62**, 915.

[169] J. K. Kim, S. I. Hong, H. N. Cho, D. Y. Kim and C. Y. Kim, *Polym. Bull.*, 1997, **38**, 169.

[170] M. Fukuda, M. Sawada and K. Joshino, *J. Polym. Sci. Part A: Polym. Chem.,* 1993, **31**, 265.

[171] T. Ahn, S.-Y. Song and H.-K. Shim, *Macromolecules,* 2000, **33**, 6764.

[172] Y. Cao, I. D. Parker, G. Yu, C. Zhang and A. J. Heeger, *Nature*, 1999, **397**, 414.

[173] a) P. Cea, Y. Hua, C. Pearson, C. Wang, M. R. Bryce, F. M. Royo and M. C. Petty, *Thin Solid Films*, 2002, **408**, 275; (b) P. Cea, Y. Hua, C. Pearson, C. Wang, M. R. Bryce, M. C. López and M. C. Petty, *Mater. Sci. and Eng. C*, 2002, **22**, 87.

[174] a) J. H. Kim and H. Lee, *Chem. Mater.*, 2002, **14**, 2270; (b) M. Jørgensen and F. C.

Krebs, *Polym. Bull.*, 2003, **51**, 23.

[175] I. N. Kang, D. H. Hwang, H. K. Shim, T. Zyung and J. J. Kim, *Macromolecules*, 1996, **29**, 165.

[176] G. Hughes, *Ph.D. Thesis*, University of Durham, 2004.

[177] T. Q. Nguyen, V. Doan and B. J. Schwartz, *J. Chem. Phys.*, 1999, **110**, 4068.

[178] (a) B. Schwartz, *Ann. Rev. Phys. Chem.*, 2003, **54**, 141. (b) T. Q. Nguyen, J. Wu, V. Doan, B. J. Schwartz and S. H. Tolbert, *Science*, 2000, **288**, 652; (c) T. Q. Nguyen, J. Wu, S. H. Tolbert and B. J. Schwartz, *Adv. Mater.*, 2001, **13**, 609; (d) B. J. Schwartz, T. Q. Nguyen, J. Wu and S. H. Tolbert, *Synth. Met.*, 2001, **116**, 35.

[179] D. R. Baigent, A. B. Holmes, S. C. Moratti, and R. H. Friend, *Synth. Met.*, 1996, **80**, 119.

[180] F. Bentiss and M. Lagrenée, *J. Heterocycl. Chem.*, 1999, **36**, 1029.

[181] S. Stockhause, M. S. Wickleder, G. Meyer, I. Orgzall and B. Schulz, *J. Mol. Struct.*, 2001, **561**, 175.

[182] a) W. Huang, H. Meng, W.-L. Yu, J. Gao and A. J. Heeger, *Adv. Mater.*, 1998, **10**, 593; (b) W.-L. Yu, H. Meng, J. Pei, Y. H. Lai, S. J. Chua and W. Huang, *Chem. Commun.*, 1998, **18**, 1957; (c) W.-L. Yu, H. Meng, J. Pei and W. Huang, *J. Am. Chem. Soc.*, 1998, **120**, 11808; (d) H. Meng and W. Huang, *J. Org. Chem.*, 2000, **65**, 3894.

[183] C. J. Goddard, *J. Heterocycl. Chem.*, 1991, **28**, 17.

[184] U. Mitschke, T. Debaerdemaeker and P. Bäuerle, *Eur. J. Org. Chem.*, 2000, 425.

[185] P.-M. Windschief and F. Vögtle, *Synthesis*, 1994, 87.

[186] N. Zhang, L. Thomas and B. Wu, *J. Org. Chem.*, 2001, **66**, 1500.

[187] For discussions on the low reactivity of aryl chlorides in cross-coupling reactions see: V. V. Grushin and H. Alper, *Chem. Rev.*, 1994, **94**, 1047.

[188] A. F. Littke, C. Dai and G. C. Fu, *J. Am. Chem. Soc.*, 2000, **122**, 4020.

[189] A. P. Monkman, L.-O. Pålsson, R. W. T. Higgins, C. Wang, M. R. Bryce, A. S. Batsanov and J. A. K. Howard, *J. Am. Chem. Soc.*, 2002, **124**, 6049.

[190] G. Hughes, D. Kreher, A. S. Batsanov, C. Wang and M.R. Bryce, *Org. Biomol. Chem.*, 2004, **2**, 3363.

[191] D. L. Horrocks, *J. Chem. Phys.*, 1969, **50**, 4962.

[192] a) J. Roncali, *Chem. Rev.*, 1997, **97**, 173; (b) M. Tachibana, S. Tanaka, Y. Yamashita and K. Yoshizawa, *J. Phys. Chem. B*, 2002, **106**, 3549.

[193] a) L. Romaner, A. Pogantsch, P. Scandiucci de Freitas, U. Scherf, M. Gaal, E. Zojer and E. J. W. List, *Adv. Funct. Mater.*, 2003, **13**, 3069; (b) M. R. Craig, M. M. de Kok, J. W.

Hofstraat, A. P. H. L. Schenning and E. W. Meijer, *J. Mater. Chem.*, 2003, **13**, 2861.

[194] For a review on the applications of PEDOT:PSS see: S. Kirchmeyer and K. Reuter, *J. Mater. Chem.*, 2005, **15**, 2077.

[195] Y. Shi, J. Liu and Y. Yang, *J. Appl. Phys.*, 2000, **87**, 4254.

[196] C. Y. Yang, F. Hide, M. A. Diaz-Garcia, A. J. Heeger and Y. Cao, *Polymer*, 1998, **39**, 2299.

[197] For an alternative route to compound **193** see: H.-N. Cho, S.-H. Chung and S.-W. Song, *US Patent*, US 2003091859.

[198] L.-O. Pålsson and A. P. Monkman, *Adv. Mater.*, 2002, **14**, 757.

[199] a) A. Chavas, J. Morgado, J. M. G. Martinho, L. Alcacer and F. Cacialli, *Chem. Commun.*, 2001, 1216; (b) A. Chavas, J. Morgado, J. M. G. Martinho, A. Fedorov, L. Alcacer and F. Cacialli, *J. Mater. Chem.*, 2002, **12**, 3523.

[200] I. Kompis and A. Wick, *Helv. Chim. Acta,* 1977, **60**, 3025.

[201] I. J. Borowitz, M. Anschel and P. D. Readio, *J. Org. Chem.*, 1971, **36**, 553.

[202] D. W. Price and J. M. Tour, *Tetrahedron,* 2003, **59**, 3131.

1 APPENDIX ONE: LUMINESCENCE SPECTROSCOPY

Luminescence can be categorised by the manner in which the excited state is formed. Photoluminescence (PL) is the type used in spectroscopy and occurs when a molecule absorbs light. Other types include electroluminescence (EL), which causes light to be emitted when an electric current is passed through a material, chemiluminescence (involving a reaction releasing energy as light rather than heat) and bioluminescence (for example in special organs of deep sea fish to help attract prey).

In phosphorescence the emission results from a triplet excited state. The transition down to the ground state is spin forbidden as the excited state is in the same spin orientation as that of the ground state. Therefore, the process is relatively slow and emission lasts well beyond the excitation, with phosphorescence lifetimes being anything from 10^{-3} s to several minutes (for example phosphorescent materials used on watch hands, allowing the time to be read in the dark).

Fluorescence on the other hand results from emission from a singlet excited state. Here the electron is of opposite spin to that of the ground state and so transition is allowed resulting in a much shorter lifetime of the order of 10^{-9} s. Therefore, to the naked eye, light appears to be emitted only whilst the sample is being excited.[1]

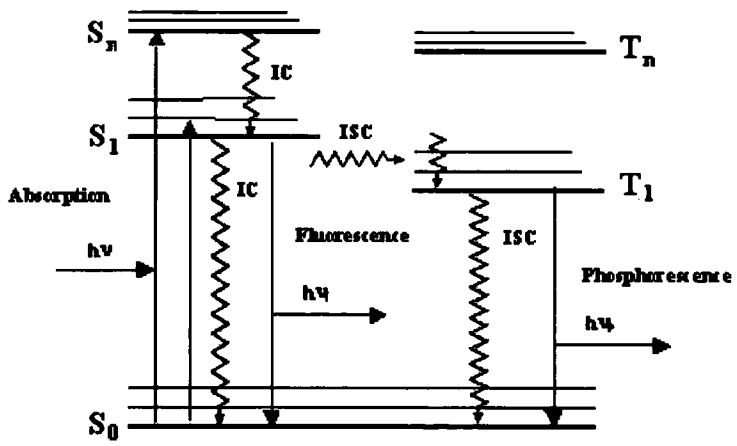

Figure A1. Typical example of a Jabloński diagram.[2]

The processes involved in luminescence are usually shown on a Jabloński diagram.[2] A typical example is given in Figure A1. In this diagram the vertical scale represents energy whilst the horizontal scale is used as an easy way of distinguishing between states of differing spin multiplicity. The singlet ground state, first excited state and higher excited states are denoted S_0, S_1 and S_n, respectively. The triplet excited states are denoted in a similar way with 'T'

replacing 'S'. Each of these energy levels is split into a number of vibrational energy levels, which result from the motion of the nuclei in the molecule. In multinuclear systems these vibrational levels cause the excited states to overlap leading to continuous spectra being observed. The vibrational levels also give rise to fine structure in the spectra.

In fluorescence the absorption of a photon of light promotes an electron from the ground state into a higher singlet energy level. The molecule then relaxes down to the lowest vibrational excited state of S_1 via one of the two non-radiative processes. These are internal conversions (IC) to a lower excited state or vibrational relaxation (VR), where the molecule loses vibrational energy by (i) collisions with solvent molecules in solution or by (ii) interactions with the vibrational motions of a solid matrix. These processes occur in general in under 10^{-12} s, which is much quicker than the alternative ($S_2 \rightarrow S_0$) radiative decay. As fluorescence lifetimes are typically between 10^{-8} and 10^{-12} s these processes are usually complete before emission commences. The molecule will then relax to the ground state (though not necessarily to the lowest energy vibrational state) with the energy lost being released as light. As the excitation does not have a large effect on the geometry of the molecule the spacing of the vibrational states is similar for both S_0 and S_1. This leads to the fluorescence emission spectra being similar (albeit reversed) in shape to the absorption spectra.[1]

Fluorescence can be effected by quenching, resulting in the intensity of fluorescence being reduced. There are ranges of mechanisms by which this process can occur. Collisional quenching occurs when the fluorophore in the excited state comes into contact with another molecule (quencher) in solution. During the encounter the quencher returns the fluorophore to the ground state by a variety of methods which can include electron transfer or spin-orbit coupling and intersystem crossing (ISC) to the triplet state (the latter occurs when the quencher is, for example, molecular oxygen or a halogen).

2 APPENDIX 2: QUANTUM CHEMICAL CALCULATIONS

2.1 NEW 2,5-DIARYL-1,3,4-OXADIAZOLE-FLUORENE HYBRIDS

Theoretical *ab initio* calculations were performed by Dr I. F. Perepichka. DFT calculations were performed to look at the geometry and the electronic state of the molecules **165, 171** and **177**. For comparison DFD **34** and OXD-7 **28c** were also included. To decrease the computational time we calculated the molecules **34a, 165a, 171a** and **177a.**

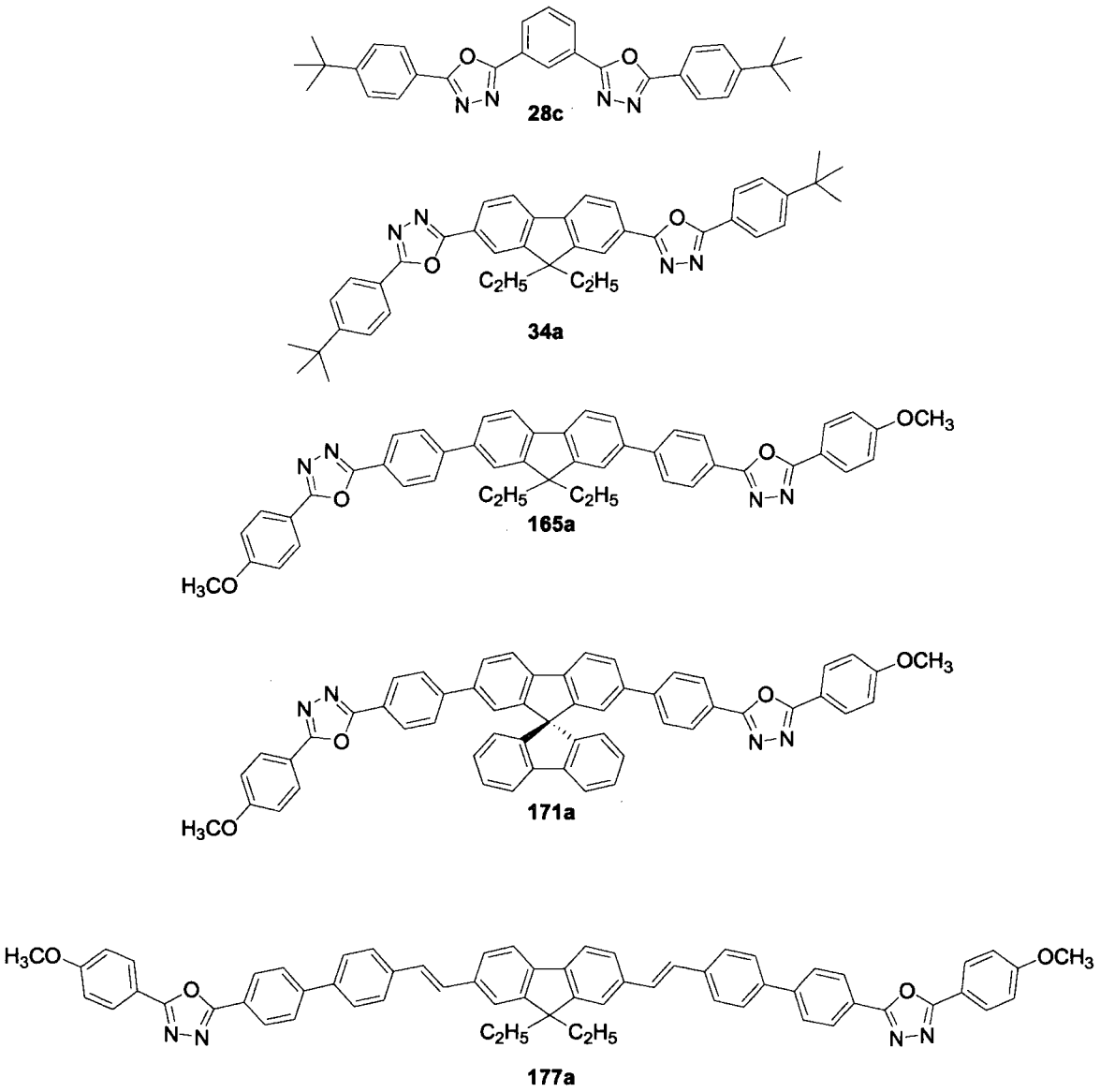

Scheme A1: Structures of compounds OXD-7 28c, 34a, 165a, 171a and 177a studied by *ab initio* calculations.

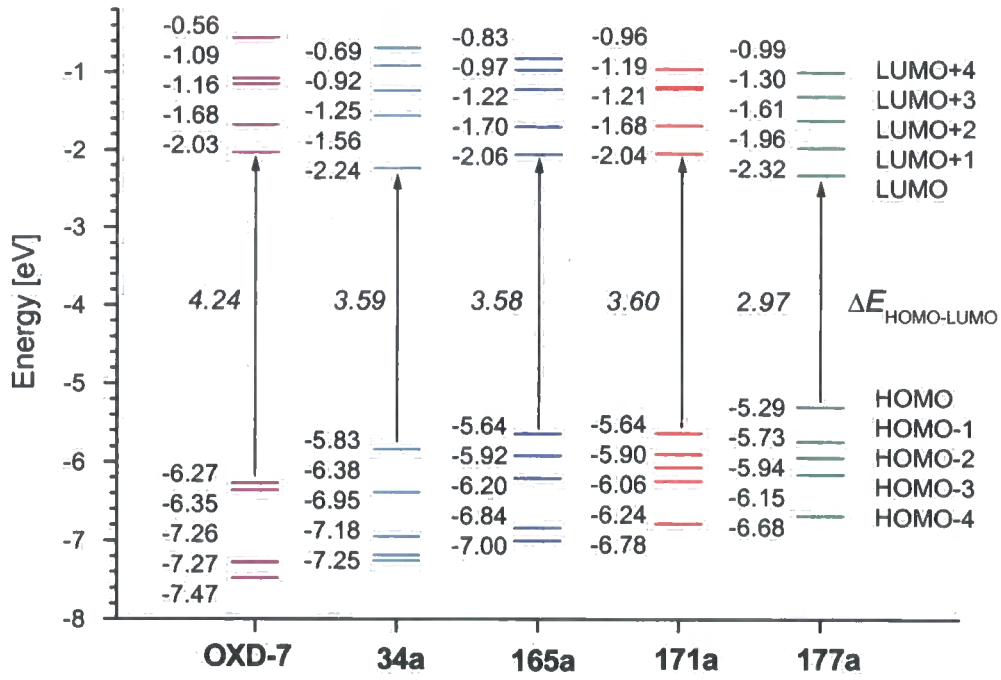

Figure A2. B3LYP/6-311G(2d,p)//B3LYP/6-31G(d) orbital energy level diagrams for compounds 28c, 34a, 165a, 171a and 177a.

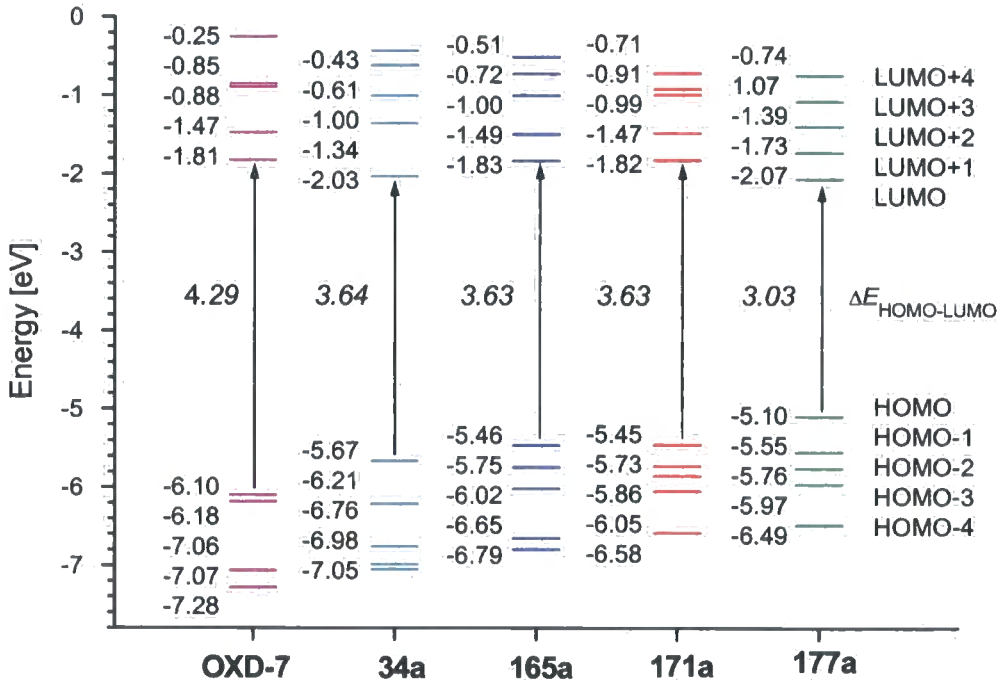

Figure A3: B3LYP/6-31G(d) orbital energy level diagrams for compounds 28c, 34a, 165a, 171a and 177a.

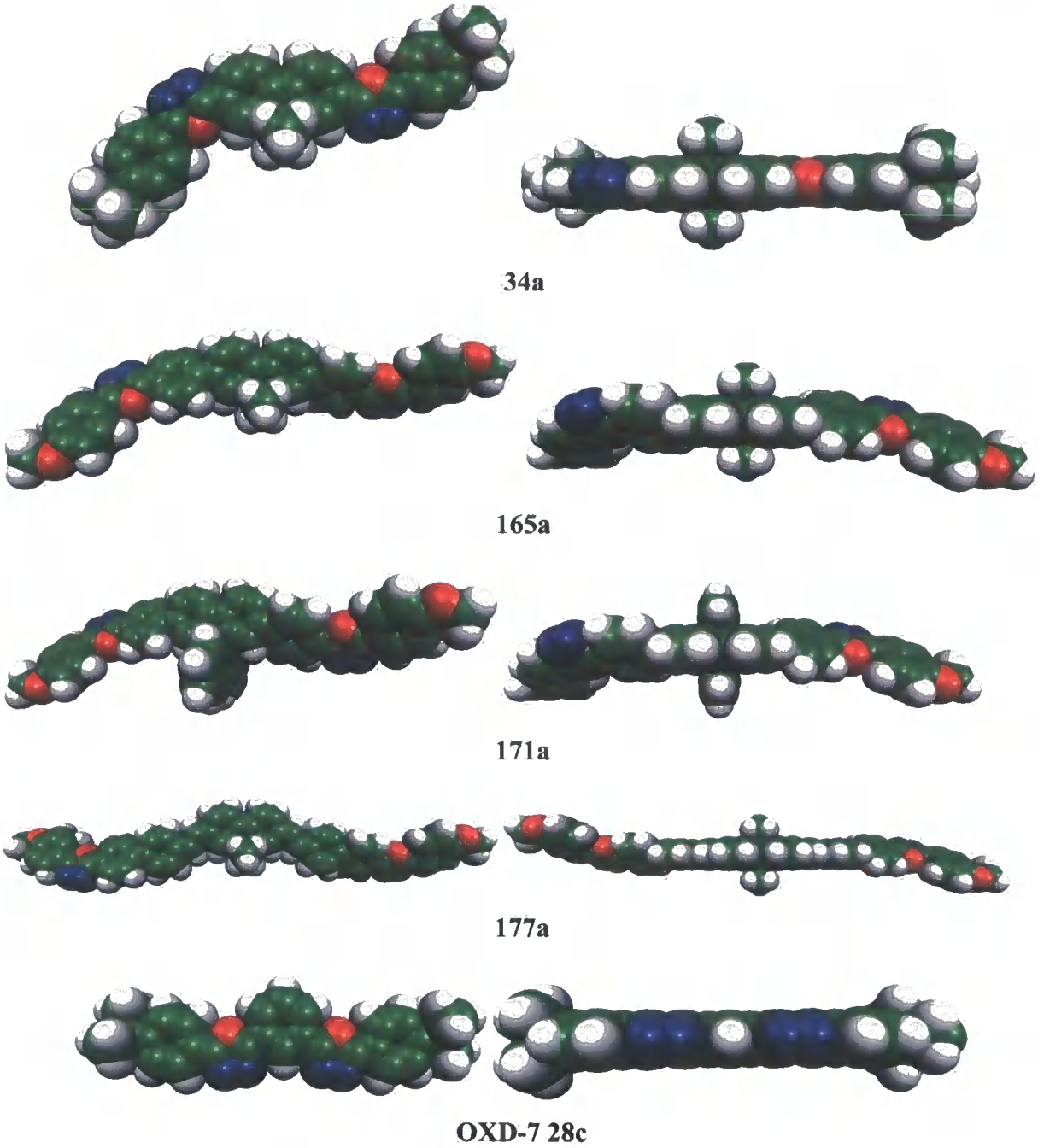

Figure A4: B3LYP/6-31G(d) optimized geometry of compounds 34a, 165a, 171a, 177a and OXD-7 28c.

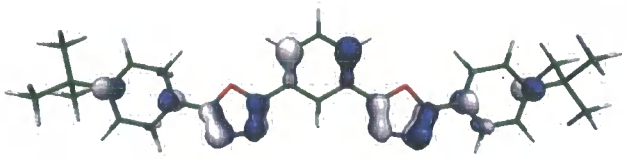

OXD-7, HOMO = –6.27 eV

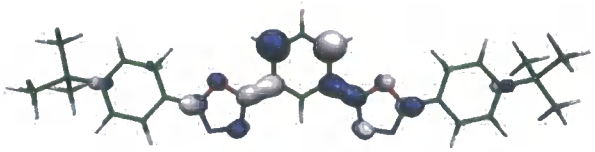

OXD-7, LUMO = –2.03 eV

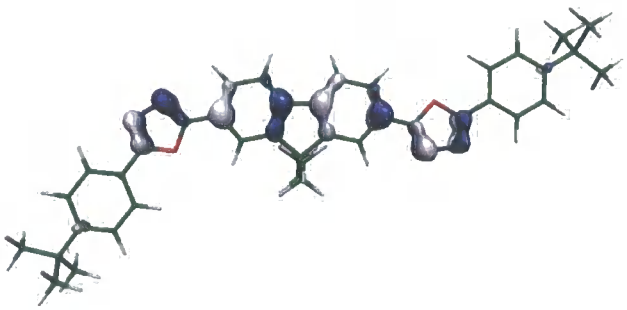

34a, HOMO = –5.83 eV

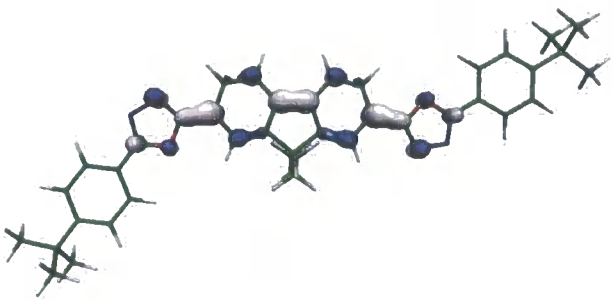

34a, LUMO = –2.34 eV

Figure A5: Frontier orbitals of compounds OXD-7 28c and 34a calculated by B3LYP/6-311G(2d,p)//B3LYP6031G(d) DFT method.

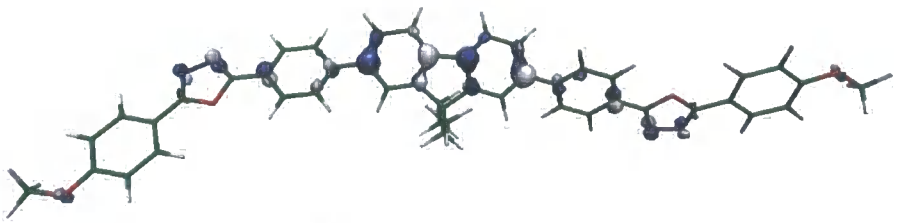

165a, HOMO = – 5.64 eV

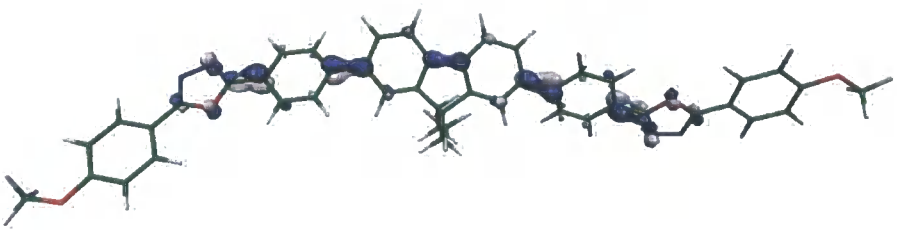

165a, LUMO = – 2.06 eV

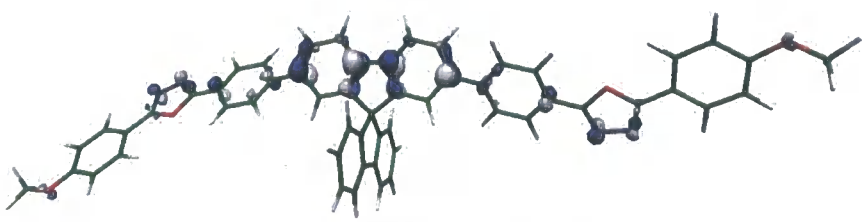

171a, HOMO = – 5.64 eV

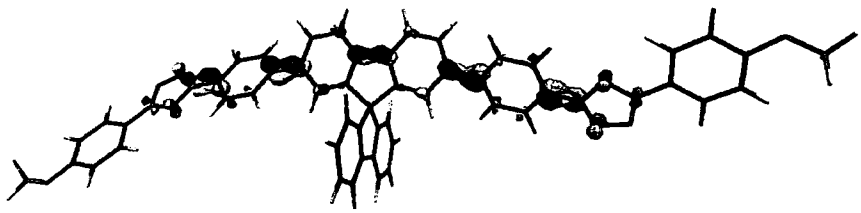

171a, LUMO = – 2.04 eV

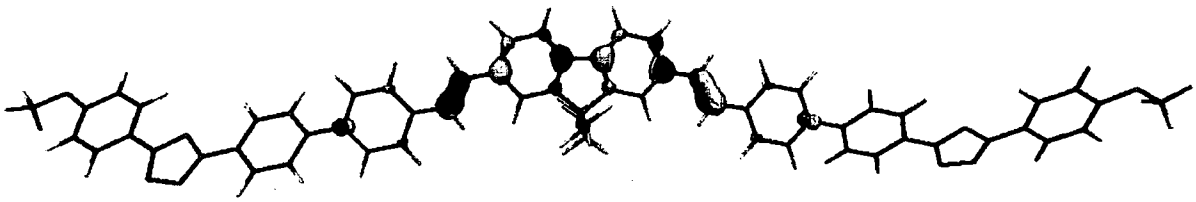

177a, HOMO = –5.29 eV

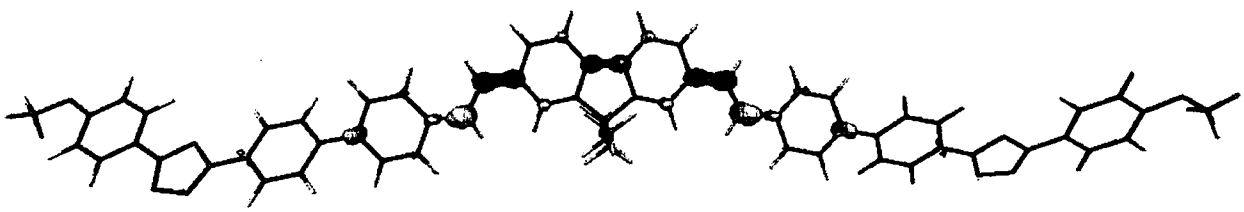

177a, LUMO = –2.32 eV

Figure A6: Frontier orbitals of compounds 165a, 171a and 177a calculated by B3LYP/6-311G(2d,p)//B3LYP6031G(d) DFT method.

2.2 New OXD–Fluorene Hybrids Incorporating Pyridine and Thiophene Units

DFT calculations were performed to elucidate the geometry and the electronic state of the new pyridyl-containing derivatives **184** and **185** in comparison with **165** and **171**. As previously to decrease the computational time calculations were performed on molecules **184a** and **185a**. Calculations were also performed on the geometrical isomers of compounds **184a** and **185a**, with different substitution positions at the pyridine rings (compounds **184a-iso** and **185a-iso**), which have not been synthesised.

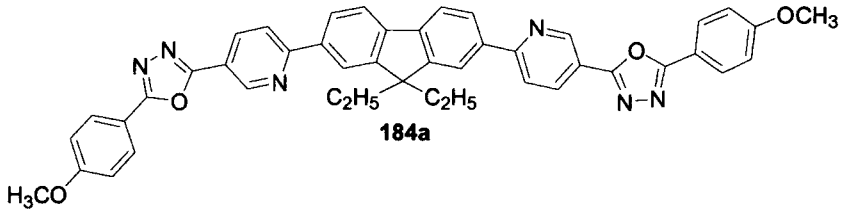

184a

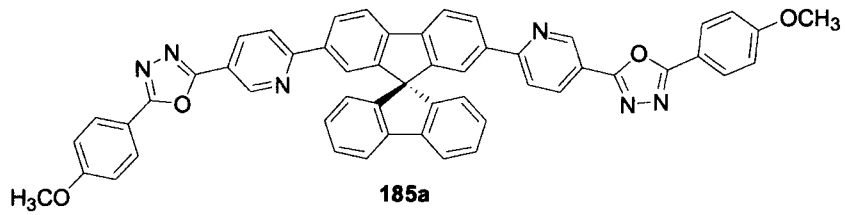

185a

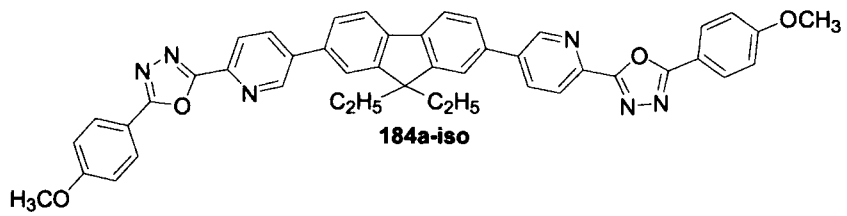

184a-iso

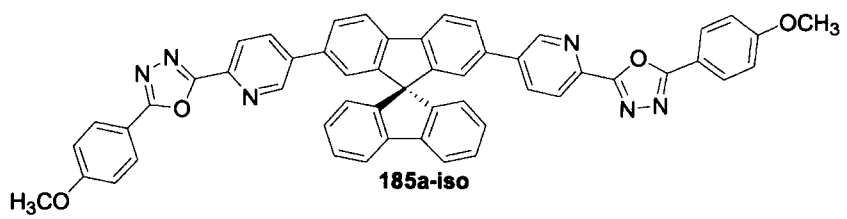

185a-iso

Scheme A2: Structure of compounds 184a, 185a, 184a-iso and 185a-iso studied by *ab initio* calculations.

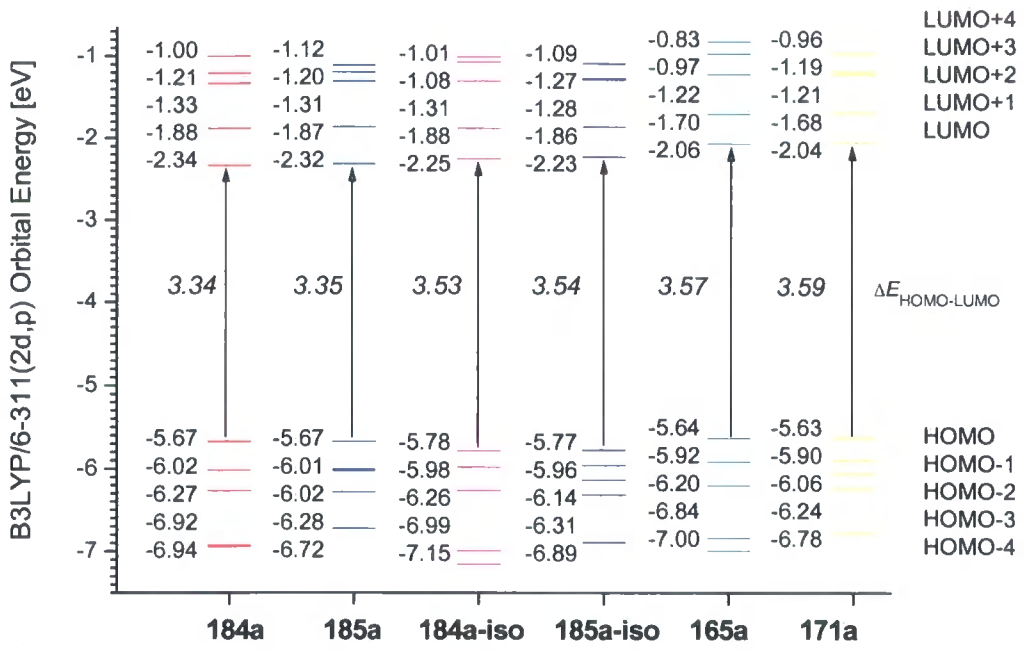

Figure A7: B3LYP/6-311G(2d,p)//B3LYP/6-31G(d) orbital energy levels diagrams for compounds 184a, 185a and a comparison with isomers 184a-iso and 185a-iso, and with phenylene analogues 165a and 171a.

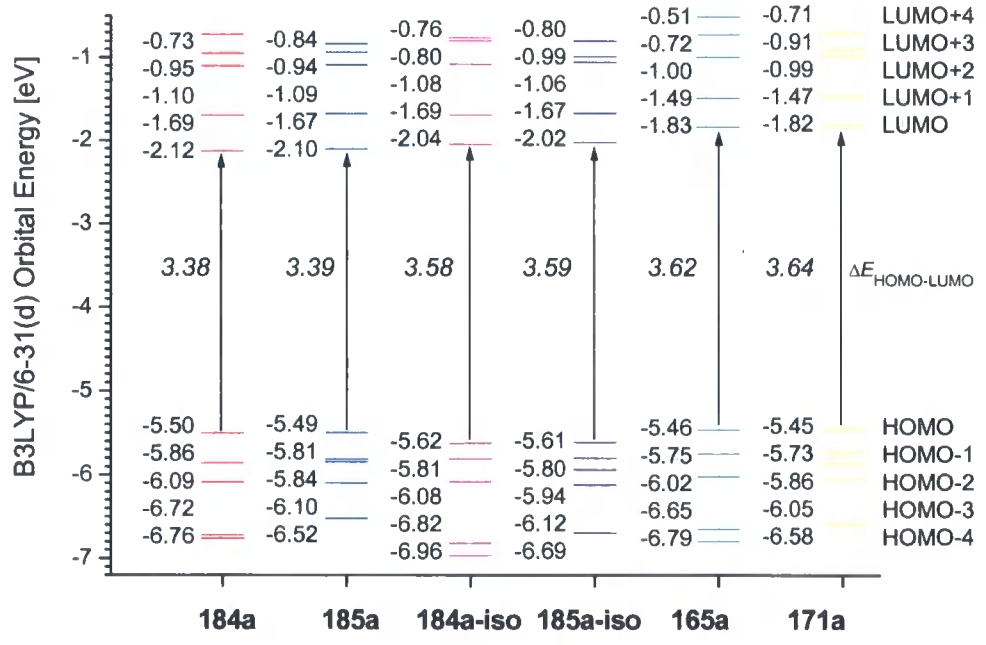

Figure A8: B3LYP/6-31G(d) orbital energy levels diagrams for compounds 184a, 185a and a comparison with isomers 184a-iso and 185a-iso, and with phenylene analogues 165a and 171a.

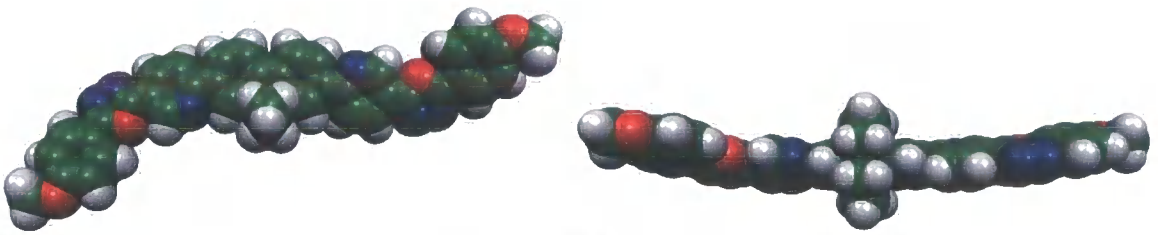

184a

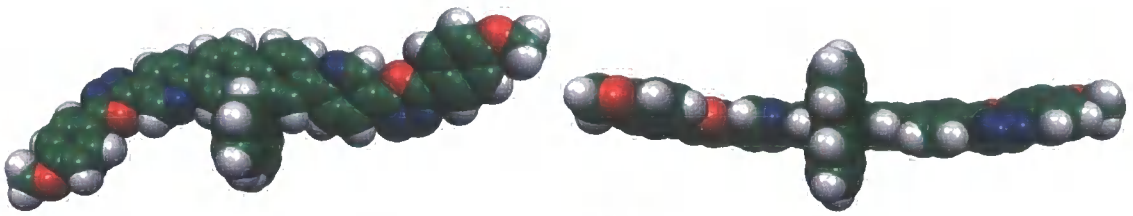

185a

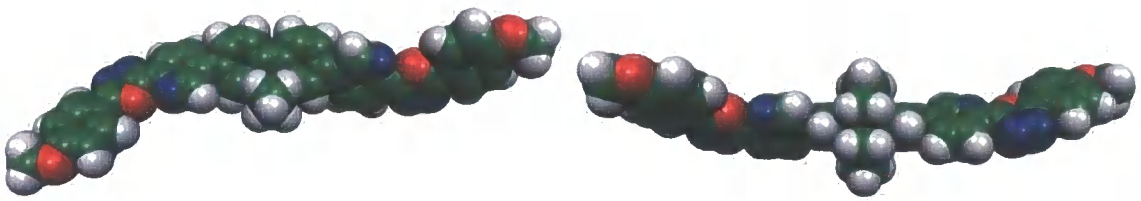

184a-iso

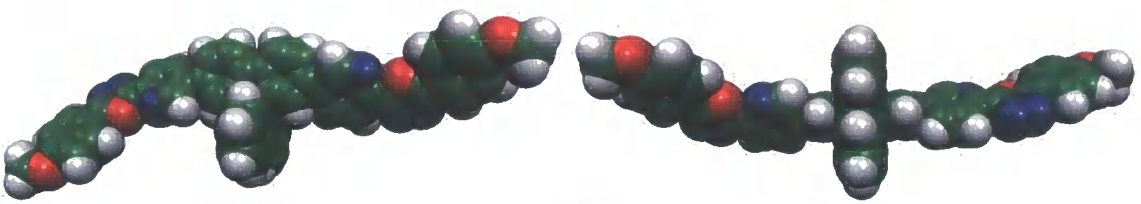

185a-iso

Figure A9: B3LYP/6-31G(d) optimised geometries of compound 184a, 185a, 184a-iso and 185a-iso.

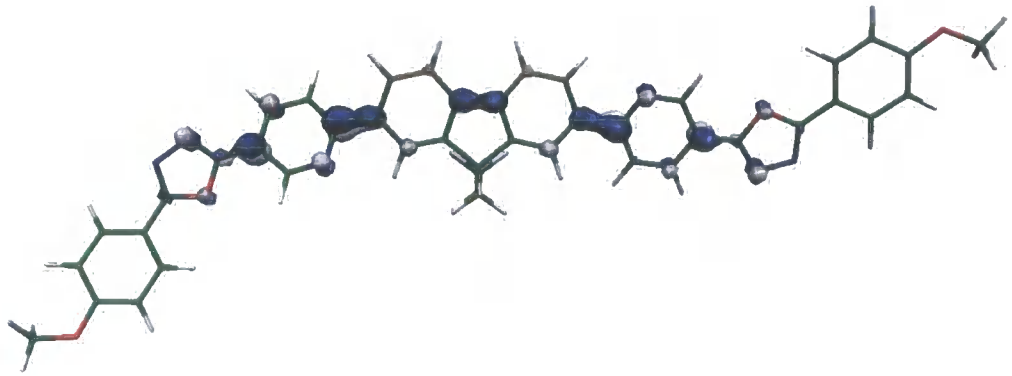

184a, LUMO = –2.34 eV

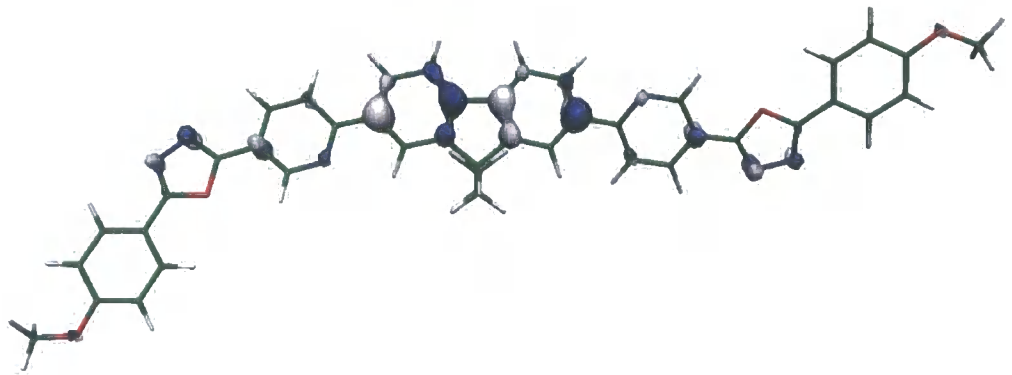

184a, HOMO = –5.67 eV

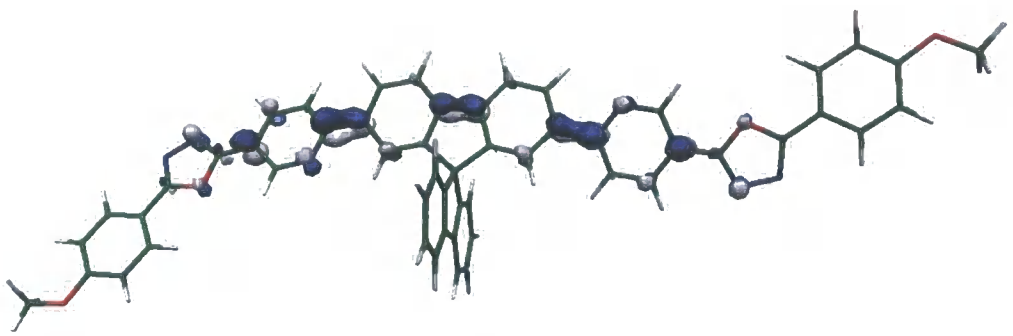

185a, LUMO = –2.32 eV

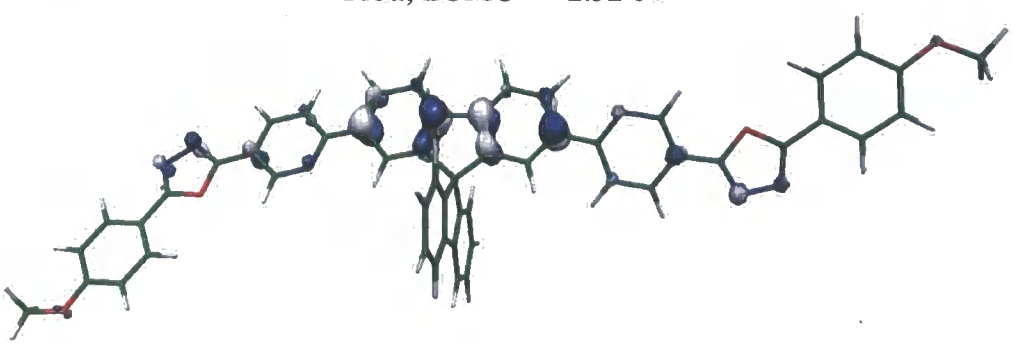

185a, HOMO = –5.67 eV

Figure A10: Frontier orbitals of compounds 184a (E_{total} = –2366.5004319 Hartree) and 185a (E_{total} = –2670.2215067 Hartree) calculated by DFT method at B3LYP/6-311G(2d,p)//B3LYP6031G(d) level.

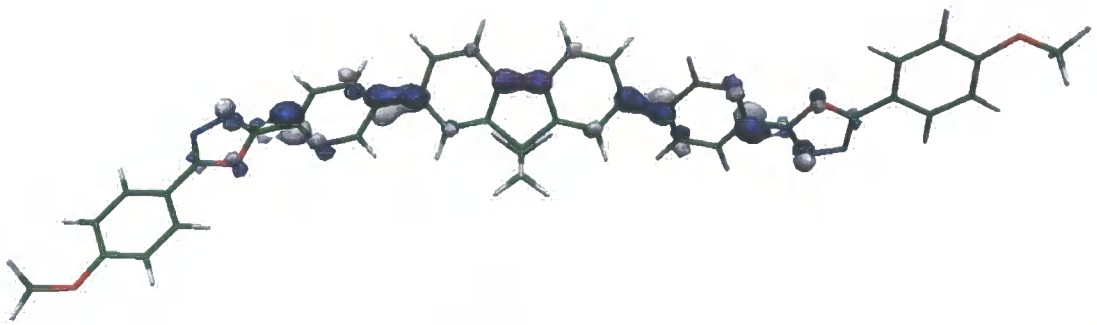

184a-iso, LUMO = –2.25 eV

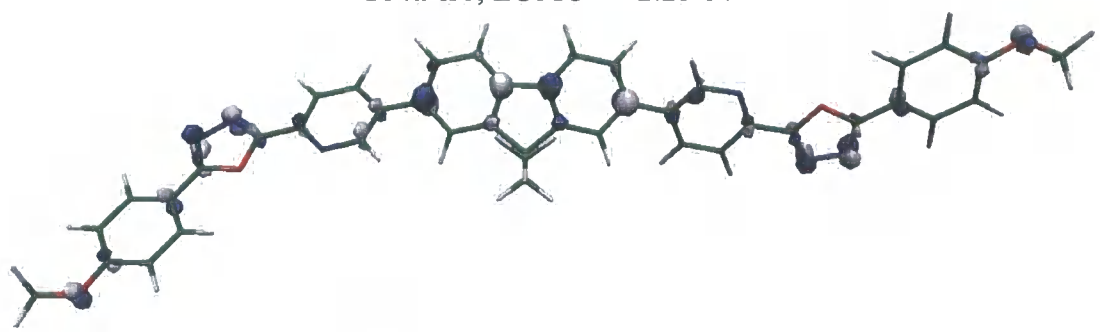

184a-iso, HOMO = –5.78 eV

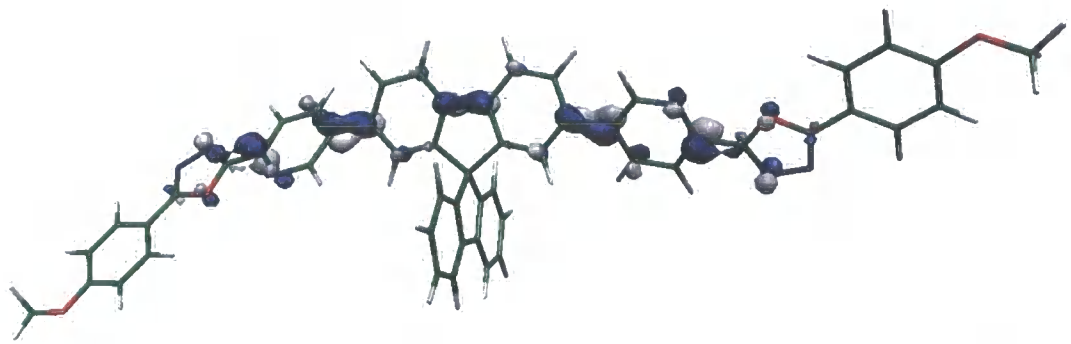

185a-iso, LUMO = –2.23 eV

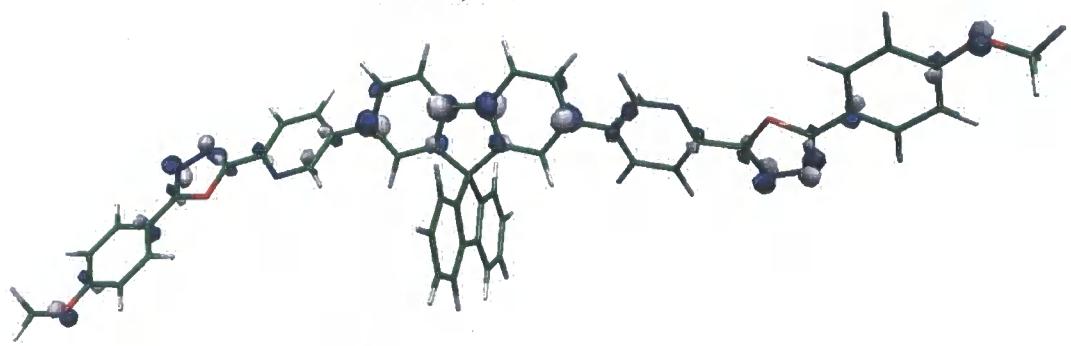

185a-iso, HOMO = –5.77 eV

Figure A11: Frontier orbitals of compounds 184a-iso (E_{total} = –2366.4931201 Hartree), 185a-iso (E_{total} = –2670.2148323 Hartree) calculated by DFT method at B3LYP/6-311G(2d,p)//B3LYP6031G(d) DFT level.

2.3 COMPUTATIONAL PROCEDURES

The *ab initio* computations of geometries of compounds **OXD-7, 34a, 165a, 171a, 177a, 184a, 185a, 184a-iso** and **185a-iso** were carried out with the Gaussian 98[3] package of programs at density-functional theory (DFT) level using Pople's 6-31G split valence basis set supplemented by *d*-polarisation functions on heavy atoms. DFT calculations were carried out using Becke's three-parameter hybrid exchange functional[4] with Lee–Yang–Parr gradient-corrected correlation functional (B3LYP).[5] Thus, the geometries were optimised with B3LYP/6-31G(d) and for all compounds and electronic structures were then calculated at both B3LYP/6-31G(d) and B3LYP/6-311G(2d,p) levels of theory. Contours of HOMO and LUMO orbitals were visualised using Molekel v.4.3 program.[6]

REFERENCES

1 J. R. Lakowicz, *Principles of Fluorescence Spectroscopy,* Kluwer Academic, New York, 2nd Ed, 1999.

2 K. J. Laidler and J. H. Meiser, *Physical Chemistry*, Houghton Mifflin Company, Boston, 2nd Ed, 1995, pg 643.

3 M. J. Frisch, G. W. Trucks, H. B. Schlegel, G. E. Scuseria, M. A. Robb, J. R. Cheeseman, V. G. Zakrzewski, J. A. Montgomery, Jr., R. E. Stratmann, J. C. Burant, S. Dapprich, J. M. Millam, A. D. Daniels, K. N. Kudin, M. C. Strain, O. Farkas, J. Tomasi, V. Barone, M. Cossi, R. Cammi, B. Mennucci, C. Pomelli, C. Adamo, S. Clifford, J. Ochterski, G. A. Petersson, P. Y. Ayala, Q. Cui, K. Morokuma, D. K. Malick, A. D. Rabuck, K. Raghavachari, J. B. Foresman, J. Cioslowski, J. V. Ortiz, A. G. Baboul, B. B. Stefanov, G. Liu, A. Liashenko, P. Piskorz, I. Komaromi, R. Gomperts, R. L. Martin, D. J. Fox, T. Keith, M. A. Al-Laham, C. Y. Peng, A. Nanayakkara, M. Challacombe, P. M. W. Gill, B. Johnson, W. Chen, M. W. Wong, J. L. Andres, C. Gonzalez, M. Head-Gordon, E. S. Replogle and J. A. Pople, Gaussian 98, Revision A.9, Gaussian, Inc., Pittsburgh PA, 1998.

4 A. D. Becke, *Phys. Rev. A*, 1988, **38**, 3098; A. D. Becke, *J. Chem. Phys.*, 1993, **98**, 5648.

5 C. Lee, W. Yang and R. G. Parr, *Phys. Rev. B*, 1988, **37**, 785.

6 (a) P. Flükiger, H. P. Lüthi, S. Portmann and J. Weber, Molekel, Version 4.3, Swiss Center for Scientific Computing, Manno (Switzerland), 2002, http://www.cscs.ch/molekel/; (b) S. Portmann and H. P. Lüthi, *Chimia*, 2000, **54**, 766.